DRAFT

BMI-2104
Volume V

Radionuclide Release Under Specific LWR Accident Conditions

Volume V
PWR-Large, Dry Containment Design (Surry Plant Recalculations)

Prepared by
J. A. Gieseke, P. Cybulskis, R. S. Denning,
M. R. Kuhlman, K. W. Lee, H. Chen

Battelle Columbus Laboratories
Columbus, Ohio 43201

July 1984

DRAFT

BMI-2104
Volume V

Radionuclide Release Under Specific LWR Accident Conditions

Volume V
PWR-Large, Dry Containment Design (Surry Plant Recalculations)

Prepared by
J. A. Gieseke, P. Cybulskis, R. S. Denning,
M. R. Kuhlman, K. W. Lee, H. Chen

Battelle Columbus Laboratories
Columbus, Ohio 43201

July 1984

Prepared for
Office of Nuclear Regulatory Research
U.S. Nuclear Regulatory Commission
Washington, D.C. 20555

ACKNOWLEDGMENTS

Battelle's Columbus Laboratories wishes to acknowledge and express appreciation for the computer codes made available for this program by Sandia National Laboratory, Battelle's Pacific Northwest Laboratories, and the Kernforschungszentrum Karlsruhe, and for the computations and consultation provided by Sandia and the Oak Ridge National Laboratories. Further, members of the Peer Review Group have contributed significantly to this effort by providing comments, suggestions, and information on various reactor systems design.

The support of the U.S. Nuclear Regulatory Commission is gratefully acknowledged, and is the untiring leadership of the NRC staff, particularly Mel Silberberg and Mike Jankowski.

The diligent efforts of many Battelle staff members contributed to the preparation of this report. The following list identifies those staff making major contributions:

RJ Ayers
GT Brooks
EP Bryant
R Freeman-Kelly
CS Jarrett
H Jordan
RG Jung
DJ Lehmicke
MB Neher
DR Rhodes
PM Schumacher
RO Wooton.

TABLE OF CONTENTS

TABLE OF CONTENTS
(Continued)

TABLE OF CONTENTS
(Continued)

1.0 EXECUTIVE SUMMARY

This is Volume 5, dealing with the Surry nuclear power plant, of a seven-volume report of work done at Battelle's Columbus Laboratories to estimate the amount of radioactive material that could be released from light water reactor (LWR) power plants under specific, hypothetical accident conditions. To make these estimates, five power plants were selected that represent the major categories of LWRs: three pressurized water reactors (PWRs) and two boiling water reactors (BWRs). Specifications and data from these plants, along with data from laboratory experiments, were input to computer codes designed to describe various conditions prevailing and physical processes occurring inside reactor systems, including the containment and other buildings. Ultimately, these computer codes provide an estimate of how much radioactive material would be able to escape to the environment if a specific series of events (an "accident sequence") took place.

This volume reports the results of the analysis of the Surry power station, a Westinghouse PWR housed in a large, dry, high-pressure containment building. The specific accident sequences investigated for the Surry plant were selected to represent cases of high risk, severe consequences, and most importantly, a wide range of physical conditions. The computer codes used to analyze the accident sequences include the new code MARCH 2. The Surry plant was previously examined in this study using an earlier version of the code, MARCH 1.1; those results were reported in Volume 1 of this series. Other power plants included in the study are Peach Bottom BWR (Volume 2); Grand Gulf BWR (Volume 3); Sequoyah PWR (Volume 4); and Zion PWR (Volume 6). The seventh volume will address technical questions raised during peer review meetings sponsored by the Nuclear Regulatory Commission.

The possibility of radioactive material being released to the environment has long been the focus of considerable public concern about the safety of nuclear power plants. Since 1962, several major reports have addressed that concern by using computer codes to estimate the release of fission products (radioactive material produced during reactor operations) to the reactor containment building, and thence to the environment, during a hypothetical severe accident. Although these analyses have improved over the years, in terms of how realistically they describe what happens during a hypothetical

accident, it has not previously been possible to apply the various codes sequentially to follow the transport of fission products along their flow path from the core to the environment. This limitation resulted in piecemeal, parametric estimates of release.

The research results reported here are intended to provide a systematic, sequential application of the codes as well as to present analyses performed with improved computational procedures. It is to be recognized that this report describes an analytical approach for estimating radionuclide transport and deposition which incorporates individual physical and chemical processes or mechanisms. This approach is being evaluated for use in predicting the amount fission product release (the "source term") to the environment for specific reactors and accident sequences. When verified, these prediction techniques are expected to be more specific and perhaps to supersede generic tables of release fractions provided by previous analyses.

The purpose of this report is then to:

(1) Develop updated release-from-plant fission product source terms for four nuclear power plant designs and for accident sequences giving a range of conditions. The estimated source terms are to be based on consistent step-by-step analyses using improved computational tools for predicting radionuclide release from the fuel and radionuclide transport and deposition.

(2) Determine the effects of major differences in plant design and accident sequences on fission product releases.

(3) Provide in-plant time- and location-dependent distributions of fission product mass for use in equipment qualification.

Approach

This study was conducted by selecting specific plants and accident sequences and then using consistent and improved analyses of fission product release from fuel and radionuclide transport and deposition to predict fission product release to the environment for these specific cases. The approach comprises a sequence of steps; in the combined analysis, the results are

specific to a particular set of accident conditions, and each step is based on results from analyses of the previous step.

The Surry Plant

Surry Unit 1 was selected to characterize large, high-pressure PWR designs. In some respects, Surry is not an ideal choice: it is not especially large, the subatmospheric design feature is representative of only a handful of plants and its power output is lower than the U.S. average. In another respect, Surry is the natural choice because it was the basis of the WASH-1400 study; by choosing to study the same plant, a direct comparison can be made with results of WASH-1400. Although clearly not a main goal, the comparison of results was judged important enough to guide the plant selection. To compensate for discrepancies between Surry and other large, high-pressure PWR designs, analyses have been performed for two accident sequences for the Zion plant. These results are reported in Volume 6 of the study.

Accident Sequences Chosen for Study

Three criteria were used in selecting accident sequences for analysis. The set of sequences was chosen to include: sequences which had been found to dominate risk in previous risk studies, sequences which would be expected to have particularly severe consequences, and sequences covering a broad range of physical conditions.

AB Sequence:

- Loss-of-Coolant Accident (LOCA), loss of AC power.
- Emergency Core Cooling injection system does not operate.
- Depressurization of the reactor coolant system occurs rapidly following the break.
- Containment safety features (containment sprays and containment cooling systems) are not available.
- A break in the hot leg is assumed for this study to examine a minimum pathway and presumably minimum fission product retention within the reactor coolant system.

TMLB' Sequence:

- Transient, loss of primary system heat removal.
- System pressure remains high during core heatup (i.e., core uncovery is delayed for a few hours).
- High pressure, essentially stagnant flow, a much longer release path, and interactions between core materials and water in the reactor cavity take place.
- Containment safety features (containment sprays and containment cooling systems) are not available.
- Rapid pressure rises in the containment following vessel failure could threaten containment integrity and lead to a potentially large release of fission products.

S_2D Sequence:

- Small pipe break, failure of Emergency Core Cooling system.
- Low flow and intermediate pressure occur in the reactor coolant system during the meltdown period.
- Containment safety features (containment sprays and containment cooling systems) are operable up to containment failure.
- This is the only sequence analyzed in which the effectiveness of containment safety features is examined.

V Sequence:

- Interfacing systems Loss-of-Coolant Accident (LOCA).
- Check valves that separate the low-pressure Emergency Core Cooling system from the high-pressure primary system fail.
- The pathway for release bypasses the protection normally provided by the containment building, so the amount of retention in the reactor coolant system is particularly important.
- This sequence potentially involves a large fission product release to the atmosphere.

Computer Codes Used in the Study

Our efforts built on previous computer modeling work performed at Battelle-Columbus, at Sandia, and in the Federal Republic of Germany, and on experimental and model evaluation studies performed at Oak Ridge, EG&G Idaho, Sandia, and Pacific Northwest Laboratories. In addition to the calculations

performed at Battelle-Columbus, calculations of thermal-hydraulic behavior and fission product release related to molten core-concrete interactions were performed by Sandia. Research efforts specifically directed toward increasing our understanding of fission product release and transport under severe accident conditions are under way at the laboratories listed above, as well as at other research installations around the world. Over the next few years, it is expected that considerable progress will be made in this area. Therefore, this report must be considered as an expression of current knowledge, with the expectation of future validation or modification of the calculated fission product releases.

The first step in analyzing accident sequences was to collect plant design data and perform thermal-hydraulic calculations. Thermal-hydraulic conditions in the reactor over time were estimated with the MARCH 2 code, and detailed thermal-hydraulic conditions for the reactor's primary coolant system were estimated with the MERGE code, developed specifically for this program.

The time-dependent core temperatures from the MARCH 2 code were used as input to another code developed for this program, CORSOR, which predicts time- and temperature-dependent releases of radionuclides from the fuel inside the reactor pressure vessel. Releases of radionuclides from the interaction of the melted reactor core with the concrete outside the reactor vessel were estimated by Sandia National Laboratories using their computer code, VANESA.

Using the MARCH/MERGE-predicted thermal-hydraulic conditions and the CORSOR-predicted radionuclide release rates as input, a newly developed version of the TRAP-MELT code was used to predict vapor and particulate transport in the primary coolant circuit. Transport and deposition of radionuclides in the containment were calculated using the NAUA-4 code. In Volume 1, analyses were also performed with the CORRAL-2 code to relate the results to WASH-1400 assumptions.

The calculations performed in this study were of a "best estimate" type. Whenever possible, input was derived from experimental measurements. Data employed in these analyses include vapor deposition velocities, aerosol deposition rates, aerosol agglomeration rates, fission product release rates from fuel, particle sizes formed from vaporizing/condensing fuel materials, engineering correlations for heat and mass transfer, and physical properties of various fuel, fission product, and structural materials.

Summary of Results

A number of accident sequences that had been analyzed previously in Volume 1 of BMI-2104 were reanalyzed in this report. The principal difference in the analyses involved the use of the MARCH 2 computer code rather than the MARCH 1.1 code used in Volume 1. In addition, a gradual fuel slumping model was used in the MARCH 2 analyses which is believed to provide a more realistic characterization of thermal-hydraulic conditions in the reactor coolant system during slumping. It is interesting to compare the results obtained in the current effort with both the earlier Volume 1 analyses and the results from WASH-1400 for the same plant and accident sequences.

The release of fission products from fuel during the period of fuel heatup and melting in-vessel and during ex-vessel attack of the concrete predicted in this study is not markedly different from the results in WASH-1400. Essentially all of the volatile fission products are predicted to be released from the fuel in all cases.

Retention of fission products during transport through the reactor coolant system was not credited in the WASH-1400 study. In the current study the amount of retention in the reactor coolant system is in many cases substantial (e.g., 85 percent of the iodine in TMLB') depending on the thermal-hydraulic conditions in the system. The uncertainty regarding the ultimate fate of fission products deposited within the reactor coolant system is very great, however. Follow-on analyses of decay heating of reactor coolant system surfaces and the reevolution of fission products are in progress and will be reported in an Appendix at a later time.

The results of the containment transport analyses performed for this study indicate that the potential for retention in the containment building and secondary buildings is somewhat greater than predicted in WASH-1400. This is partially because of an underestimation of removal processes in the WASH-1400 CORRAL code and partially because of an increased time to containment failure in the current analyses.

In general the results of the current study indicate that for many important accident sequences the source term in WASH-1400 is overestimated by approximately an order of magnitude. The effect of a reduction of this magnitude on estimated risk would be essentially proportional for the risk of latent

fatalities (i.e., an order of magnitude) but would be even more dramatic for the risk of early fatalities because of the threshold behavior of this measure.

Of the important sequences analyzed, the one in which a major reduction in consequences was not observed is the interfacing LOCA sequence, V, for the assumption of no overlying pool of water at the entry point into the safeguards building. If there is an overlying water layer, the source term is considerably reduced. Although this is no longer considered a risk-dominant sequence because of steps taken to suppress its likelihood, the existence of credible sequences with potentially large consequences can have public perception and regulatory implications regardless of the risk significance of the sequence.

It is important that the reader recognize the magnitude of the uncertainties in the "best estimate" release terms presented in this report. The prediction of fission product release has been shown in this study to be sensitive to accident thermal-hydraulics and core melting and slumping behavior as well as to the mechanisms of fission product release, transport, and deposition. The reader is referred to the companion QUEST study being undertaken by Sandia National Laboratory to obtain a perspective on the magnitude of the uncertainties in these results.

2. INTRODUCTION

The possibility of radioactive material being released to the environment from LWRs has long been the focus on public concern about the safety of nuclear power plants and the impetus for safety research. Most reactors in the United States were designed, and their sites were chosen, on the basis of accidental release assumptions described in research report TID-14844.[2.1] Published in 1962, TID-14844 prescribes a formula for the release of fission products (radioactive material produced during reactor operations) to the reactor containment area during a hypothetical severe accident. Although these assumptions are representative of the state of knowledge at the time, the behavior of fission products has become better understood in the intervening years. In the period 1972 to 1975, the Nuclear Regulatory Commission conducted the Reactor Safety Study to assess the accident risks in U.S. commercial nuclear power plants. The report of that study, known as WASH-1400,[2.2] provided a more comprehensive and physically accurate description of fission product behavior. The amount of fission product release (the "source term") estimated in WASH-1400 has since been used extensively in planning and evaluating reactor operations.

The WASH-1400 source term to the environment for accident sequences has had broad implications for operating LWRs--in licensing, emergency planning, safety goals, and indemnification policy. However, additional research continued to provide even better methods for estimating fission product release and transport. In 1981, the Nuclear Regulatory Commission issued the report "Technical Bases for Estimating Fission Product Behavior During LWR Accidents",[2.3] a review of the state of knowledge at the time. As part of the Technical Bases report, the assumptions, analytical procedures, and available data were evaluated, and new estimates were made. One advantage of the new estimates was that they took into account the fact that some radioactive material would be deposited inside the reactor during an accident and would therefore not escape from the reactor core to the environment. On the other hand, because of the limitations of the computer codes available at that time, the new estimates could not follow the transport of fission products along their flow path from the core to the environment by applying the various codes sequentially. This resulted in piecemeal, parametric estimates of release.

The research results reported here are intended to provide this systematic, sequential application of the codes as well as to present analyses performed with computational procedures improved since the "Technical Bases" report. It is to be recognized that in this study, an analytical approach was developed for estimating radionuclide transport and deposition which incorporates individual physical and chemical processes or mechanisms. This approach is being evaluated for use in predicting fission product source terms for release to the environment for specific reactors and accident sequences. When verified, predictions made with the approach used here are expected to replace the generic tabular release fractions such as those in Table 6, Appendix V of WASH-1400, where release fractions are given for broad classes of accidents.

The purpose of this report is then to:

(1) Develop analytical procedures and use them to predict updated release-from-plant fission product source terms for four types of nuclear power plants and for accident sequences giving a range of conditions. The estimated source terms are to be based on consistent step-by-step analyses using improved computational tools for predicting radionuclide release from the fuel and radionuclide transport and deposition.

(2) Determine the effects on fission product releases associated with major differences in plant design and accident sequences.

(3) Provide in-plant time- and location-dependent distributions of fission product mass for use in equipment qualification.

It is not necessarily the intent of this work to produce an all-encompassing definition of source terms, but rather to make best estimates of source terms for a range of typical plants and several risk-significant sequences covering a wide range of conditions. These analyses are to be made with the best available techniques, in a consistent manner, following along release pathways for fission products, and at a level of detail consistent with current knowledge of pertinent physical processes. Based on state-of-the-art techniques, these best-estimate analyses should provide an indication of the conservatisms inherent in current source term assumptions and guidance for the development of new source terms. The analytical methods and

corresponding predictions presented here are based on currently available information and are subject to revision and improvement as better analytical procedures are developed and as a more extensive experimental base evolves. The preparation of this report, therefore, is an evolutionary process which will be carried out over a period of time, with verification and possibly revision of the procedures continuing over several years.

As a part of this evolutionary process, it should be noted that this report is expected to be revised using improved analytical procedures and incorporating predictions of possible fission product reevolution during decay heating of deposits. The results of these calculations are to be published as an appendix to this report.

2.1 References

(2.1) DiNunno, J. J., et al, "Calculation of Distance Factors for Power and Test Reactors Sites", TID-14844 (March 23, 1962).

(2.2) "Reactor Safety Study--An Assessment of Accident Risks in U.S. Commercial Nuclear Power Plants", WASH-1400, NUREG-75/014 (October, 1975).

(2.3) "Technical Bases for Estimating Fission Product Behavior During LWR Accidents", NUREG-0772 (June, 1981).

3. GENERAL APPROACH

The general philosophy behind this study is that mechanistic predictions of radionuclide release and transport are possible if proper modeling is performed to represent the physical and chemical processes occurring during LWR accidents. The study, then, represents an attempt to describe in a reasonably complete but tractable fashion the processes influencing radionuclide release to the environment for selected plants and accident conditions.

The objectives of this study originally called for a consistent analysis of radionuclide behavior by following fission product transport along flow paths, starting with release into the core region and ending with final release to the environment. To meet these objectives, numerous decisions and assumptions were required for the analyses: selection of plants and sequences for consideration; choice of analytical tools to be used or upgraded; evaluation and incorporation of experimental data; and determination of major physical effects which would be considered on a parametric variation basis to determine the sensitivity of calculations to such variations. Some of the major considerations will be reviewed and discussed in this section.

The general approach in this study was to select specific plants and accident sequences for consideration and then to use consistent and improved analyses of fission product release from fuel, transport, and deposition to predict fission product release to the environment for these specific cases. The approach consists of a series of steps performed in sequence such that in the combined analysis, the results are specific to an individual set of accident conditions, and each step is based on results from analyses of the previous step.

3.1 Plant Selection

The first major step in the process was the selection of types of nuclear power plant designs to be considered and a specific plant to represent each type. The types to be considered were: large, dry PWRs; Mark I BWRs; Mark III BWRs; and ice-condenser containment PWR designs. The specific plants chosen to represent each type, respectively, are the Surry and Zion, Peach Bottom, Grand Gulf, and Sequoyah plants. These selections were made on a

combined basis of typicality of design and availability of design details needed for analysis.

3.2 Selection of Accident Sequences

Accident sequences were chosen for each plant such that significant contributions to risk and a wide range of physical conditions were represented in the analyses. The selected plants and accident sequences are listed below:

PWR: Large Dry Containment (Surry-Volumes 1 and 5)	PWR: Large Dry Containment (Zion-Volume 6)	BWR: Mark I (Peach Bottom-Volume 2)
AB	TMLB'	TC
S_2D	S_2D	AE
V		TW
TMLB'		

BWR: Mark III (Grand Gulf-Volume 3)	PWR: Ice Condenser Containment (Sequoyah-Volume 4)
TPI	S_2HF
TQUV	TMLB'
TC	TML
S_2E	

The accident sequences for each plant are described in detail in Section 4.2 of the volume of the report dealing with that plant.

3.3 Computer Codes Used in the Study

Following the selection of plants and sequences, the required plant design data were collected and thermal-hydraulic analyses performed for each accident sequence. Overall thermal-hydraulic conditions on a time-dependent basis were estimated with the MARCH code,(3.1) and detailed thermal-hydraulic conditions for the primary system were estimated with the MERGE code(3.2) developed specifically for this program.

The time-dependent core temperatures were used as input to another code developed for this program, CORSOR(3.3), which predicts time- and

temperature-dependent mass releases of radionuclides from the fuel within the pressure vessel. Releases during core-concrete interactions of radionuclides remaining with the melt were provided by Sandia National Laboratories using their newly developed model, VANESA[3.4].

Using the MARCH/MERGE-predicted thermal-hydraulic conditions and the CORSOR-predicted radionuclide release rates as input, a newly developed version of the TRAP-MELT code (TRAP-MELT 2)[3.5] was used to predict vapor and particulate transport in the primary coolant circuit.

Transport and deposition of radionuclides in the containment were calculated using the NAUA-4[3.6] code.

The basic stepwise procedure described above is illustrated in Figure 3.1, which shows the relationships among the computational models. The calculations were of a "best estimate" type using input derived from experimental measurements whenever possible. Types of data employed in the analyses include vapor deposition velocities, aerosol deposition rates, aerosol agglomeration rates, fission product release rates from fuel, particle sizes formed from vaporizing/condensing fuel materials, engineering correlations for heat and mass transfer, and physical properties of various fuel, fission product and structural materials.

3.3.1 Assumptions

In preparation for performing calculations of thermal-hydraulic conditions and radionuclide transport and deposition, it was necessary to make a number of assumptions or to select conditions from among several options. Major assumptions used in this study of the Surry plant, using the MARCH-2 code, are listed below in the categories of geometry, thermal hydraulics, mechanisms, and sequences.

Geometry

(1) Surfaces within the containment building available for radionuclide deposition include only the major geometrical features of the building.

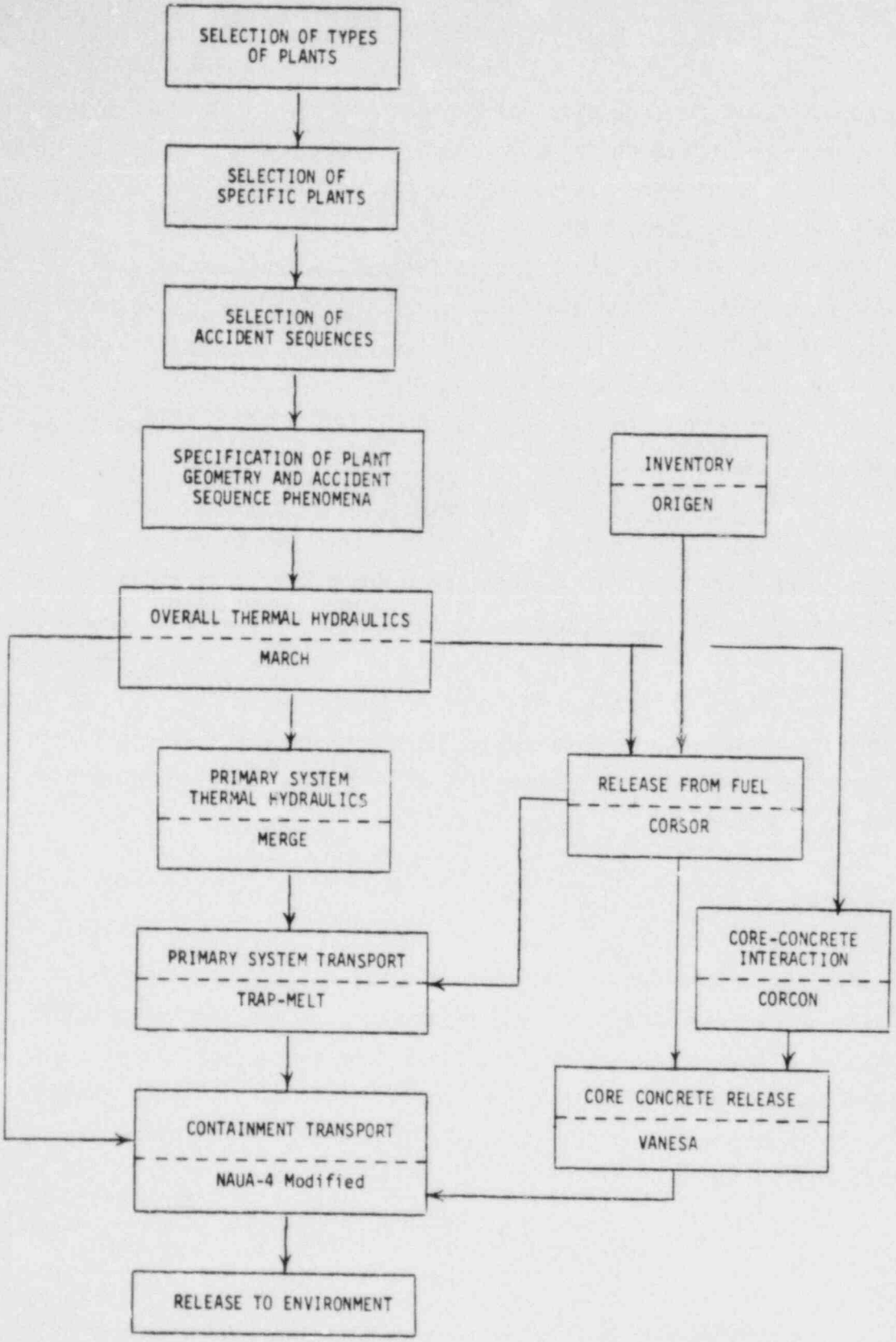

FIGURE 3.1. INFORMATION FLOW FOR RELEASE, TRANSPORT, AND DEPOSITION CALCULATION

(2) There is no attenuation of radionuclides as they pass through leak paths in the containment shell.

Thermal Hydraulics

(3) Before pressure vessel failure, flow in the primary coolant system is restricted to direct leak paths.

(4) The upper plenum geometry is modeled in terms of surface areas, steel thickness, and compartment heights rather than with exact geometries.

(5) Decay heating of surfaces by deposited fission products is neglected in the calculations reported in the main body of this volume but is considered in the Appendix (to be added later).

(6) No operator intervention occurs that would lead to cooling of the steam generators.

Mechanisms

(7) Neither deposition nor resuspension of radionuclides occurs during rector coolant system depressurization at the time of pressure vessel melt-through.

(8) In the long term (after pressure vessel failure), deposited radionuclides remain in the primary system indefinitely. The effects of this assumption are considered in the Appendix (to be added later).

(9) No change in fission product physical or chemical properties results from radioactive decay.

Sequences

(10) In the V sequence, all fission products released from the fuel after pressure vessel failure are assumed to mix in the containment volume prior to flowing back through the reactor coolant system to the environment.

(11) Vaporization release is scrubbed by an overlying layer of water in the S_2D sequence.

Some of the above assumptions have been relaxed or changed to accommodate best estimates of conditions and occurrences in specific cases. These are discussed in greater detail for each plant in Section 6.1 of the volume of the report dealing with that plant.

3.3.2 Uncertainty Considerations

The computation of radionuclide release and transport using mechanistic models is subject to many uncertainties of various magnitudes and importance. Quantitative estimates of uncertainties in individual parameters, and hence the overall importance of such uncertainties, has been outside the scope of this study. Where practical, however, qualitative (and in some cases quantitative) estimates of uncertainties have been noted.

Some of the uncertainties in the analyses and procedures can be identified that are currently considered significant. The following is a list of some uncertainties that are believed significant and warrant further evaluation through more detailed analyses:

(1) The simplified fuel melting model in MARCH (i.e., a single melting temperature) could bias the predicted release of material from overheated fuel, particularly regarding the source of inert and low volatility fission product aerosols.

(2) The rate coefficients for the release of fission products from overheated fuel are empirical, rather than mechanistically based, and rely largely on scaled, simulant experiments.

(3) The model for the release of fission products and inert materials during the attack of concrete has a very limited experimental basis.

(4) The flow patterns in the reactor coolant system are uncertain. The adequacy of the simple thermal-hydraulic models used in this study will require experimental verification.

(5) Primary system transport models used in these analyses have not been validated against integral experiments.

(6) The mode and timing of containment failure in severe accident sequences can have a major influence on fission product behavior but are subject to large uncertainty.

(7) The calculation methods for water condensation in the containment are based on limited, small-scale experiments and require verification at larger scales.

(8) Deposition velocities for vapor species used in the TRAP-MELT calculations were taken as a mid-points in order-of-magnitude ranges of experimental data. More accurate data would reduce the uncertainty in these parameters and in the resulting rates for deposition by sorption.

3.4 References

(3.1) Wooton, R. O. and Avci, H. I., "MARCH (Meltdown Accident Response Characteristics) Code Description and Users' Manual", NUREG/CR-1711, BMI-2064 (October, 1980).

(3.2) MERGE Manual.

(3.3) CORSOR Manual.

(3.4) VANESA Manual.

(3.5) TRAP-MELT 2 Manual.

(3.6) Bunz, H., Koyro, M., and Schock, W., "A Code for Calculating Aerosol Behavior in LWR Core Melt Accidents Code Description and Users' Manual".

4. PLANT SELECTION AND ACCIDENT SEQUENCES

4.1 General Plant Description

The plant selected to characterize pressurized water reactors with large, high-pressure containment designs is Surry Unit 1. In some respects, the selection is not ideal: the Surry plant is an older design, and in comparison with average parameters for U.S. plants, its power output is low, its containment volume is small, and its containment design pressure is low. However, the Surry plant was chosen because its design was analyzed in the Reactor Safety Study, and, a direct comparison of our predicted source terms and those predicted in the Reactor Safety Study was judged important enough to guide our selection. Important differences between Surry and the "ideal" choice have been examined by parametric variation.

The Surry unit is a pressurized water reactor (157-inch diameter vessel with 157 fuel assemblies) designed by Westinghouse. A detailed description of plant data is provided in Table 4.1. The reactor is designed to operate at a nominal power of 2441 MW(t) and a reactor coolant system pressure of 2250 psia. The containment is a steel-lined reinforced concrete structure with a free volume of 1.8×10^6 ft^3; it is operated subatmospheric with initial pressure and temperature of 10 psia and 100 F. Figure 4.1 illustrates the layout of the containment.

4.2 Selection Basis and General Description of Accident Sequences

The four accident sequences selected for analyzing the large, high-pressure containment PWR plant design were AB, TMLB', S_2D, and V. (Table 4.2 relates the letter used in the accident identifier to the type of event and to the failure of the engineered safety systems.) Two criteria were used in selecting sequences. First, the selected sequences were to be risk dominant for a number of design variations within the large high-pressure containment category of PWRs. Second, these sequences were to cover a range of accident conditions and engineered safety system performance within the reactor coolant system and containment building.

TABLE 4.1. PWR DATA

Nominal power	2,441 MW(t)	
	8,331 x 10^6 Btu/hr	
Internal energy of water	246.9 x 10^6 Btu	(2.66 x 10^{10} kg-m)
Sensible heat in the core	16.35 x 10^6 Btu	(1.76 x 10^9 kg-m)
Total water in the system	423,200 lb	(192,000 kg)
Avg temperature (Excl. pres.)	571.8 F	(300 C)
Pressure	2280 psia	(15.7 MPa)
Reactor coolant system volume	10,370	(293.7)
Pressurizer volume, total	1,336 ft^3	(37.83 m^3)
water	816 ft^3	(23.1 m^3)
steam	520 ft^3	(14.7 m^3
Three accumulators, total volume	4,350 ft^3	(123.2 m^3)
water volume	2,775 ft^3	(78.58 m^3)
pressure	665 psig	(4.585 MPa)
temperature	120 F	(48.9 C)
Containment recirculation spray		
2 systems, flow each	3,500 gpm	(220.8 l/s)
Containment free volume	1.8 x 10^6 ft^3	(5.1 x 10^4 m)
Initial temperature	100 F	(3.778 C)
Initial pressure	10 psia	(6.89 x 10^4 Pa)
Dewpoint	80 F	(26.7 C)
Primary system hot metal	1,686,285 lb	(766,000 kg)
Temperature	572 F	(300 C)

Containment Heat Sinks

	Thickness		Area	
Walls inside containment	1.0 ft	(0.3048 m.)	3,320 ft^2	(308.4 m^2)
Walls inside containment	2.0	(0.6096	27,600	(2564)
Walls inside containment	3.0	(0.9144	19,400	(1802)
Walls inside containment	4.0	(1.219)	5,000	(464.5)
Walls inside containment	6.5	(1.981)	2,100	(195.1)
Containment wall	4.5	(1.372)	46,747	(4343)
Dome	2.5	(0.762)	25,000	(2323)
Floor above foundation mat	2.0	(0.6096)	11,250	(1045)
Foundation mat	10.0	(3.048)	11,250	(1045)
Containment liner				
Walls	0.38 in.	(0.9652 cm)	46,747	(4343)
Dome	0.50 in.	(1.27 cm)	25,000	(2323)
Floor	0.25	(0.635 cm)	11,250	(1045)
Miscellaneous metal - 1,200,000 lb	(544,308 kg)			
Core				
Equivalent diameter	119.7 in.	(3.04 m)		
Active height	144.0 in.	(3.658 m)		
Total cross sectional area	78.3 ft^2	(7.27 m^2)		

TABLE 4.1. PWR DATA (CONTINUED)

Core (Continued)		
No. of fuel assemblies	157	
Rods per assembly	204	
Pitch	0.563 in.	(1.430 cm)
Assembly dimensions	8.426 in. square	
Fuel rod diameter	0.422 in.	(1.072 cm)
Clad (Zr-4) thickness	0.0243 in.	(0.0617 cm)
Total number of fuel rods	32,028	
Core weight	226,200 lb	(102,700 kg)
UO_2	175,600 lb	(79,820 kg)
Zircaloy	36,300 lb	(16,500 kg)
Misc.	14,300 lb	(6,500 kg)
Fuel pellet diameter, Region 1	0.3669 in.	(0.9319 cm)
2 and 3	0.3659 in.	(0.9294 cm)
Fuel pellet length	0.6 in.	(1.524 cm)
Diametral gap, Region 1	0.0065 in.	(0.01651 cm)
2 and 3	0.0075 in.	(0.01905 cm)
Fuel density, Region 1	94%	
2	92	
3	91	
Fuel enrichment, Region 1	1.85 w/o	
2	2.55	
3	3.10	
No. of grid spacers	7	
Neutron adsorber	Ag-In-Cd	
Clad	304 ss	
Clad thickness	0.024 in.	(0.06096 cm)
No. of control assemblies	53	
Full length	48	
Part length	5	
Rods per assembly	20	
Burnable poison rods	816	
No. per assembly	12	
No. of assemblies	68	
Material	Borosilicate glass	
O.D.	0.4395 in.	(1.116 cm)
I.D.	0.2365 in.	(0.6007 cm)
Clad	304 ss	
Boron (natural) loading	0.0429 g/cm	
Reactor vessel		
I.D. of shell	157 in.	(3.99 m)
Belt line thickness (w/o clad)	7.875 in.	(0.2000 m)
Head thickness	5.0 in.	(0.127 m)
Clad thickness	0.125 in.	(0.3175 m)
Overall height	40 ft-5 in.	(12.32 m)

TABLE 4.1. PWR DATA (CONTINUED)

Reactor vessel (continued)	
Inlet nozzles	27.5 in. (0.699 m) tapered to 35.4 in. (0.899 m)
Outlet nozzles	29 in. (0.737 m)
Water volume with core and internals in place	3,718 ft^3 (1.053 x 10^2 m^3)
Core barrel I.D.	133.9 in. (3.401 m)
O.D.	137.9 in. (3.503 m)
Thermal shield I.D.	142.6 in. (3.622 m)
O.D.	148.0 in. (3.759 m)
Safety Injection Charging Pumps	
Number	3
Design pressure, discharge	2750 psig (18.96 MPa)
Design pressure, suction	250 psig (1.724 MPa)
Design temperature	250 F (121 C)
Design flow	150 gpm (9.46 l/s)
Maximum flow	600 gpm (37.8 l/s)
Design head	5800 ft (1768 m)
Low Head Safety Injection Pumps	
Number	2
Design pressure, discharge	300 psig (2.07 MPa)
Design temperature	300 F (148.9 C)
Design flow	3000 gpm (189.2 l/s)
Design head	225 ft (68.58 m)
Maximum flow	4000 gpm (252.3 l/s)
Containment Spray Pumps	
Number	2
Design flow	3,200 gpm (201.9 l/s)
Design head	225 ft (68.58 m)
Design pressure	250 psig (1.724 MPa)
Recirculation Spray Pumps Inside Containment	
Number	2
Design flow	3500 gpm (220.8 l/s)
Design head	230 gpm (14.5 l/s)
Recirculation Spray Pumps Outside Containment	
Number	2
Design flow	3,500 gpm (220.8 l/s)
Design head	249 ft (75.89 m)
Recirculation Spray Coolers	
Number	4
Design duty, each	55,534,520 Btu/hr (16.3 MW)
Refueling Water Storage Tank	
Volume	350,000 gal (1.32 x 10^6 l)
Boron concentration	2,500 ppm
Design pressure	Hydraulic head
Design temperature	150 F (65.6 C)
Water temperature	45 F (7.22 C)

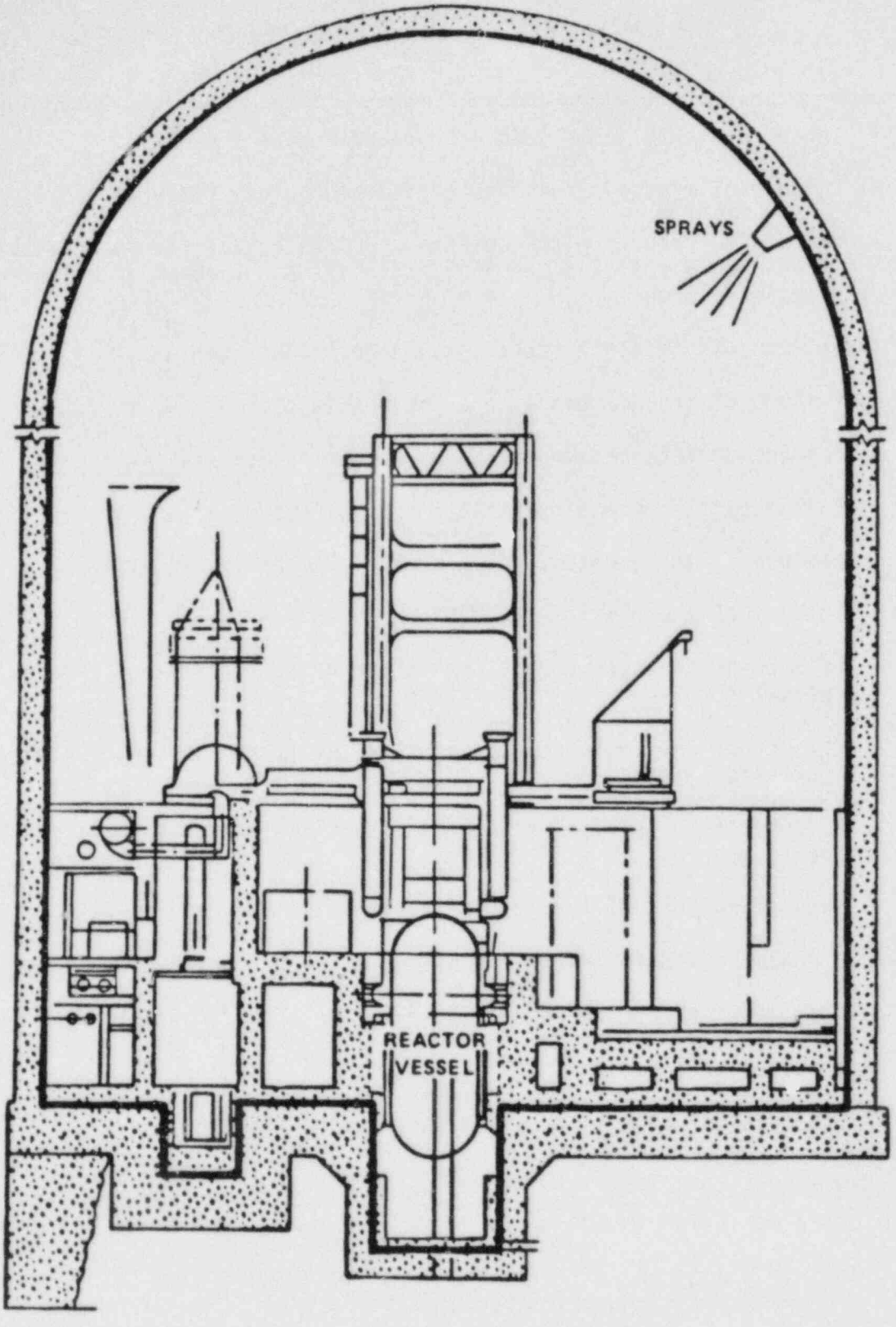

FIGURE 4.1. LARGE, HIGH PRESSURE CONTAINMENT PWR DESIGN

TABLE 4.2. KEY TO PWR ACCIDENT SEQUENCE SYMBOLS

A - Intermediate to large loss of coolant accident (LOCA).

B - Failure of electric power to engineered safety features (ESF).

B' - Failure to recover either onsite or offsite electric power within about 1 to 3 hours following an initiating transient which is a loss of offsite AC power.

C - Failure of the containment spray injection system.

D - Failure of the emergency core cooling injection system.

F - Failure of the containment spray recirculation system.

G - Failure of the containment heat removal system.

H - Failure of the emergency core cooling recirculation system.

K - Failure of the reactor protection system.

L - Failure of the secondary system steam relief valves and the auxiliary feedwater system.

M - Failure of the secondary system steam relief valves and the power conversion system.

Q - Failure of the primary system safety relief valves to reclose after opening.

R - Massive rupture of the reactor vessel.

S_1 - A small LOCA with an equivalent diameter of about 2 to 6 inches.

S_2 - A small LOCA with an equivalent diameter of about 1/2 to 2 inches.

T - Transient event.

V - Low pressure injection system check value failure.

Containment Failure Modes:

α = steam explosion

β = containment isolation failure

γ = overpressurization due to hydrogen combustion

δ_e = early overpressure failure due to steam and noncondensible gases

δ_l = delayed overpressure failure due to steam and noncondensible gases

ϵ = basemat melt-through

Although the large, high pressure PWR containment design is often referred to as "dry", a great quantity of steam would be released to the containment building in each of the sequences analyzed (except V, in which steam would be released to the safeguards building). In these cases, steam condensation on the walls and on aerosols can enhance the natural removal of radionuclides from the containment atmosphere. The containment spray systems would be even more effective, in those sequences in which they operate; sequences were selected to illustrate the performance of the containment system with and without spray operation.

In the Three Mile Island accident, the release of radionuclides to the containment atmosphere was significantly limited by a large quantity of water in the pathway of release to the environment. This is not characteristic of accident sequences leading to complete core melting of the type selected for the present analysis. In the sequences studied here, fuel heatup would not begin until the water level had dropped below the top of the core, and very hot steam and hydrogen from the melting core would superheat the structures in the pathway to the containment.

There are large variations in the volume and design pressure of large high-pressure containments. To some extent, generic accident sequences can be defined which are independent of variations in plant designs; for example, the sequence AB-δ (large LOCA, loss of all AC power, and failure of containment by overpressurization) could occur in any PWR, because the general safety philosophy and safety functions provided to protect the plants are the same. Different vendors and architect-engineers have chosen different approaches to satisfy these safety functions, however, so the likelihood of each sequence may vary greatly between plants. Similarly, the timing and order of events in an accident sequence may also vary, depending on the design.

4.2.1 Sequence AB (Loss of Coolant Accident, Loss of AC Power)

A large pipe break accident was selected for analysis because it represents one extreme of reactor coolant system conditions during core meltdown. Depressurization of the reactor coolant system is expected to occur rapidly following the break. If all AC power is lost, the accumulators discharge into the vessel to supply some emergency coolant, but the pumped ECC

injection systems does not operate. As the water level decreases in the core, heatup of the fuel and fission product release occur at the same pressure as the containment building atmosphere. A break in the hot leg break rather than the cold leg was selected in order to examine a case involving a minimum pathway and, presumably, minimum fission product retention within the reactor coolant system. The flow path for fission products from the core, to the upper plenum, and to the hot leg brak is illustrated in Figure 4.2. In this sequence, flow through the other loops is assumed to be blocked by hydrogen, and possibly by water seals, in the low points of the system. The flow path during the vaporization release period is shown in Figure 4.3.

In terms of reactor coolant system response, there is little difference between AB and AD (involving failure of pumped ECC injection rather than loss of all AC power). The containment conditions for AD would be very similar to those of S_2D, which was also analyzed. It was felt that AB provided an opportunity to examine a number of containment failure modes in which fission products would be retained by natural deposition.

Three failure modes were examined for the AB sequence: containment isolation failure (β), early overpressure failure resulting from hydrogen combustion (γ), and basemat melt-through failure (ε). For the Surry plant, the probability of isolation failure is quite small, since the plant's operating containment pressure is significantly less than atmospheric; for other PWR designs, however, this may be a major potential failure mode. The conditions leading to early overpressure failure are not expected to occur in AB, but because of the potentially large consequences of this failure mode and the uncertainty in the processes associated with it, the associated fission product release was evaluated. Delayed overpressure failure and melt-through of the basemat without aboveground failure (ε) are the most likely modes of containment failure. Because of the long delay to failure, the consequences of these two modes of failure are expected to be similar and to differ primarily in the magnitude of noble gas release.

4.2.2 Sequence TMLB' (Transient, Loss of Primary System Heat Removal)

The TMLB' sequence was found to be a major risk contributor in WASH 1400. The predicted release fractions for the containment overpressurization

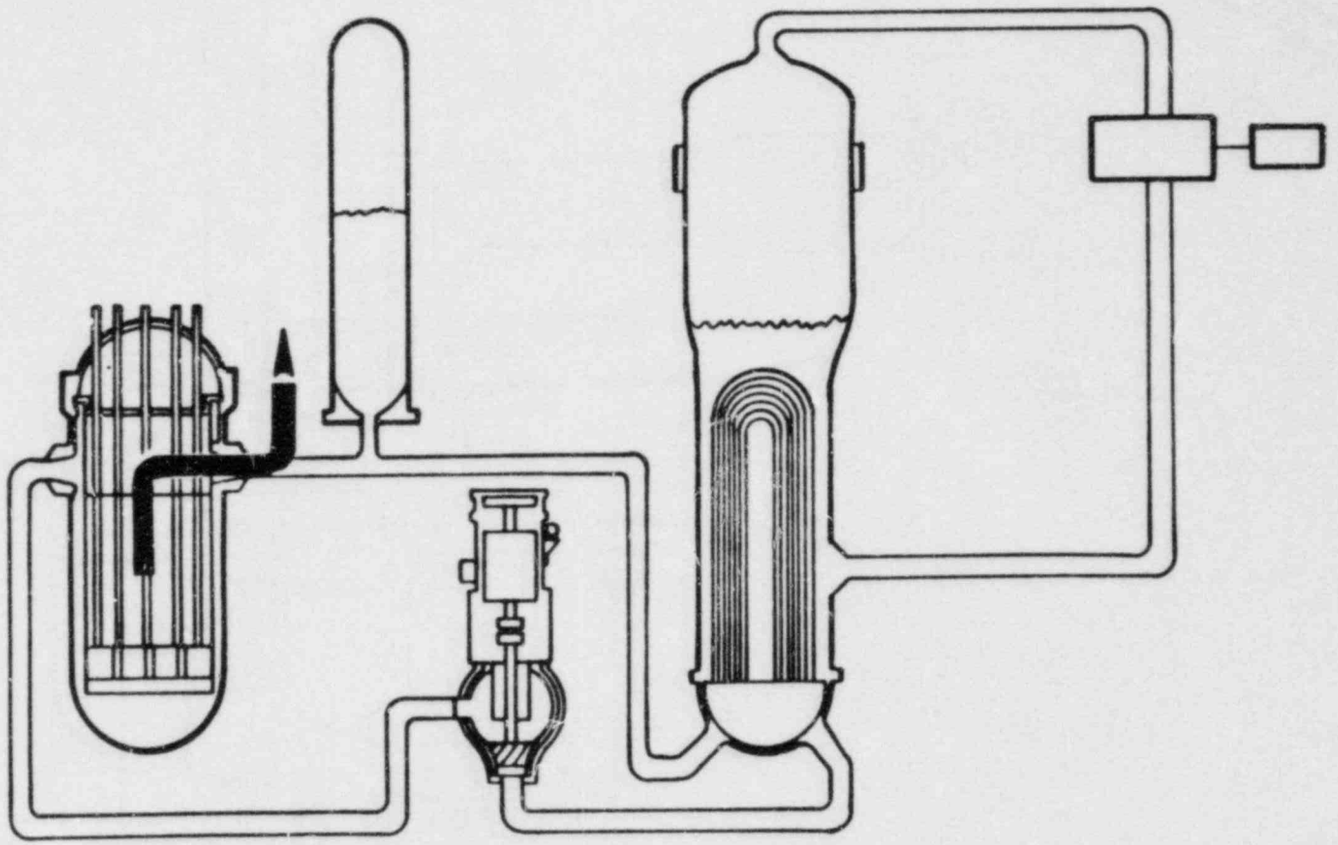

FIGURE 4.2. FLOW PATH FOR PRIMARY SYSTEM FISSION PRODUCT TRANSPORT IN SEQUENCE AB

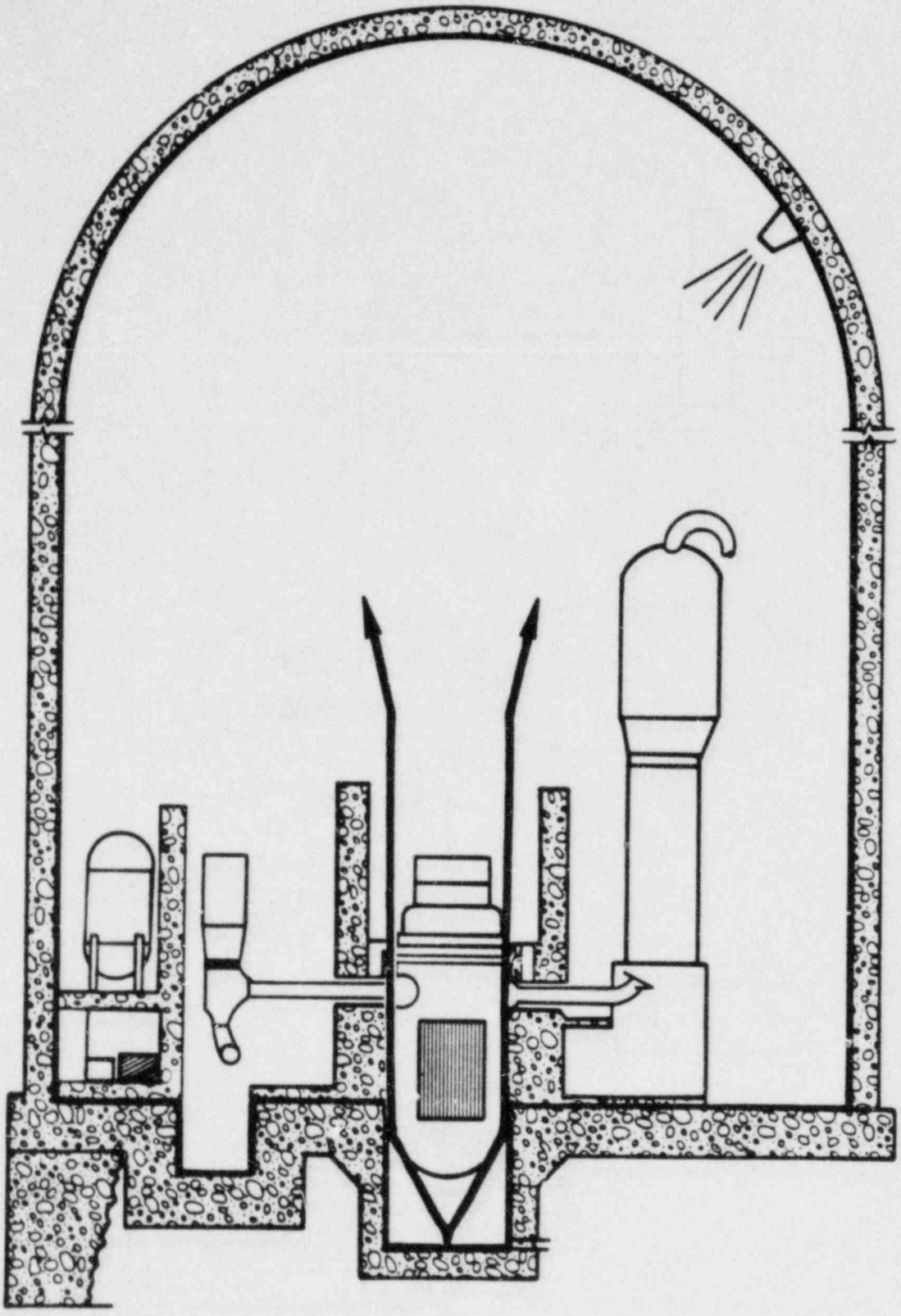

FIGURE 4.3. FLOW PATH FOR VAPORIZATION RELEASE

failure mode for this sequence were used to characterize release category PWR 2. The reactor coolant system behavior of TMLB' contrasts sharply with AB because the reactor coolant system pressure remains elevated (~2500) during core heatup and fission product release. The beginning of core uncovery is also delayed for a few hours, providing some time for the decay heat power to be reduced.

The flow path for fission products through the reactor coolant system is illustrated in Figure 4.4. Prior to core uncovery, the water in the pressurizer is predicted to be carried from the pressurizer with the steam flow or to fall back into the hot leg during periods when the relief valve is closed. If the reactor pump seals were to fail in this sequence, the results are expected to be similar to a cold leg break.

As in AB, containment sprays are assumed to be inoperable in this sequence. One reason for selecting TMLB' was to investigate the effect of containment failure time on fission product retention. Early and late failure of the containment by overpressurization (δ, ε) are considered. Although early failure is considsered unlikely, it was evaluated because of its potentially large consequences. Interaction between molten core material and accumulator water in the reactor cavity could lead to early failure of the containment. The magnitude of the ensuing steam pressure spike depends on mixing and heat transfer processes that are uncertain.

4.2.3 Sequence S_2D (Small Pipe Break, Failure of ECC System)

Because containment cooling and the containment spray systems are operable in this sequence, the expected release of fission products to the environment would be quite small. As a result, the contribution to the predicted public health risk would also be expected to be small. This type of event is believed to be comparatively likely, however, and is of interest for this reason. Also, this is the only sequence analyzed in which the effectiveness of the containment safety features is examined. The possibility of hydrogen combustion is of particular interest in this case because steam inerting will not be present as in other sequences. Core meltdown occurs with elevated reactor coolant system pressure, as in TMLB', but at slightly lower

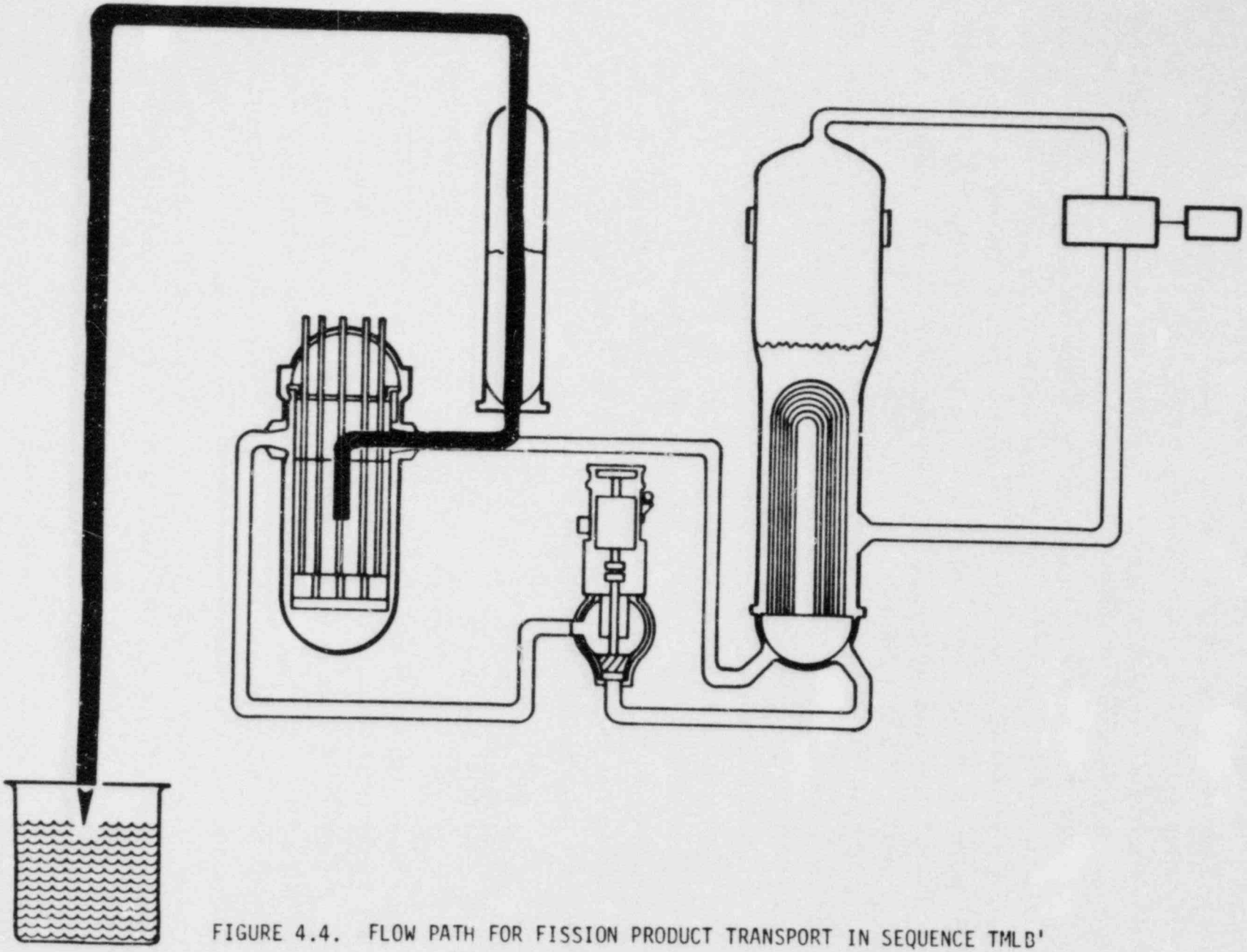

FIGURE 4.4. FLOW PATH FOR FISSION PRODUCT TRANSPORT IN SEQUENCE TMLB'

pressures and with leakage from the reactor coolant system augmented by the depressurization.

The flow path of fission products in the primary system is illustrated in Figure 4.5. Other possible flow paths to the break through the intact loops were assumed to be sealed by water in the low points of the primary system. If these flow paths were available, the residence time and retention of fission products in the primary system would be greater than for the case analyzed.

4.2.4 Sequence V (Interfacing Systems Loss of Coolant Accident)

This sequence was the largest individual contributor to risk identified in WASH 1400. Having recognized the potential system weakness, it has been possible to reduce the likelihood of the sequence substantially. The interfacing LOCA is of interest even at reduced probability, however, because the pathway for release bypasses the protection normally provided by the containment building. Retention in the reactor coolant system is particularly important in this sequence.

The flow path for release from the reactor coolant system is illustrated in Figures 4.5 and 4.6.

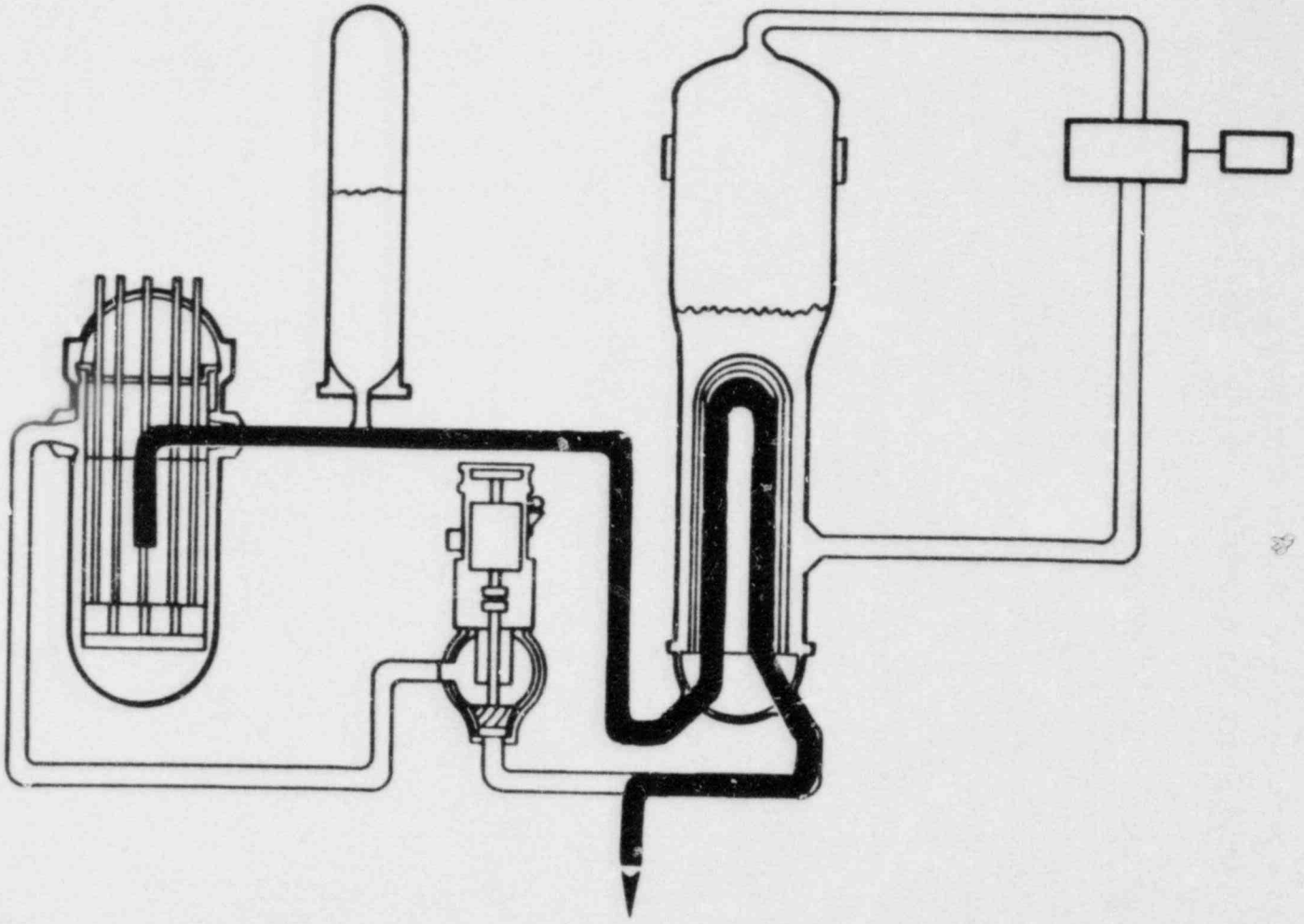

FIGURE 4.5. FLOW PATH FOR FISSION PRODUCTS IN SEQUENCES S_2D AND V

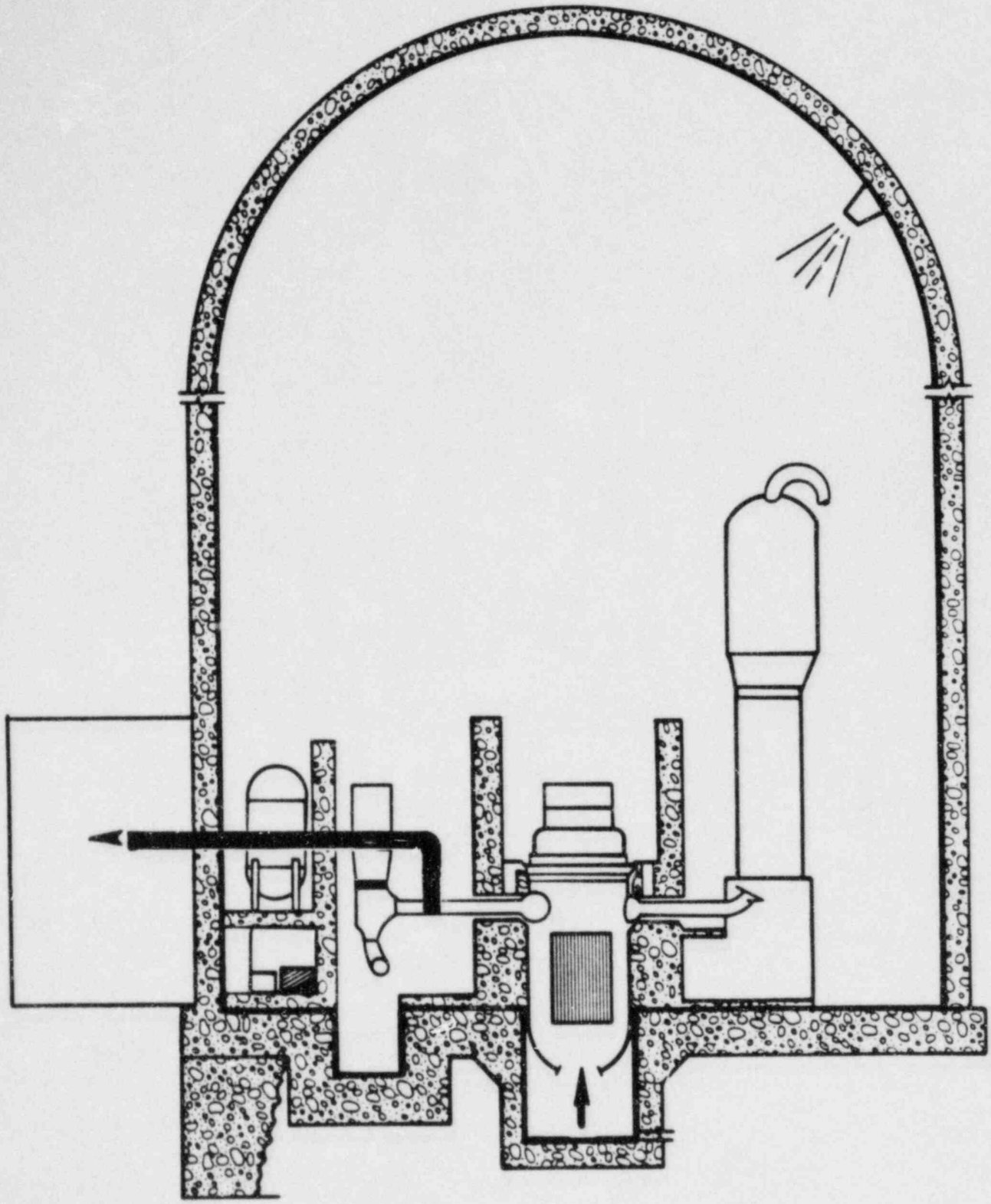

FIGURE 4.6. RELEASE PATHWAY TO SAFEGUARDS BUILDING IN SEQUENCE V

5. ANALYTICAL METHODS

This section describes the analytical methods used in reassessing the source term to the environment for the Surry plant, a PWR with a large, high pressure containment. The methods employed here differ significantly from those used to analyze the Surry plant, as described in Volume 1 of this report[5.1].

The first major difference between the methods used here and those described in Volume 1 is that the MARCH 2 code (which includes an improved model for core slumping) is used here for the overall thermal-hydraulic calculations, replacing the MARCH 1.1 code used for Volume 1. The second major change is that in the present analysis, an accounting is made for the effect of Zircaloy cladding oxidation on the release rate for tellurium. Finally, a new code called SPARC is used here to predict the retention of aerosols in suppression pools.

Some other, less significant changes have been made as well. These are discussed in the text.

5.1 Thermal Hydraulic Behavior

This section describes the computer code MARCH 2, which, along with the MERGE code, was used to analyze the thermal-hydraulic response of the reactor core, the primary coolant system, and the containment system for the selected accident sequences.

5.1.1 Overall System Thermal Hydraulics: MARCH 2

The MARCH 2[5.2] (Meltdown Accident Response CHaracteristics) computer code describes the physical processes involved in severe fuel-damage accidents in light water reactors. Version 2 of the code replaces Version 1.1.[5.3] The differences between the two versions include changes in models, code structure, and programming language. The new models in MARCH 2 were developed at a number of institutions, including Battelle, Sandia National Laboratories, Oak Ridge National Laboratories, Brookhaven National Laboratory, and the Tennessee Valley Authority. In many cases, these models are provided as options to

existing models. The changes in MARCH were largely undertaken to address recognized deficiencies in the early version related to modeling approximations, time-step control, and transportability of the code to other installations.

The MARCH 2 code was developed primarily for use in probabilistic risk assessment. The uncertainties in many of the MARCH 2 models are large, and in many cases the extent to which the models have been validated against experiments is limited. More mechanistic codes are being developed by the NRC, such as SCDAP and HECTR, but they were not available for use in this program.

The MARCH 2 code examines the behavior of a large variety of accident processes including depressurization or leakage from the reactor coolant system, core uncovery, core heatup, oxidation of Zircaloy cladding, fuel melting, fuel slumping, fuel-coolant interaction in the lower vessel head, vessel head failure, fuel-coolant interaction in the reactor cavity, debris bed coolability, core-concrete interactions, production of combustible gases, gas combustion in the containment, containment heat transfer, intercompartment flows, and the effect of engineered safety features on containment thermal hydraulic behavior. Some of the principal modeling improvements in Version 2 of the MARCH code are described below.

5.1.1.1 Containment Response. The containment response modeling in MARCH 2 includes the following principal changes: provision for expanded blowdown input via subroutine INITIAL, the ability to accept two input terms from the primary system, completely revised treatment of burning of combustibles, addition of a heat sink for radiation heat transfer from the debris in the reactor cavity, and removal of a number of restrictions in the earlier code.

The expanded blowdown table input capability is intended to facilitate the interfacing of the MARCH code with more detailed thermal-hydraulic codes that may be used to describe the initial portion of the accident sequence.

The containment response subroutine, MACE, has been changed to accommodate simultaneous break and relief/safety valve flows from the primary system. The two inputs can be directed to different compartments if desired, e.g., break flow to the drywell and relief/safety valve flow to the suppression pool of a BWR.

5.1.1.2 Primary System Response. The MARCH 2 treatment of the primary system includes both improvements in the treatment of initial (early) primary system response and the addition of several phenomenological models to treat the processes following core collapse into the bottom head. Included are changes in the steam generator model to remove some of the restrictions and limitations of the earlier version, improved break flow models, changes in the flashing model in response to primary system pressure changes, provisions for simultaneous break and relief/safety valve flow, changes in the treatment of heat transfer to structures, and consideration of the transport of fission products within the primary system.

5.1.1.3 Water and Steam Properties. The representation of the properties of water and steam has been improved in MARCH 2. This has included expansion of the property tables and correlations incorporated in the code as well as inclusion of additional properties required by the new phenomenological models. The input parameters are based on the ASME steam tables.

5.1.1.4 Decay Heat. MARCH 2 incorporates the current American National Standard[5.4] for evaluating fission product decay heating as a function of time after shutdown and time at power, including the contributions from heavy element decay. This replaces the earlier, simplified version incorporated in MARCH 1.1. Alternatively, decay heat as a function of time may be input in tabular form; this approach would be particularly appropriate for transients with failure to scram, where the power history would be provided by more detailed system codes.

5.1.1.5 Core Heat Transfer. MARCH 2 retains the basic model of the core as developed for the earlier version, but incorporates additional models for a more detailed treatment of heat transfer processes. Heat transfer between the fuel rods and the steam-hydrogen gas mixture is now calculated using either the full Dittus-Boelter correlation[5.5] for turbulent flow or a laminar flow correlation. A subroutine has also been added to approximate axial conduction heat transfer in the fuel rods using the Fourier law of heat conduction and the BOIL-calculated node temperatures. The effect of axial and radial thermal radiation heat transfer within the core, as well as between the core and

surrounding structures and water surfaces, can now be calculated. The heatup of the core support barrel by thermal radiation is included. Additional changes include corrections in the heat transfer analysis of partially covered core nodes and improvements in the metal-water reaction model.

5.1.1.6 Core Debris. A number of phenomenological models have been added for the treatment of the core debris in the reactor vessel bottom head. These include a flat plate critical heat flux model, a fragmented debris-to-water heat transfer correlation, and several options that consider formation of debris beds within the vessel head while water is still in the vessel. The bottom head heatup model utilizes a calculated heat transfer coefficient between the molten debris and the vessel head.

A major area of concern and controversy in the analysis of core meltdown accidents has been the behavior of core and structural debris upon contact with water in the reactor cavity. The highly simplified models of MARCH 1.1 have been supplemented with a flat plate critical heat flux model, a part culate heat transfer model with more mechanistic heat transfer coefficients, and several debris bed heat transfer correlations. If desired, the switchover from one model to another can be based on calculated conditions, e.g., debris temperature. The production of hydrogen from steel-water reactions has been incorporated into these models in addition to the zirconium-water reaction previously available. Also included are the heating of the evolved gases by the debris beds and the effect of hydrogen flow on bed floodings.

A heat sink has been provided for the thermal radiation from the top of the core debris as calculated by the INTER subroutine. The decomposition of concrete due to radiated heat flux is treated by an ablation-type model with the resulting gases added to the containment atmosphere. Also, the geometry of the corium-concrete mixture is fixed following solidification of the melt.

5.1.1.7 Burning in Containment. The treatment of combustible gases now includes consideration of the burning of hydrogen and carbon monoxide if their concentrations exceed flammability limits. Included are explicit considerations of inerting due to high steam concentrations and oxygen depletion, direction-dependent compositions for flame propagation between compartments, and burn velocities as functions of composition. Various options are available

to explore the effects assumptions about the burning of hydrogen and carbon monoxide.

5.1.2 Primary System Thermal Hydraulics: MERGE

When the MERGE[5.6] code was written, the existing computer codes describing the thermal-hydraulic behavior of a core meltdown accident were not capable of analyzing the flow and temperatures in the individual volumes of the reactor coolant system downstream of the core in the pathway for release to the containment. The report "Technical Bases for Estimating Fission Product Behavior During LWR Accidents"[5.7], published by the NRC in 1981, indicated that in at least some accident sequences, the retention of fission products in the reactor coolant system (RCS) could be significant. To support more realistic analyses of fission product retention with the TRAP-MELT code discussed in Section 5.3.1, an effort was undertaken to write a simple stand-alone code, MERGE, to predict gas temperature, surface temperature, and flow within the reactor coolant system.

MERGE calculations are based on the output of MARCH, and the output of MERGE is input to the TRAP-MELT code. The MARCH results used by MERGE are: the primary system pressure, the flow rate of hydrogen leaving the core, the flow rate of steam leaving the core, and the average temperature of gases leaving the core. The MERGE analysis accounts for conservation of energy and conservation of mass by species. It is assumed that the gases within a volume are well mixed and have the same temperature, and that the pressure differential between volumes is negligible.

In MERGE, the equations are solved with an explicit time difference scheme. At a particular time step, conditions within the first volume downstream of the core are calculated first, and the solution proceeds from each volume to the next downstream volume. Knowing the initial and inlet flow conditions for each volume, MERGE solves for the value of the outlet flow from the volume that yields the known pressure. Heat transfer from flowing gas to structures is accounted for. Forced laminar, forced turbulent, and natural convection heat transfer coefficients are utilized as appropriate, with a radiative term added to the coefficient. In addition, the MERGE-calculated

radiative heat transfer from the core to the first structure is calculated based on a MARCH-calculated radiative flux.

The MERGE code involves certain approximations and limitations. In the MERGE analysis, the flow of gases in the upper plenum is assumed to be one-dimensional; in reality, circulation patterns would more probably be established in this region due to the strong temperature gradients. Whether a more detailed analysis is required for this region must be determined by the results of sensitivity studies with the TRAP-MELT code. The need for validation experiments must also be evaluated.

5.2 Radionuclide Release from Fuel

5.2.1 Source Within Pressure Vessel: CORSOR

CORSOR[5.8] is a simple correlative code which estimates aerosol and fission product release rates from the core during the period of core melting in a light water reactor. Quantifying the aerosol and fission product release from the core region is an important first step in determining the radionuclide source term to the containment during a hypothetical severe core damage accident. The timing of the release of various materials influences their retention in the reactor coolant system because it determines which species emanating from the core will be able to interact. The timing also determines the residence time of the released materials and the temperatures in the reactor coolant system, since these are both dynamic parameters. Simplistic source terms, such as constant or linearly increasing release rates with concurrent releases for all radionuclides, may therefore lead to unrealistic estimates of radionuclide transport behavior.

The reassessment of the Surry plant includes the most recent adjustments of CORSOR. In comparison with the initial assessment of Surry reported in Volume 1 of this report, this analysis uses a refined method for calculating tellurium release from fuel and a physically-based method for calculating aerosol release from silver-indium-cadmium control rods.

For the present analysis, the core has been divided into 240 nodes, 10 radial and 24 axial, which have distinct temperatures as predicted by MARCH.

The core inventory, determined from the program ORIGEN[5.9], has been divided equally among the nodes. In an actual reactor, the distribution would vary both axially and radially and would change with time. Typically, fuel is shifted between three radial zones during its irradiation history. To flatten the power distribution across the core, the freshest fuel is placed in the outside zone of the core and the most highly burned-up fuel is placed in the central region. Thus, an abrupt change in the spatial distribution of radionuclides occurs at the time of refueling but then continues to shift during the cycle as the fissile inventory is preferentially depleted in the regions of higher flux.

Alternative distributions of fission products can be used in the CORSOR program, and the effect on fission product release rates of the "flat-flux" assumption can be quantitatively assessed by examining the results of parametric studies such as those described in Appendix B of Volume 1[5.1]. Uncertainties in the release rate coefficients are expected to have a more significant effect on release rates than will the assumptions regarding fission product distribution among core regions.

Temperatures at each of the nodes are obtained from the MARCH code for each of a number of time steps, beginning at the start of the accident and continuing to a user-specified time. An average temperature is computed over each time span during core heatup and melting, and if the temperature is less than 900 C for any node, no release will occur from that node. The average temperature for failure of the cladding of a fuel rod is taken to be 900 C.[5.7] The sensitivity of CORSOR release estimates to the temperature set for cladding failure was also discussed in Appendix B of Volume 1.[5.1] When any axial position in a fuel bundle achieves a temperature of 900 C, CORSOR calculates a gap release of certain volatile fission products for all fuel rods in that radial zone. This is intended to simulate the gap release accompanying the bursting of individual fuel rods. This release occurs because certain fission products accumulate in the fuel-cladding gap because of migration within the fuel. The amount of the gap release is taken to be 5 percent of the initial amount present for cesium, 1.7 percent for iodine, 3 percent for the noble fission gases, 0.01 percent for tellurium and antimony, and 0.0001 percent for barium and strontium. Since this emission is very small in comparison with the melt release, and is concurrent with the melt release, it is not treated separately in any of the transport analyses. Clearly, the gap release would

require more careful analysis if less severe hypothetical accident conditions were considered.

Subsequent mass release as the nodes progress toward melting is calculated on a nodal basis as the product of the amount of each species remaining, the release rate coefficient, and the time interval of integration. The mass released is then summed over all the nodes in the core for each species to give the total mass released during the time step. It should be noted that the MARCH code predictions for core temperatures do not take into account the heat of vaporization of materials released from the core.

The computation of the fractional release rate coefficients for fission products is based on empirical correlations derived from experiments performed by Lorenz, Parker, Albrecht, and others.[5.10-5.16] The data from these experiments were graphed and curves developed of the releases. A fractional release rate coefficient, K(T), is derived for species by fitting an equation of the form

$$K(T) = Ae^{BT}$$

to each of these curves. The resulting values of A and B for three different temperature regions of the graph are given in Table 5.1 and are basically the same as those defined in Appendix B of the "Technical Bases Report"[5.8] but have, in many cases, been adjusted to account for updated evaluations.[5.17] It should be noted that the fractional release rate is a function of temperature and elemental species only, and any effects of pressure and specific surface area of the melt on the release rate are not considered. Additionally, details of complex phase interactions of various components within the melting core are, for the most part, not known quantitatively; hence the release rates are valid only to the extent that the experiments upon which the release rates are based adequately modeled a core meltdown situation.

The release rate coefficients used in CORSOR in the analyses presented in this volume are similar to those presented in Volumes 1-3, except that the method for calculating tellurium release from the fuel elements has been refined. Tellurium release is dependent on the extent of oxidation of the zirconium cladding.

In the equation shown above, depending upon the local extent of zirconium oxidation, different A values are used. For a node where zirconium oxidation is nearly complete, one A value is used, and for a node at which

zirconium oxidation is less than some specified fraction, the A value is lowered by a factor of 40. For the two-side oxidation of zirconium fuel-rod cladding, the extent of oxidation used as the delimiter between higher and lower release rates is 0.70 in CORSOR. For one-side oxidation this figure would be 0.96-1.0. It is recognized that this is a simplistic treatment of a complex process, but it is believed to be the best representative of the limited available information.

Several uncertainties associated with the CORSOR predictions must be mentioned. These uncertainties most strongly impact the predicted release rates for aerosols, rather than for the more volatile materials. One difficulty in predicting aerosol release is that as core melting progresses, the temperatures increase throughout the core until, eventually, a loss of geometry would be expected to occur. In the BWR analyses, core slumping occurs in such a way as to remove radial regions from the core in an incremental fashion. Thus, the emission of fission products from the fuel rods which have fallen to the lower structures is included in the calculations of the source to the primary system. This represents a change from the PWR analysis reported in Volume 1, in which emission into the primary system was halted at the time of core slumping. A further difference between the two sets of analyses is that for the BWR sequences, significant periods of time elapse between vessel dryout and bottom head failure. Thus, during a portion of the melt period, the core is emitting fission products into an essentially stagnant volume.

The behavior of the control rods during core melting is still a source of uncertainty with respect to aerosol generation, as it was in the first three volumes of this report. In this analysis, however, a physical model for the release of control rod materials has been adopted, based on the recommendations of ORNL. The calculations proceed as follows: silver-indium-cadmium control rods in a radial zone are assumed to fail when, at any axial node within the radial zone a temperature of 1400 C is reached. At this time, 0.05 of the silver, 0.05 of the indium, and 0.50 of the cadmium are released from the control rods. The masses of these species released increases linearly (regardless of heating rate) so that when the melting point (2300 C) is reached, 0.50 of the silver, 0.15 of the indium, and 0.80 of the cadmium has been released. For temperatures greater than 2300 C, the mass released increases linearly with temperature, so that at 2800 C the balance of the local inventory has been

released from the rod. While this release model is physical, there is no adequate set of experimental observations against which its predictions can be objectively assessed.

One further point regarding the calculation of release rate coefficients should be noted. During core melting, the MARCH code predicts some core nodal temperatures above the UO_2 melting point (approximately 2880 C)[5.19] which are not regarded as being realistic. Using these high values in the expression for the release rate coefficients would lead to excessively high estimates of release rates for the lower-volatility materials. Thus, the release rates calculated in this work are calculated using a temperature value of 2760 C in place of any values predicted by MARCH in excess of this value. The "Technical Bases Report"[5.8] states that the melting point of UO_2 may be lowered by up to 300 C with the addition of ZrO_2, and even lower with other compounds, such as control rod material. Thus, it is not yet clear what this maximum achievable temperature should be. The sensitivity of the CORSOR predictions to uncertainties in the maximum temperature, the core temperature, and the release rate coefficients used in the calculations is discussed in Appendix B of Volume 1.[5.1]

5.2.2 Source from Melt-Concrete Interactions: VANESA

The release of fission products and nonradioactive aerosols during the interaction of molten core materials with concrete plays an important role in determining the risk of severe reactor accidents and is modeled with the VANESA code. Aerosol production and fission product release from core debris outside the reactor vessel can persist for many hours. The aerosols produced in this way do not usually have to traverse a convoluted pathway before they enter the reactor containment as do aerosols produced in the reactor vessel. The increased inventory of aerosols in the reactor containment brought on by ex-vessel core-debris interactions could lead to rapid agglomeration and settling of the condensed fission products released during the in-vessel phases of an accident. If containment failure is delayed, the primary source of radioactivity released to the environment would come from ex-vessel sources.

Release of fission products from core-concrete interactions can compensate for any inhibition in the release of volatile species during the

in-vessel phase of an accident because gases from the thermal decomposition of concrete sparge through the melt and drive the release processes. Ex-vessel processes can also lead to the release of fission product elements that are ordinarily quite refractory. This, again, is because of the strong driving force produced by gas sparging and the unusual melt chemistry that arises during ex-vessel interactions of core debris with concrete.

Also of importance is the generation of aerosols from nonradioactive materials, such as concrete and steel, during ex-vessel interactions. The additional concentrations of suspended particulates in the containment brought on by these aerosols naturally mitigate the inventory of radioactivity released from the fuel that would then be available for release to the environment. This additional material, on the other hand, poses yet another threat to equipment in the containment whose performance is degraded by the presence of aerosols.

VANESA is a mechanistic model of fission product release and aerosol generation during core-concrete interactions. This model was based on observation from experiments involving high-temperature melts on concrete and information from analogous industrial processes. Two broad mechanisms of aerosol formation are considered in the model:vaporization of melt species accentuated by gas sparging, and mechanical formation of aerosols by violent agitation of the molten debris sparged with decomposition gases. Vaporization processes produce the most intense aerosol generation during ex-vessel core debris interactions, while mechanical processes provide a mechanism for aerosol formation that persists even when debris temperatures are so low that little vaporization of species in the debris can occur.

Input to this model includes melt temperature, concrete erosion rate, and gas generation rate predicted by the CORCON model of melt-concrete interactions. It computes the thermochemical limits of vaporization from the melt, and then compares the extent of vaporization recognizing kinetic barriers, such as mass transport, to the approach to the thermochemical limits for vaporization. Mechanical aerosol generation is estimated by analogy to experimental data with simulant systems.

More complete descriptions of the model are provided in the users' manual[5.19] and its uncertainties are discussed further in Appendix C of Volume 1.[5.1]

5.3 Radionuclide Transport and Deposition

5.3.1 Transport in Reactor Coolant System: TRAP-MELT

The TRAP-MELT code that was used for the primary system radionuclide transport analyses of this study was developed from the published TRAP-MELT code[5.20] used for the "Technical Bases" report[5.8]. Major changes were made in the treatment of aerosol particle transport and behavior and in radionuclide condensation on and evaporation from particles. In addition, the internal data base of the code was increased to include physical property data for tellurium and cesium hydroxide. An outline of the code, highlighting these changes, is given below. A more detailed description is given in the TRAP-MELT Users' Manual[5.20].

The TRAP-MELT model is designed to treat radionuclide transport in an arbitrary flow system whose thermal-hydraulic conditions are given as functions of time. For this study, the data needed by TRAP-MELT to define the thermal-hydraulic conditions of the primary system were generated by MERGE. In addition, TRAP-MELT requires the definition of source terms for each radionuclide; these terms were developed by CORSOR.

Once the flow system is defined, it is subdivided into a series of control volumes that can, in principle, be arbitrary in number and flow connections and that are chosen on the basis of characteristic geometry, thermal-hydraulic conditions, and suspected significant radionuclide behavior such as change of phase, agglomeration, or deposition. Radionuclides in each control volume are assigned, with uniform distribution, to one of two carriers: the wall surfaces and the gas phase. Each radionuclide is allowed to reside on these carriers in either particulate (liquid or solid) or vapor form so that by combining carrier with form in the concept of "state", the condition of a radionuclide in a given control volume is completely determined by its state. TRAP-MELT thus considers five states:

- Radionuclide vapor carried by gas
- Radionuclide particle carried by gas
- Radionuclide vapor carried on wall surface

- Radionuclide particle carried on wall surface
- Radionuclide vapor chemisorbed on wall surface.

This list of states is not exhaustive (for instance, in two-phase flow, the carrier water must be considered) and the logic of the code has been chosen to accept an arbitrary number of states readily .

Radionuclide transport can occur among the five states of an individual control volume or between certain states of different control volumes are connected by fluid flow. The former types of transport are modeled or correlated in the code itself. The latter are assumed to occur in phase with the fluid flow (as developed by codes such as MERGE) and are imposed on the system. Sources of radionuclides to the system may occur in any volume and any state, and they must be input to the code as mass rate functions of time.

At present, the intravolume transport mechanisms contained in TRAP-MELT are:

- Competitive condensation on, or evaporation from, wall surfaces and particles of cesium iodide, cesium hydroxide, and tellurium
- Irreversible sorption of molecular iodine, cesium hydroxide, and tellurium on stainless steel surfaces
- Particle deposition on surfaces due to
  - Settling
  - Diffusion from laminar and turbulent flow
  - Inertial impaction from turbulent flow
  - Thermophoresis.

Particle transport (and evaporation or condensation from or on particles) depends on particle size. TRAP-MELT takes this into account by considering a discretized particle size distribution that is subject to change, in each volume, by the deposition processes themselves, by possible particle sources, by flow of particles from other volumes, by flow of particles out of the volume in question, and by agglomeration. The last can be due to many mechanisms. TRAP-MELT considers the following agglomeration mechanisms:

- Brownian
- Gravitational
- Turbulent (shear and inertial).

Considerations of stiffness and linearity split the system of first-order differential equations resulting from the above-listed transport mechanisms into three classes. Most of the deposition mechanisms (transfer from gas to wall surface) are taken as first order in the concentration of radionuclide species on the carrier (gas, particle, or wall) from which the transfer occurs. They constitute the first class, whose transport scheme can be written in the form:

$$\frac{dC}{dt} = S + MC, \tag{5.1}$$

where C is the concentration vector of the species in question for each state and volume, S is the source rate vector for each state and volume, and M is the transport matrix between all states and volumes. Because the deposition terms are taken as first order, M is independent of C and depends, with S, on time only. It is thus possible to solve Equation (5.1) as a set of first-order differential equations with constant coefficients by standard techniques. This is done in TRAP-MELT for the class of linear mechanisms. Condensation and evaporation, which have a much shorter time constant than the linear processes, constitute the second class and are treated outside this framework but parallel to it, as is particle agglomeration, which constitutes the third class of mechanisms in the TRAP-MELT code.

The approach to this parallel treatment is as follows: Equation (5.1) is taken as the master time-translation operation of the radionuclide system. Time steps are adjusted so that S and M change little over a time step and so that the time step does not exceed one-third of the smallest flow residence time for any control volume. The latter assures that the system does not translate excessively between couplings to the other two classes of mechanisms. In addition, the characteristic coagulation time for the aerosol in each volume is evaluated and compared to the master time step. If the former is short compared to the latter, the master time step is appropriately reduced.

At the beginning of each time step, phase transitions of radionuclides are modeled by examining each control volume in turn and solving the molecular mass transport equations for vapor transport among the gas phase, particles, and wall surfaces. Because of the low heats of vaporization of the

radionuclides in question, this transport is assumed to be isothermal. Transfer to the walls assumes the Dittus-Boelter correlation[5.5] for pipe flow and transfer to the particles occurs by diffusion based on the size distribution at the beginning of the time step. Redistribution of the vapor phase occurs in a time that is small compared to the master time step; therefore, this redistribution is essentially decoupled from the other processes considered which justifies the use of a time parallel solution treatment.

Once redistribution of the vapor phase has been effected, its effect on the existing particle size distribution (in the volume in question) is calculated by assuming that each size class gains (or loses) mass in proportion to the rate of vapor transfer to (or from) that size class. Conservation of number for each size class then dictates redistribution between, in general, two new contiguous size classes, the number in each size class being determined by mass conservation.

At the end of a time step, the particle size distribution in each volume is reevaluated over that time step to account for possible particle agglomeration, sources, and flow terms. The agglomeration algorithm has been excerpted from the QUICK aerosol behavior code[5.22], which is based on a size discretization scheme.

The approximations inherent in this parallel treatment are minimized by relegating mass redistribution and conservation to the master Equation (5.1), except for redistribution due to radionuclide phase change. Agglomeration and particle evaporation/condensation serve only to modify the particle size distribution and therefore affect particle deposition indirectly through mass-distribution-averaged deposition velocities. Thus the aerosol aspect is solved (over a master time step) completely in parallel to Equation (5.1), using all sources, flow terms, and particle removal terms evaluated for each size class considered. The resultant distribution is used to evaluate average particle deposition terms for use in the master equation only. Similarly, reevaluation of the particle size distribution due to radionuclide phase change affects these average deposition terms only.

In addition to the time-dependent thermal-hydraulic conditions and mass input rates by species, the TRAP-MELT code requires input information on the initial particle size distribution of the source, the control volume geometry, and the physical properties of species (including deposition veloci-

ties on surface materials). The code provides output in terms of time- and location-dependent mass by species and state, as well as size distribution of suspended particulate material.

There are a number of uncertainties which affect the TRAP-MELT code predictions of primary system retention of materials. Any errors or imprecisions in the input to the code will clearly affect the quality of the results, both for the primary system thermal-hydraulics provided by MERGE and for the core release rates determined by CORSOR. The extent of interaction among the materials released from the melting core is determined largely by the timing of their releases, and this represents a less straightforward, but no less important, potential effect on the code's results due to input inaccuracies.

The experimentally determined vapor deposition velocities for Te, CsOH and I_2 on hot surfaces may not represent an accurate description of the process as it occurs in the reactor coolant system (RCS) because of the imprecision in the available data and because the experimental systems may differ from the actual RCS conditions. Nevertheless, what data are available have been incorporated, since these analyses are intended to reflect the state of the art. Additional uncertainties affecting vapor and aerosol deposition arise from possibly inadequate specifications of primary system geometry and flow patterns.

The disposition of materials suspended in the coolant system at the time of core slumping or at depressurization of the pressure vessel can have significant impact on retention calculated for some of the sequences analyzed. This is because some fission products and aerosols emitted from the core have not escaped the RCS at the time of core slumping and are still available for injection into the containment. The large burst of steam which accompanies core slumping or depressurization when the pressure vessel fails will rapidly sweep out the coolant system, and the very short transit time to the containment is expected to lead to minimal retention of these materials. Thus, in the analyses in this document, the material suspended in the RCS at the time of core slump or pressure vessel failure is assumed to be injected into the containment as a "puff" release, with no further retention in the primary system.

The analyses in the main body of this document are subject to some uncertainties which may overpredict retention in the primary system. One

mechanism not included in the current analysis is the structure heatup due to decay heat from the deposited fission products. Heatup of surfaces where species of intermediate volatility (e.g., CsI and CsOH) are deposited would lead to reevolution and transport of the previously deposited materials through the reactor coolant system to regions of lower surface temperature or to the containment. Thus, the deposition of these species may be self-limiting to some extent. This effect is analyzed in the Appendix to this volume.

5.3.2 Transport in Containment: SPARC

Many BWR accident sequences involve a fission-product flow path which passes through a suppression pool. Although the importance of the suppression pool in removing fission products has long been recognized, comprehensive analytical models that consider all pertinent parameters (such as particle size, bubble size, pool dimensions, and pressure and temperature conditions) have not been available. The SPARC code was written specifically for the analysis reported here and was used to calculate removal of particulate matter by a suppression pool.

The SPARC code was developed by Owczarski, et al[5.23]. The model includes particulate removal due to steam condensation, gravitational settling, inertial impaction both inside the gas bubbles and in the gas injection regime, diffusion deposition, and mechanical entrainment of pool liquid at the pool surface. In addition, a mechanism which retards particle deposition due to evaporation of steam is considered. Details of the model are provided in the SPARC Users' Manual[5.23].

Recognizing that the role of the suppression pool in removing particulates was neglected in the past, or a fixed removal efficiency or decontamination factor was arbitrarily assumed, use of the SPARC code in this program represents an improvement over previous source term analyses by accounting mechanistically for the effects of the suppression pool.

5.3.3 Transport in Containment: NAUA 4

The NAUA code was developed at the Kernforschungszentrum Karlsruhe, West Germany, for calculating aerosol behavior in LWR core melt accidents.[5.24] It is based on mechanistic modeling of aerosol agglomeration and deposition

within a containment vessel where a condensing steam atmosphere may exist. The model for steam condensation on particles was validated by small-scale experimental measurements[5.25], and larger-scale validation is being planned.

The NAUA code calculates physical processes, excluding chemical changes and radioactive decay. The removal processes considered include gravitational settling and diffusional plateout. Interactive processes include Brownian and gravitational agglomeration and steam condensation. Aerosol sources and leakage are also included. Compositional changes resulting from time-dependent compositions for the input aerosol are tracked by the code.

The particle size distribution is defined by a number of monodisperse fractions. In this approach, the governing integro-differential equation is transformed into a system of coupled first-order differential equations. In effect, the particle size fractions interact and deposit according to the included mechanisms, generating a time-dependent distribution of mass among the various size fractions. Steam condensation is handled in a separate integration. Output from the code includes mass concentrations of condensed water and dry aerosol materials (airborne and on surfaces), as well as particle size distributions at various times throughout the calculation.

Since the original version of the NAUA code has no provision for engineered safeguards, calculations were made to account for removal of aerosol particles by sprays, as follows:

$$\frac{dn}{dt} = -\varepsilon\pi R^2 N\,(V_g - v_g)n, \qquad (5.2)$$

where

n is the aerosol particle concentration,

ε is the collision efficiency,

V_g and v_g are settling velocities of the spray drops and aerosol particles, respectively,

R is the radius of the spray drop, and

N is the water drop concentration.

Due to hydrodynamic interaction between a falling water drop and airborne particles, only a small fraction of the particles within the cross-sectional area of the water drop is removed by spraying. To account for this hydrodynamic effect, the collision mechanisms due to inertial impaction, interception, and

Brownian diffusion of aerosol particles were used by defining ε in Equation (5.2) as:

$$\varepsilon = \varepsilon_I + \varepsilon_R + \varepsilon_D, \tag{5.3}$$

where ε_I, ε_R and ε_D are the collision efficiencies due to intertial impaction, interception, and Brownian diffusion, respectively. The following collision efficiency models were utilized for the three mechanisms:

$$\varepsilon_I = \frac{Stk^2}{(Stk + 0.35)2} \tag{5.4}$$

$$\varepsilon_R = \frac{1.5(r/R)^2}{(1+r/R)^{1/3}} \tag{5.5}$$

$$\varepsilon_D = 3.5\ Pe^{-2/3}, \tag{5.6}$$

where Stk is the Stokes number for aerosol particles based on a characteristic length of water drop with radius R; r is the particle radius; and Pe is the Peclet number. The Stokes number and the Peclet number are defined as

$$Stk = \frac{2\ r^2 \rho_p V_g C}{9\mu R} \text{ and} \tag{5.7}$$

$$Pe = \frac{2V_g R}{\bar{D}} \tag{5.8}$$

where $\bar{D}$ is the diffusion coefficient of aerosol particle
V_g is the settling velocity of water drop
C is the Cunningham slip correction factor
ρ_p is the particle density
μ is the gas viscosity.

In general, for relatively large particles, the inertial effects on the overall collision efficiency are larger than the interception term because the water drops are much larger than the aerosol particles. As particle size becomes smaller, the Brownian diffusion term will become increasingly important. It should also be mentioned that Equation (5.4) is given by Hetsroni[5.26] and Equations (5.5) and (5.6) are based on the work of Lee and Gieseke[5.27, 5.28].

Another particle deposition mechanism, diffusiophoresis, was added to the NAUA code. Diffusiophoresis results from steam condensation onto containment walls and involves two mechanisms: a net flow of gas toward the wall surface (known as Stephan flow), and a molecular weight gradient caused by the steam concentration gradient. In general, the effects of Stephan flow are much larger than those of the molecular weight gradient and result in deposition of particles on the wall surface. The condensation rate toward wall surfaces calculated by the MARCH code has been used to calculate deposition due to diffusiophoresis.

In utilizing the NAUA computer code for calculating aerosol behavior during various accident sequences, it was noted that in certain cases the code requires a long computing time to calculate the rate of condensation of water vapor onto particles. This type of problem takes place when a large amount of condensible water vapor was used as an input. It was noted that a supersaturation ratio of much greater than 1.0 was frequently encountered even after the condensation calculation was completed.

Some literature suggests that pure water vapor at 20 C will spontaneously form water droplets in the absence of condensation nuclei when the supersaturation ratio exceeds 3.5, and at 0 C a saturation ratio of 4.3 is required for homogeneous nucleation. This mechanism has been implemented in NAUA in addition to the existing condensation calculation. As the critical supersaturation for the homogeneous nucleation, the following correlation equation given by Green and Lane[5.29] was used:

$$S = \exp(0.557 \cdot (\sigma/T)^{3/2} \cdot M),$$

where

S is the critical supersaturation
σ is surface tension
T is the temperature in °C
M is the molecular weight of water.

No nucleation or self-condensation rates are calculated in the code. Rather, if critical supersaturation is realized at a given time, the excess water vapor is assumed to form water particles of a uniform size spontaneously. Of course, these small pure water droplets are subsequently subject to NAUA's usual condensation and coagulation processes both among themselves and with

other particles containing solids. Although the effects of this mechanism on the overall aerosol concentration change are insignificant, the computational time is reduced considerably by this implementation.

References

(5.1) Gieseke, J. A., et al, "Radionuclide Release Under Specific LWR Accident Conditions, Volume 1", BMI-2104 (July, 1983).

(5.2) Wooton, R. O., et al, "MARCH 2 Code Description and Users' Manual", Draft (December, 1982).

(5.3) Wooton, R. O. and Avci, H. I., "MARCH (Meltdown Accident Response Characteristics) Code Description and Users' Manual", NUREG/CR-1711, BMI-2064 (October, 1980).

(5.4) "American National Standard for Decay Heat Power in Light Water Reactors", ANSI/ANS-5.1-1979.

(5.5) Geankoplis, C. J., "Mass Transport Phenomena", Holt, Rinehart, and Winston (1972).

(5.6) Freeman-Kelly, R., "A Users' Guide for MERGE", Battelle's Columbus Laboratories, October, 1982.

(5.7) "Technical Basis for Estimating Fission Product Behavior During LWR Accidents", NUREG-0772 (June, 1981).

(5.8) CORSOR Manual.

(5.9) Bell, M. J., "ORIGEN, The ORNL Isotope Generation and Depletion Code", ORNL-4628 (1973).

(5.10) Lorenz, R. A., et al, "Fission Product Release from Highly Irradiated LWR Fuel", NUREG/CR-0722 (1980).

(5.11) Lorenz, R. A., Collins, J. L., and Malinauskas, A. P., "Fission Product Source Terms for the LWR Loss-of-Coolant Accident", NUREG/CR-1288 (1980).

(5.12) Lorenz, R. A., et al, "Fission Product Release from Highly Irradiated LWR Fuel Heated to 1300-1600 C in Steam", NUREG/CR-1386 (1980).

(5.13) Lorenz, R. A., "Fission Product Release from BWR Fuel Under LOCA Conditions", NUREG/CR-1773 (1981).

(5.14) Parker, G. W., Martin, W. J., and Creek, G. E., "Effect of Time and Gas Velocity of Distribution of Fission Products from UO_2 Melted in

a Tungsten Crucible in Helium", Nuclear Safety Program Semi-Annual Report for period ending June 30, 1963, ORNL-3483, 19-20 (1967).

(5.15) Albrecht, H., Matschoss, V., and Wild, H., "Experimental Investigation of Fission and Activation Product Release from LWR Fuel Rods at Temperatures Ranging from 1500-2800 C", proceedings of the Specialists' Meeting on the Behavior of Defected Zirconium Alloy Clad Ceramic Fuel in Water Cooled Reactors, 141-146 (September, 1979).

(5.16) Albrecht, H., Matschoss, V., and Wild, H., "Release of Fission and Activation Products During Light Water Reactor Core Meltdown", Nuclear Technology, 46, 559-565 (1979).

(5.17) Niemczyk, S. J. and McDowell-Boyer, L. M., "Technical Considerations Related to Interim Source Term Assumptions for Emergency Planning and Equipment Qualification", ORNL/TM-8275 (1982).

(5.18) Weast, Robert C., Ed., CRC Handbook of Chemistry and Physics, 59th Edition, (1978).

(5.19) VANESA Manual.

(5.20) Jordan, H., Gieseke, J. A., and Baybutt, P., "TRAP-MELT Users' Manual", NUREG/CR-0632, BMI-2017 (February, 1979).

(5.21) TRAP-MELT 2.1 Users' Manual.

(5.22) Jordan, H., Schumacher, P. M., and Gieseke, J. A., "QUICK Users' Manual", NUREG/CR-2105, BMI-2082 (April, 1981).

(5.23) Owczarski, P. C., Postma, A. K., and Schreck, R. I., "Technical Bases and Users' Manual for SPARC -- Suppression Pool Aerosol Removal Code", report to the U.S. NRC, NUREG/CR-3317 (May, 1983).

(5.24) Bunz, H., Koyro, M., and Schock, W., "A Code for Calculating Aerosol Behavior in LWR Core Melt Accidents Code Description and Users' Manual".

(5.25) Schock, W., Bunz, H., and Koyro, M., "Messungen der Wasserdampfkondensation an Aerosolen unter LWR-un-falltypischen Bedingungen", KfK 3153 (August, 1981).

(5.26) Hetsroni, G., "Handbook of Multiphase Systems", McGraw Hill Book Company and Hemisphere Pub. Co. (1982).

(5.27) Lee, K. W. and Gieseke, J. A., J. Aerosol Science, 11, 335 (1980).

(5.28) Lee, K. W. and Gieseke, J. A., Environ. Sci. & Technol., 13, 446 (1979).

(5.29) Green, H. L. and Lane, W. R., Particulate Clouds: Dust, Smokes and Mists, D. Van Nostrand Co., Princeton, New Jersey (1957).

6. BASES FOR TRANSPORT CALCULATIONS

6.1 Plant Geometry and Thermal Hydraulic Conditions

MARCH 2 code calculations were performed for several variations of each of the four accident sequences considered. The results of the MARCH analyses are used as input for three aspects of the fission product release and transport calculations:

(1) The predicted time-dependent temperatures of the fuel are used by CORSOR to calculate fission product release.

(2) The primary system pressure and flow of steam and hydrogen from the core are input to MERGE to calculate primary system thermal-hydraulic input to TRAP-MELT.

(3) The thermal-hydraulic conditions in the containment building as well as leak rates out are input to the containment transport codes.

A summary of MARCH modeling options utilized in the analyses is presented in Table 6.1*. The design parameters for the Surry plant were summarized in Table 4.1.

One of the many areas of modeling uncertainty for thermal-hydraulic analysis for this study has been the behavior of the flow in the reactor coolant system in the pathway of release to the containment. In particular the conditions in the upper plenum and upper dome region are quite uncertain and could have a significant effect on the transport of radionuclides. The first problem in describing flow behavior in this region is in obtaining an adequate characterization of the structures. These structures are not described in detail in publicly available reports because of proprietary design features. This problem was alleviated by input from Westinghouse Electric Corporation, the reactor manufacturer for the Surry plant. In addition, even if the geometries of these structures had been well known, there is significant uncertainty as to the nature of the flow patterns in the upper plenum and dome during accident conditions, and as a result how much of the flow reaches the

*All tables in this section of the report have been placed at the end of the section.

available surfaces. The current version of TRAP only considers one structure with a given surface to mass ratio within a volume. While this limitation can be circumvented by subdividing the volume of interest into a number of smaller subvolumes, each with a particular structure, such an approach would require information on the possible series/parallel flow splits among the subvolumes, i.e., how much of the flow is seen by each of the structures. Such fine detail was not warranted by the existing level of understanding of flow patterns in the upper plenum. As a practical matter the gases leaving the core were assumed to flow in series through the upper core support structures, past the control rod guide tubes and support columns, past the top support structure, along the upper core barrel, and out the hot legs. Clearly alternate flow paths are possible, e.g., after passing through the upper core plate some of the flow could go directly to the hot legs without passing past the other structures. The sensitivity of results to this approximation will be investigated later in the program.

In the following sections of the report, the results obtained with the MARCH and MERGE codes are described for each of the accident sequences. In Section 6.1.6, some of the uncertainties in the analyses and sensitivities to assumptions are discussed.

6.1.1 Sequence AB (Hot Leg)

A large pipe-break accident with failure of the active emergency core coolant injection system, as would result from total loss of AC power, would be expected to result in comparatively rapid core meltdown. This is because core uncovery would occur essentially at the start of the accident with the decay heat level relatively high. The loss of electric power would also preclude the operation of containment safety features. Table 6.2 indicates the times of key events as predicted by the MARCH code for the input and modeling assumptions utilized. Table 6.3 provides details of the core and primary system conditions for this sequence. Core uncovery, heatup, and melting would occur at low primary system pressure, corresponding to the pressure of the containment. The temperature of selected fuel regions is illustrated as a function of time in Figures 6.1a and 6.1b. In this, as well as in subsequent plots of core node temperatures, the designation ROD (X,Y) denotes the core

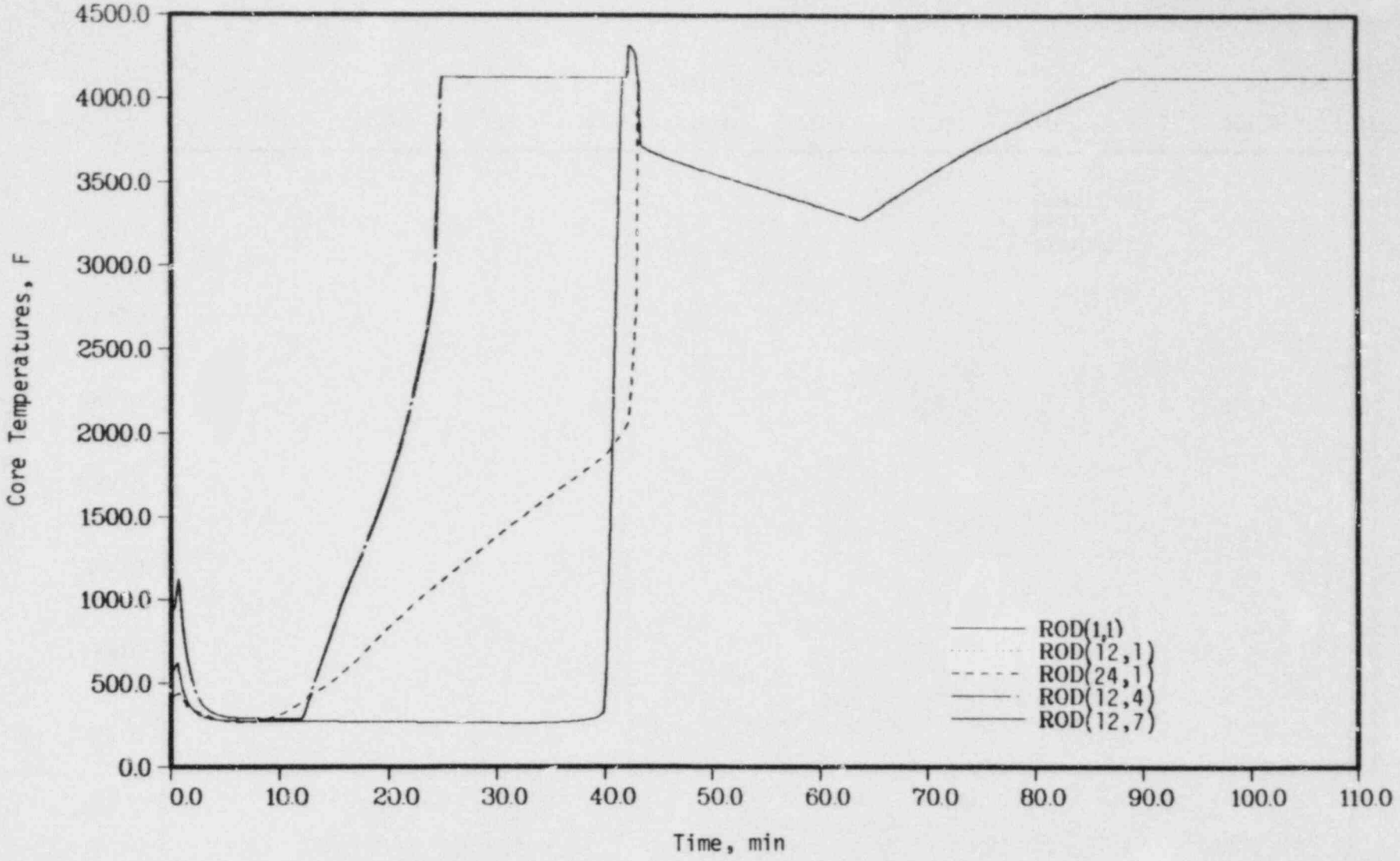

FIGURE 6.1a. SELECTED CORE NODE TEMPERATURES FOR SURRY AB SEQUENCE

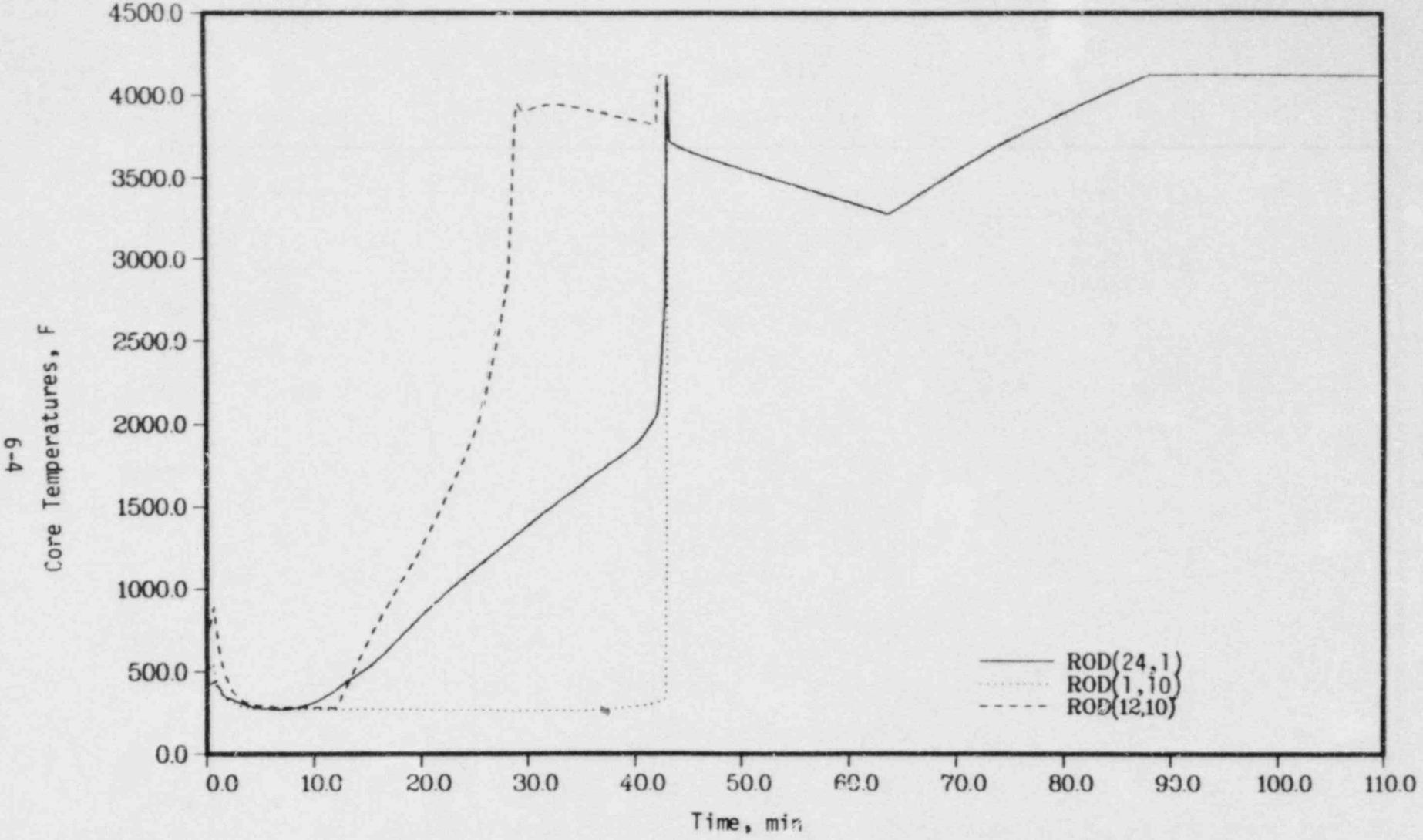

FIGURE 6.1b. SELECTED CORE NODE TEMPERATURES FOR SURRY AB SEQUENCE

node in axial position X and radial region Y. For these analyses the core was divided into 24 axial nodes and 10 radial regions.

Prior to the accident, the piping and structures in the reactor coolant system would be in the temperature range of 290-315 C. Because heatup of the fuel and the release of fission products would occur at about 172 kPa (25 psia), these surfaces would be expected to be considerably superheated. In addition, because of the high boiloff rate (high decay heat level) and low density of gases in the primary system (low primary system pressure), the velocity of gases passing through the reactor coolant system would be high in comparison to other accident sequences. At the time of core uncovery, the velocity of steam in the upper plenum is estimated to be approximately 1/2 meter/sec (2 feet/sec). The total residence time in the system, from leaving the core to exiting the break in the hot leg, would be less than 1 minute. As the water level in the core drops, the production of steam decreases accordingly. Just prior to slumping into the lower plenum, most of the steam that is being generated is predicted to be reduced to hydrogen.

Temperatures of the structure in the reactor coolant system are illustrated in Figure 6.2. Structure 1 represents the upper core plate, Structure 2 represents the control rod guide tubes and support columns, and Structure 3 represents the top support structures and core barrel. (In this figure, time is measured from the start of core uncovery.) The gas temperatures leaving the core rise rapidly as the core melts and begins to slump. When the core collapses into the bottom head of the reactor vessel, large quantities of steam are generated, resulting in a sharp decrease in gas temperatures as well as cooldown of the structures in the upper plenum. The maximum temperature of gases leaving the hot leg is estimated to be in the range of 650 C (1200 F), but these persist only a short time. A schematic of the gas flow path for the AB sequence is illustrated in Figure 6.3.

Several possible times and modes of containment failure have been investigated for this sequence: failure to isolate (β), early failure due to hydrogen burning (γ), and basemat melt-through (ϵ). Table 6.4 presents the details of the containment response for the various cases considered. For this analysis, the containment isolation failure is assumed to exist at the start of the accident and to be in one of the penetrations from the containment

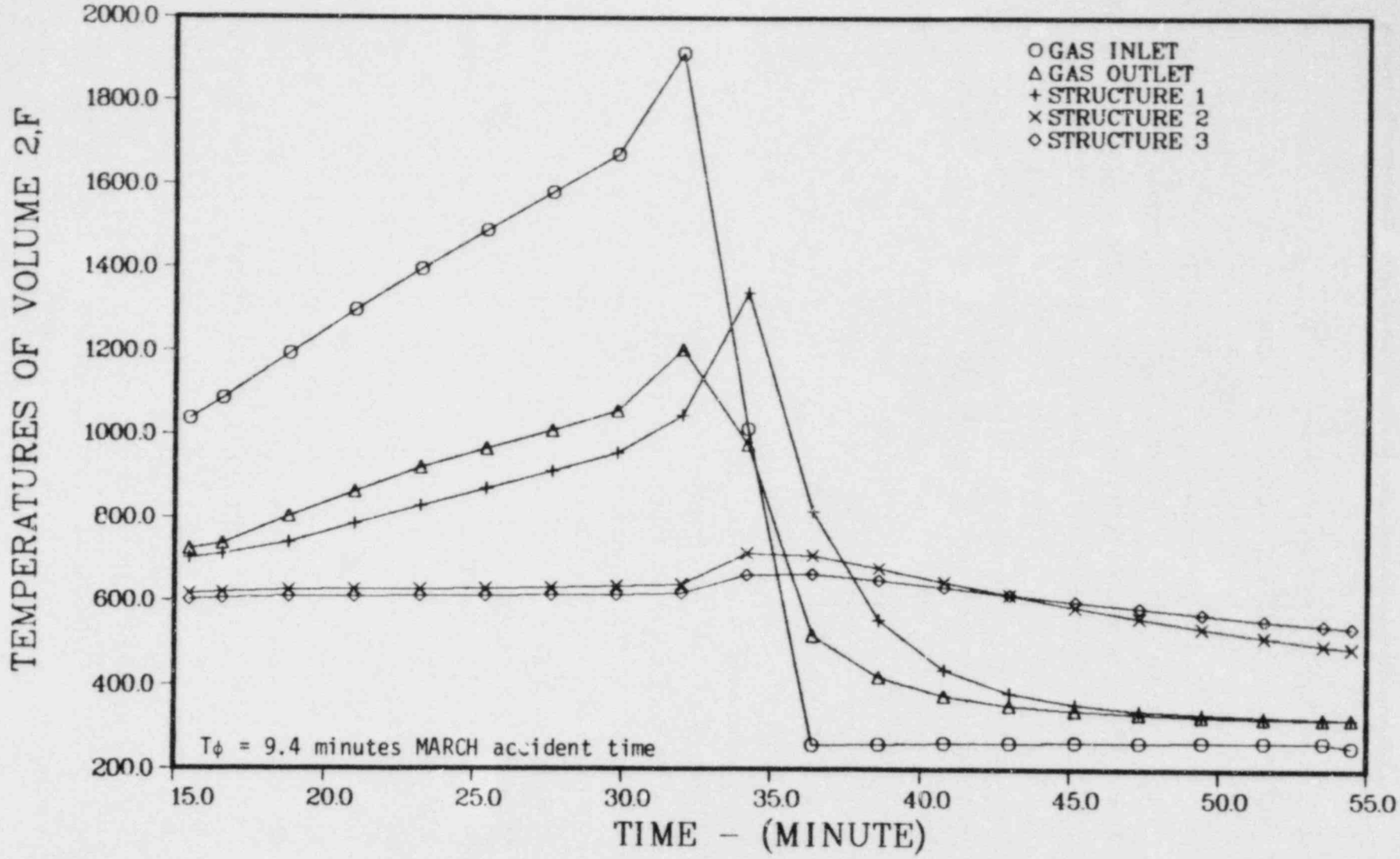

FIGURE 6.2 UPPER PLENUM GAS AND STRUCTURE TEMPERATURES FOR SURRY AB-ε SEQUENCE

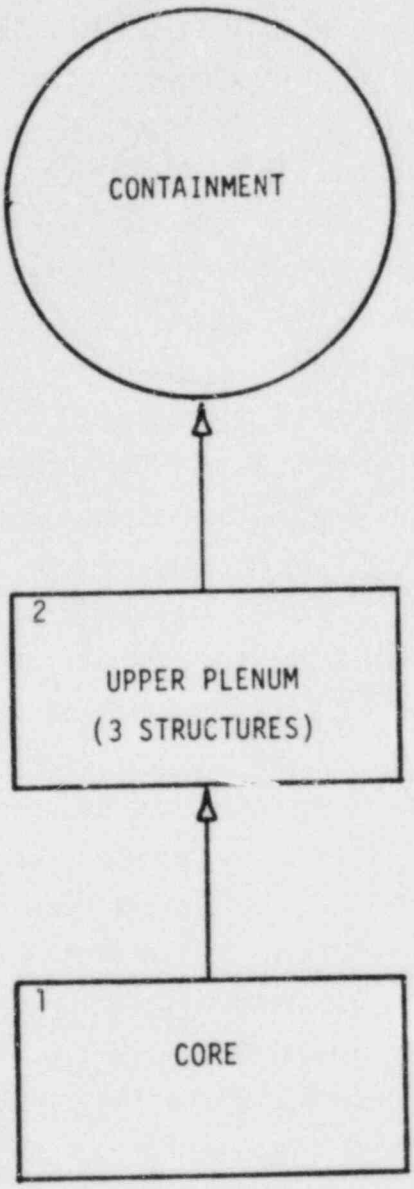

FIGURE 6.3 SCHEMATIC OF MERGE CONTROL VOLUMES FOR SURRY AB SEQUENCE

to the safeguards or auxiliary buildings. Thus, both these volumes were considered in the analyses for the AB-8 sequence.

The containment pressure and temperature histories for this sequence are illustrated in Figures 6.4 and 6.5. In these figures, Compartments 1 and 2 represent the containment and the safeguards building, respectively. As a result of leakage through the isolation failure, the containment pressure decreases fairly rapidly after primary system blowdown. The large steam generation associated with the collapse of the core into the bottom head leads to a temporary increase in the pressure. The pressure in the safeguards building is seen to stay near atmospheric except for a sharp increase at about 200 minutes, when a hydrogen burn is predicted to take place. At other times, the leakage from the safeguards building is able to keep the pressure low. It should be noted that a pressure rise of the type calculated could lead to the failure of the safeguards building.

The timing of the burn is controlled by the combination of increasing hydrogen concentration due to leakage from the containment and decreasing steam concentration due to condensation. (High steam concentration tends to inert the containment atmosphere early in the sequence.) The early overpressure containment failure (γ) considered was associated with a hydrogen burn taking place during the concrete-attack phase of the accident. The hydrogen was allowed to burn when flammable conditions were reached. The timing of the burn was determined by the increasing hydrogen concentration from concrete attack and decreasing steam concentration due to condensation.

The containment pressures and temperatures for the AB-γ sequence are illustrated in Figures 6.6 and 6.7. Different containment pressure responses would be predicted if the assumptions regarding hydrogen generation and burning were varied. The likelihood of containment failure due to a hydrogen burn or other event would, of course, depend on the failure pressure as well as the magnitude of the pressure; however, quantifying the probability of containment failure is not a part of this effort. If the containment is able to withstand earlier challenges, long-term overpressure failure or basemat melt-through may be the eventual outcome for this sequence.

The current MARCH calculations, using as input a concrete composition representative of that actually used at Surry, indicate that melt-through of the basemat would take place before long-term overpressurization. This is the

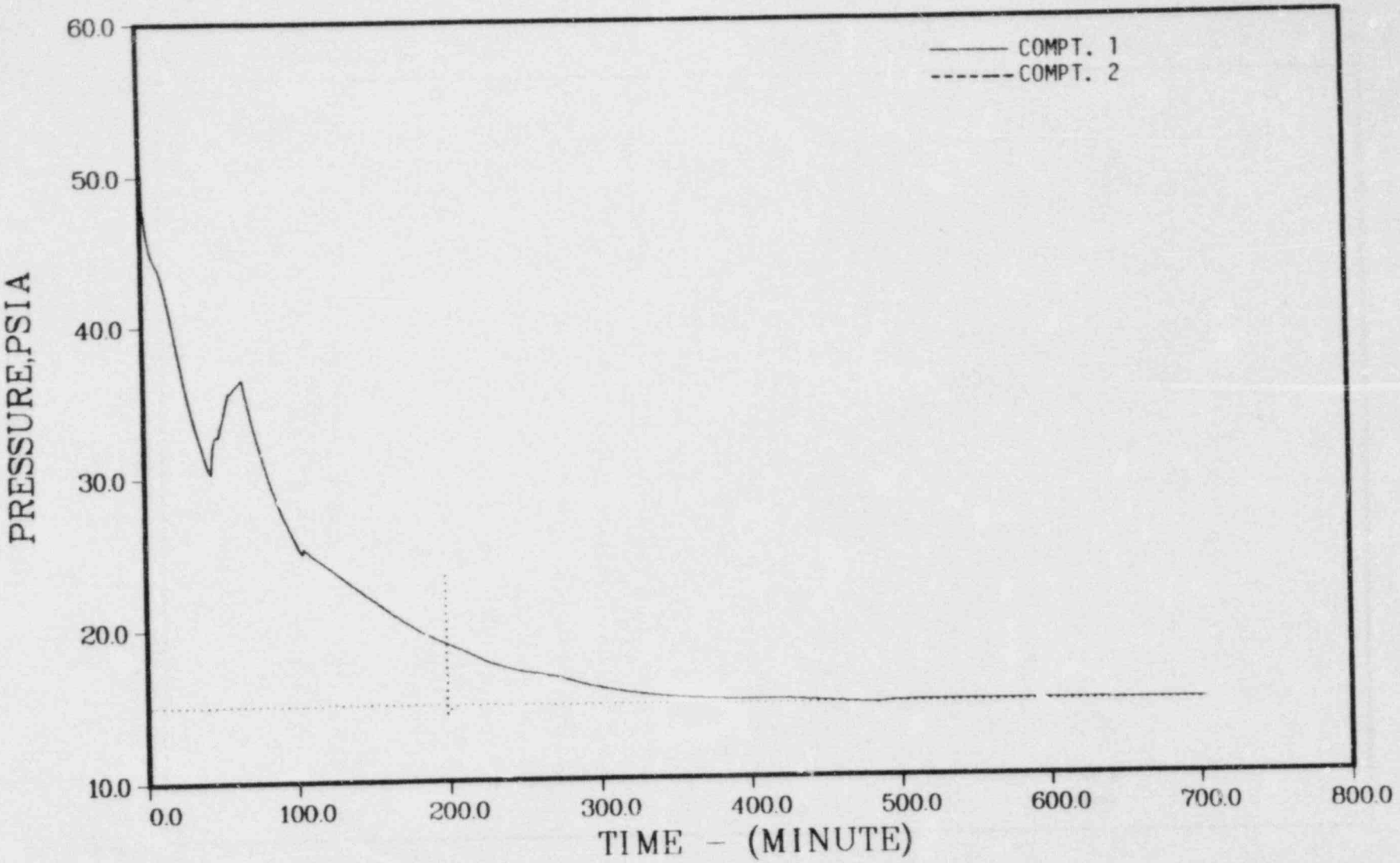

FIGURE 6.4 CONTAINMENT PRESSURE RESPONSE FOR SURRY AB-B SEQUENCE

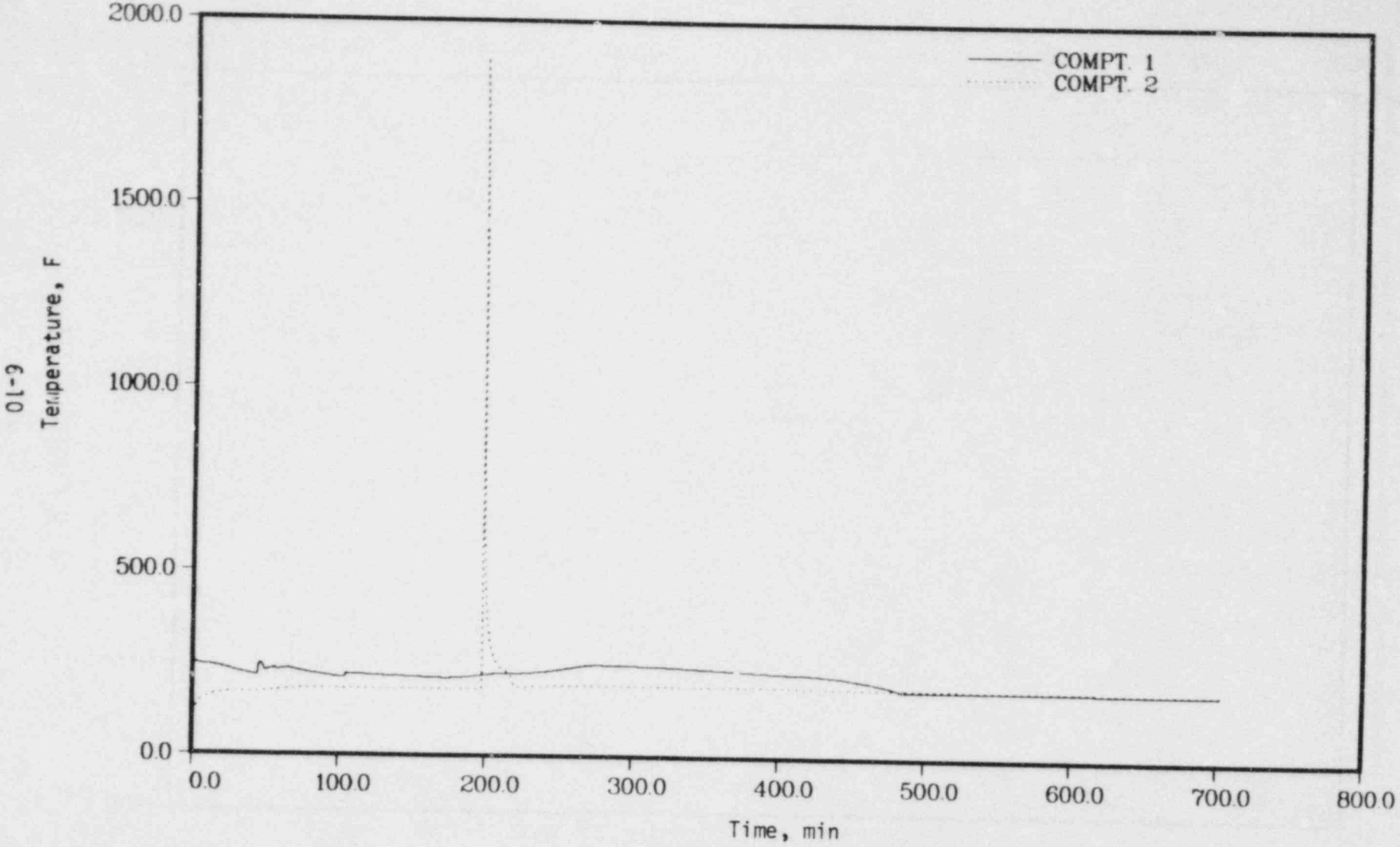

FIGURE 6.5 CONTAINMENT TEMPERATURE RESPONSE FOR SURRY AB-β SEQUENCE

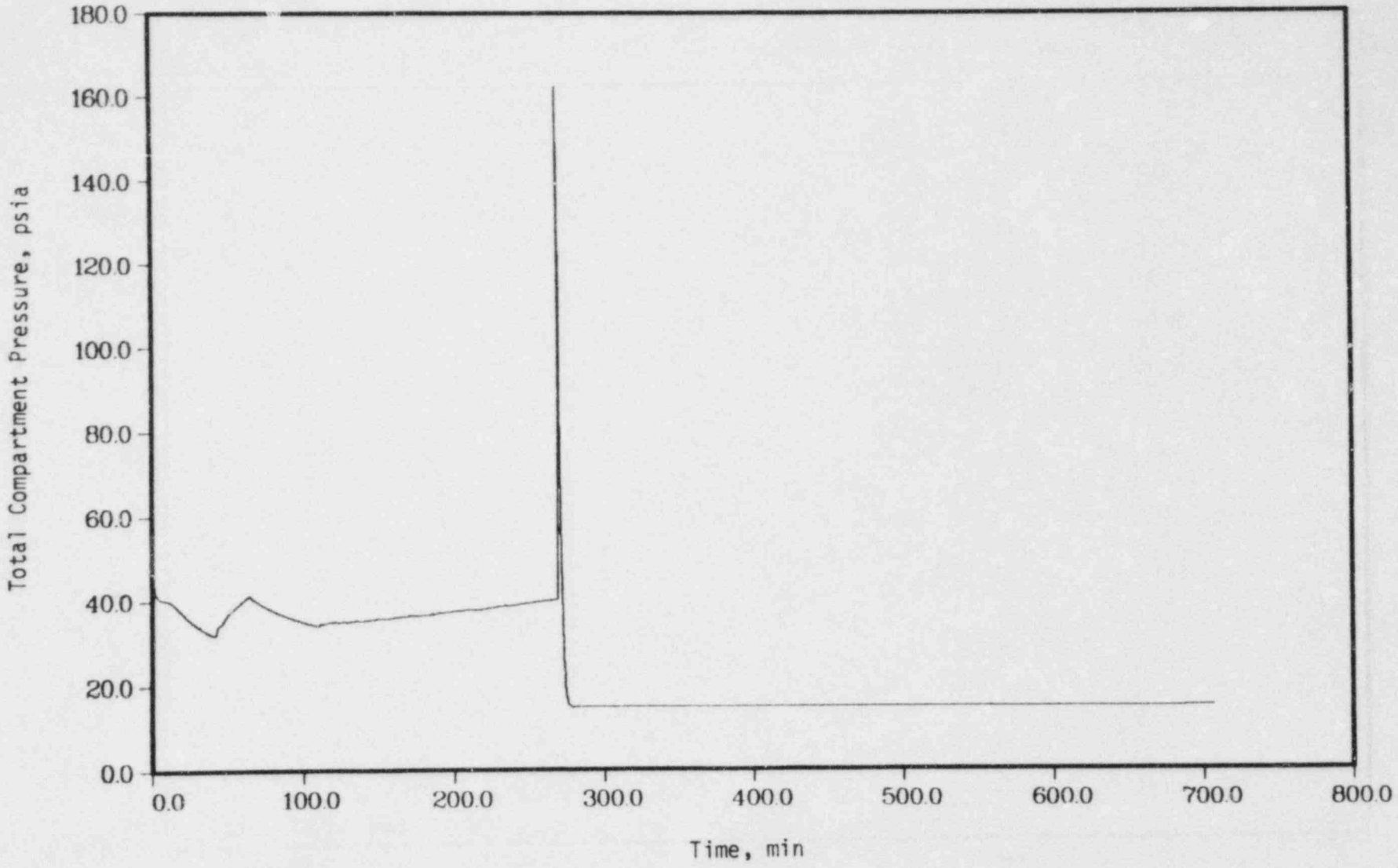

FIGURE 6.6 CONTAINMENT PRESSURE RESPONSE FOR SURRY AB-γ SEQUENCE

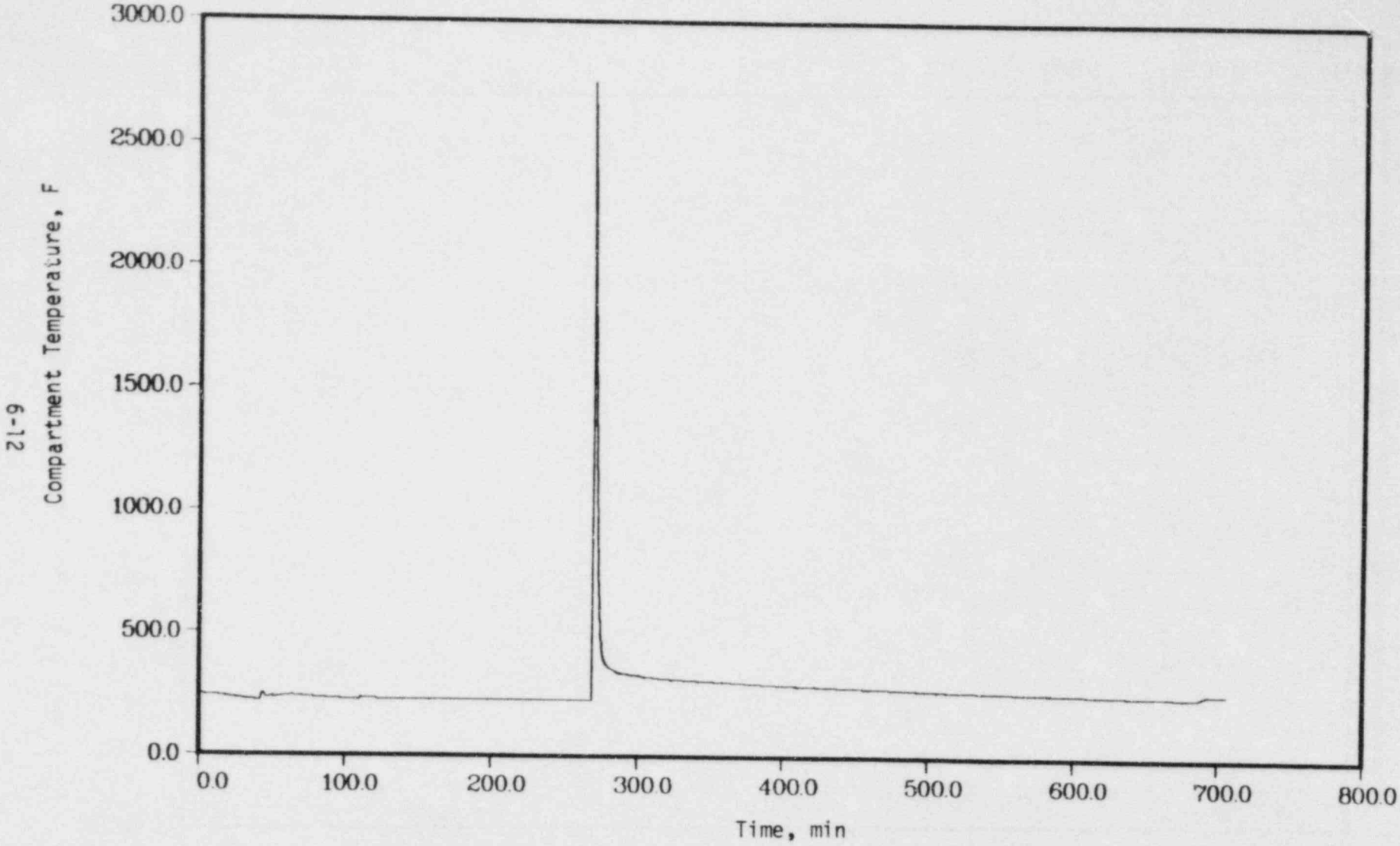

FIGURE 6.7 CONTAINMENT TEMPERATURE RESPONSE FOR SURRY AB-γ SEQUENCE

case that was analyzed as representative of delayed failure modes. The containment pressure and temperature histories for this sequence are shown in Figures 6.8 and 6.9. Containment melt-through is predicted to take place at about 1450 minutes into the accident. Since upon melt-through the containment depressurizes through the ground, only a small change in the containment pressure is seen for the conditions encountered here.

It should be noted that there is substantial uncertainty regarding the progression of concrete attack, and the timing of the occurrence of melt-through could vary considerably. It is also possible that overpressure failure could precede melt-through. In the Surry design, the reactor cavity and the containment sump are not connected; thus sump water evaporation is not a source of containment pressurization. After reactor vessel penetration, the principal driving force for pressurization would be the release of gases from the decomposition of the concrete. The time required to reach the assumed failure level of 0.69 MPa (100 psia) would be longer than the melt-through time predicted for the particular case considered here. If, however, lateral attack of the concrete by the core debris leads to the ingress of sump water into the reactor cavity, the rate of containment pressurization could be increased.

Table 6.5 summarizes the containment leakages for the various cases considered that were derived from the MARCH results and used in the evaluation of the fission product release from containment.

6.1.2 Sequence TMLB'

In the transient sequence TMLB', the ability to remove heat from the reactor coolant system is lost, and containment safety features are not available due to loss of all electric power. Decay heating following reactor shutdown boils off the water in the secondary side of the steam generators. After steam generator dryout, the primary system pressure rises to the relief valve setpoint, and reactor coolant is discharged through the relief line to the discharge tank and ultimately to the containment building. Table 6.2 indicates the times of key events as predicted by the MARCH code. Core and primary system conditions are given in Table 6.3. The temperature transient of selected fuel regions is illustrated in Figures 6.10a and 6.10b. Core uncovery, heatup, and melting occur with the primary system pressure at approximately 17.24 MPa (2500

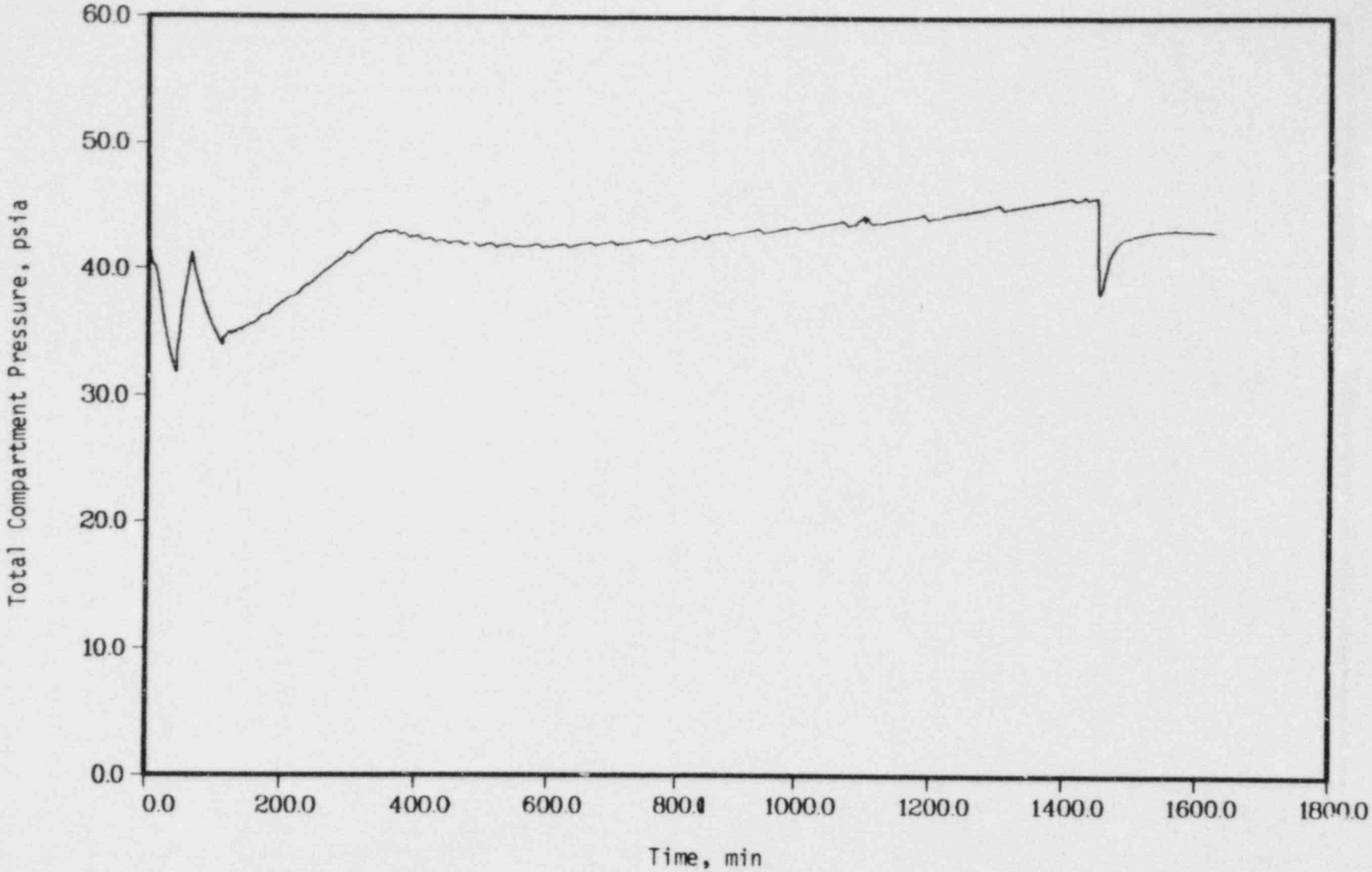

FIGURE 6.8 CONTAINMENT PRESSURE RESPONSE FOR SURRY AB-ε SEQUENCE

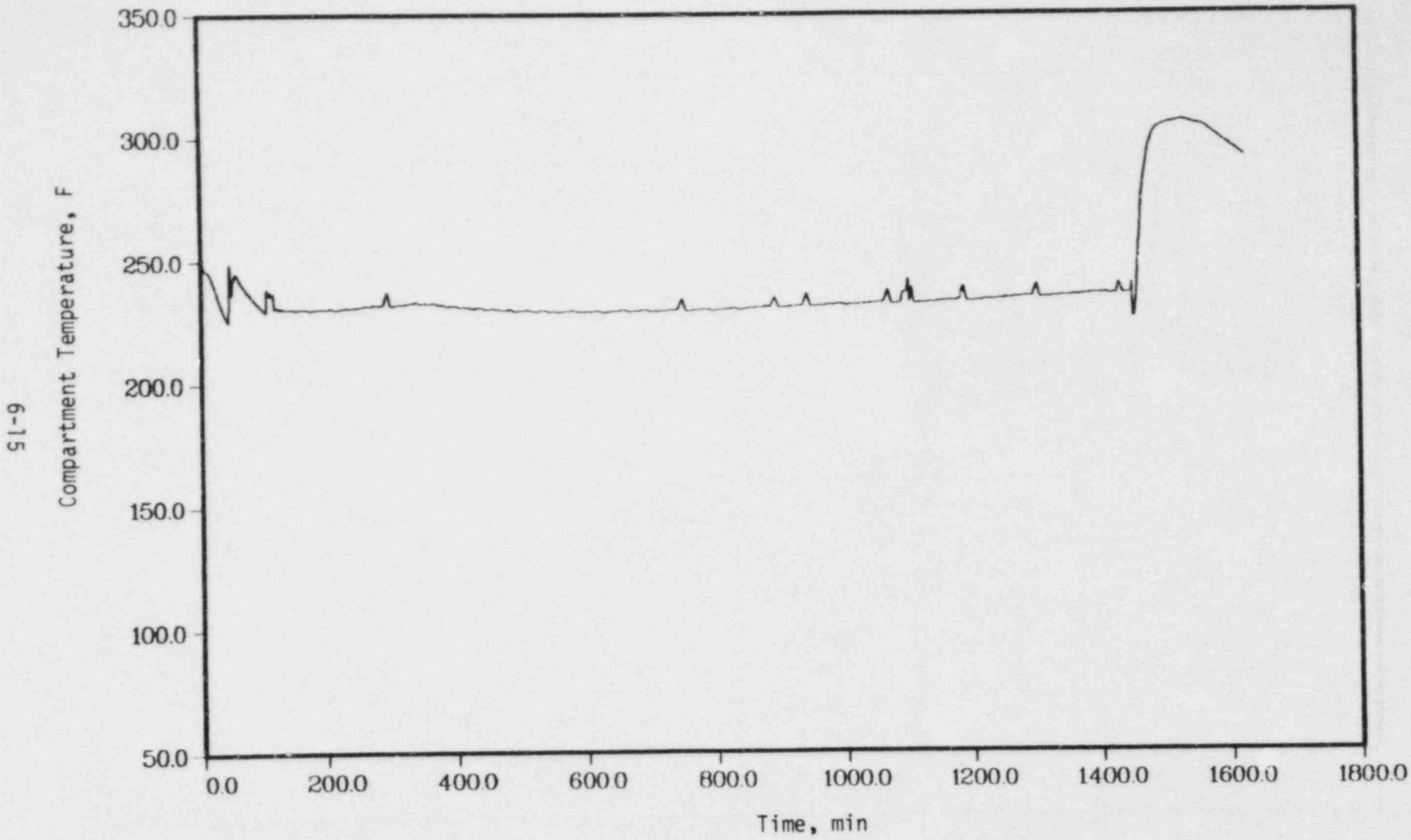

FIGURE 6.9 CONTAINMENT TEMPERATURE RESPONSE FOR SURRY AB-ε SEQUENCE

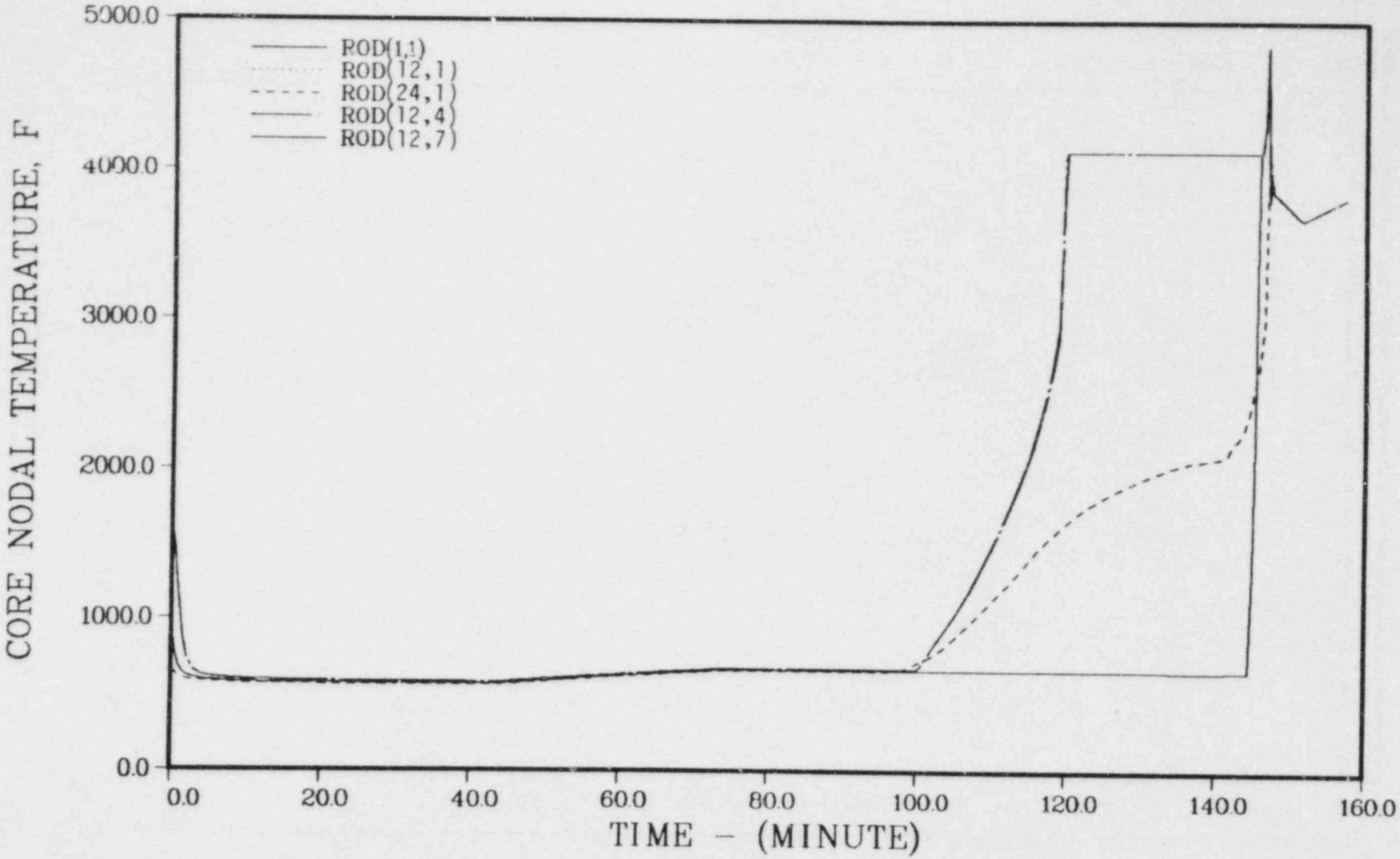

FIGURE 6.10a SELECTED CORE NODE TEMPERATURES FOR SURRY TMLB' SEQUENCE

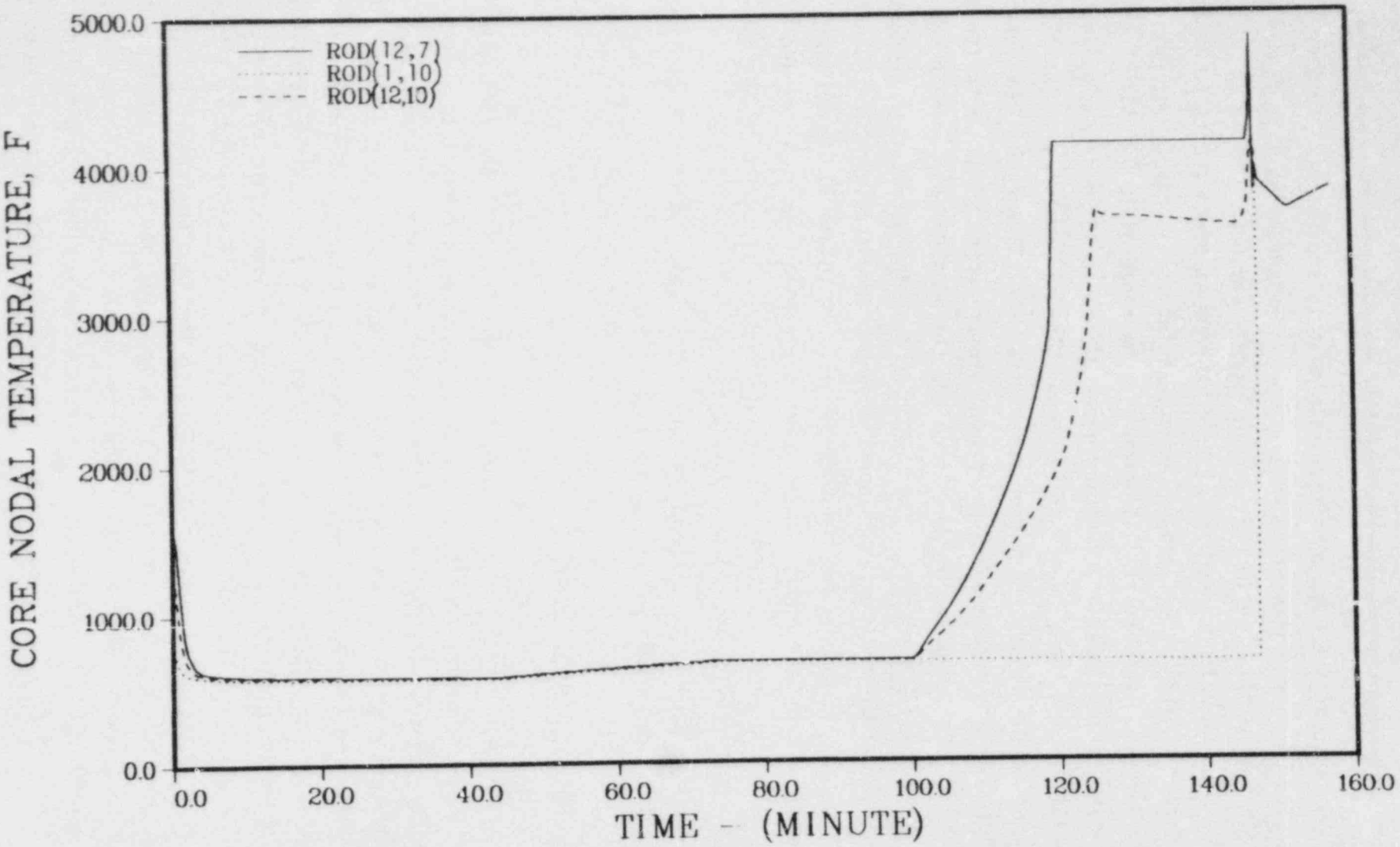

FIGURE 6.10b SELECTED CORE NODE TEMPERATURES FOR SURRY TMLB' SEQUENCE

psia). Because of the high density of steam at this pressure, the flow velocity in the primary system would be quite small -- generally less than 1/2 cm/sec (1 foot/min) -- until the start of core slumping.

The Reynolds Number in the upper plenum is predicted to be in the laminar regime until core slumping begins, as for the AB case. The Rayleigh Number, however, is substantially larger in the range of 10^{11}-10^{14}. Thus, significant mixing could occur in the upper plenum could be driven by temperature gradients and the buoyancy of hydrogen. The temperatures of the gas and structures in the volumes of the primary system are illustrated in Figures 6.11a and 6.11b. Volume 2 represents the reactor vessel upper plenum with its structures and Volume 3 represents the piping and the pressurizer. Within Volume 2 (the upper plenum), Structure 1 is the top core plate, Structure 2 represents the control rod guide tubes and support columns, and Structure 3 represents the top support structure and the core barrel. In Volume 3, Structure 1 is the pressurizer and Structure 2 represents the piping. In these figures, the time is measured from the start of core uncovery. A schematic of the gas flow path for TMLB' is illustrated in Figure 6.12.

Two specific containment failure mode possibilities were considered for the TMLB' sequence, an early and a late failure.

6.1.2.1 Early Failure: TMLB' (δ)

The early failure was assumed to be the result of the rapid steam generation from the interaction of the core debris with accumulator water in the reactor cavity. The failure of the vessel bottom head releases the high pressure steam from the primary system to the containment and discharges the core debris into the reactor cavity; the resulting drop in the primary system pressure allows the accumulators to discharge onto the top of the core debris. Figures 6.13 and 6.14 give the containment pressure and temperature histories for TMLB-δ, in which the containment is assumed to fail early due to the pressure rise from the debris water interacting in the reactor cavity.

MARCH calculates the rate of steam and hydrogen production resulting from the debris-water interaction in the reactor cavity. Several user-selected options in MARCH can be used to describe these interactions, ranging from a simple quenching model to several debris-bed models; combinations of models

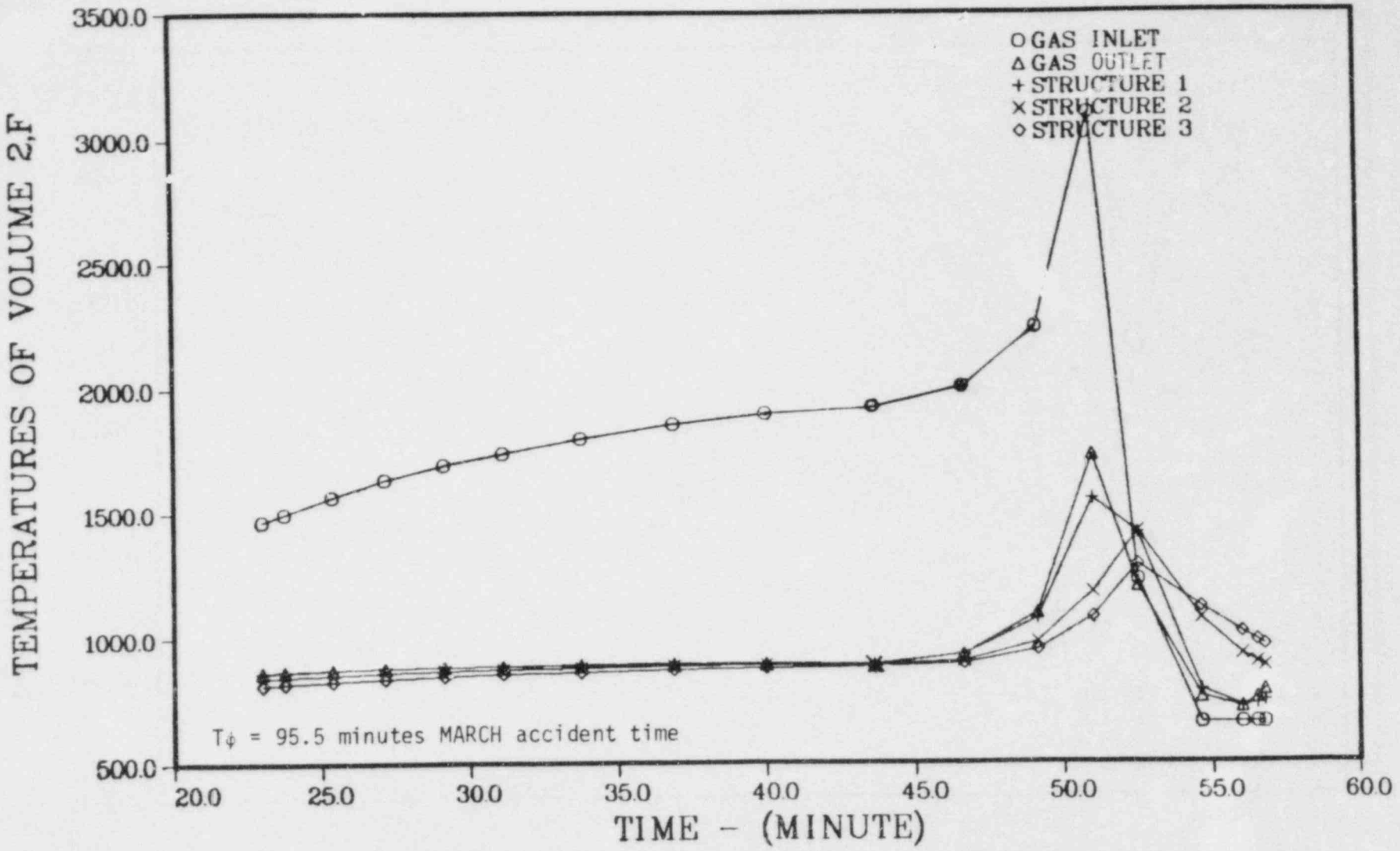

FIGURE 6.11a. PRIMARY SYSTEM GAS AND STRUCTURE TEMPERATURES FOR SURRY TMLB' SEQUENCE

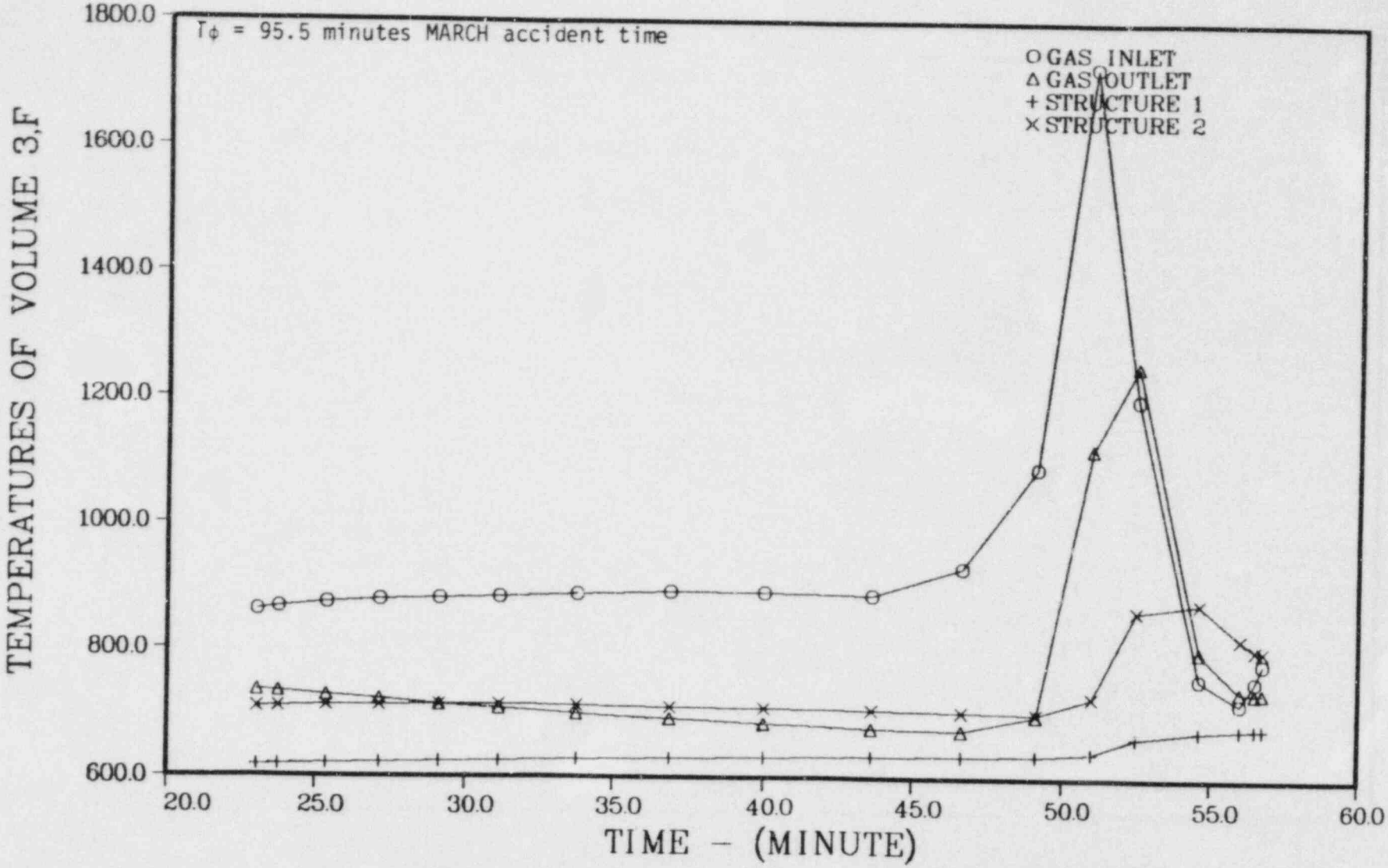

FIGURE 6.11b. PRIMARY SYSTEM GAS AND STRUCTURE TEMPERATURES FOR SURRY TMLB' SEQUENCE

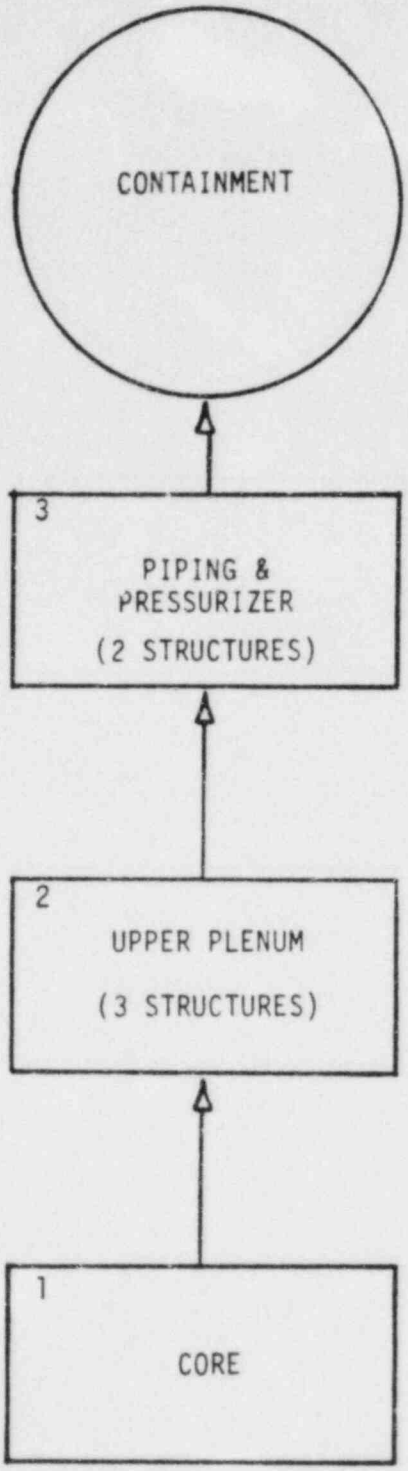

FIGURE 6.12 SCHEMATIC OF MERGE CONTROL VOLUMES FOR SURRY TMLB' SEQUENCE

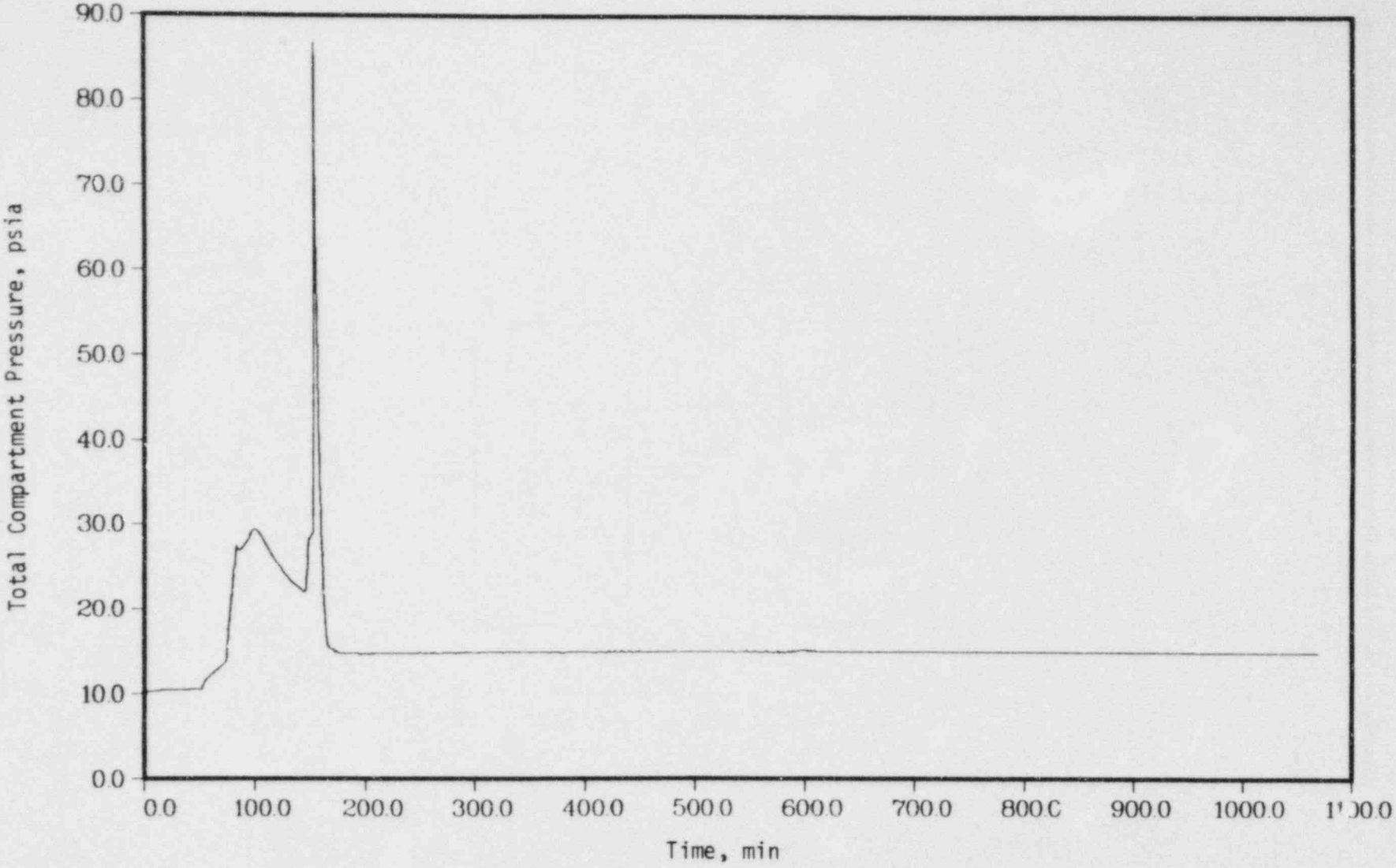

FIGURE 6.13 CONTAINMENT PRESSURE RESPONSE FOR SURRY TMLB'-δ SEQUENCE

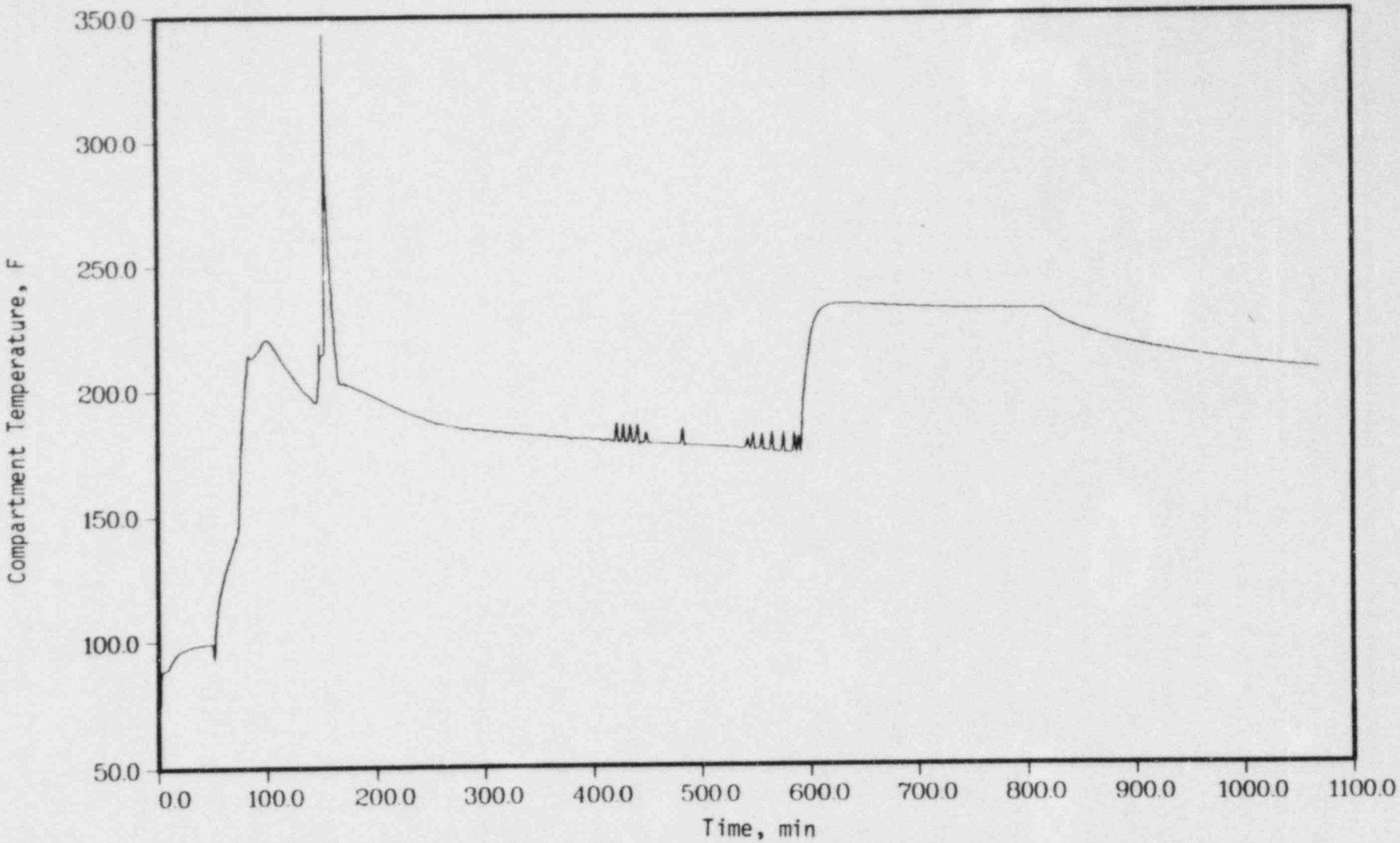

FIGURE 6.14 CONTAINMENT TEMPERATURE RESPONSE FOR SURRY TMLB'-δ SEQUENCE

are also possible. All the models require user inputs for which there is little basis. Perhaps the most important input parameter is the assumed debris-particle size; additional inputs that may be required relate to such items as debris-bed porosity, bed area, and criteria for transition from particulate to debris bed heat transfer. The rate and magnitude of the calculated containment pressure rise can obviously be sensitive to the input and modeling assumptions utilized. The use of the simple quench models in conjunction with small particle sizes tends to maximize the amount as well as rate of steam production from debris-water interaction; since in such cases the debris are quenched rapidly, only small amounts of hydrogen are predicted to be generated under these assumptions. The debris bed models can also predict large amounts and rates of steam generation, depending on the input parameters, but generally lead to slower rates of containment loading. In some cases, associated with marginally coolable debris beds, large amounts of hydrogen generation can be predicted.

6.1.2.2 Late Failure: TMLB' (ϵ)

The containment pressures and temperatures for a representative TMLB-ϵ sequence are given in Figures 6.15 and 6.16. The effect of the debris-water interaction is seen in the sharp pressure increase at about 160 minutes in Figure 6.15. In the particular case illustrated, the pressure rise would probably not challenge containment integrity; higher pressures could be predicted if alternate assumptions were used.

If the containment maintains its integrity through the above early pressure transient, the containment pressure will decline somewhat due to condensation of steam on internal structures, but will later increase again due to the attack of the concrete basemat by the hot core and structural debris. Since the gas and vapor input rates from concrete decomposition are low, except when the debris is very hot, a long time would be required for the pressure to build up to levels at which the likelihood of failure is significant. While the pressure is slowly building up, basemat melt-through could precede and preclude a long-term overpressure failure.

Melt-through of the concrete basemat, with venting of the gases through the ground, is reflected in the sharp pressure decrease at about 740

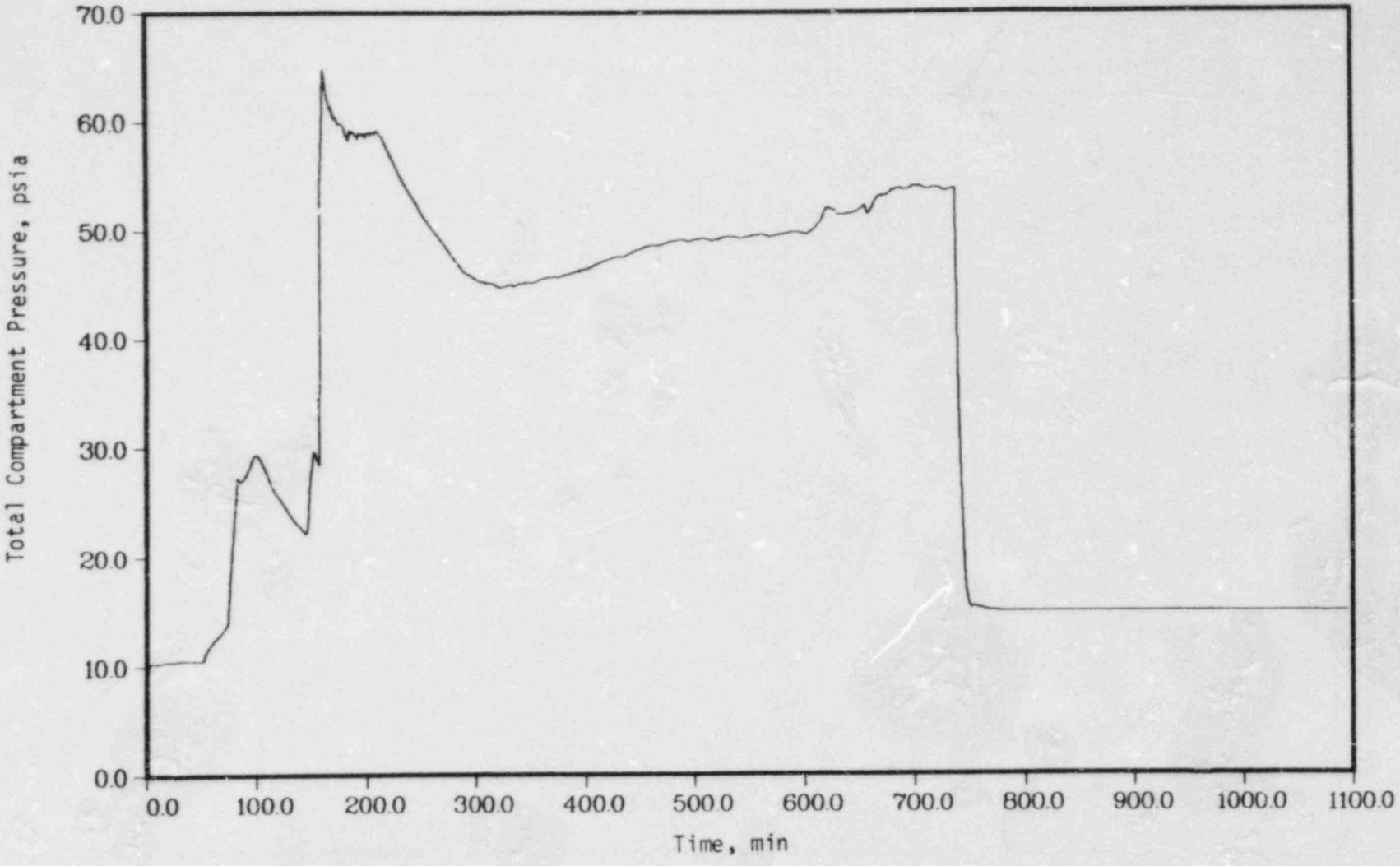

FIGURE 6.15 CONTAINMENT PRESSURE RESPONSE FOR SURRY TMLB'-ε SEQUENCE

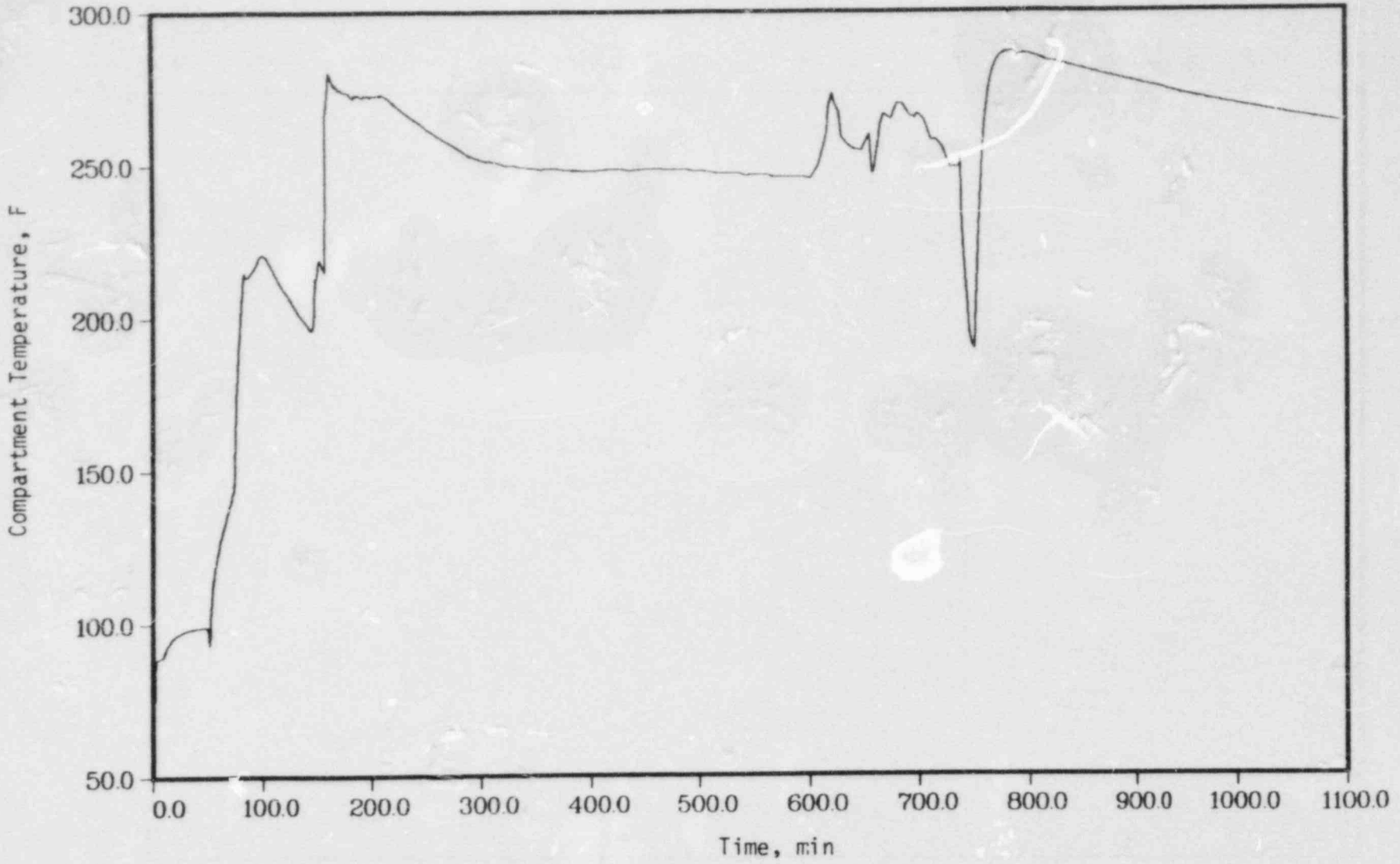

92-9

FIGURE 6.16 CONTAINMENT TEMPERATURE RESPONSE FOR SURRY TMLB'-ε SEQUENCE

minutes in Figure 6.15. It should be noted that the progression of concrete attack by the core debris, and hence the possible timing of melt-through, are highly uncertain, and that the high partial pressures of steam in the containment atmosphere throughout most of this sequence are predicted to preclude hydrogen burning.

It may be noted that some of the input parameters for the TMLB-δ sequence were changed from those in TMLB-ε, leading to a higher containment pressure peak. In considering the occurrence of an early containment failure, no representation is made as to the likelihood of such failure; the quantification of the probability of containment failure due to such interactions is beyond the scope of this study. It is suggested, however, that the magnitude of the pressures resulting from debris-water interactions may be sufficiently high that the possibility of failure should be considered.

Table 6.5 summarizes the containment leak rate information derived from the MARCH results and used in the evaluation of the fission product release from the containment.

6.1.3 Sequence V

The V sequence, or interfacing systems LOCA, is initiated by the failure of the check valves separating the low pressure emergency core cooling system from the primary coolant system. The release of the high pressure primary coolant inventory to the low pressure piping would not only lead to the failure of the emergency core cooling system but also provide a path for the release of radioactivity that bypasses the primary containment. It is also possible that the primary system blowdown would result in the failure of the safeguards or the auxiliary building.

The interfacing systems LOCA sequence is of particular interest because the containment building is bypassed for much of the sequence, and the primary system could represent the principal location for the retention of fission products released from the core. The possibility of retention in the safeguards (or auxiliary) building also exists if it does not also fail; this possibility would be quite design dependent.

The thermal-hydraulic behavior of the system during the period of fuel melting is similar to that of the Sequence AB. Following a period of 1/2

hour, during which blowdown and loss of reactor coolant inventory lead to the point of core uncovery, melting of fuel would occur over an interval of another 1/2 hour. The temperature histories of selected core nodes are given in Figures 6.17a and 6.17b. The timing of key events is presented in Table 6.2.

The core and primary system characteristics at key times during the sequence are given in Table 6.3. In this case, the primary system pressure would be slightly more elevated (0.68 MPa), and the velocity in the upper plenum would be reduced to approximately 10 cm/s. The velocity of the steam and hydrogen flowing back through the ECC injection line to the auxiliary building would be greater than 1 m/s. The residence time in the reactor coolant system from core exit to the atmosphere of the auxiliary building would be on the order of 1 minute, with the majority of the time spent in the upper plenum.

The predicted temperatures of gases and structures in the flow path to the auxiliary building are illustrated in Figures 6.18a-d. In these figures, Volume 2 represents the reactor vessel upper plenum, Volume 3 the hot leg piping, Volume 4 the steam generator, and Volume 5 the emergency core cooling system piping. The three structures in the upper plenum (Volume 2) are as previously described. Figures 6.19a-d show the results for an alternate breakdown in which the emergency core cooling system piping was represented as four connected volumes rather than a single volume. In both sets of figures, the time is measured from the start of core uncovery. The results are similar to those obtained for the AB sequence.

A schematic of the gas flow path for V is illustrated in Figure 6.20. The auxiliary building and containment characteristics at various times during the sequence are given in Table 6.4. Table 6.5 summarizes the containment leakage flows derived from the MARCH analyses and used to evaluate fission product release to the environment.

6.1.4 Sequence S_2D

This small-pipe-break accident sequence with failure of ECC injection involves conditions intermediate to the high pressure meltdown sequence TMLB' and the low pressure sequences AB and V. In the S_2D sequence, the containment sprays and heat removal systems are operating; thus the containment pressure would be maintained at low levels, except perhaps for brief

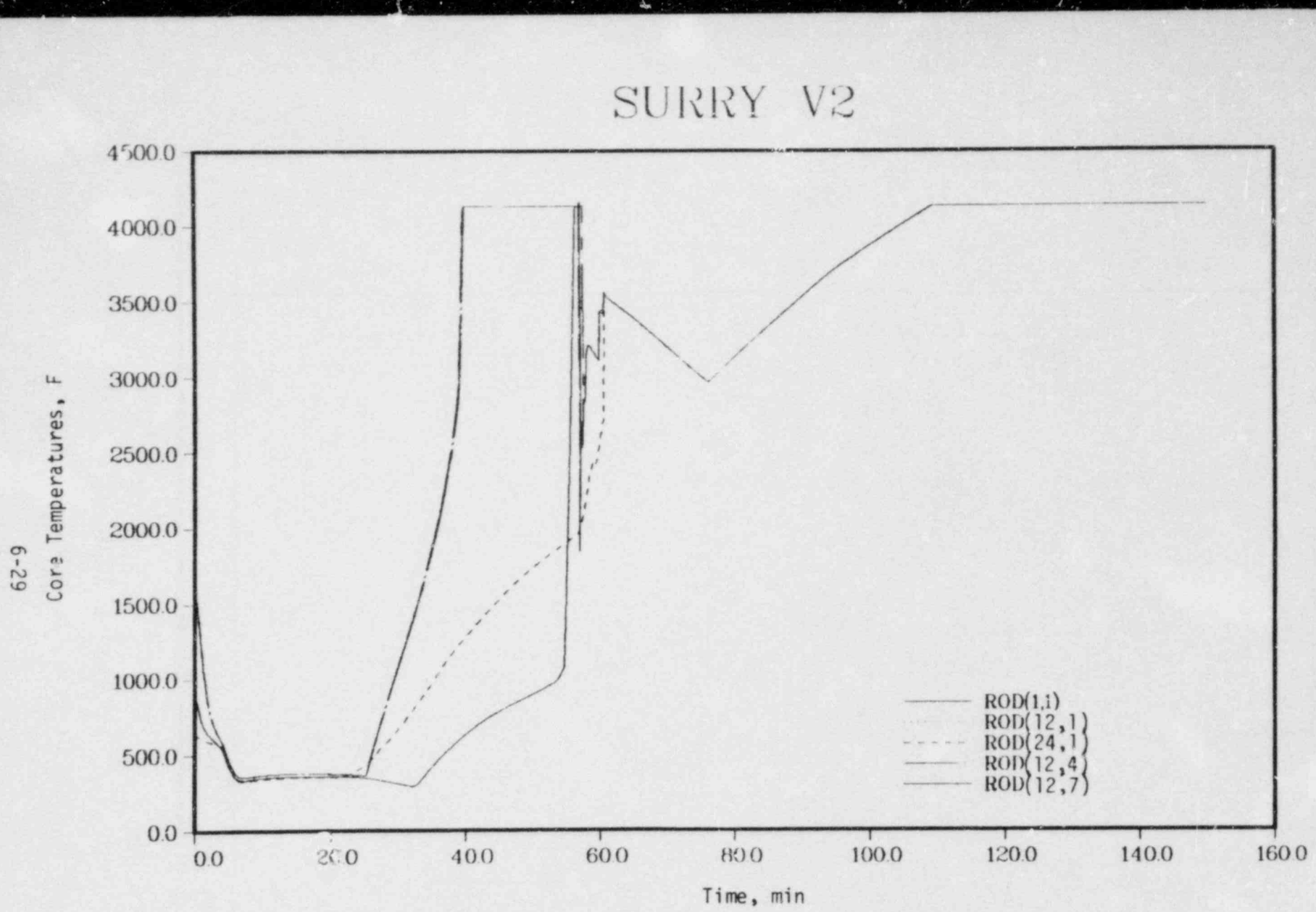

FIGURE 6.17a. SELECTED CORE NODE TEMPERATURES FOR SURRY V SEQUENCE

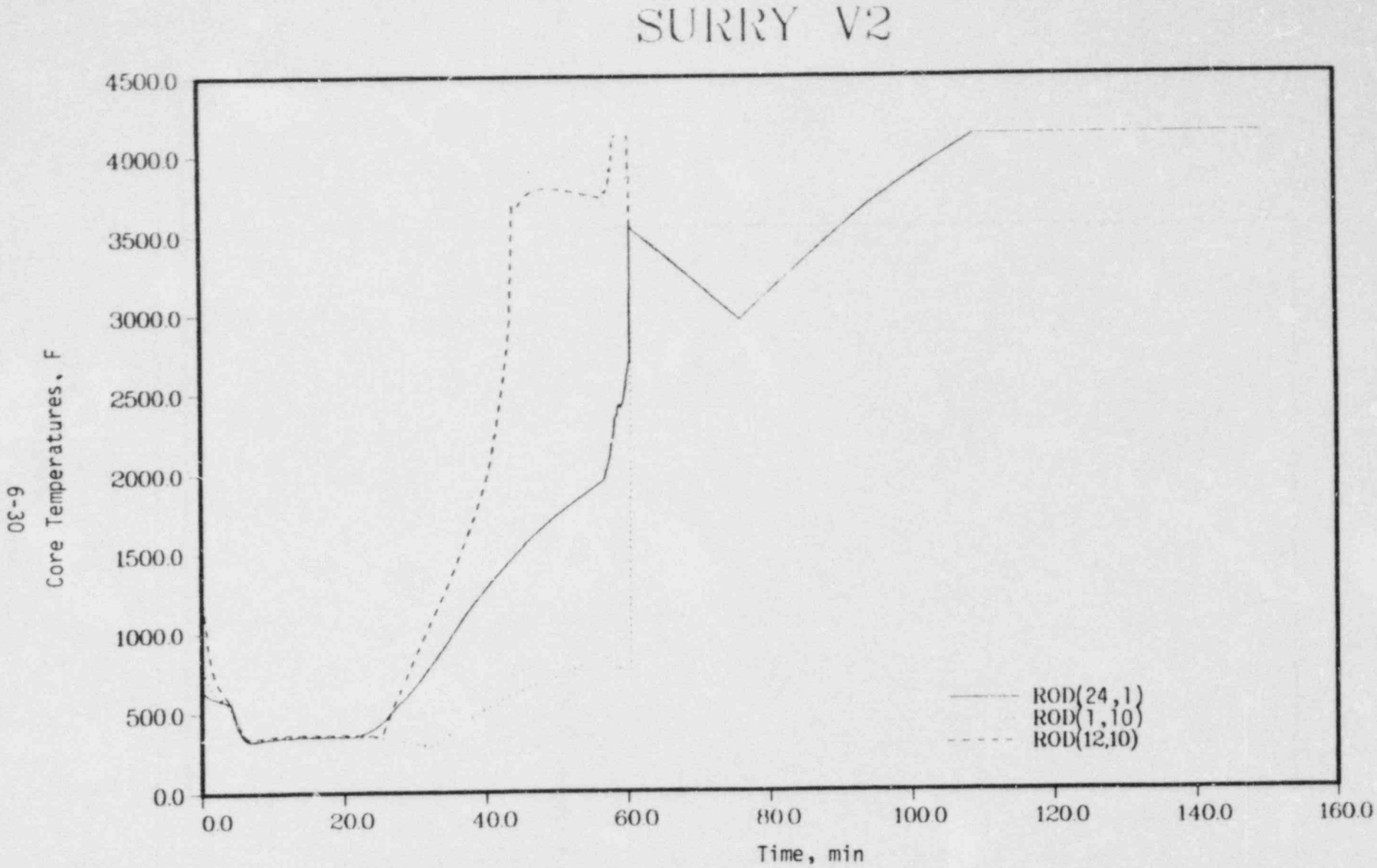

FIGURE 6.17b. SELECTED CORE NODE TEMPERATURES FOR SURRY V SEQUENCE

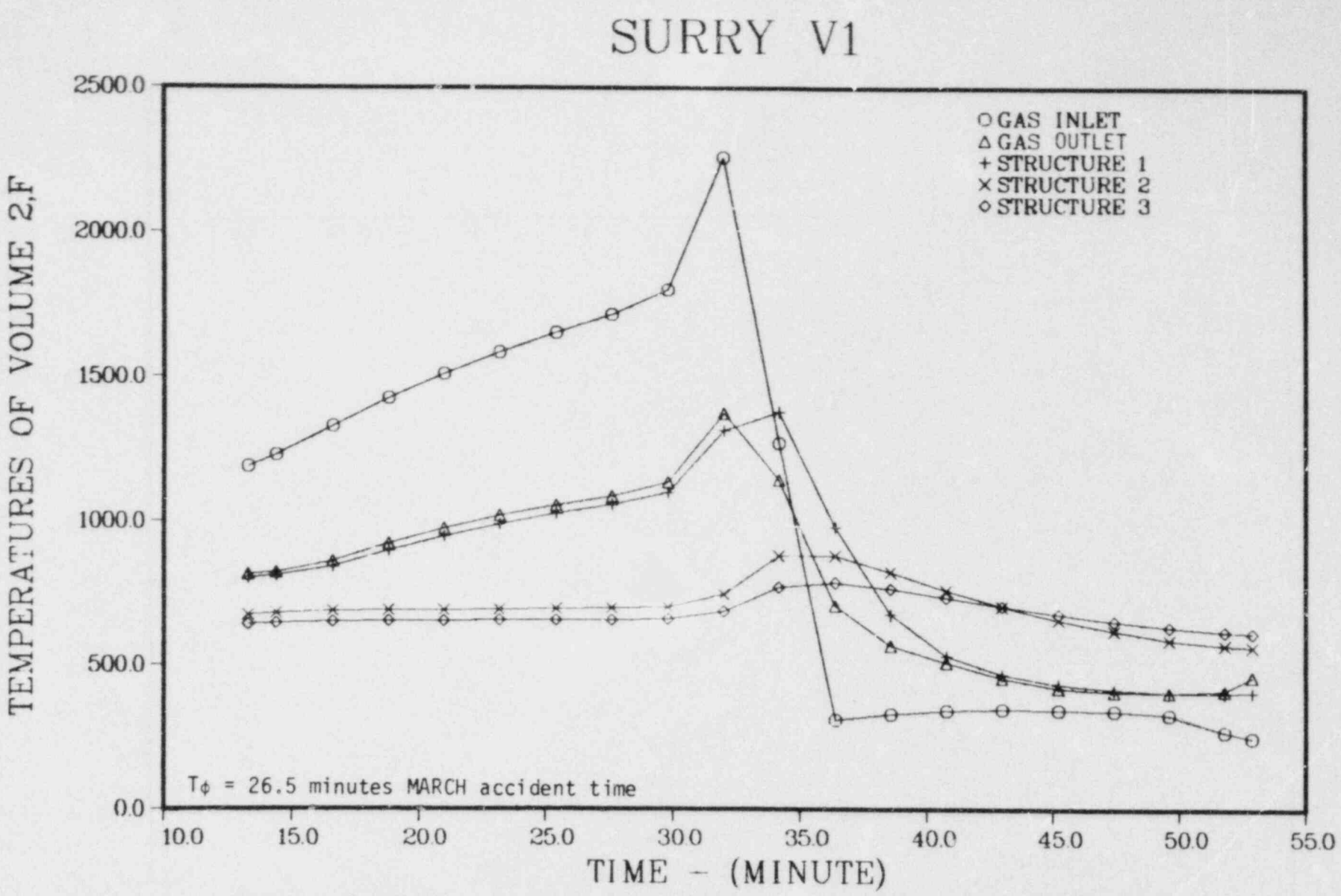

FIGURE 6.18a. PRIMARY SYSTEM GAS AND STRUCTURE TEMPERATURES FOR SURRY V SEQUENCE

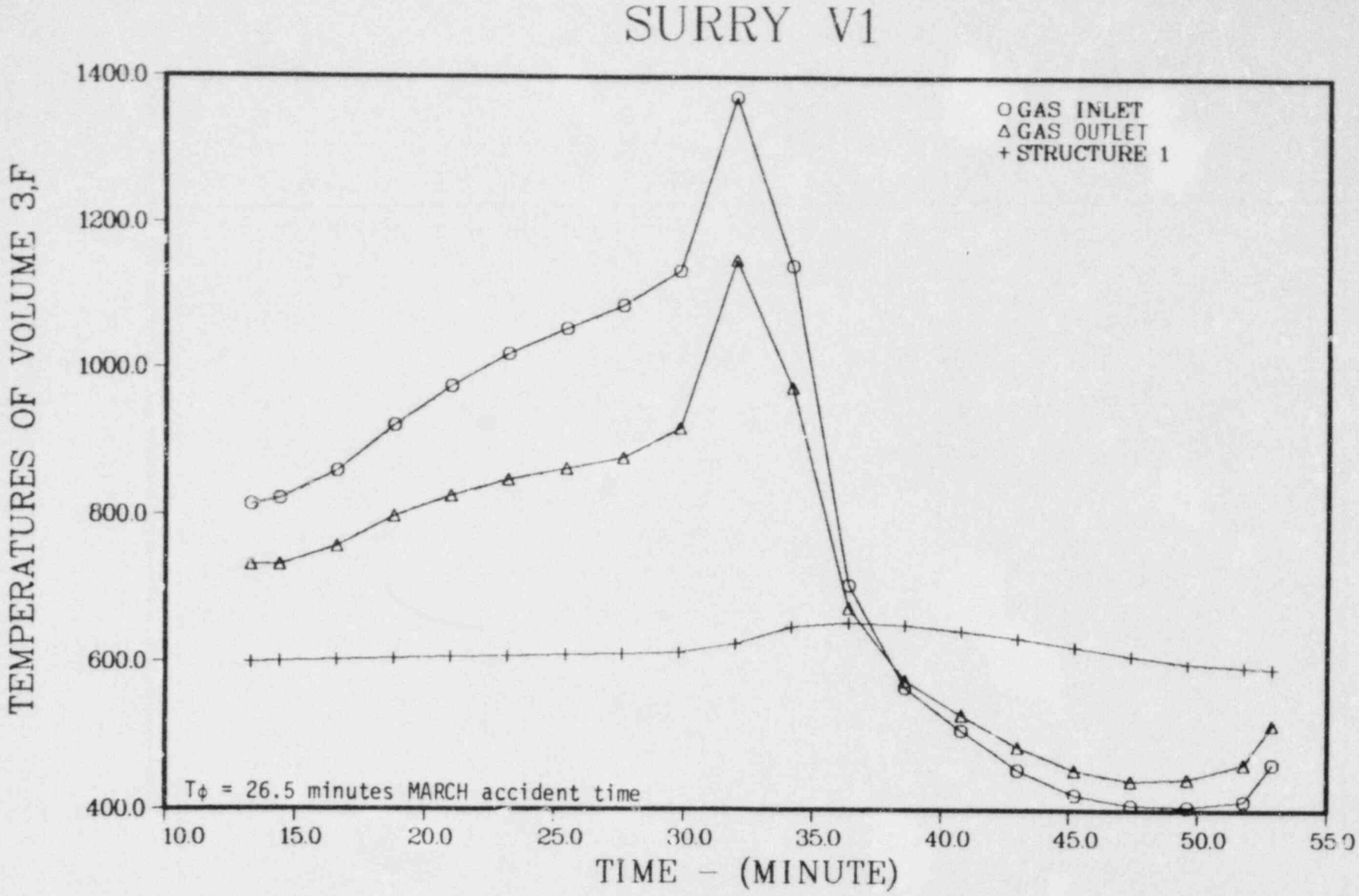

FIGURE 6.18b. PRIMARY SYSTEM GAS AND STRUCTURE TEMPERATURES FOR SURRY V SEQUENCE

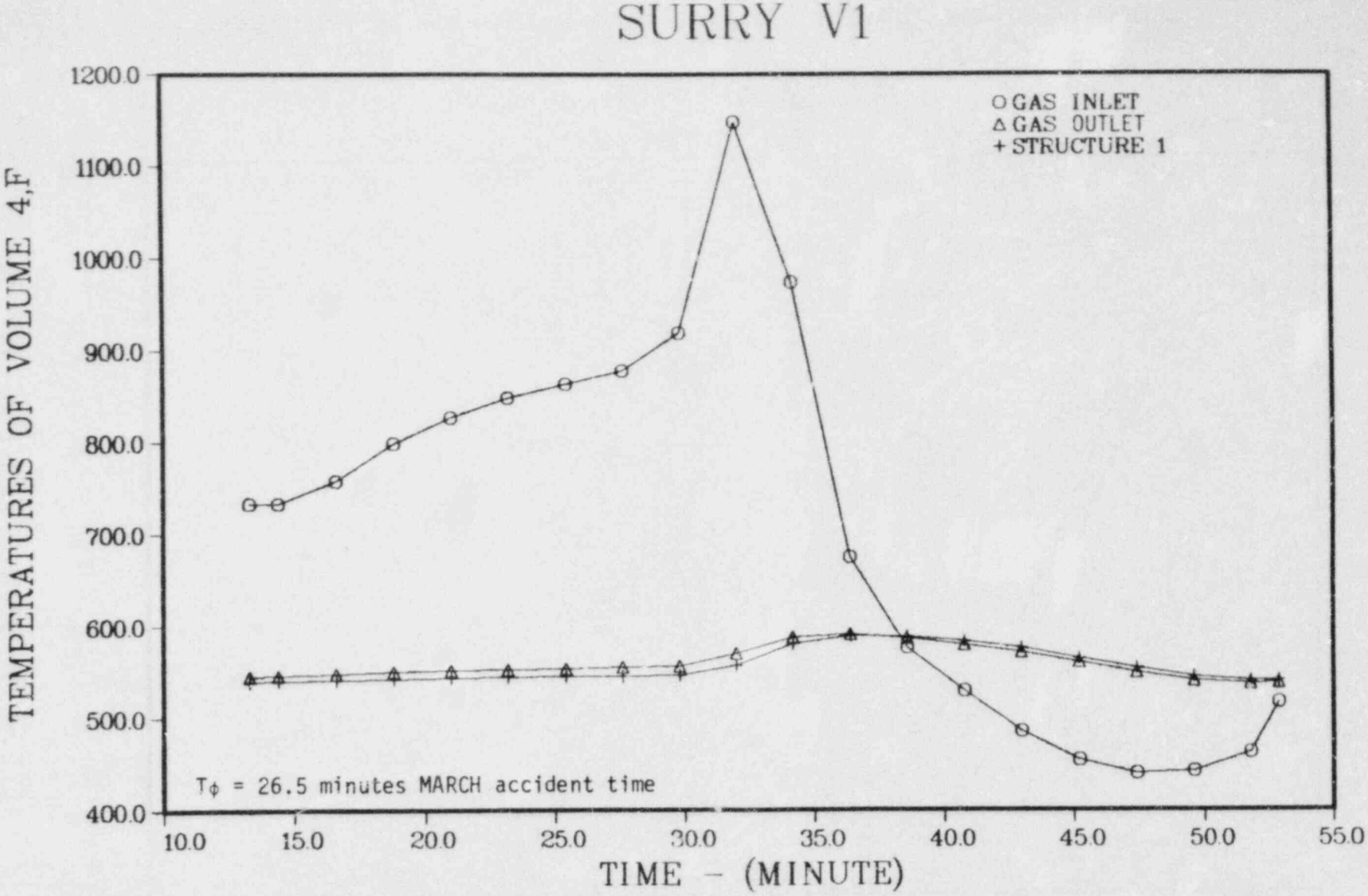

FIGURE 6.18c. PRIMARY SYSTEM GAS AND STRUCTURE TEMPERATURES FOR SURRY V SEQUENCE

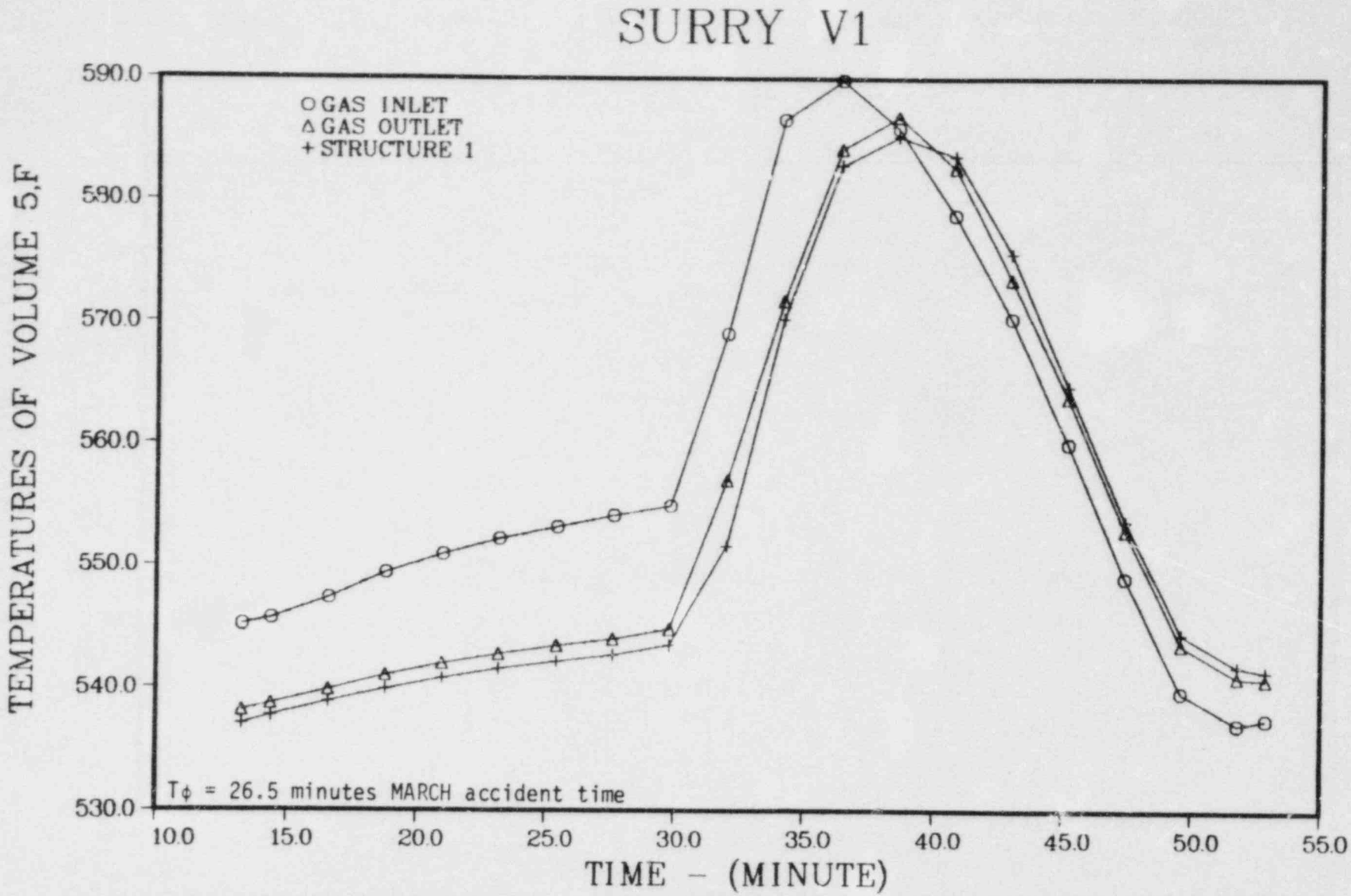

FIGURE 6.18d. PRIMARY SYSTEM GAS AND STRUCTURE TEMPERATURES FOR SURRY V SEQUENCE

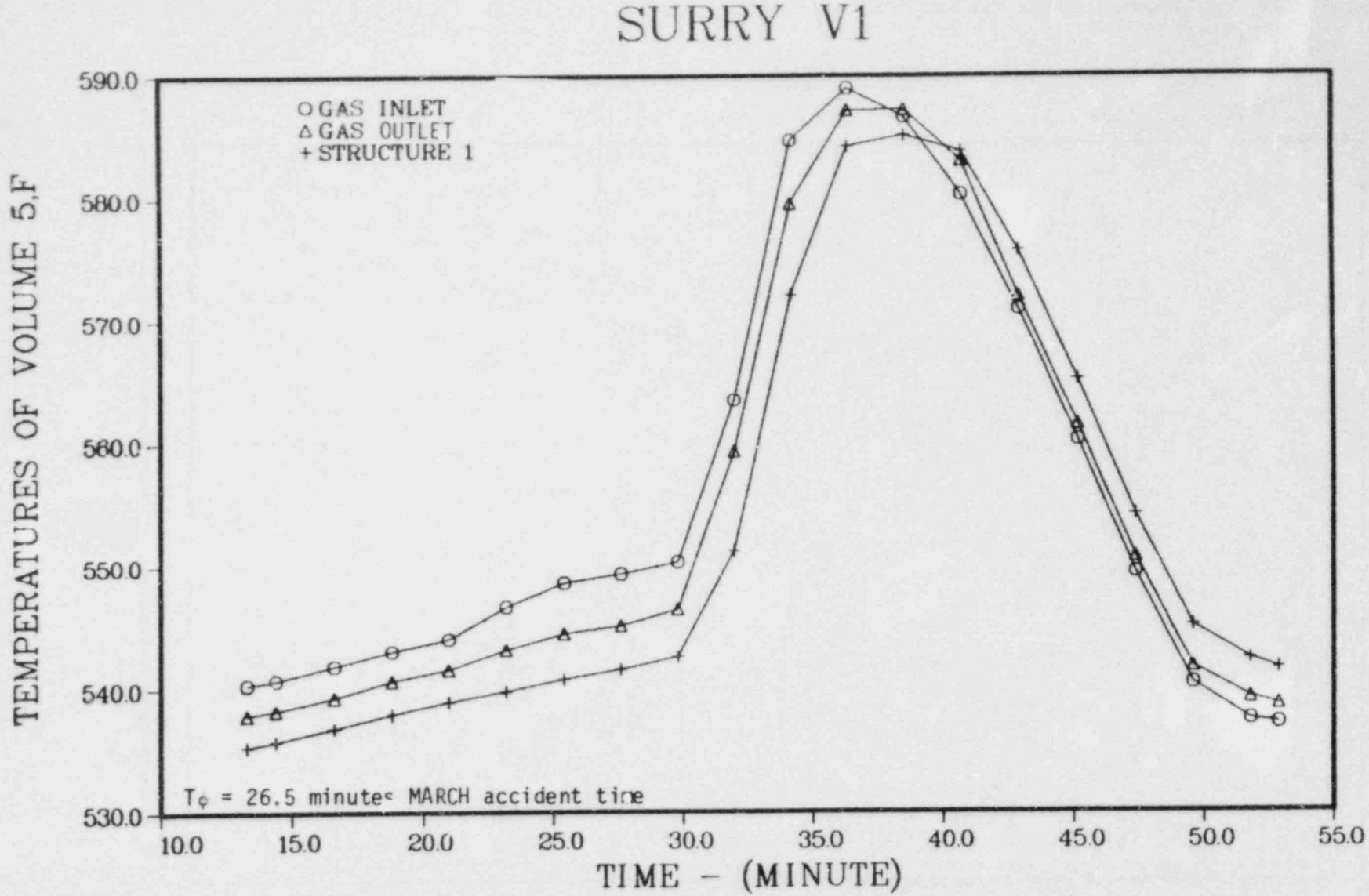

FIGURE 6.19a. EMERGENCY CORE COOLING SYSTEM PIPING TEMPERATURES FOR SURRY V SEQUENCE

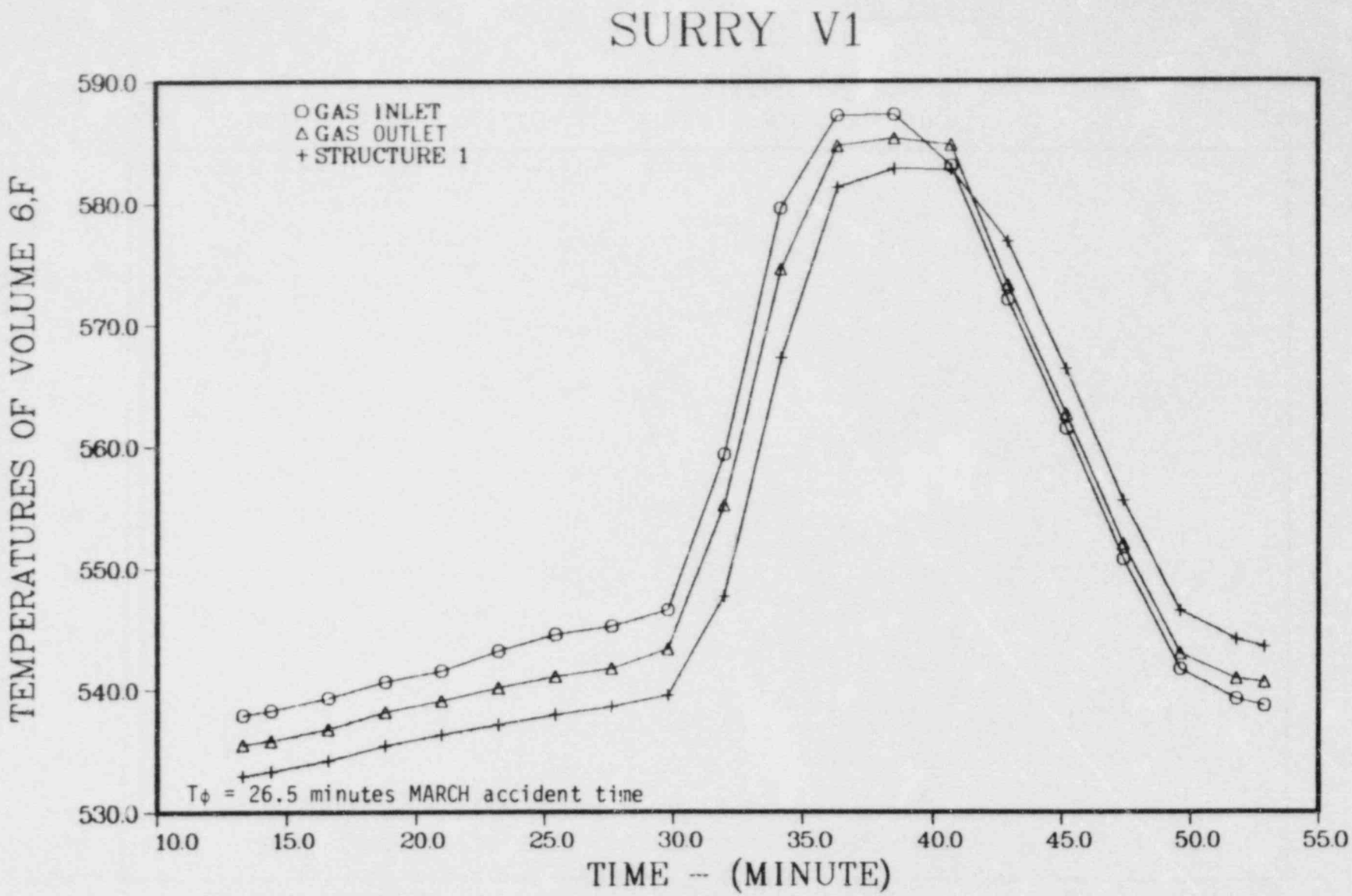

FIGURE 6.19b. EMERGENCY CORE COOLING SYSTEM PIPING TEMPERATURES FOR SURRY V SEQUENCE

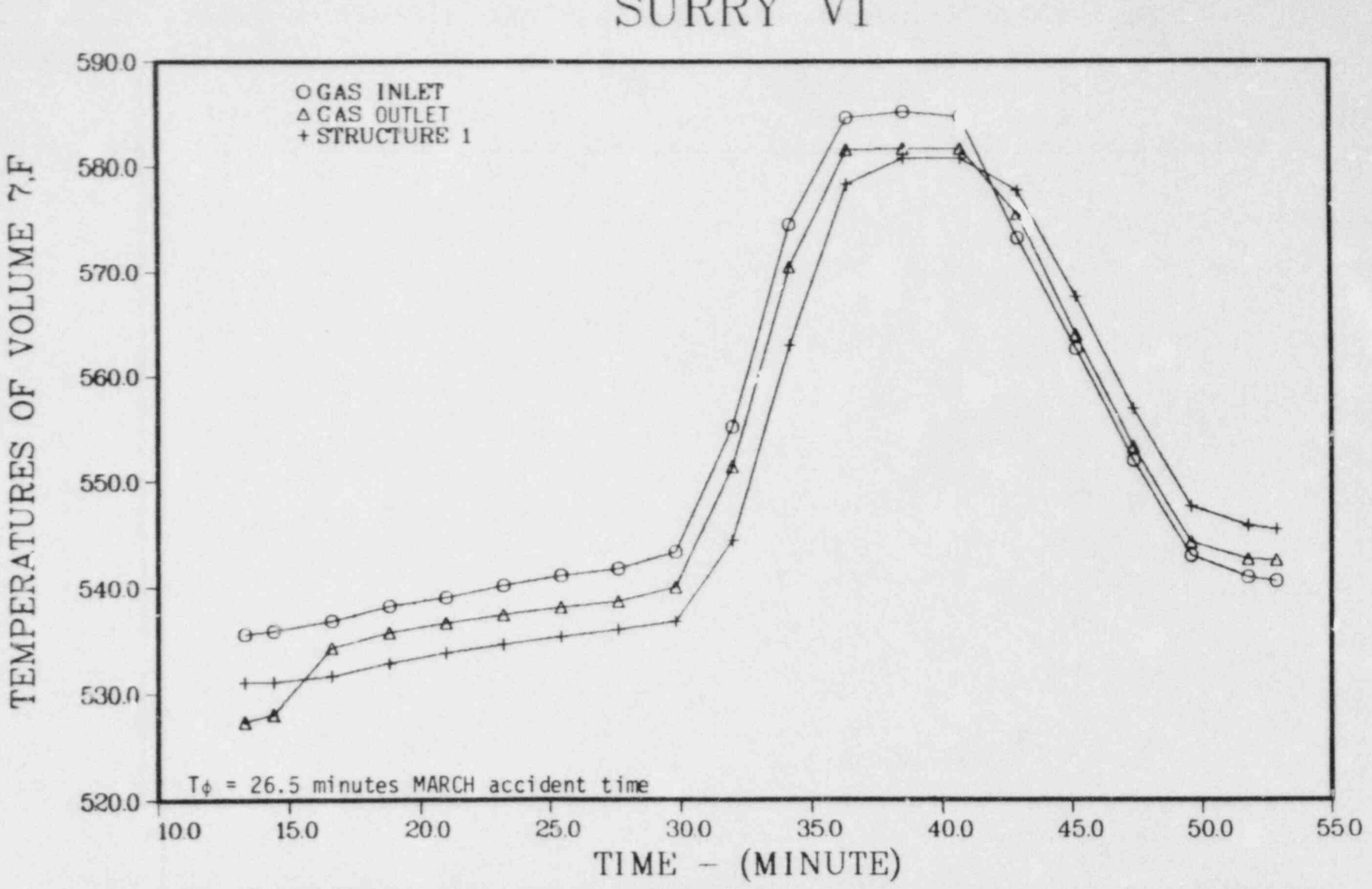

FIGURE 6.19c. EMERGENCY CORE COOLING SYSTEM PIPING TEMPERATURES FOR SURRY V SEQUENCE

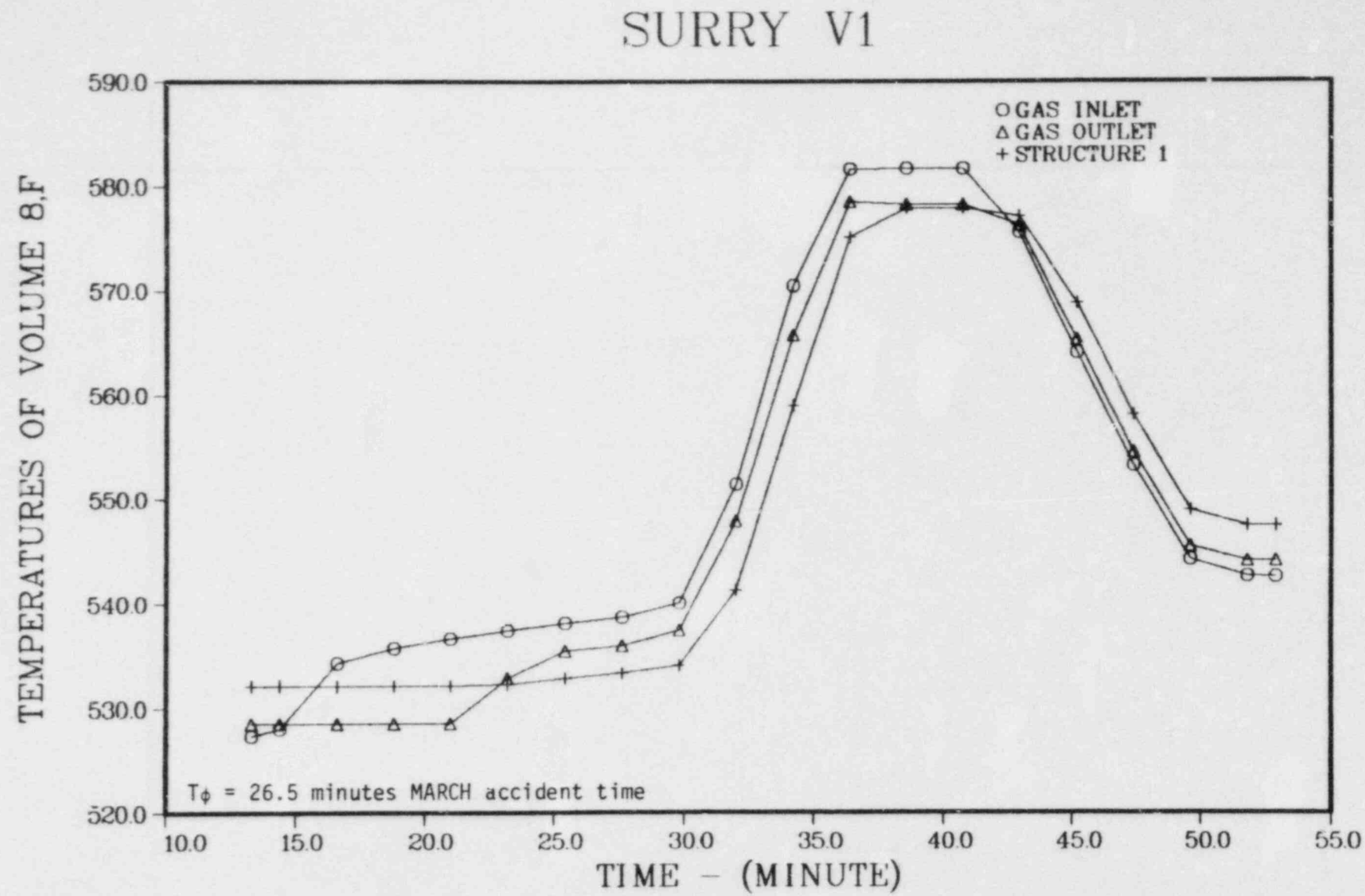

FIGURE 6.19d. EMERGENCY CORE COOLING SYSTEM PIPING TEMPERATURES FOR SURRY V SEQUENCE

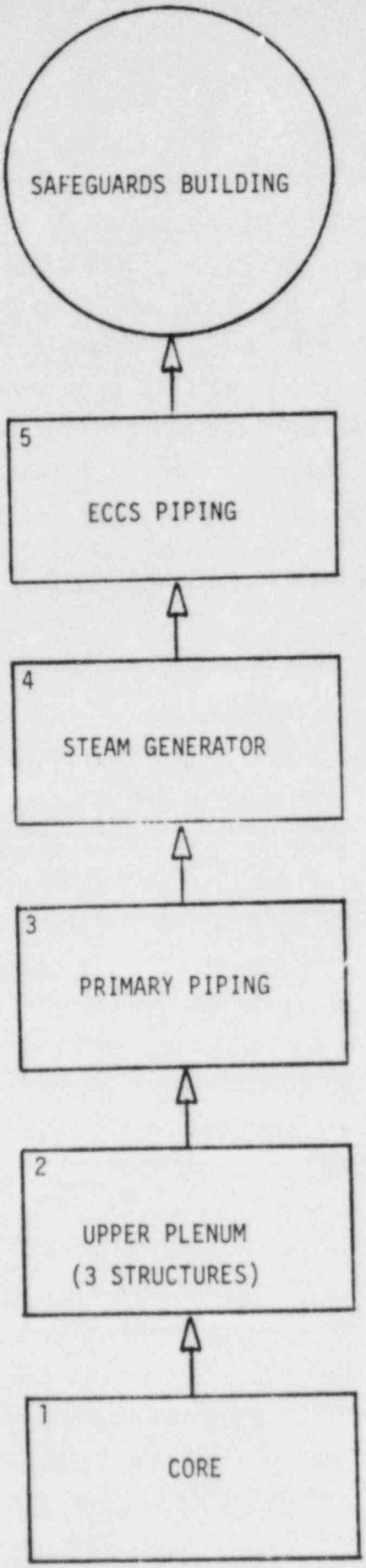

FIGURE 6.20 SCHEMATIC OF MERGE CONTROL VOLUMES FOR SURRY V SEQUENCE

periods when rapid transient loadings may be encountered. Two containment failure modes were considered for this sequence: an early overpressure failure resulting from hydrogen combustion (S_2D-γ), and basemat melt-through failure with no direct atmospheric failure of the containment (S_2D-ϵ). The timing of significant events is given in Table 6.2. Core and primary system parameters are summarized in Table 6.3. Selected core node temperatures are illustrated in Figures 6.21a and 6.21b. The predicted temperatures of gases and structures in the primary system are illustrated in Figures 6.22a, 6.22b, and 6.22c. Volume 2 again represents the upper plenum with its associated structures, Volume 3 represents the hot leg piping, and Volume 4 represents the steam generator. In these figures, the time is measured from the start of core uncovery. A schematic of the gas flow path for S_2D is illustrated in Figure 6.23.

Table 6.4 summarizes the containment response at key times during the accident sequence. Since the rate of primary coolant loss is restricted by the break size and the containment sprays are operational, pressure in the containment would remain relatively low during most of this accident sequence. This is illustrated by the pressure history for the melt-through case in Figure 6.24; the corresponding temperature history is given in Figure 6.25. Substantial containment pressure increases would require the accumulation and subsequent coherent burning of large amounts of hydrogen.

For the case of failure due to a hydrogen burn, the latter was assumed to take place following vessel failure when the hot core debris entered the reactor cavity. The ejection of the hot core debris into the containment would provide the ignition source for the burn. The containment pressure and temperature histories for such a hydrogen burn are given in Figures 6.26 and 6.27. This burn produced a peak pressure of about 0.62 MPa (90 psia); the calculated peak pressure can be sensitive to the timing of the assumed burn.

In assuming containment failure due to such a burn, no representation is made as to the likelihood of failure. If the containment maintains its integrity through challenges such as hydrogen burning, it is likely that the basemat will eventually be penetrated due to the attack of the concrete by the core and structural debris. The time required for melt-through would provide ample opportunity for fission product removal by the sprays. If sufficient spray water can continuously reach the reactor cavity, a coolable debris

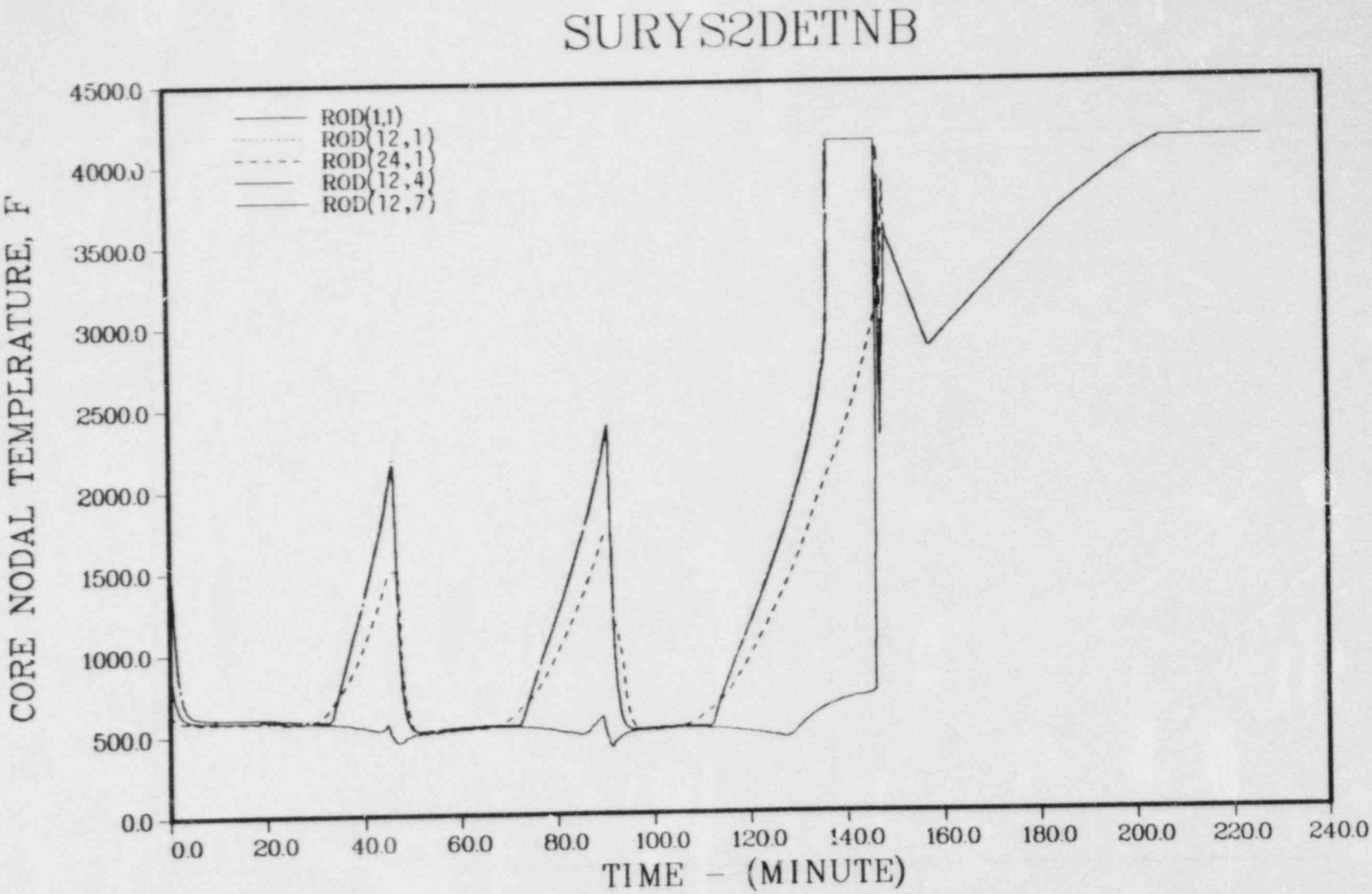

FIGURE 6.21a. SELECTED CORE NODE TEMPERATURES FOR SURRY S_2D

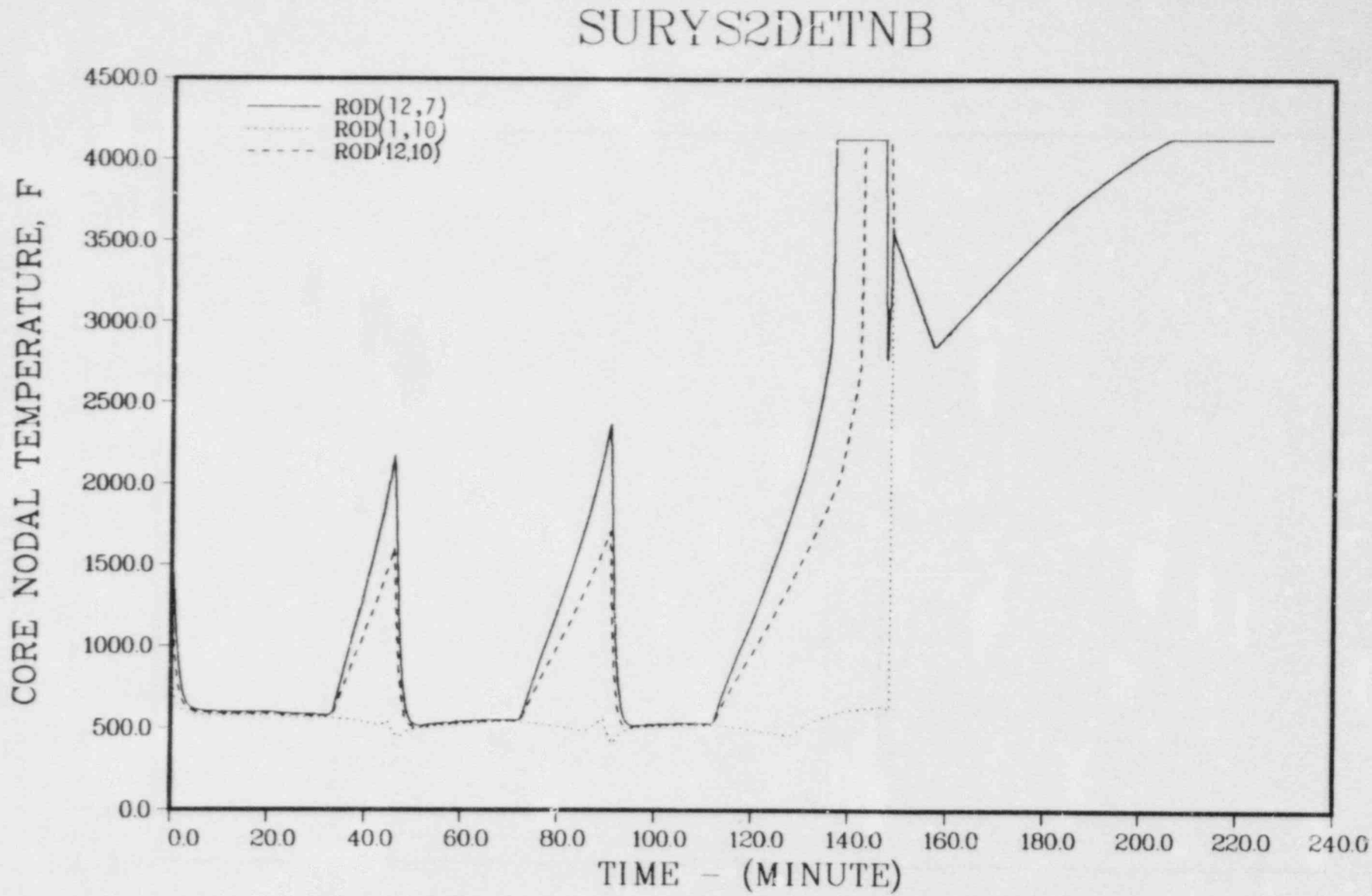

FIGURE 6.21b. SELECTED CORE NODE TEMPERATURES FOR SURRY S_2D

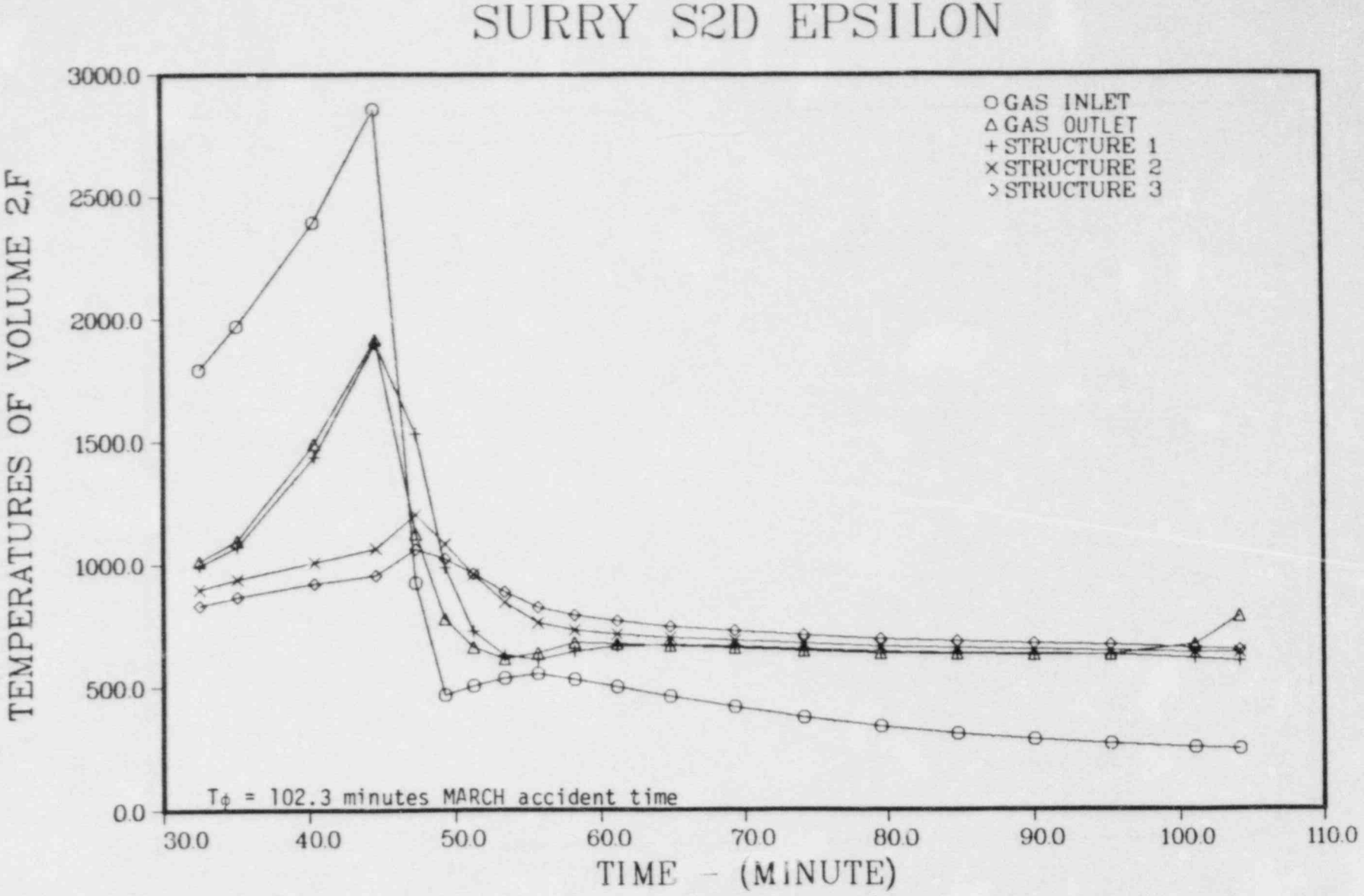

FIGURE 6.22a. PRIMARY SYSTEM GAS AND STRUCTURE TEMPERATURES FOR SURRY S_2D-ϵ SEQUENCE

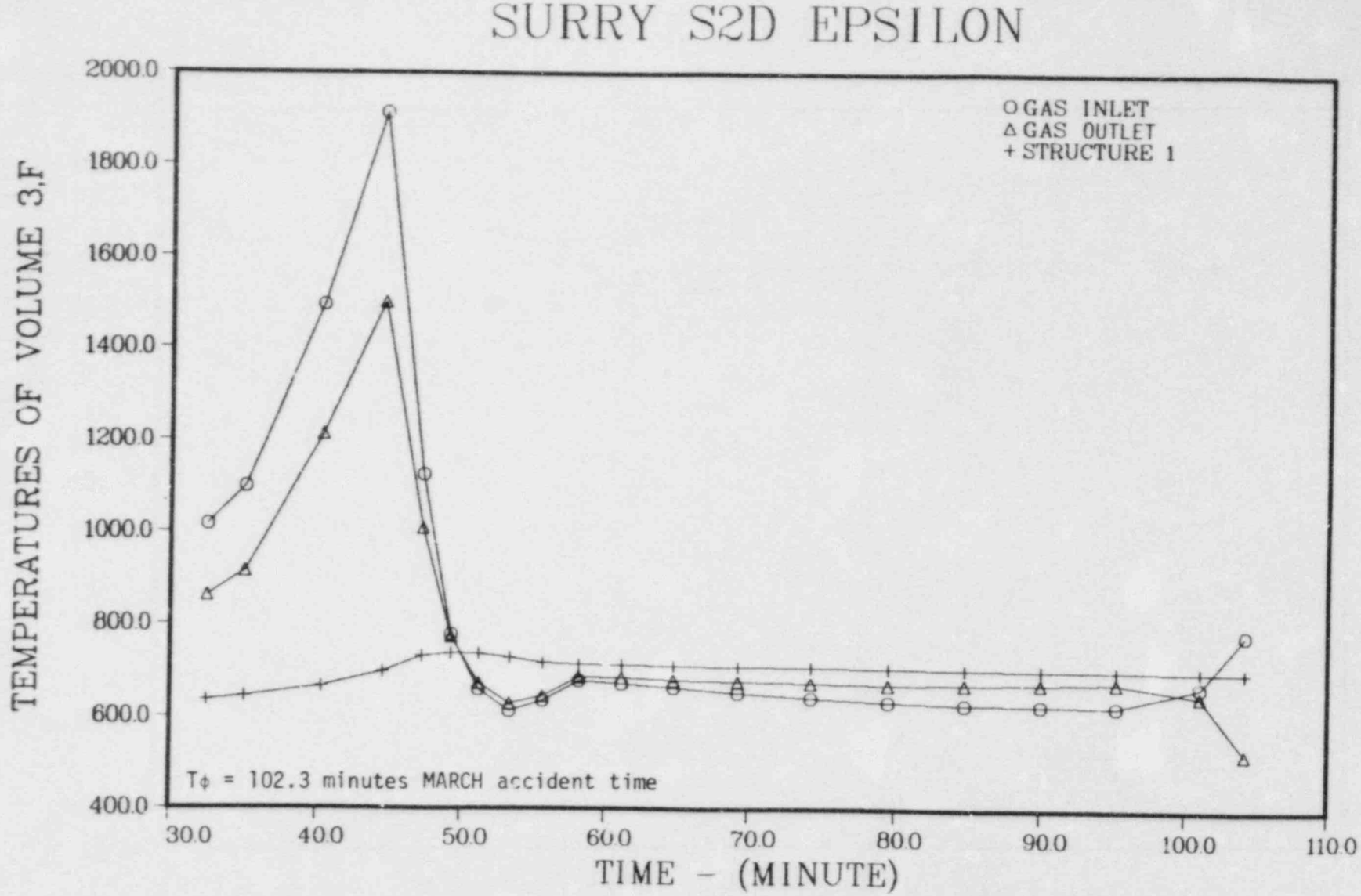

FIGURE 6.22b. PRIMARY SYSTEM GAS AND STRUCTURE TEMPERATURES FOR SURRY S_2D-ϵ SEQUENCE

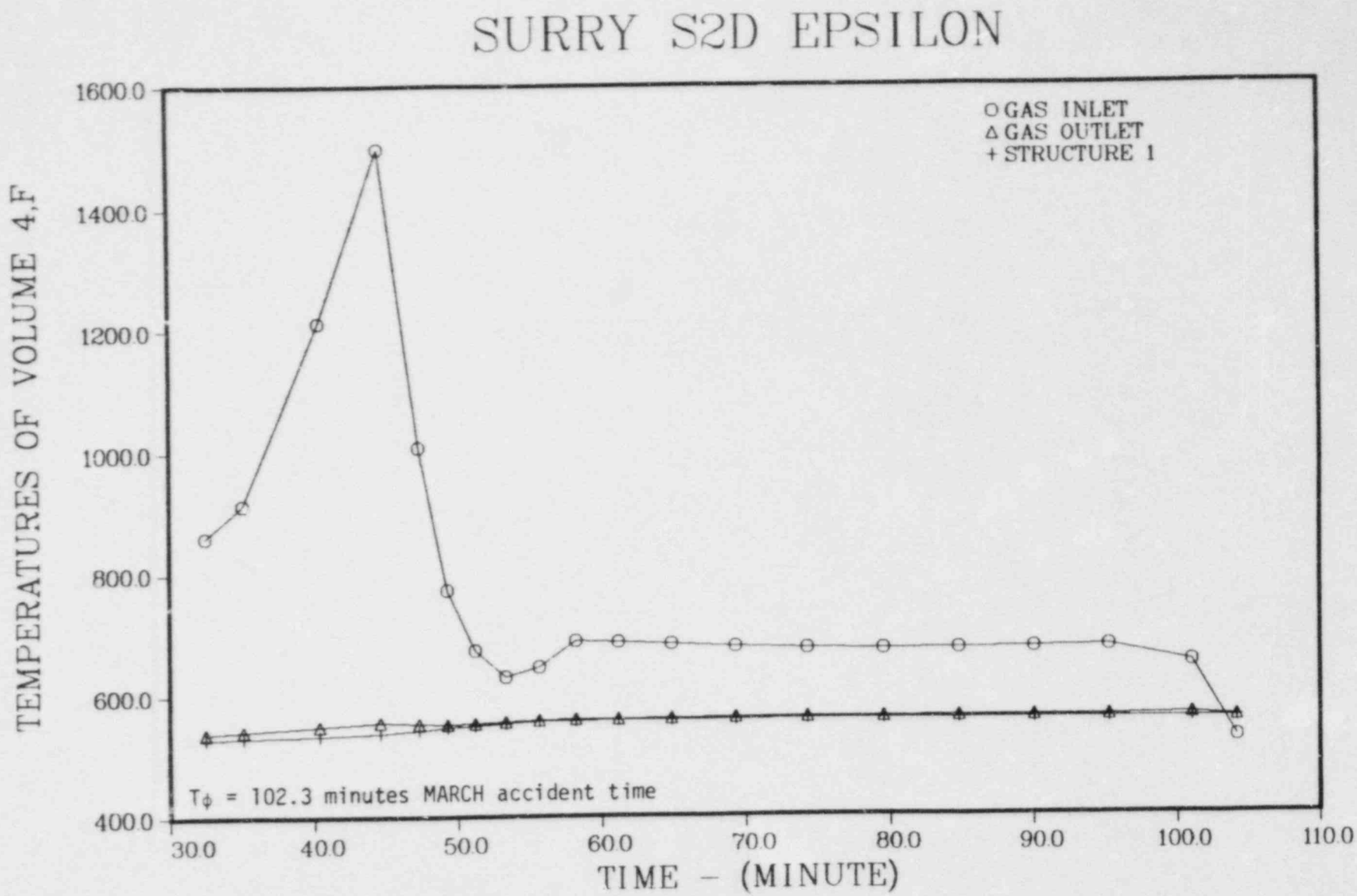

FIGURE 6.22c. PRIMARY SYSTEM GAS AND STRUCTURE TEMPERATURES FOR SURRY S_2D-ϵ SEQUENCE

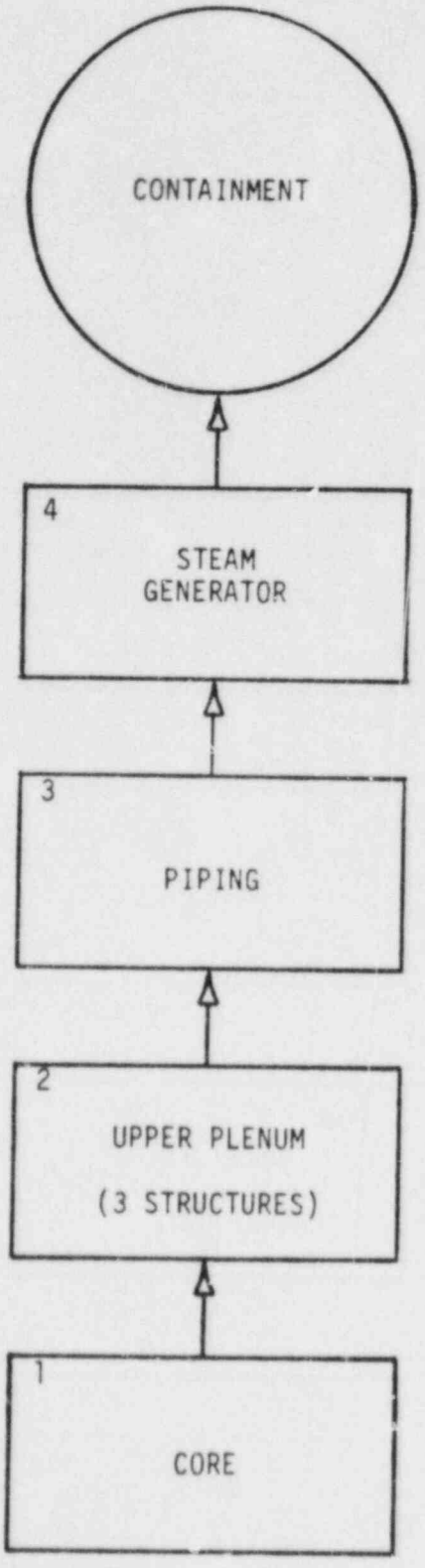

FIGURE 6.23 SCHEMATIC OF MERGE CONTROL VOLUMES FOR SURRY S_2D SEQUENCE

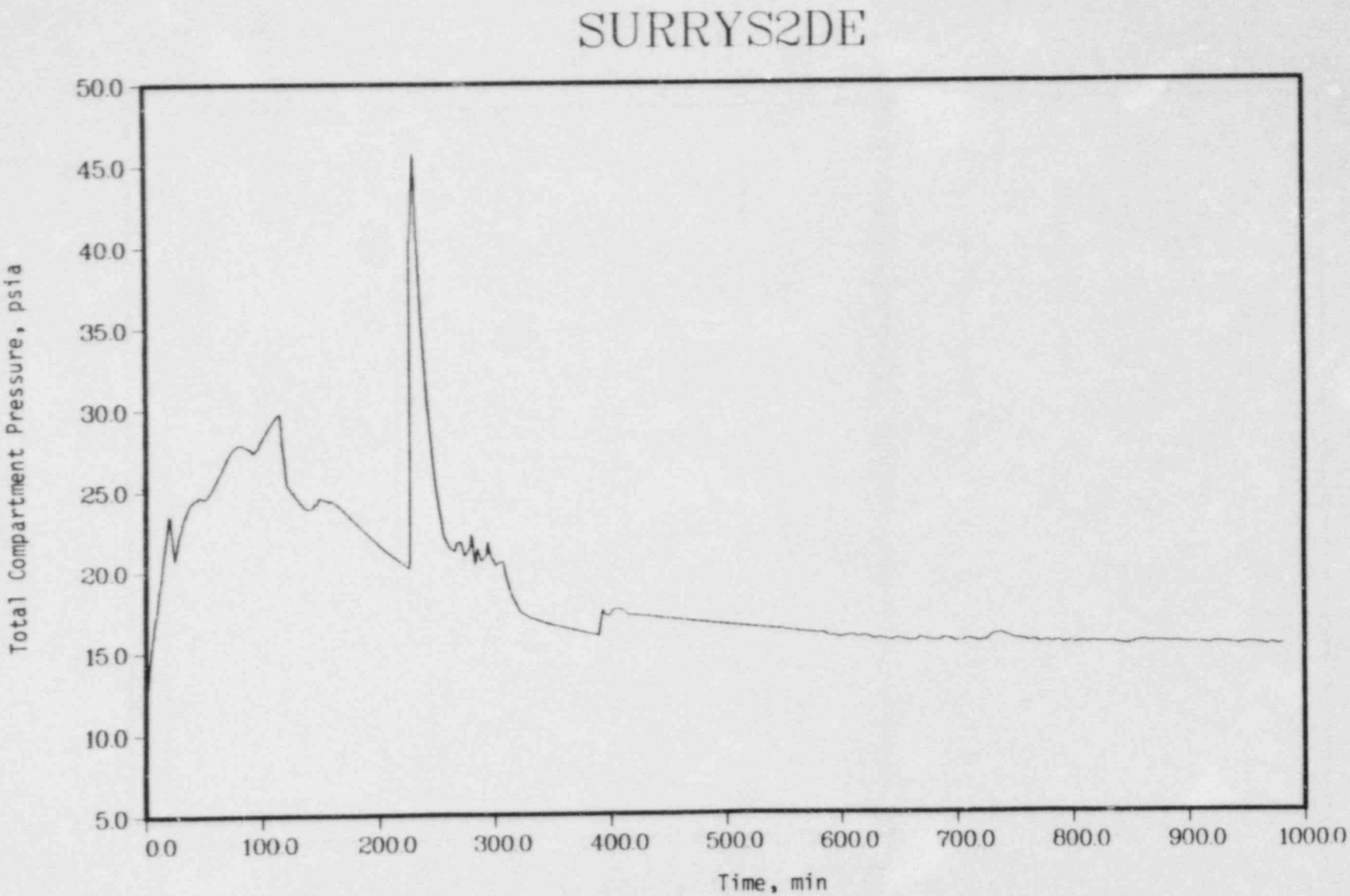

FIGURE 6.24 CONTAINMENT PRESSURE RESPONSE FOR SURRY S_2D-ϵ SEQUENCE

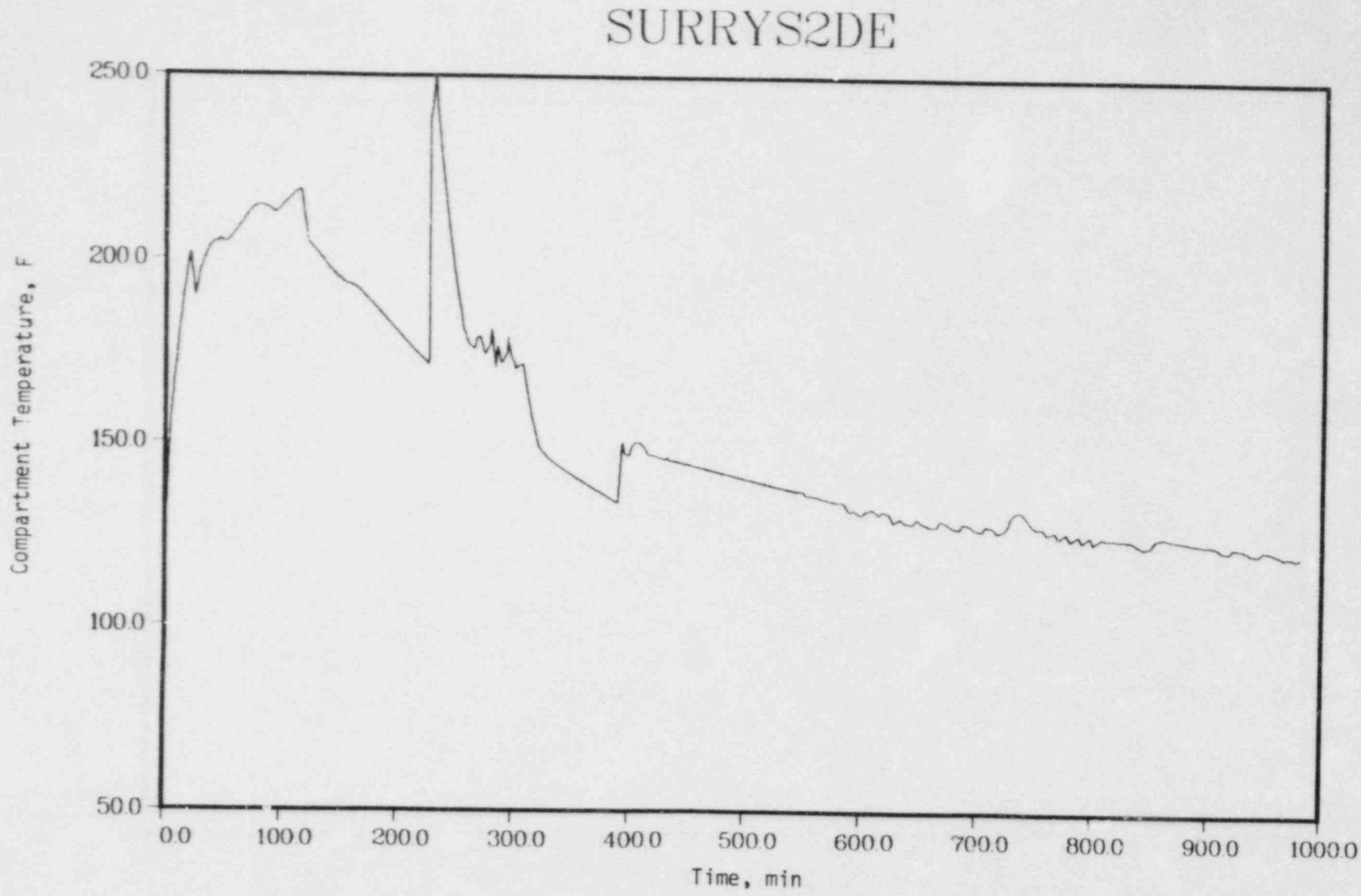

FIGURE 6.25 CONTAINMENT TEMPERATURE RESPONSE FOR SURRY S_2D-ϵ SEQUENCE

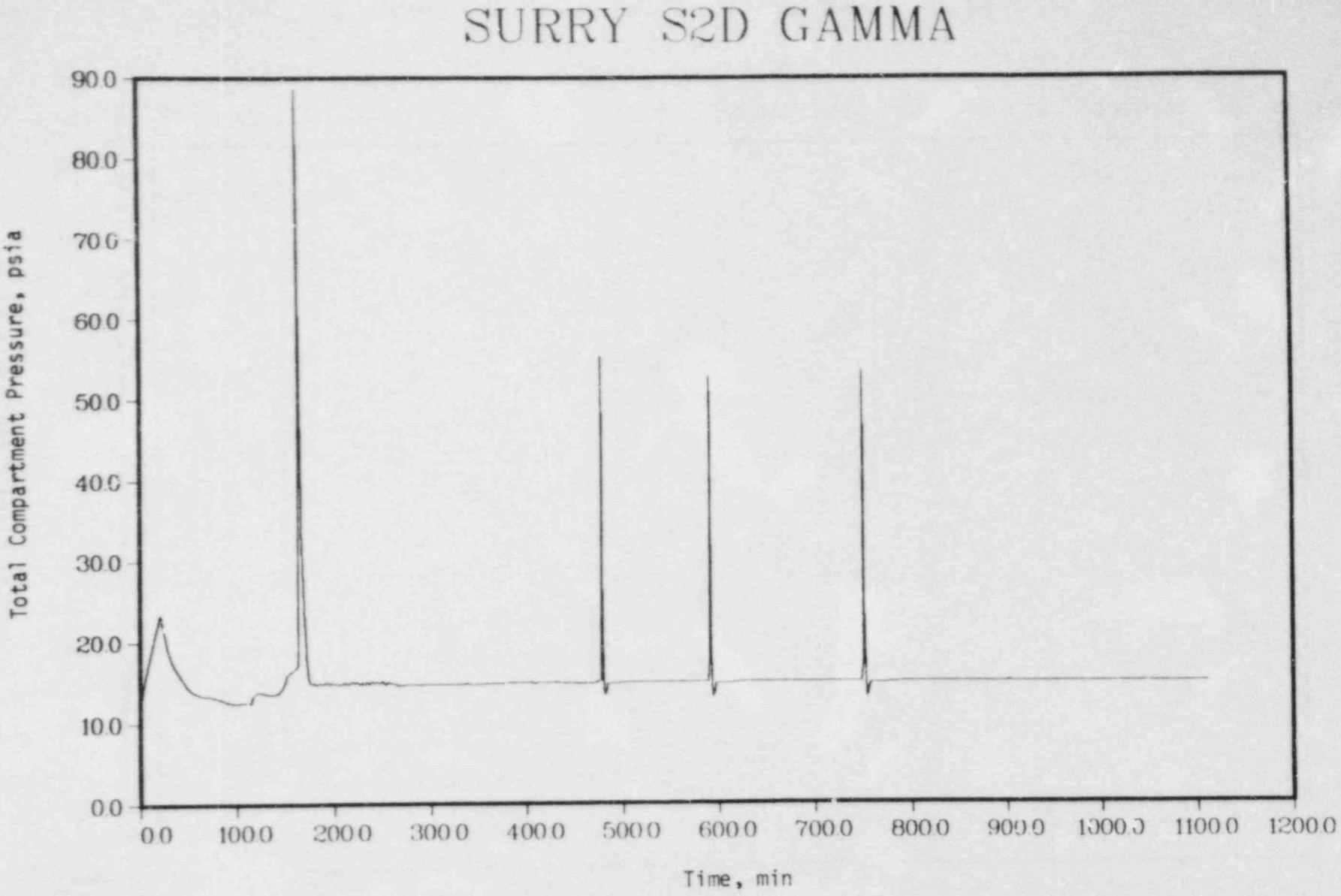

FIGURE 6.26 CONTAINMENT PRESSURE RESPONSE FOR SURRY S_2D-Y SEQUENCE

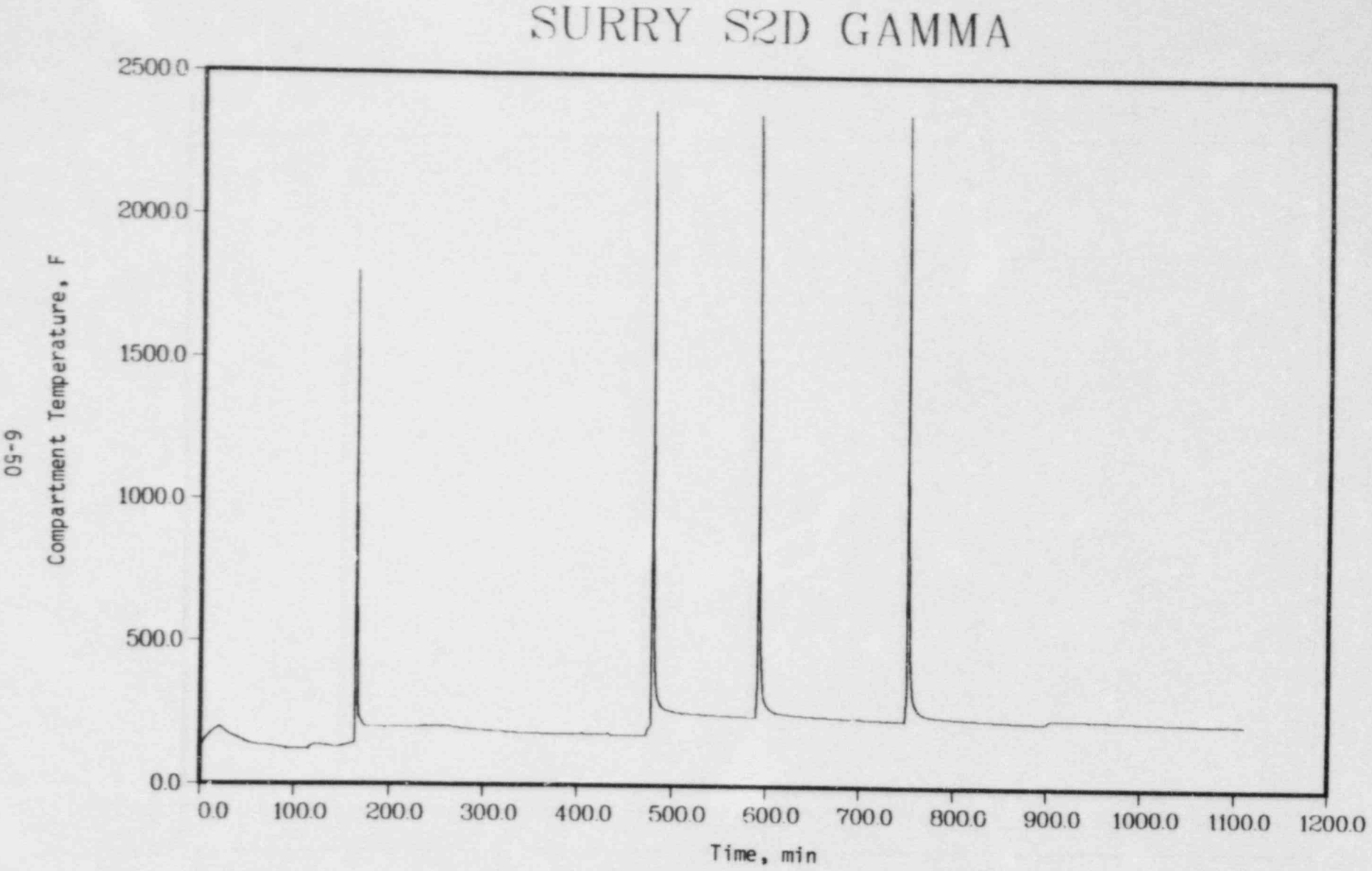

FIGURE 6.27 CONTAINMENT TEMPERATURE RESPONSE FOR SURRY S_2D-Y SEQUENCE

bed could form. In such a case, the S_2D sequence would be terminated without containment breach.

Table 6.5 summarizes the containment leakages derived from the MARCH calculations that were used in the evaluation of fission product releases from the containment.

6.1.5 Other Cases Considered

The primary containment in the above cases was modeled as a single compartment with its inherent assumption of being well mixed. For the AB-β and V sequences, the releases from the primary containment were input into the safeguards building before their release to the atmosphere. Thus the potential for fission product deposition in the safeguards building was included in the analyses for these two cases. In the other sequences, the release from the primary containment was directly to the environment.

To investigate the possible effects of containment compartmentalization on the release of radioactivity to the environment, the AB-β sequence was reformulated to model the primary containment as a system of four interconnected compartments. While the Surry containment has many internal structures and partitions, the flow paths between adjacent subcompartments are typically very large, and multiple flow paths are possible. Thus there is no obvious unique approach to containment compartmentalization. The containment model in MARCH is restricted to handling only compartments connected in series. The four-volume representation utilized was a practical compromise between the actual containment design and the code modeling capabilities. With the four-compartment containment model, the melt release took place into a different compartment than the vaporization release, i.e., the melt release was assumed to enter one of the steam generator cubicles and the vaporization release was into the reactor cavity. The location of the containment leak was in still another compartment.

In the V sequence, the rupture of the coolant system takes place in the low pressure emergency core cooling system piping outside the primary containment. There is a long length of pipe between the core where the fission products leave the fuel and the safeguards building where they leave the piping. In the base-case analysis, this piping was represented as a single volume. To

gain insight on the possible sensitivity of the predictions this analysis was repeated with the piping being divided into four equal volumes.

The analyses for this sequence as discussed up to this point have included consideration of fission product deposition in the safeguards building but have taken the safeguards building as an open structure.

A number of variations of the V sequence are possible. The effect of the primary system blowdown on the secondary structures may result in significant changes in secondary building integrity. Other questions relate to the operability of various engineered safety feature systems and/or components: e.g., does the failure of the low pressure emergency core cooling system piping necessarily imply failure of the emergency core cooling system pumps? If some of these pumps are operable, they could serve to delay the time of core uncovery and subsequent overheating, or in the least they could flood the area in which the break in the system is postulated and thus provide a possible mechanism for fission product removal.

While many variations of the V sequence can be postulated, it has been suggested by Stone & Webster, the Architect-Engineer for the Surry plant, that a realistic consideration of the building layout in the area where the emergency core cooling piping is located and where the break in the system is postulated, would lead to the conclusion that this area would be flooded by the water from the refueling water storage tank. Representatives of Stone & Webster have indicated that the compartment where the system break is likely to occur, given the other assumptions related to the definition of this sequence, would be flooded to a depth of 5 feet above the floor of the compartment. The water depth would be limited to this height by an opening in the wall at this level; additional water would spill through this opening to other parts of the plant. Since the piping is aproximately 2 feet off the floor, the effluent from the primary system would have to pass through about 3 feet of water before being released to the safeguards building atmosphere and subsequently to the environment. The volume of water contained on the floor of this compartment is understood to be approximately 30,000 gallons.

An additional analysis was performed to investigate the possible fission product attenuation by passage through the 3 feet of water if the sequence of events is as described above. The water in the Surry refueling water storage tank is maintained at a temperature of 45 F to improve its

IMAGE EVALUATION
TEST TARGET (MT-3)

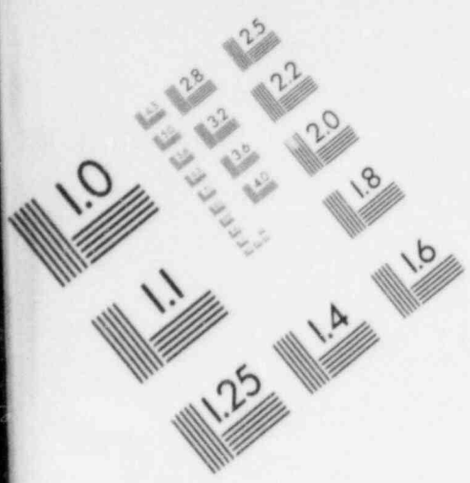

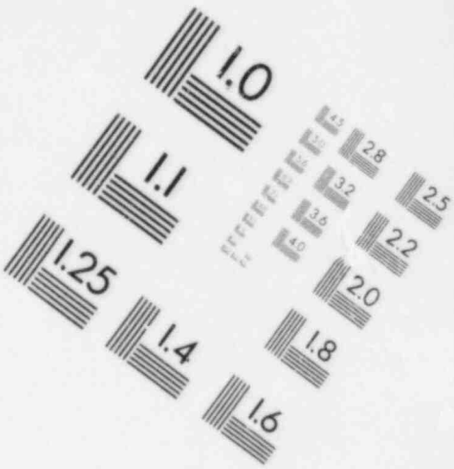

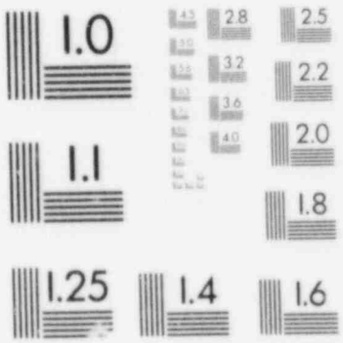

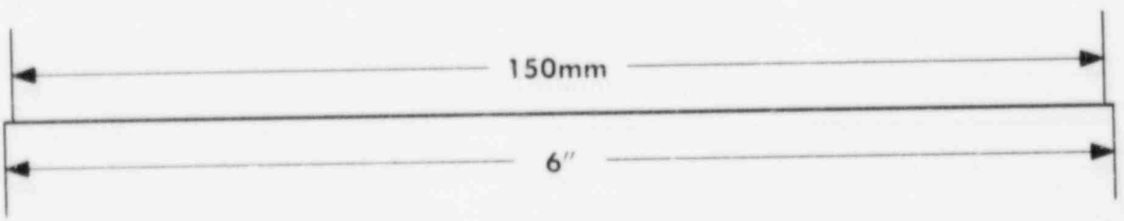

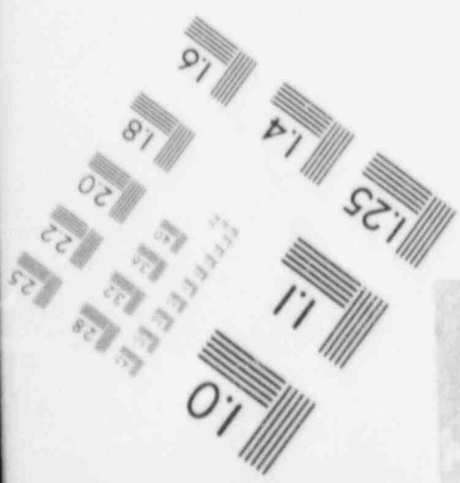

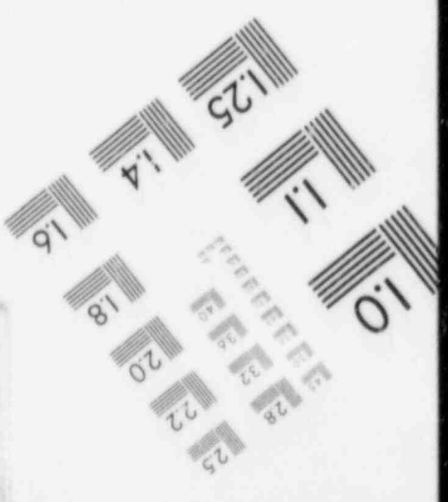

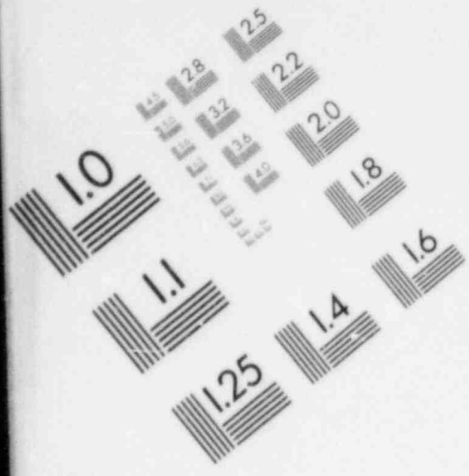

IMAGE EVALUATION TEST TARGET (MT-3)

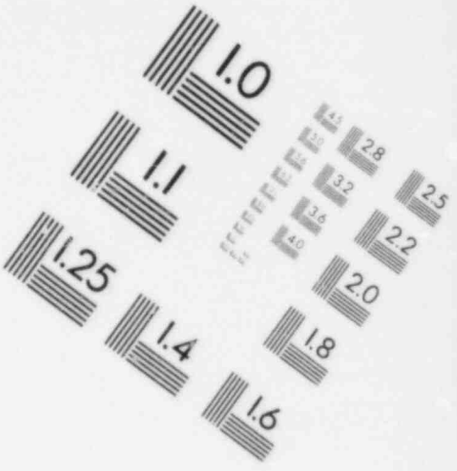

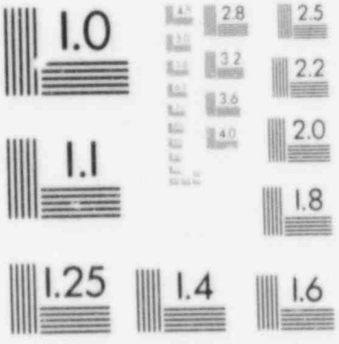

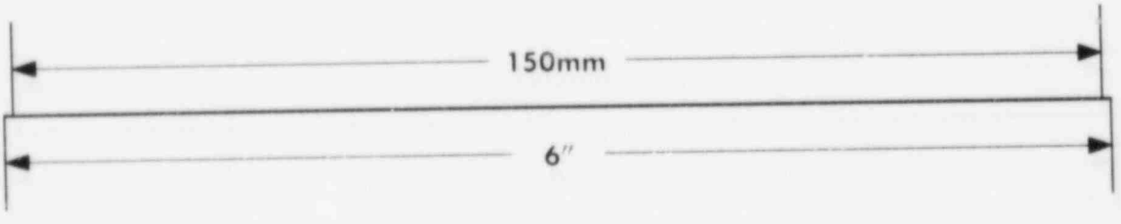

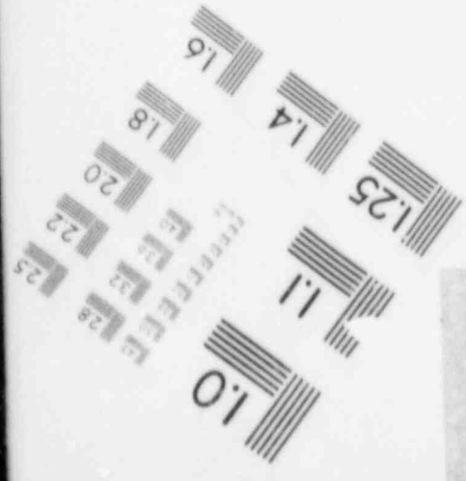

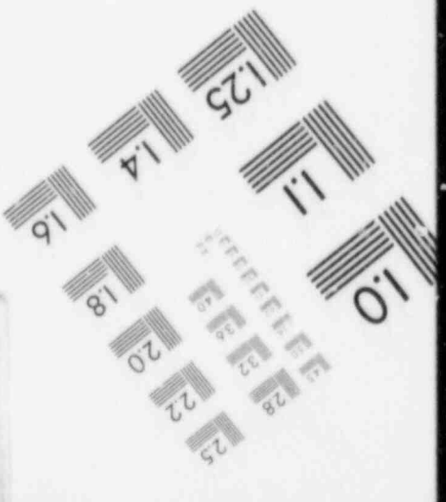

effectiveness for emergency core cooling purposes. After spilling to the floor of the compartment, this water would be heated by the passage of steam generated during core uncovery and subsequently by the high temperature steam and hydrogen during core melting. It is possible that some of the water on the floor would be boiled off during these stages of the accident, and this has been calculated by Stone & Webster staff to give a reduction in water depth of a few inches. For purposes of the additional fission product attenuation analyses, it was assumed that the water was heated to saturation at atmospheric pressure and that the submergence of 3 feet was maintained throughout the duration of the accident sequence. The releases from the primary system were then input into the SPARC code to determine aerosol attenuation by this pool of water.

An additional calculation was performed accounting for water spilled on the floor of the safeguards building for the V sequence. The water was assumed saturated and a submergence of 3 feet was used as discussed in Section 6.1.5. Table 7.18b shows the calculated locational distribution of fission products in various compartments as predicted by the additional calculation. When compared with 7.18a, the additional fission product attenuation due to the water present in the safeguards building is found to be significant. It should be noted that for a rigorous calculation, it is necessary to perform a complete thermal-hydraulic analysis for this sequence to obtain the accurate temperature conditions of water and of the safeguard atmosphere.

6.1.6 General Discussion

The release and transport of fission products are strongly influenced by the thermal-hydraulic behavior of the accident. The computer codes MARCH 2 and MERGE that have been used to predict the thermal-hydraulic conditions treat various aspects of accident behavior with different degrees of confidence. In the following paragraphs, the principal areas of uncertainty in the analyses, simplifying assumptions and approximations, and the implications for fission product transport will be discussed.

In the MARCH 2 analyses of fuel heatup, the reactor core was subdivided into 24 axial and 10 radial mesh regions. The variation that would occur in the timing of heatup and fission product release across the core is well characterized. Up to the point of cladding melting and fuel/cladding

liquefaction, the theoretical treatments of the thermal behavior of the fuel and oxidation of the cladding are supported by experimental data. Reasonable agreement has been obtained in the past between different computer codes in analyzing this behavior. The MARCH code makes the simplifying approximation that the fuel would melt at a single characteristic temperature which is input. The selected input melting temperature of 2550 K (4130 F) has been chosen to be between the temperature at which the fuel would dissolve into molten zirconium and the melting point of uranium dioxide. In the actual system, melting would occur over the above range of temperatures up to the melting point of uranium dioxide, with the actual melting or liquidus temperature being a function of local composition and state of oxidation. As a result of the single melting point approximation, the peak fuel temperatures predicted by MARCH may be underestimated for some quantity of fuel. The time for which fuel stays at elevated temperature is also very dependent on modeling uncertainties. These uncertainties will have little effect on the predicted release of volatile fission products but could affect the vaporization of involatile materials, most likely by underprediction.

The MARCH analyses for the present study utilized meltdown model "A" with no movement of fuel out of the core until the bottom node in any radial region was molten. At that point, the molten nodes in that region were allowed to slump to the core support plate. As the bottom nodes in successive radial regions melted, these regions were allowed to slump. When 75 percent of the core was molten, the entire core was assumed to slump into the lower head of the reactor vessel. The assumptions regarding fuel slumping and ultimate collapse into the vessel bottom head also affect the driving forces for fission product transport, the timing of reactor vessel dryout, and subsequent analyses of head heatup and failure. MARCH does not attempt to describe fuel melting and movement mechanistically. There is no actual redefinition of core geometry. The slumping models attempt to treat mathematically what would happen if the fuel were to move in accordance with the selected scenario. These representations are highly intuitive but have some support from core meltdown simulation experiments.

The MERGE code was developed specifically for the analysis of reactor coolant system temperatures in this study. There is very little past experience in performing this type of analysis. The flow patterns in the system could be

quite complex, particularly in the upper plenum region, and are treated approximately. If there is substantial internal recirculation, both the fission product residence time and the heating of structures could be higher than calculated here. The flow within the reactor coolant system is treated as one-dimensional, with well-mixed volumes. Natural convection within the upper plenum is considered in predicting the heat transfer to structures. Although convection patterns are not examined explicitly, the mixing which is expected to result would be consistent with the well-mixed approximation. The one-dimensional treatment of the upper plenum does not take into account the radial temperature profile of gases leaving the core and transporting through the upper plenum. The calculated temperatures are averages across the flow cross section and would be expected to be higher near the center and lower near the periphery.

As demonstrated later in this report, the timing of containment failure has a major impact on the predicted release of fission products to the environment. The pressure level at which the containment would be expected to fail is input into MARCH. To the extent that this failure pressure is uncertain (typically it is quite uncertain), it would tend to compound any uncertainties associated with MARCH code calculations. The thermal-hydraulic conditions within the containment can be predicted with relative confidence if the driving forces are well defined. The principal early challenges to containment integrity are the rapid steam generation from core debris interaction with water and the burning of hydrogen. The analysis of steam generation from debris quenching is particularly uncertain and is sensitive to the input and modeling assumptions utilized. This phenomenology is inherently uncertain and one in which unique answers, except in a bounding sense, cannot be expected.

The prediction of the pressures due to hydrogen burning is fairly straightforward if the initial conditions and the timing of the burn are known; however, this is generally not the case, and key assumptions must be made. The amount of hydrogen present in the containment at any point in time is subject to the uncertainties in the prediction of core slumping, vessel failure, debris interactions in the cavity, etc. For any set of conditions, the composition of the atmosphere and its potential flammability can be tracked as a function of time. Except in the presence of igniters, however, the occurrence of ignition cannot be predicted and must be assumed. Typically containment integrity

would be challenged by large coherent burns, but it would not be challenged by extended combustion; the timing of the ignition is the key difference between the two predictions.

Tables 6.6 and 6.7 provide the information on which the calculations of radionuclide transport and deposition in the containment were based. Table 6.6 gives containment geometrical data, and Table 6.7 provides containment spray parameters.

6.2 Radionuclide Sources

6.2.1 Source Within Pressure Vessel

Inventory

The reactor fission product inventory which was used in all four sequences considered in this report is based upon ORIGEN calculations for the Surry plant with a three region model, with the maximum burnup corresponding to 33,000 MW days/ton. Table 6.8 contains the inventory of the fission products and control rod structural materials. Since release rate information is not available for all these species, rates for members of the various groups considered in the Reactor Safety Study were taken to be equal when no other information was available.

The nonfission product materials constitute the bulk of the aerosol mass released during core melting. The value for Ag in this table is based on a total of 1060 control rods composed of 81 mol percent Ag, 14 mol percent In, and 4.9 mol percent Cd. The inventory of fission products was distributed according to the power peaking factors in Table 6.9, and the control rod and structural materials were distributed according to the volume of each radial node.

Release From Fuel

The rates for radionuclide release from the fuel were computed using the CORSOR code for the core temperature profiles specific to each accident sequence. The mass of each species of interest released as a function of time

is shown in Figures 6.28 through 6.32 for the AB, TMLB', V, and S_2D sequences. Two runs of CORSOR were performed for the S_2D sequences, ϵ and γ. This was done because the conditions which give rise to the γ containment failure mode engender somewhat different temperatures in the melting fuel and produce a significantly different time to bottom head failure. In these figures, aerosol materials were considered to be the sum of fission products Sb, Sr, Ba, Ru, Mo, Zr, and A[illegible], along with nonfission products Fe, UO_2, Zr (cladding), Ag, In, Cd, and Sn. After melt-through of the reactor pressure vessel, the release during the core-concrete interaction was taken as a release to the containment. The inventory available for release during the core-concrete interaction is listed in Tables 6.10 and 6.11.

Regrouping of Released Species

In order to track the Reactor Safety Study groups independently, an additional CORSOR run was performed for the AB and TMLB' sequences which produced release rates for all groups. A description of the makeup and methodology for release of each group follows.

- Group 1 (Xe, Kr) -- Xe and Kr releases were summed and a release rate computed. This group was not previously computed.

- Group 2 (I, Br) -- Br release was not considered due to an absence of data concerning Br release and its small inventory relative to I (1:16).

- Group 3 (Cs, Rb) -- Thermodynamic and physical properties of Rb justify treating it identically to Cs. As a result, the Rb inventory was lumped into the Cs inventory for treatment by CORSOR. Releases for I and Cs were combined to produce release rates for CsI and CsOH which were the forms assumed to be transporting through the primary system. This assumption is based on the predicted temperatures and gas compositions combined with consideration of the likely chemical thermodynamic equilibrium states.(6.1,6.2)

- Group 4 (Te, Se, Sb) -- Se and Sb were not considered based on their small inventory and lack of data concerning their behavior. Their inclusion in this group would be further complicated by the dependence of Te release on Zircaloy oxidation.

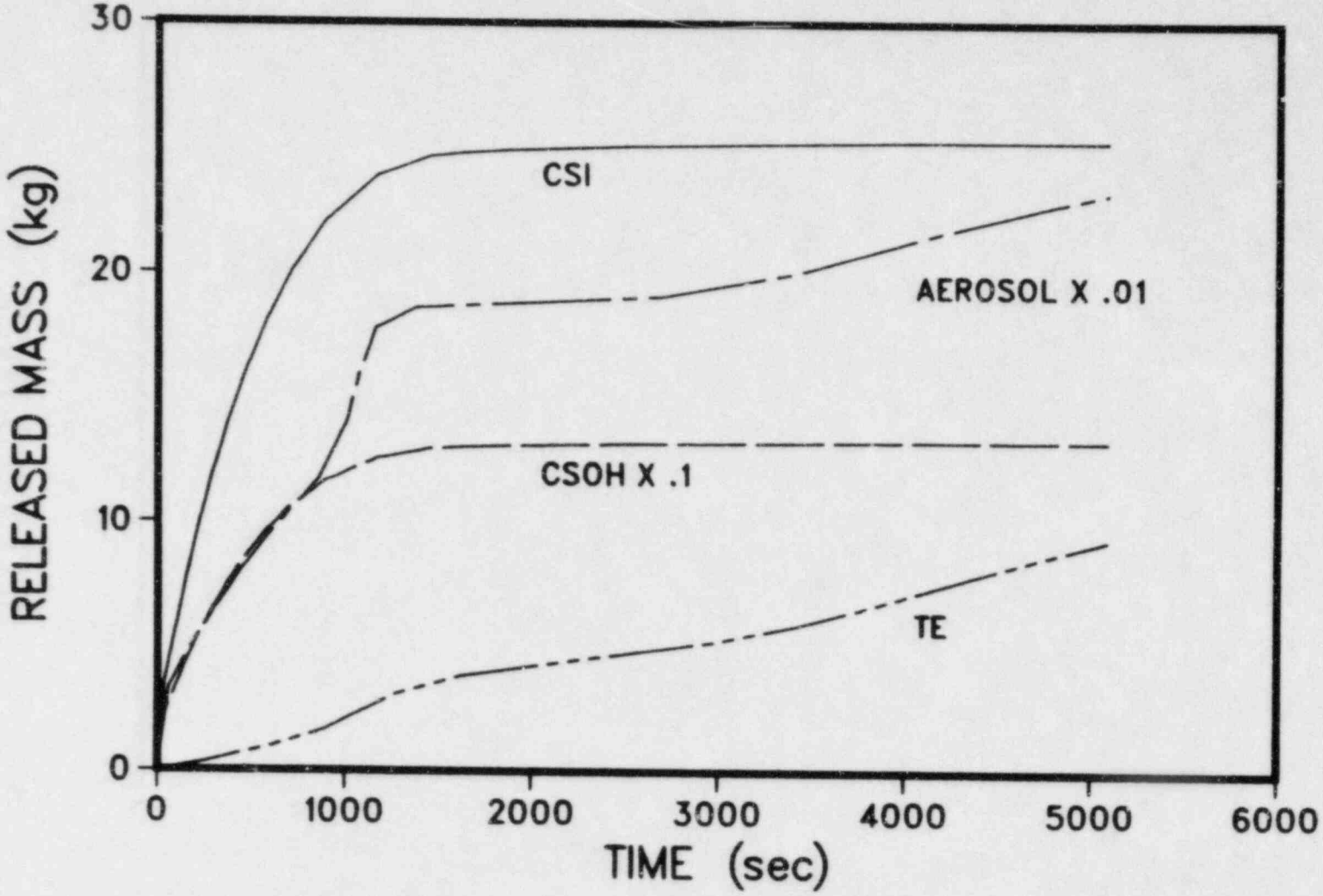

FIGURE 6.28. CORSOR PREDICTIONS OF SPECIES MASS RELEASED FROM THE CORE DURING THE AB SEQUENCE FOR THE SURRY PLANT

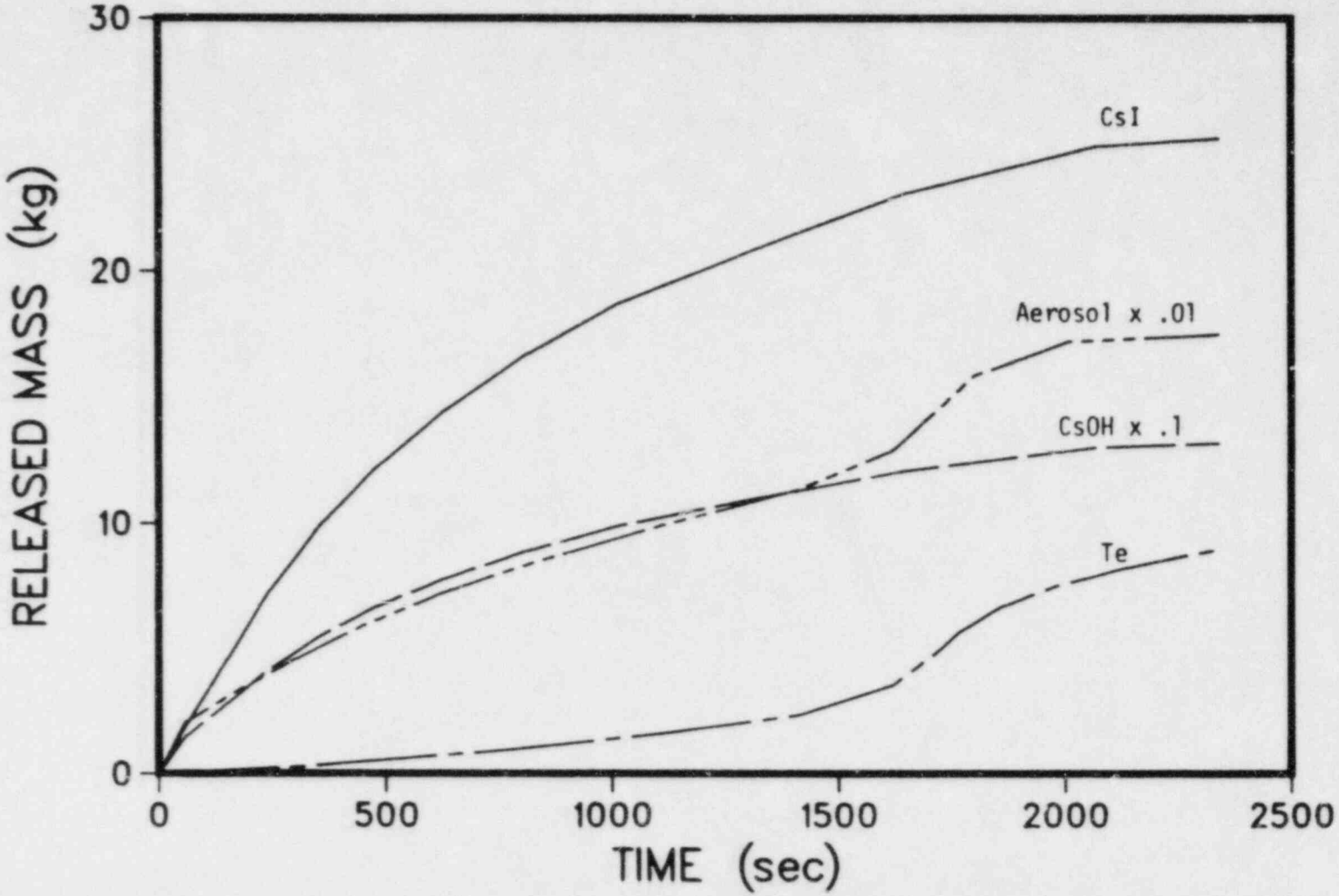

FIGURE 6.29. CORSOR PREDICTIONS OF SPECIES MASS RELEASED FROM THE CORE DURING THE TMLB SEQUENCE FOR THE SURRY PLANT

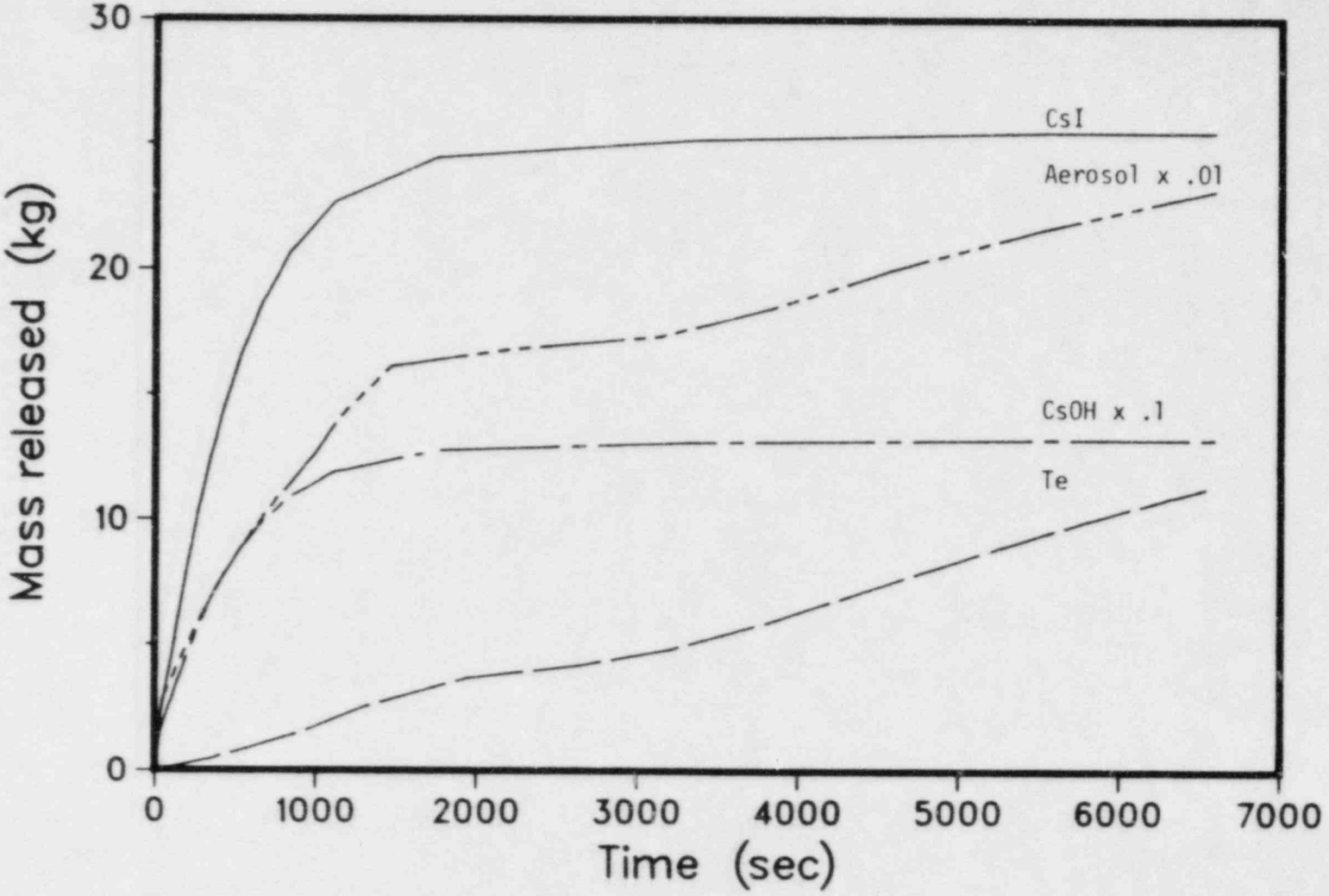

FIGURE 6.30. CORSOR PREDICTIONS OF SPECIES MASS RELEASED FROM THE CORE DURING THE V SEQUENCE FOR THE SURRY PLANT

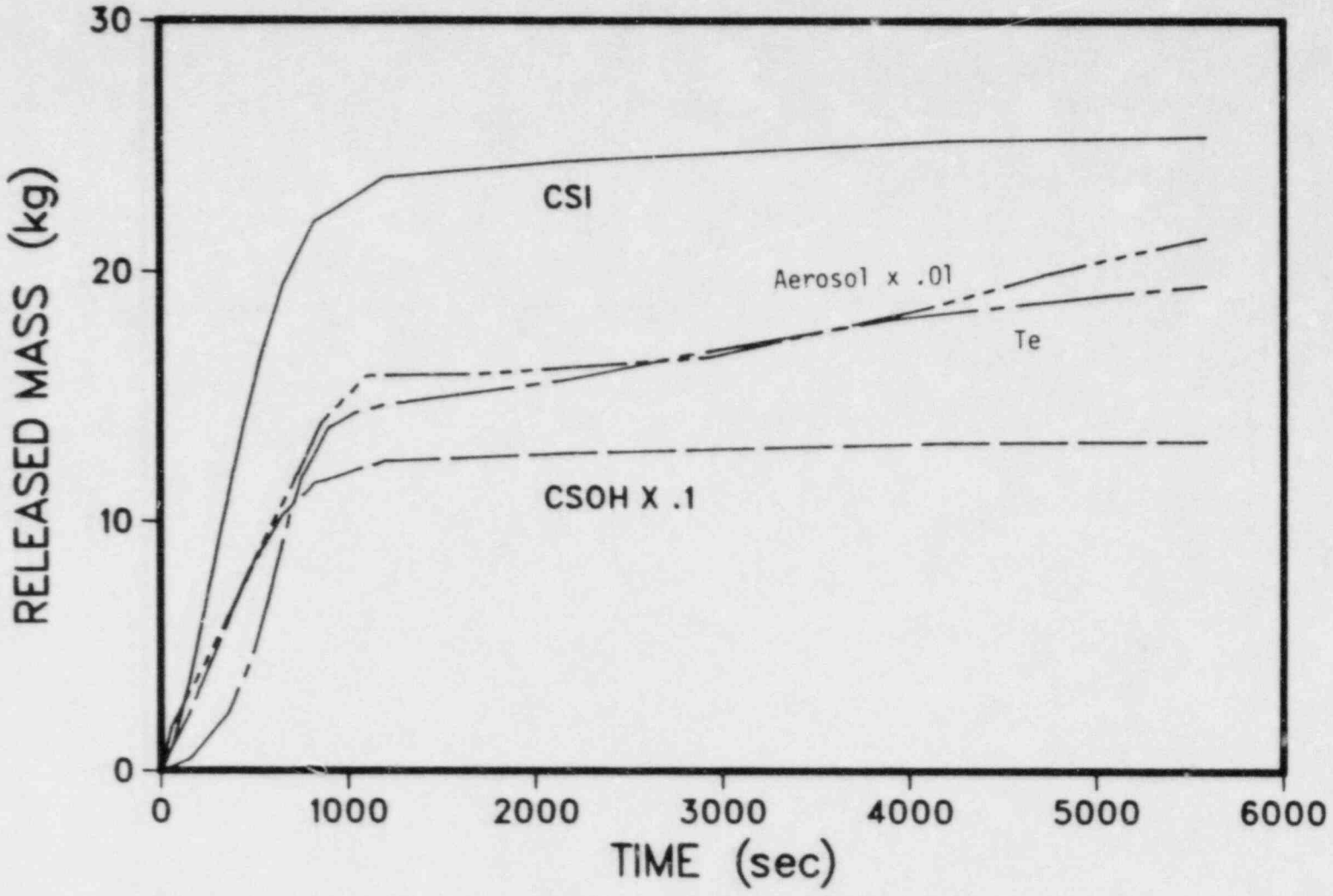

FIGURE 6.31. CORSOR PREDICTIONS OF SPECIES MASS RELEASED FROM THE CORE DURING THE S_2D-ϵ SEQUENCE FOR THE SURRY PLANT

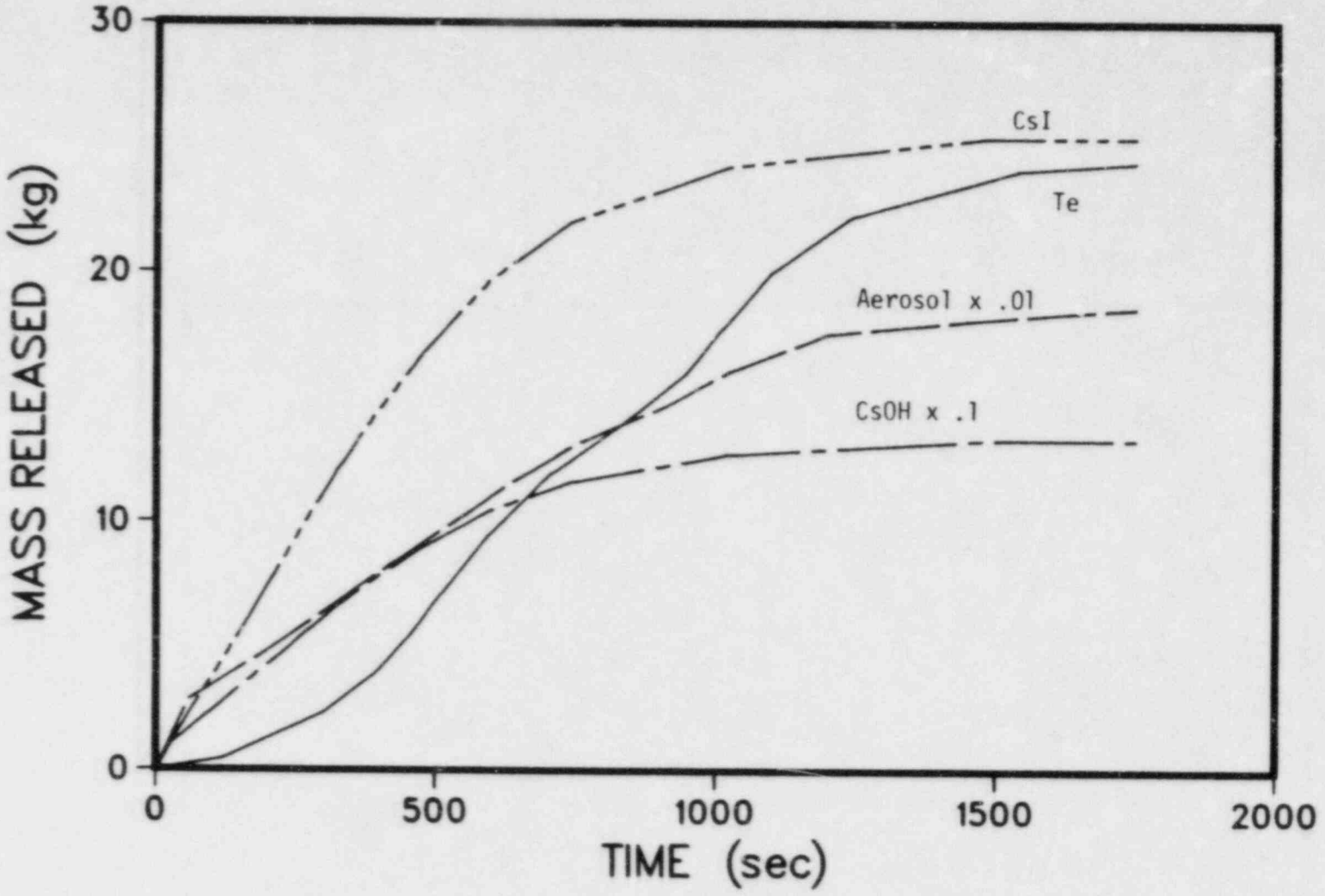

FIGURE 6.32. CORSOR PREDICTIONS OF SPECIES MASS RELEASED FROM THE CORE DURING THE S_2D-γ SEQUENCE FOR THE SURRY PLANT

- Group 5 (Ba, Sr) -- Ba and Sr were released separately and their releases summed to form the release rates for this group. Further, their releases were not included in the aerosol materials sum.

- Group 6 (Rh, Pd, Tc, Ru, Mo) -- Rh, Pd, and Tc inventories were added to the Ru inventory for purposes of release. The releases of Ru and Mo were then summed to produce release rates for this group. The aerosol materials sum does not include Mo or Ru releases.

- Group 7 (La, Y, Eu, Nd, Np, Sm, Pm, Pu, Zr, Ce, Nb, Pr) -- All members of Reactor Safety Study Group 7 with the exception of Zr were treated identically for purposes of release, using UO_2 release rate coefficients. Their release and the release of Zr were summed to produce release rates for this group. Table 6.8.B lists initial inventories of Group 7 members not included in Table 6.8.

- Aerosol Materials (Fe, UO_2, Zr (cladding), Sn, control rod: Ag, Cd, In) -- The release rate for this group includes only nonfission products.

Table 6.8.C lists initial inventories and final CORSOR releases for the Reactor Safety Study groups and compares the results from AB and TMLB' sequences.

It is necessary to select an initial particle size for those materials forming the aerosol species. It has been shown[6.3] that when significant agglomeration occurs, the initial aerosol size has a negligible effect on subsequent aerosol behavior after agglomeration has proceeded for a very short time. Nevertheless, initial particle sizes were chosen to correspond to the best available information. Numerous reviews of experimental mean aerosol sizes from vaporizing and condensing fuel will be from slightly below 0.01 μm to about 0.1 μm with the most likely size being about 0.05 μm.[6.4,6.5] A number median radius of 0.05 μm and a geometric standard deviation of 1.7 were assumed for the primary particles in the current analyses, and a bulk density of 3 g/cc was assumed for the particles.

6.2.2 Sources within the Containment

Radionuclides enter the containment as they are transported through the primary system and on melt-through of the reactor pressure vessel. Material that is still suspended in the RCS is transported into the containment as the RPV and containment pressures equalize. The final source considered is material that is released during the core-concrete interaction. Because of a lack of release information or, even more generally, a lack of evidence that they are of potential importance, sources sometimes postulated as arising from steam explosions (oxidation release) or from jet emission of hot, molten corium at the time of RPV failure were not included in these analyses.

Release from Primary System

The source to the containment of material penetrating the primary system is defined in mass input rate by species of interest and on a time-dependent basis by the output from the TRAP-MELT calculations. Also provided in the TRAP-MELT output is the size distribution of the particulate material. This calculated information is included in Chapter 7.

Volatile metals, leaving the primary system are assumed to be condensed as they enter the containment to particles having the same size distribution as the particles otherwise predicted to be released from the primary system.

Release from Core-Concrete Interaction

VANESA was used to predict aerosol and gas release rates and compositions as a function of time. The composition of the core materials contacting the concrete was, as determined with the CORSOR code, to be the materials remaining in the melt at the time of head melt-through. These compositions for the various sequences are given in Tables 6.10 and 6.11. The concrete was taken to be basaltic ($CaCO_3$ = 0.05, CaOH = 0.09, SiO_2O = 0.60, H_2O = 0.04, Al_2O_3 = 0.22), and the initial temperature of the molten material was as calculated with the MARCH code. The total release rates and composition of

the release are given in Tables 6.12 through 6.16. These rates and compositions define the source to the drywell after vessel failure.

Source Term for Volatile Iodides

In a previous section it has been shown that the thermodynamics of the cesium-iodine-hydrogen-oxygen system indicate that iodine will be present primarily as a nonvolatile iodide in the primary coolant system. After release from the primary system, a small fraction of the iodine inventory in the containment is believed to be present as volatile iodides.[6.1] The presence of volatile iodide species in containment-type systems has been observed in experiments[6.6] and in the TMI-2 post-accident containment atmosphere.[6.7] At present, the mechanisms responsible for the generation of these volatile iodides are not well understood. Since a theoretical model is not available, an empirical approach has been selected for the formulation of a source term for volatile iodides. This source term consists of two components. One component represents the fraction of the containment iodine inventory which is present as volatile iodides before containment failure. The second component represents a generation rate for volatile iodides after containment failure. The containment inventory of volatile iodides present prior to containment failure was estimated from levels observed in TMI-2[6.7] and from estimates of the probable detection limits in relevant experiments.[6.8] The volatile iodide generation rate was estimated from a conservative evaluation of the measurements of the airborne iodine levels in the TMI-2 containment over the time period from 100-2000 hours after reactor trip. Based on these estimates it has been assumed for this study that 0.05 percent of the containment iodine inventory will be present as volatile iodides prior to containment failure and after containment failure, additional volatile iodides will be generated at a rate of 2×10^{-7} fraction/hour of the containment iodine inventory.

Of this volatile iodine source, it is believed that a fraction of the iodine inventory in a reactor containment will be present as volatile organic iodides (predominantly CH_3I).[6.1] (Other volatile species may also be present.) Therefore, in the analysis of reactor accidents involving a radionuclide release from the reactor system and containment failure, formation in the containment and subsequent release of organic iodides should be considered.

Unfortunately, the mechanism responsible for the generation of organic iodides has not yet been elucidated. As a result, it is not yet possible to establish a definitive source of organic iodides. Early estimates of the organic iodine source terms were based on a conservative interpretation of experimental systems studies.[6.6,6.9] Early thermodynamic studies predicted that organic iodides should be present in much smaller concentrations than observed in experiments.[6.10] These calculations predicted that CH_3I would comprise only 10^{-4} percent of the total gaseous iodine inventory modeled. Experimental data[6.6] and "chemical species specific" measurements of the TMI-2 airborne iodine inventory[6.7] imply that the concentration of organic iodides present in a reactor containment during and following an accident may be higher than the concentrations predicted by thermodynamic calculations for an equilibrium system. Additionally, observations of the airborne iodine behavior at TMI-2[6.7] imply the presence of competing sources and sinks for volatile iodine species. In light of these data, a kinetic description may be required to adequately quantify the time dependence of the organic iodide concentration in reactor containments during and following reactor accidents. Pending results of studies, such as those which are currently under way,[6.2] use of a general source term for volatile iodides rather than separate source terms for CH_3I, I_2, etc., has been assumed as noted above.

References

(6.1) Technical Base for Estimating Fission Product Behavior During LWR Accidents, NUREG-0772, (June, 1981).

(6.2) Torgerson, D. F., et al., Fission Product Chemistry Under Reactor Accident Conditions, presented at the International Meeting on Thermal Nuclear Reactor Safety, Chicago, Illinois, U.S.A. (September 1982).

(6.3) Jordan, H., Schumacher, P. M., and Gieseke, J. A., "Comparison of QUICK Predictions with Results of Selected, Recent Aerosol Behavior Experiments", NUREG/CR-2922, BMI-2089 (September, 1982).

(6.4) Gieseke, J. A., et al, "Aerosol Source Term for Fast Reactor Safety Analysis", BMI-X-637 (August 11, 1972).

(6.5) Nuclear Aerosols in Reactor Safety, CSNI/SOAR No. 1 (June, 1979).

(6.6) Postma, A. K. and Zavodoski, R. W., Review of Organic Iodide Formation Under Accident Conditions in Water-Cooled Reactors, WASH-1233 (1972).

(6.7) Pelletier, C. A., et al., Preliminary Radioiodine Source Term and Inventory Assessment for TMI-2, SAI-139-82-12-RV (September, 1982).

(6.8) Lin, C. C., Chemical Effecs of Gamma Radiation on Iodine in Aqueous Solutions, J. Inorg. Nucl. Chem., 42, pp. 1101-1107 (1980).

(6.9) Reactor Safety Study: An Assessment of Accident Risks in U.S. Commercial Nuclear Power Plants, WASH-1400 (1974).

(6.10) Barnes, R. H., Kircher, J. F., and Townley, C. W., Chemical Equilibrium Studies of Organic Iodide Formation Under Nuclear Reactor Accident Conditions, BMI-1816 (1966).

TABLE 6.1. REACTOR CHARACTERISTICS, CONTAINMENT PARAMETERS, AND MARCH OPTIONS FOR LARGE DRY PWR CONTAINMENT

ECC storage and injection tanks

	Accumulator		RWST	
Weight of water	171,300 lb	77,700 kg	2.92×10^6 lb	1.3245×10^6 kg
Initial pressure	665 psia	45.9 MPa	14.7 psia	0.1 MPa
Temperature	120 F	48.89 C	45 F	7.22 C

Fractional value of RWST to start ECC recirculation: 0.01

Fractional value of RWST to start spray recirculation: 0.143

Large LOCA blowdown

Time, min	Enthalpy		Blowdown Rate	
	Btu/lb	J/kg	lb/min	kg/s
0	602.7	288,400	2.115×10^6	1.599×10^4
.20	602.7	288,400	2.115×10^6	1.599×10^4
.201	89.73	42,930	2.770×10^5	2.094×10^3
.401	89.73	42,930	2.770×10^5	2.094×10^3

Calculated model input

Core heatup section:

Number of radial zones: 10

Number of axial zones: 24

Meltdown model: BOIL model A

Core melting temperature: 4130 F (2277 C)

Core slumping: Starts when lowest node in a zone has melted

Core collapse: Occurs when 75 percent of core has melted

Zircaloy - water reaction: Urbanic-Heidrick reaction rate data, hydrogen blanketing, steam limited, continues for melted nodes, reaction of molten Zircaloy in the bottom head calculated.

TABLE 6.1. (Continued)

End of blowdown conditions for large LOCA:

Water in vessel: core covered

Peak core temperature: 1700 F (927 C)

Accumulators: empty

Bottom head failure section:

Head melting temperature: 2800 F (1538 C)

Debris melting temperature: 4130 F (2277 C)

Heat loss from top of debris: Radiation to core barrel

Debris thermal conductivity: 8 Btu/hr ft F (0.1384 w/cm/C)

Tensile strength of vessel: σ = min (80,000, 1.49×10^{16} TEMP-3.9105), lb/in^2

Reactor cavity processes, debris fragmentation:

Particle diameter: 0.5 inch (1.27 cm)

Particle thermal conductivity: 2.0 Btu/hr ft F (0.0346 w/cm/C)

Reactor cavity processes, concrete decomposition:

Metal-concrete interface heat transfer coefficient: HIM = 0.01 w/cm^2 K

Oxide-concrete interface heat transfer coefficient: HIO = 0.01 w/cm^2 K

Top surface emissivity: E = 0.5

Heat to cover water: film boiling plus 50 percent of area radiating at internal temperature of top layer.

Containment Section:

Atmosphere-wall heat transfer coefficient:

$h = h_c$ (TSAT-TWALL) + 0.19 $(T-TWALL)^{4/3}$ /(T-TWALL)

h_c = 0 if TSAT < TWALL

2.0 < h_c = Uchida data < 280 Btu/hr ft^2 F

Containment break area: 7.0 ft^2 overpressure failure (0.65 m^2)

0.349 ft^2 isolation failure (0.0324 m^2)

TABLE 6.1. (Continued)

Failure of safety systems:
(1) Containment failure fails the containment sprays
(2) Containment failure fails ECR if sump is saturated.

TABLE 6.2 ACCIDENT EVENT TIMES

Event	Time, minutes
	Surry AB-ε
Core Uncover	9.4
Start Melt	24.8
Core Slump	42.1
Core Collapse	43.3
Bottom Head Dry	64.4
Bottom Head Fail	110.1
Start Concrete Attack	110.1
Containment Leak	1450.6
End Calculation	1639.6
	Surry AB-Y
Core Uncover	9.4
Start Melt	24.8
Core Slump	42.1
Core Collapse	43.5
Bottom Head Dry	64.4
Bottom Head Fail	110.1
Start Concrete Attack	110.1
Hydrogen Burn	268.9
Containment Fail	268.9
End Calculation	710.7

TABLE 6.2 (Continued)

Event	Time, minutes	
	Surry AB-8	
	4 Volumes	2 Volumes
Core Uncover	7.1	9.4
Start Melt	24.6	27.2
Core Slump	41.5	44.6
Core Collapse	42.5	45.6
Bottom Head Dry	62.5	65.8
Bottom Head Fail	97.9	104.3
Start Concrete Attack	97.95	104.4
Hydrogen Burn	108.1	198.2
Hydrogen Burn	129.1	
Hydrogen Burn	145.4	
Hydrogen Burn	226.9	
End Calculation	698.3	704.6
	Surry TMLB'-8	
Steam Generator Dry	67.5	
Core Uncover	95.5	
Start Melt	118.3	
Core Slump	146.3	
Core Collapse	148.0	
Bottom Head Fail	152.8	
Containment Fail	152.9	
Reactor Cavity Dry	177.2	
Start Concrete Attack	254.2	
End Calculation	1073.4	

TABLE 6.2 (Continued)

Event	Time, minutes
Surry TMLB'-ε	
Steam Generator Dry	67.5
Core Uncover	95.5
Start Melt	118.3
Core Slump	146.3
Core Collapse	147.3
Bottom Head Fail	157.3
Reactor Cavity Dry	214.9
Start Concrete Attack	289.9
Containment Fail	738.2
End Calculation	1100.0
Surry S2D-ε	
Containment Spray Injection On	20.0
Containment Spray Recirculation On	25.0
Core Uncover	27.8
Accumulators Empty	91.5
Containment Spray Injection Off	114.7
Start Melt	134.6
Core Slump	147.3
Core Collapse	148.8
Bottom Head Fail	227.5
Reactor Cavity Dry	325.7
Start Concrete Attack	407.7
End Calculation	2210.4

TABLE 6.2 (Continued)

Event	Time, minutes
Surry S2D-Y	
Containment Spray Injection On	20.0
Containment Spray Recirculation On	25.0
Core Uncover	27.8
Accumulators Empty	91.4
Containment Spray Injection Off	114.7
Start Melt	134.0
Core Slump	146.6
Core Collapse	150.8
Bottom Head Fail	163.6
Containment Fail	163.7
Reactor Cavity Dry	264.9
Start Concrete Attack	336.9
End Calculation	1114.6
Surry V	
Containment Fails	0.0
Core Uncover	20.6
Start Melt	39.7
Core Slump	56.6
Core Collapse	60.5
Bottom Head Fail	149.9
Start Concrete Attack	149.9
End Calculation	750.2

TABLE 6.3 CORE AND PRIMARY SYSTEM RESPONSE

Accident Event	Time, minutes	Primary System Pressure, psia	Primary System Water Inventory, lbm	Average Core Temperature, F	Peak Core Temperature, F	Fraction Core Melted	Fraction Clad Reacted
			Surry TMLB-ε				
Core Uncover	95.5	2369	8.58×10^4	669	675	0.	0.
Start Melt	118.3	2366	5.65×10^4	1990	4130	0.00	0.06
Start Slump	146.3	2362	5.37×10^4	3709	4147	0.55	0.33
Core Collapse	147.3	2364	4.79×10^4	4130	---	0.82	0.58
Bottom Head Fail	157.3	2368	1.95×10^4	3820	---	---	0.59
			Surry TMLB-δ				
Core Uncover	95.5	2369	8.68×10^4	669	675	0.	0.
Start Melt	118.3	2366	5.65×10^4	1990	4130	0.00	0.06
Start Slump	146.3	2362	5.37×10^4	3658	4150	0.55	0.33
Core Collapse	148.0	2367	4.52×10^4	4130	---	0.79	0.89
Bottom Head Fail	152.8	2369	9.33×10^4	4130	---	---	0.93
			Surry S2D-γ				
Core Uncover	27.8	1164	1.01×10^5	577	585	0.	0.
Start Melt	134.0	292	7.03×10^4	2067	4130	0.00	0.08
Start Slump	146.6	131	6.37×10^4	3688	4139	0.58	0.48
Core Collapse	150.8	337	5.88×10^4	4207	---	0.77	0.89
Bottom Head Fail	163.6	617	2.46×10^5	3925	---	---	0.89

TABLE 6.3 (Continued)

Accident Event	Time, minutes	Primary System Pressure, psia	Primary System Water Inventory, lbm	Average Core Temperature, F	Peak Core Temperature, F	Fraction Core Melted	Fraction Clad Reacted
			Surry S2D-ε				
Core Uncover	27.8	1164	1.01×10^5	577	585	0.	0.
Start Melt	134.6	293	7.04×10^4	2046	4130	0.00	0.07
Start Slump	147.3	129	6.38×10^4	3658	4147	0.58	0.48
Core Collapse	148.8	213	6.20×10^4	4130	---	0.76	0.59
Bottom Head Fail	227.5	18	2.46×10^5	4130	---	---	0.60
			Surry V				
Core Uncover	20.6	129	1.11×10^5	367	380	0.	0.
Start Melt	39.7	24	7.97×10^4	2094	4130	0.00	0.05
Start Slump	56.6	17	7.74×10^4	3597	4135	0.49	0.22
Core Collapse	60.5	122	7.31×10^4	4130	---	0.75	0.41
Bottom Head Fail	149.9	15	0.	4130	---	---	0.41
			Surry AB-β (2 Volumes)				
Core Uncover	9.4	44.2	8.32×10^4	288	296	0.	0.
Start Melt	27.2	36.3	5.64×10^4	1952	4130	0.00	0.05
Start Slump	44.6	30.2	5.34×10^4	3629	4132	0.54	0.24
Core Collapse	45.6	31.7	5.05×10^4	3729	---	1.0	0.40
Bottom Head Dry	65.8	36.4	0.	3234	---	---	0.40
Bottom Head Fail	104.3	24.9	0.	4130	---	---	0.40

TABLE 6.3 (Continued)

Accident Event	Time, minutes	Primary System Pressure, psia	Primary System Water Inventory, lbm	Average Core Temperature, F	Peak Core Temperature, F	Fraction Core Melted	Fraction Clad Reacted
			Surry AB-B (4 Volumes)				
Core Uncover	7.1	41.3	8.40×10^4	286	295	0.	0.
Start Melt	24.6	29.8	5.62×10^4	1962	4130	0.00	0.05
Start Slump	41.5	24.0	5.34×10^4	3623	4131	0.54	0.24
Core Collapse	42.5	25.2	5.08×10^4	4207	---	0.76	0.39
Bottom Head Dry	62.5	28.4	0.	3236	---	---	0.39
Bottom Head Fail	97.9	18.7	0.	4130	---	---	0.39
			Surry AB-C/Y				
Core Uncover	9.4	40.2	7.50×10^4	296	357	0.	0.
Start Melt	24.8	35.6	5.70×10^4	1960	4130	0.00	0.05
Start Slump	42.1	31.8	5.33×10^4	3644	4139	0.54	0.24
Core Collapse	43.5	33.5	5.02×10^4	3732	---	1.0	0.40
Bottom Head Dry	64.4	41.2	0.	3299	---	---	0.40
Bottom Head Fail	110.1	33.9	0.	4130	---	---	0.40

TABLE 6.4 CONTAINMENT RESPONSE

Accident Event	Time, minutes	Compartment Pressure, psia	Compartment Temperature, F	RWST or CST Water Mass, lbm	Sump Water Mass, lbm	Sump Water Temp., F	Reactor Cavity Water Mass, lbm	Reactor Cavity Water Temp., F	Steam Cond. on Walls lbm/min
				Surry TMLB-ε					
Steam Generator Dry	67.5	13.0	136	3.0×10^6	3.39×10^4	138	0.	---	1,051
Core Uncover	95.5	28.8	219	3.0×10^6	2.07×10^5	197	0.	---	2,498
Start Melt	118.3	25.7	209	3.0×10^6	2.47×10^5	200	0.	---	994
Start Slump	146.3	22.5	197	3.0×10^6	2.69×10^5	198	0.	---	684
Core Collapse	147.3	24.9	205	3.0×10^6	2.70×10^5	197	0.	---	1,378
Bottom Head Fail	157.3	45.9	253	3.0×10^6	2.82×10^5	198	1.71×10^5	120	11,810
Start Debris/ Water Interaction	157.3	46.0	253	3.0×10^6	2.82×10^5	198	1.71×10^5	120	12,400
Cavity Dry	214.9	58.6	272	3.0×10^6	4.06×10^5	221	0.	---	1,405
Start Concrete Attack	289.9	46.0	253	3.0×10^6	4.54×10^5	225	0.	---	653
Containment Fail	738.2	53.7	249	3.0×10^6	4.85×10^5	227	0.	---	0
End Calculation	1100.0	14.8	263	3.0×10^6	4.66×10^5	180	0.	---	0
				Surry TMLB-δ					
Steam Generator Dry	67.5	13.0	136	3.0×10^6	3.39×10^4	138	0.	---	1051
Core Uncover	95.5	28.7	219	3.0×10^6	2.07×10^5	197	0.	---	2498
Start Melt	118.3	25.8	209	3.0×10^6	2.47×10^5	200	0.	---	990
Start Slump	146.3	22.3	196	3.0×10^6	2.68×10^5	196	0.	---	668
Core Collapse	148.0	26.5	210	3.0×10^6	2.68×10^5	196	0.	---	0

TABLE 6.4 (Continued)

Accident Event	Time, minutes	Compartment Pressure, psia	Compartment Temperature F	RWST or CST Water Mass, lbm	Sump Water Mass, lbm	Sump Water Temp., F	Reactor Cavity Water Mass, lbm	Reactor Cavity Water Temp., F	Steam Cond. on Walls lbm/min
			(Surry TMLB-A Continued)						
Bottom Head Fail	152.8	46.5	252	3.0×10^6	2.75×10^5	197	0.	---	12,300
Start Debris/ Water Interaction	152.8	46.6	252	3.0×10^6	2.75×10^5	197	1.71×10^5	120	12,510
Containment Fail	152.9	86.0	336	3.0×10^6	2.76×10^5	197	8.82×10^3	109	0
Cavity Dry	177.2	14.7	202	3.0×10^6	3.16×10^5	202	0.	---	238
Start Concrete Attack	254.2	14.6	187	3.0×10^6	3.30×10^5	187	0.	---	278
End Calculation	1073.4	14.8	207	3.0×10^6	3.33×10^5	159	0.	---	0
			Surry S2D-C						
Containment Spray Injection On	20.0	23.4	201	2.90×10^6	2.14×10^5	194	3.96×10^2	196	3,184
Containment Spray Recirculation On	25.0	20.9	191	2.77×10^6	3.58×10^5	191	4.14×10^4	189	1,301
Core Uncover	27.8	19.4	183	2.70×10^6	4.00×10^5	184	6.53×10^4	185	823
Accumulators Empty	91.5	12.6	126	1.04×10^6	2.08×10^6	131	2.46×10^5	128	0.
Start Melt	134.6	13.5	136	4.12×10^5	2.75×10^6	131	2.46×10^5	128	113
Core Slump	147.3	14.2	132	4.12×10^5	---	---	2.46×10^5	128	27
Core Collapse	148.3	14.4	132	4.12×10^5	---	---	2.46×10^5	128	45
Bottom Head Fail	227.5	13.6	144	4.12×10^5	2.81×10^6	141	2.46×10^5	128	355

TABLE 6.4 (Continued)

Accident Event	Time, minutes	Compartment Pressure, psia	Compartment Temperature, F	RWST or CST Water Mass, lbm	Sump Water Mass, lbm	Sump Water Temp., F	Reactor Cavity Water Mass, lbm	Reactor Cavity Water Temp., F	Steam Cond. on Walls lbm/min
			(Surry S2D-C Continued)						
Start Debris/ Water Interaction	227.5	13.6	144	4.12×10^5	---	---	2.46×10^5	128	375
Reactor Cavity Dry	325.7	16.1	162	4.12×10^5	3.06×10^6	164	0.	---	15
Start Concrete Attack	407.7	13.7	141	4.12×10^5	3.06×10^6	147	0.	---	0
End Calculation	2210.4	13.8	131	4.12×10^5	2.88×10^6	132	2.39×10^5	212	12
			Surry S2D-Y						
Containment Spray Injection On	20.0	23.4	201	2.90×10^6	2.14×10^5	194	4.76×10^2	196	3,185
Containment Spray Recirculation On	25.0	20.9	190	2.77×10^6	3.58×10^5	191	4.15×10^4	189	1,299
Core Uncover	27.8	19.4	183	2.70×10^6	3.99×10^5	184	6.52×10^4	185	824
Accumulators Empty	91.4	12.6	126	1.04×10^6	2.08×10^5	131	2.46×10^5	131	0
Start Melt	134.0	13.5	136	4.15×10^5	2.75×10^6	130	2.46×10^5	128	114
Core Slump	146.6	14.2	132	4.15×10^5	2.76×10^6	132	2.46×10^5	128	24
Core Collapse	150.8	15.4	136	4.15×10^5	2.76×10^6	132	2.46×10^5	128	188
Bottom Heat Fail	163.6	23.1	186	4.15×10^5	2.77×10^6	134	2.46×10^5	128	6,254
Start Debris/ Water Interaction	163.6	24.0	191	4.15×10^5	2.77×10^6	134	2.46×10^5	128	6,561

TABLE 6.4 (Continued)

Accident Event	Time, minutes	Compartment Pressure, psia	Compartment Temperature, F	PWST or CST Water Mass, lbm	Sump Water Mass, lbm	Sump Water Temp., F	Reactor Cavity Water Mass, lbm	Reactor Cavity Water Temp., F	Steam Cond. on Walls lbm/min
				(Surry S2D-Y Continued)					
Containment Fail	163.7	88.6	1696	4.15×10^5	2.78×10^6	134	0.	---	0
Reactor Cavity Dry	264.9	14.6	203	4.15×10^5	2.88×10^6	137	0.	---	491
Start Concrete Attack	336.9	14.7	184	4.15×10^5	2.89×10^6	137	0.	---	0
End Calculation	1114.6	14.8	228	4.15×10^5	2.90×10^6	137	0.	---	0
				Surry AB-ε					
Core Uncovers	9.4	40.2	246	3.0×10^6	3.45×10^5	247	0.	---	3,878
Start Melt	24.8	35.5	236	3.0×10^6	3.78×10^5	237	0.	---	1,797
Start Slump	42.1	31.8	225	3.0×10^6	---	---	0.	---	0
Core Collapse	45.3	33.6	249	3.0×10^6	---	---	0.	---	0
Bottom Head Dry	64.4	41.1	245	3.0×10^6	---	---	0.	---	1,793
Bottom Head Fail	110.1	34.0	205	3.0×10^6	4.42×10^5	227	0.	---	777
Start Concrete Attack	110.1	34.0	205	3.0×10^6	4.42×10^5	227	0.	---	0
Containment Leak	1450.6	45.8	239	3.0×10^6	4.93×10^5	227	0.	---	0
End Calculation	1639.6	43.0	288	3.0×10^6	4.93×10^5	227	0.	---	0
				Surry AB-Y*					
Containment Fail	268.9	87.4	1152	3.0×10^6	4.52×10^5	227	0.	---	0
End Calculation	710.7	14.9	271	3.0×10^6	4.45×10^5	213	0.	---	0

* Containment response same as Surry AB-ε out to Start of Concrete Attack.

TABLE 6.4 (Continued)

Accident Event	Time, minutes	Compartment Pressure, psia		Compartment Temperature, F		RWST or CST Water Mass, lbm	Sump Water Mass, lbm	Sump Water Temp., F	Reactor Cavity Water Mass, lbm	Reactor Cavity Water Temp., F	Steam Cond. on Walls lbm/min
		1	2	1	2						
					Surry V						
Containment Fails	0.0	10.0	15.7	100	161	3.0×10^6	0.	0.	0.	---	0/1163*
Core Uncover	20.6	10.1	15.8	101	216	3.0×10^6	---	---	0.	---	0/0
Start Melt	39.7	10.1	14.8	100	210	3.0×10^6	3.38×10^4	45	0.	---	0/225
Start Slump	56.6	10.1	14.9	100	428	3.0×10^6	3.38×10^4	45	0.	---	0/0
Core Collapse	60.5	10.1	15.0	100	739	3.0×10^6	3.38×10^4	45	0.	---	0/0
Bottom Head Fail	149.9	12.3	12.3	114	141	3.0×10^6	3.70×10^4	50	0.	---	1084/0
Start Concrete Attack	149.9	12.8	12.8	116	131	3.0×10^6	3.89×10^4	54	0.	---	1413/0
End Calculation	750.2	14.9	14.9	135	150	3.0×10^6	6.62×10^4	81	0.	---	0/0

* Volume 1/Volume 2

TABLE 6.4 (Continued)

Accident Event	Time, minutes	Compartment Pressure, psia		Compartment Temperature, F		RWST or CST Water Mass, lbm	Sump Water Mass, lbm	Sump Water Temp., F	Reactor Cavity Water Mass, lbm	Reactor Cavity Water Temp., F	Steam Cond. on Walls lbm/min
		1	2	1	2						
					Surry AB-B (2 Volumes)						
Containment Fail	0.6	54.2	15.7	260	99	3.0×10^6	2.24×10^5	258	0.	---	3026/0*
Core Uncover	9.4	44.2	15.0	244	155	3.0×10^6	3.40×10^5	245	0.	---	3815/319
Start Melt	27.2	36.3	15.0	230	170	3.0×10^6	3.76×10^5	231	0.	---	1525/250
Start Slump	44.6	31.7	15.0	241	171	3.0×10^6	3.89×10^5	218	0.	---	0/0
Core Collapse	45.6	31.9	15.0	244	171	3.0×10^6	3.89×10^5	218	0.	---	0/0
Bottom Head Fail	104.3	24.9	15.0	211	181	3.0×10^6	4.18×10^5	212	0.	---	521/0
Start Concrete Attack	104.4	24.9	14.8	211	181	3.0×10^6	4.18×10^5	212	0.	---	534/0
End Calculation	704.6	14.9	14.8	184	186	3.0×10^6	4.03×10^5	176	0.	---	0/0

* Volume 1/Volume 2

TABLE 6.4 (Continued)

Accident Event	Time, minutes	Compartment Pressure, psia				Compartment Temperature F				RWST or CST Water Mass, lbm	Sump Water Mass, lbm	Sump Water Temp., F	Reactor Cavity Water Mass, lbm	Reactor Cavity Water Temp., F	Steam Cond. on Walls lbm/min			
		1	2	3	4	1	2	3	4						1	2	3	4
Surry AB-β (4 Volumes)																		
Containment Fail	0.0	15.7	15.7	15.7	15.7	110	109	90	174	3.0×10^6	---	---	0.	---	0/0*		0/6155*	
Core Uncover	7.1	41.3	41.3	41.3	41.3	126	193	255	268	3.0×10^6	9.80×10^2	120	0.	---	18/1530		2082/1694	
Start Melt	24.6	29.9	29.8	29.8	29.8	103	163	235	246	3.0×10^6	1.008×10^3	104	0.	---	0/310		697/0	
Start Slump	41.5	23.9	23.9	23.9	23.9	98	154	220	377	3.0×10^6	1.006×10^3	98	0.	---	0/262		453/0	
Core Collapse	42.5	25.2	25.2	25.2	25.2	109	163	239	614	3.0×10^6	1.008×10^3	98	0.	---	0/584		0/0	
Bottom Head Fail	97.9	18.8	18.8	18.8	18.8	124	187	221	215	3.0×10^6	1.139×10^3	99	0.	---	50/0		0/172	
Start Concrete Attack	98.0	18.8	18.8	18.8	18.8	127	187	221	215	3.0×10^6	1.143×10^3	100	0.	---	66/0		0/156	
End Calculation	698.3	14.8	14.8	14.8	14.8	468	148	279	173	3.0×10^6	2.141×10^3	118	0.	---	0/42		0/0	

* Volume 1/Volume 2 Volume 3/Volume 4.

TABLE 6.5 SUMMARY OF CONTAINMENT LEAK RATES

Subsequence	CSIS Start, min	CSIS End, min	CSRS Start, min	CSRS End, min	Leakage Time Interval, min	Leakage Leak Rate,(a) v/hr	Pressure MPa	Pressure psia	Temp. °F	Temp. °C	Remarks
TMLB-δ					95.5	4.2E-4	0.20	29	219	104	Core uncovers
					95.5-118	4.2E-4	0.19	28	217	103	Core heats
					118-146	4.2E-4	0.16	24	201	94	Core melts
					146-148	4.2E-4	0.17	25	204	96	Core slumps and collapses
					148-152.8	4.2E-4	0.20	29	216	102	Reactor vessel heatup
					152.8	4.2E-4	0.31	46	251	122	Reactor vessel fails
					152.8-152.9	4.2E-4	0.51	75	327	164	Boiloff of H_2O
					152.9	4.2E-4	0.58	86	337	169	Containment fails
					152.9-164.4	7.5	0.26	38	245	118	Boiloff of H_2O
					164.4-166.4	3.8	0.11	16	204	95	Boiloff of H_2O
					166.4-168.4	1.9	0.10	15	203	95	Boiloff of H_2O
					168.4-173.2	0.9	0.10	15	203	95	Boiloff of H_2O
					173.2-254.2	0.01	0.10	15	194	90	Boiloff of H_2O
					254.2-272	4.2E-4	0.10	15	186	86	Concrete decomposition
					272-325	0.02	0.10	15	184	84	Concrete decomposition
					325-567	0.09	0.10	15	180	82	Concrete decomposition
					567-627	0.19	0.10	15	204	96	Concrete decomposition
					627-1073	0.08	0.10	15	222	106	Concrete decomposition
TMLB-ε					95.5	4.2E-4	0.20	29	219	104	Core uncovers
					95.5-118.3	4.2E-4	0.19	28	217	102	Core heats
					118.3-146.3	4.2E-4	0.16	24	203	95	Core melts

(a) Normalized to a containment free volume of 1.8×10^6 ft^3. Units are volume fractions per hour.

TABLE 6.5 SUMMARY OF CONTAINMENT LEAK RATES

Subsequence	CSTS Start, min	CSTS End, min	CSRS Start, min	CSRS End, min	Leakage Time Interval, min	Leakage Leak Rate,(a) v/hr	Pressure MPa	Pressure psia	Temp. °F	Temp. °C	Remarks
TMLB-ε (Continued)					146.3-147.3	4.2E-4	0.15	22	197	92	Core slumps and collapses
					147.3-157.3	4.2E-4	0.20	29	216	102	Reactor vessel heatup
					157.3	4.2E-4	0.31	45	252	122	Reactor vessel fails
					157.3-290	4.2E-4	0.37	55	267	130	Boiloff of H_2O
					290-620	4.2E-4	0.32	48	248	120	Concrete decomposition
					620-738.2	4.2E-4	0.35	52	248	120	Concrete decomposition
					738.2	4.2E-4	0.36	54	249	120	Containment fails
					738.2-742.8	7.7	0.26	38	231	111	Concrete decomposition
					742.8-770	1.97	0.11	16	236	114	Concrete decomposition
					770-1100	0.10	0.10	15	275	135	Concrete decomposition
S2D-ε	20	2210	20	2210	27.8	4.2E-4	0.13	19	183	84	Core uncovers
					27.8-134.6	4.2E-4	0.09	14	140	60	Core heats
					134.6-147.3	4.2E-4	0.09	14	133	56	Core melts
					147.3-148.3	4.2E-4	0.10	14	132	56	Core slumps and collapses
					148.3-148.8	4.2E-4	0.17	25	580	305	Hydrogen burns
					148.8-148.82	4.2E-4	0.31	46	1424	773	Hydrogen burns
					148.82-148.83	4.2E-4	0.37	55	1789	976	Hydrogen burns
					148.83-149	4.2E-4	0.32	48	1337	725	Hydrogen burns
					149-149.2	4.2E-4	0.23	34	659	348	Hydrogen burns
					149.2-227.5	4.2E-4	0.10	15	153	67	Reactor vessel heatup

(a) Normalized to a containment free volume of 1.8×10^6 ft^3. Units are volume fractions per hour.

TABLE 6.5 (Continued)

Subsequence	CSIS Start, min	CSIS End, min	CSRS Start, min	CSRS End, min	Leakage Time Interval, min	Leakage Leak Rate,(a) v/hr	Pressure MPa	Pressure psia	Temp. °F	Temp. °C	Remarks
S2D-ε (Continued)					227.5	4.2E-4	0.10	14	142	61	Reactor vessel fails
					227.5-227.6	4.2E-4	0.13	19	153	67	Initial boiloff of H_2O
					227.6-233	4.2E-4	0.21	32	226	108	Boiloff of H_2O
					233-407.7	4.2E-4	0.11	17	164	73	Boiloff of H_2O
					407.7-1248	4.2E-4	0.10	14	145	63	Concrete decomposition
					1248-2210	4.2E-4	0.10	14	134	57	Concrete decomposition
S2D-γ	20	91.4	20	163.7	27.8	4.2E-4	0.13	19	183	84	Core uncovers
					27.8-134.0	4.2E-4	0.09	14	140	60	Core heats
					134.0-150.8	4.2E-4	0.09	14	133	56	Core slumps and collapses
					150.8-163.6	4.2E-4	0.11	16	142	61	Reactor vessel heatup
					163.6	4.2E-4	0.16	23	186	85	Reactor vessel fails
					163.6-163.7	4.2E-4	0.34	50	825	441	Hydrogen burns
					163.7	4.2E-4	0.60	87	1795	980	Hydrogen burns
					163.7	4.2E-4	0.60	88	1726	941	Containment fails
					163.7-164.5	11.1	0.50	73	1308	709	Hydrogen burns
					164.5-166.7	8.7	0.31	46	588	309	Hydrogen burns
					166.7-201.5	1.7	0.16	17	207	97	Boiloff of H_2O
					201.5-407.7	0.2	0.10	15	190	88	Boiloff of H_2O
					407.7-477.6	4.6	0.14	20	478	248	Hydrogen burns
					477.6-479.1	11.8	0.24	36	1599	870	Hydrogen burns

(a) Normalized to a containment free volume of 1.8×10^6 ft^3. Units are volume fractions per hour.

TABLE 6.5 (Continued)

Subsequence	CSIS Start, min	CSIS End, min	CSRS Start, min	CSRS End, min	Leakage Time Interval, min	Leak Rate,(a) v/hr	Pressure MPa	Pressure psia	Temp. °F	Temp. °C	Remarks
S2D-γ (Continued)					479.1-480.7	5.1	0.11	16	694	368	Hydrogen burns
					480.7-591.3	0.1	0.10	15	256	124	Concrete decomposition
					591.3-591.5	9.2	0.23	34	1260	682	Hydrogen burns
					591.5-592.3	12.3	0.26	38	1785	974	Hydrogen burns
					592.3-593.3	9.6	0.14	20	973	523	Hydrogen burns
					593.3-750.7	0.1	0.10	15	250	121	Concrete decomposition
					750.7-750.8	9.0	0.23	34	1249	676	Hydrogen burns
					750.8-751	13.2	0.34	50	2252	1233	Hydrogen burns
					751-752.2	11.3	0.22	32	1470	799	Hydrogen burns
					752.2-758	1.2	0.10	14	425	218	Concrete decomposition
					758-1115	0.07	0.10	15	238	114	Concrete decomposition
AB-ε	--	--	--	--	9.4	4.2E-4	0.28	40	246	119	Core uncovers
					9.4-24.8	4.2E-4	0.27	39	244	118	Core heats
					24.8-42.1	4.2E-4	0.23	33	230	110	Core melts
					42.1-43.3	4.2E-4	-.23	33	238	114	Core slumps and collapses
					43.3-110.1	4.2E-4	0.25	37	238	114	Reactor vessel heats
					110.1	4.2E-4	0.23	34	229	110	Reactor vessel fails
					110.1-1451	4.2E-4	0.29	42	232	111	Concrete decomposition
					1451	4.2E-4	0.31	46	236	113	Containment leaks
					1451-1452.4	5.8	0.28	41	230	110	Concrete decomposition
					1452.4-1639.8	4.2E-4	0.29	42	295	146	Concrete decomposition

(a) Normalized to a containment free volume of 1.8×10^6 ft^3. Units are volume fractions per hour.

TABLE 6.5 (Continued)

Subsequence	CSIS Start, min	CSIS End, min	CSRS Start, min	CSRS End, min	Leakage Time Interval, min	Leak Rate,(a) v/hr	Pressure MPa	Pressure psia	Temp. °F	Temp. °C	Remarks
AB-Y	--	--	--	--	9.4	4.2E-4	0.32	46	246	119	Core uncovers
					9.4-24.8	4.2E-4	0.27	40	245	118	Core heats
					24.8-42.1	4.2E-4	0.23	34	230	110	Core melts
					42.1-43.5	4.2E-4	0.23	33	243	117	Core slumps and collapses
					43.5-110.1	4.2E-4	0.25	37	238	114	Reactor vessel melts
					110.1	4.2E-4	0.23	34	230	110	Reactor vessel fails
					110.1-268.9	4.2E-4	0.25	37	230	110	Concrete decomposition
					268.9	4.2E-4	0.46	68	770	410	Containment fails/H burns
					268.9-269.6	14.7	0.93	137	2567	1408	Hydrogen burns
					269.6-271	12.9	0.56	82	1809	987	Hydrogen burns
					271-271.9	11.1	0.33	48	1211	655	Hydrogen burns
					271.9-274.2	9.5	0.19	28	769	409	Hydrogen burns
					274.2-277.4	4.4	0.11	16	443	228	Hydrogen burns
					277.4-299	4.2E-4	0.11	15	345	174	Concrete decomposition
					299-710.7	0.07	0.11	15	281	138	Concrete decomposition

(a) Normalized to a containment free volume of 1.8 x 10 ft . Units are volume fractions per hour.

TABLE 6.5 (Continued)

Subsequence	CSIS Start, min	CSIS End, min	CSRS Start, min	CSRS End, min	Leakage in Compartment 1: Time Interval, min	Leak Rate,(a) v/hr	Pressure MPa	Pressure psia	Temp. °F	Temp. °C	Leakage in Compartment 2: Leak Rate,(b) v/hr	Pressure MPa	Pressure psia	Temp. °F	Temp. °C	Remarks
AE-B(2V)	--	--	--	--	9.4	0.32	0.30	44	244	118	4.2E-4	0.10	15	86	30	Core uncovers
					9.4-27.2	0.70	0.29	42	241	116	2.3	0.10	15	156	69	Core heats
					27.2-44.6	0.50	0.22	33	223	106	2.2	0.10	15	170	77	Core melts
					44.6-46.0	0.59	0.22	32	244	118	2.3	0.10	15	170	77	Core slumps and collapses
					46.0-104.3	0.57	0.21	31	226	108	2.3	0.10	15	179	82	Reactor vessel heats
					104.3	0.45	0.17	25	212	100	2.3	0.10	15	181	83	Reactor vessel fails
					104.3-104.4	1.96	0.17	25	212	100	2.3	0.10	15	181	83	Boiloff of H_2O
					104.4-198.2	0.42	0.15	22	215	102	2.3	0.10	15	181	83	Concrete decomposition
					198.2-198.3	94.1	0.13	19	219	104	0.44	0.14	20	1345	730	Hydrogen burns
					198.3-201.5	4.2E-4	0.13	19	219	104	2.3	0.10	15	540	282	Hydrogen burns
					201.5-257.4	0.29	0.12	18	228	109	1.95	0.10	15	210	99	Concrete decomposition
					257.4-442.1	0.13	0.11	16	238	115	1.0	0.10	15	192	89	Concrete decomposition
					442.1-704.6	0.05	0.10	15	125	87	0.43	0.10	15	125	87	Concrete decomposition
V (2V)	--	--	--	--	0.04-4.0	4.2E-4	0.07	10	100	38	169.0	0.12	18	232	111	Core uncovers
					4.0-40.0	4.2E-4	0.07	10	100	38	14.7	0.10	15	214	101	Core heats
					40.0-57.0	4.2E-4	0.07	10	100	38	1.6	0.10	15	253	123	Core melts
					57.0-61.0	4.2E-4	0.07	10	100	38	13.0	0.10	15	583	306	Core slumps and collapses
					61.0-149.9	4.2E-4	0.07	10	100	38	3.3	0.10	15	248	120	Reactor vessel melts

(a) Normalized to a containment free volume of 1.8×10^6 ft^3. Units are volume fraction/hr.

(b) Normalized to a compartment free volume of 2.746×10^5 ft^3. Units are volume fraction/hr.

TABLE 6.5 (Continued)

Subsequence	CSIS Start, min	CSIS End, min	CSRS Start, min	CSRS End, min	Leakage in Compartment 1: Time Interval, min	Leak Rate, v/hr(a)	Pressure MPa	Pressure psia	Temp. °F	Temp. °C	Leakage in Compartment 2: Leak Rate, v/hr(b)	Pressure MPa	Pressure psia	Temp. °F	Temp. °C	Remarks
V (2V)* (Continued)					149.9	4.2E-4	0.08	12	113	45	4.2E-4	0.08	12	142	61	Reactor vessel fails
					149.9-159.8	4.2E-4	0.10	15	118	48	4.2E-4	0.10	15	127	53	Concrete decomposition
					159.8-371.5	0.11	0.10	15	126	52	0.76	0.10	15	165	74	Concrete decomposition
					371.5-750.2	0.09	0.10	15	133	56	0.64	0.10	15	158	70	Concrete decomposition
AB-8(4V) (Compartments 1 & 2 are given first. Compartments 3 & 4 are on page 9)	--	--	--	--	7.1-24.6	0.9	0.26	38	121	49	0.01/0.18/ 1.03	0.26	38	185	85	Core uncovers and heats
					24.6-41.5	0.7	0.18	26	100	38	0.01/ 1.6E-3/ 1.00	0.18	26	156	69	Core melts
					41.5-42.5	0.1	0.17	25	104	40	0.2/ 4.2E-4/ 1.01	0.17	25	159	71	Core slumps and collapses
					42.5-97.9	0.9	0.16	24	107	42	0.04/0.55/ 0.69	0.16	24	185	85	Reactor vessel melts
					97.9	52.3	0.13	19	122	50	4.2E-4/ 2.8/0.64	0.13	19	187	86	Reactor vessel fails
					97.9-97.95	4.2E-4	0.13	19	124	51	0.11/ 4.2E-4 0.64	0.13	19	197	86	Boiloff of H_2O

(a) Normalized to a containment free volume of 4.199×10^4 ft^3. Leakage, in volume fraction/hr, is from Compartment 1 to Compartment 2.

(b) Normalized to a compartment free volume of 5.380×10^5 ft^3. Leakages are respectively, Compartment 2 to Compartment 1, Compartment 2 to Compartment 3, and Compartment 2 to the environment.

* See footnotes on Page 6 for V(2V).

TABLE 6.5 (Continued)

Subsequence	CSIS Start, min	CSIS End, min	CSRS Start, min	CSRS End, min	Leakage in Compartment 1: Time Interval, min	Leak Rate,(a) v/hr	Pressure MPa	Pressure psia	Temp. °F	Temp. °C	Leakage in Compartment 2: Leak Rate,(b) v/hr	Pressure MPa	Pressure psia	Temp. °F	Temp. °C	Remarks
AB-8(4V)(Continued)					97.95	79.6	0.13	19	129	54	4.2E-4/ 3.8/0.61	0.13	19	187	86	Initial concrete attack
					97.95-108.1	6.9	0.12	18	174	79	0.32/0.17/ 0.90	0.12	18	178	81	Concrete decomposition
					108.1	173.4	0.12	18	225	107	4.2E-4/ 9.1/0.88	0.12	18	175	79	Hydrogen burns
					108.1-129.1	9.6	0.11	16	409	209	0.96/0.09 0.74	0.11	16	175	79	Concrete decomposition
					129.1	89.5	0.11	16	493	256	5.88/151.1/ 0.62	0.11	16	189	87	Hydrogen burns
					129.1-145.4	10.5	0.11	16	508	264	4.2E-4/ 0.14/0.56	0.11	16	219	104	Concrete decomposition
					145.4	76.9	0.10	15	518	270	6.07/155.4/ 0.25	0.10	15	197	92	Hydrogen burns
					145.4-226.9	8.7	0.10	15	528	276	2.4E-3/ 0.43/0.13	0.10	15	188	87	Concrete decomposition
					226.9	56.5	0.10	15	530	277	1.61/ 4.2E-4/ 0.26	0.10	15	172	78	Hydrogen burns
					226.9-698.3	5.2	0.10	15	502	261	0.05/0.16/ 0.17	0.10	15	161	72	Concrete decomposition

(a) Normalized to a containment free volume of 4.199×10^4 ft^3. Leakage, in volume fraction/hr, is from Compartment 1 to Compartment 2.

(b) Normalized to a compartment free volume of 5.380×10^5 ft^3. Leakages are respectively, Compartment 2 to Compartment 1, Compartment 2 to Compartment 3, and Compartment 2 to the environment.

TABLE 6.5 (Continued)

Subsequence	CSIS Start, min	CSIS End, min	CSRS Start, min	CSRS End, min	Leakage in Compartment 3: Time Interval, min	Leak Rate,(c) v/hr	Pressure MPa	Pressure psia	Temp. °F	Temp. °C	Leakage in Compartment 4: Leak Rate,(d) v/hr	Pressure MPa	Pressure psia	Temp. °F	Temp. °C	Remarks
AB-β(4V) (Continued)					7.1-24.6	0.89/0.11	0.26	38	250	121	5.8	0.26	38	263	128	Core uncovers and heats
					24.6-41.5	0.43/0.46	0.18	26	227	108	2.2	0.18	26	253	123	Core melts
					41.5-42.5	2.67/ 4.2E-4	0.17	25	230	110	30.3	0.17	25	521	272	Core slumps and collapses
					42.5-97.9	0.86/0.40	0.16	24	232	111	4.6	0.16	24	253	123	Reactor vessel melts
					97.9	4.2E-4/ 0.46	0.13	19	221	105	4.2E-4	0.13	19	215	102	Reactor vessel fails
					97.9-97.95	0.51/0.20	0.13	19	221	105	0.35	0.13	19	215	102	Boiloff of H_2O
					97.95	4.2E-4/ 0.54	0.13	19	221	105	4.2E-4	0.13	19	215	102	Initial concrete attack
					97.95-108.1	0.46/0.13	0.12	18	219	104	0.23	0.12	18	212	100	Concrete decomposition
					108.1	2.19/1.2	0.12	18	217	103	1.09	0.12	18	210	99	Hydrogen burns
					108.1-129.1	0.39/0.17	0.11	16	213	101	0.32	0.11	16	205	96	Concrete decomposition
					129.1	4.2E-4/ 15.0	0.11	16	213	101	4.2E-4	0.11	16	202	95	Hydrogen burns
					129.1-145.4	1.71/0.13	0.11	16	299	149	1.18	0.11	16	199	93	Concrete decomposition
					145.4	2.21/15.94	0.10	15	288	142	1.67	0.10	15	196	91	Hydrogen burns
					145.4-226.9	0.68/0.18	0.10	15	302	150	0.78	0.10	15	189	87	Concrete decomposition
					226.9	12.9/ 4.2E-4	0.10	15	298	148	155.4	0.10	15	236	113	Hydrogen burns
					226.9-698.3	0.15/0.13	0.10	15	289	143	0.37	0.10	15	182	83	Concrete decomposition

(c) Normalized to a compartment free volume of 9.136×10^5 ft^3. Leakages are respectively, Compartment 3 to Compartment 2 and Compartment 3 to Compartment 4.

(d) Normalized to a compartment free volume of 1.731×10^5 ft^3. Leakage is from Compartment 4 to Compartment 3.

TABLE 6.6. DIMENSIONS OF PWR USED FOR CALCULATIONS

Containment Design	Compartment	Volume		Wall Area		Floor Area	
		ft^3	m^3	ft^2	m^2	ft^2	m^2
Large, high pressure	Containment	1.80×10^6	5.097×10^4	2.36×10^5	2.19×10^4	1.374×10^4	1.277×10^3
General, for V sequence	Containment	1.80×10^6	5.097×10^4	2.36×10^5	2.19×10^4	1.347×10^4	1.277×10^3
	Aux Building	1.50×10^5	4.248×10^3	5.25×10^3	4.88×10^2	1.875×10^3	1.742×10^2

TABLE 6.7. PWR CONTAINMENT SPRAY PARAMETERS

Pumps	Flow Rate		Height		Temperature		Droplet Diameter, μm
	lb/min	kg/s	ft	m	F	C	
Injection	2.60×10^4	1.966×10^2	90	27.4	120	48.89	400
Recirculation	5.80×10^4	4.385×10^2	90	27.4	120	48.89	400

TABLE 6.8. INVENTORIES OF RADIONUCLIDES AND STRUCTURAL MATERIALS FOR SURRY DURING IN-VESSEL PERIOD OF MELTING

Fission Products		Actinides/Structural	
Element	Mass (kg)	Element	Mass (kg)
Kr	13.4	U	70,210
Rb	14.7	Pu	469
Sr	47.6	Zr	16,460
Y	22.9	Sn	262
Zr	179	Ag	2,750
Mo	155	In	505
Tc	37.1	Cd	173
Ru	104	Fe	6,486
Rh	20.9		
Pd	52.5		
Te	25.4		
I	12.4		
Xe	260		
Cs	131		
Ba	61.2		
La	62.3		
Ce	131		
Pr	50.7		
Nd	171		
Sm	34.0		

TABLE 6.8.B. INITIAL INVENTORIES OF ADDITIONAL SPECIES INCLUDED IN GROUPED RELEASE CALCULATIONS

Element	Mass (kg)
Eu	8.9
Nb	2.7
Np	26.0
Pm	7.2

TABLE 6.8.C. CORSOR RESULTS WITH AND WITHOUT RSS GROUPING

	Without RSS Grouping			With RSS Grouping		
	Initial Inventory	Final CORSOR Releases (kg)		Initial Inventory	Final CORSOR Releases (kg)	
Group	(kg)	AB	TMLB	(kg)	AB	TMLB
Xe	273	273	272	273	273	271
I	12.4	12.4*	12.3	12.4	12.4*	12.3
Cs	131	131*	130	146	146*	145
Te	25.4	9.3	9.0	25.4	9.3	8.8
Sr	NA	NA	NA	109	71.1	35.7
Ru	NA	NA	NA	369	34.7	16.7
La	NA	NA	NA	986	0.82	0.29
Aerosol	106900	2330	1750	106300	2220	1710

	Not Grouped		Grouped	
	AB	TMLB	AB	TMLB
CsI	25.4	25.2	25.4	25.2
CsOH	133	132	150	148

*CORSOR releases these species in the form of CsI and CsOH.

TABLE 6.9. GEOMETRIC AND POWER PEAKING FACTORS FOR CORE CONFIGURATION OF THE SURRY PLANT

Radial Power Peaking Factor	Axial Power Peaking Factor	Fraction of Core in Radial Zone
1.03	0.09	0.047
1.055	0.26	0.062
1.04	0.43	0.083
1.04	0.59	0.062
1.055	0.74	0.062
1.05	0.89	0.062
1.03	1.02	0.083
1.04	1.14	0.124
0.95	1.24	0.166
0.71	1.32	0.249
	1.39	
	1.43	
	1.44	
	1.45	
	1.43	
	1.41	
	1.35	
	1.27	
	1.18	
	1.07	
	0.94	
	0.80	
	0.63	
	0.49	

TABLE 6.10. MATERIAL PRESENT IN MELT AT TIME OF RPV FAILURE FOR THE SURRY PLANT

Species	AB-δ Melt Content (kg)	TMLB-δ Melt Content (kg)	S_2D-ε Melt Content (kg)	S_2D-γ Melt Content (kg)	V Melt Content (kg)
Cs	0.0	0.7	0.0	0.0	0.0
I	0.0	0.1	0.0	0.0	0.0
Xe	0.0	1.5	0.0	0.0	0.0
Kr	0.0	0.1	0.0	0.0	0.0
Te	16.4	16.4	5.9	0.61	14.0
Ba	38.6	49.1	38.2	49.1	31.0
Sn	38.0	152	44.0	123	20.0
Ru	102	103	102	103	101
UO_2	79594	79630	79591	79624	79559
Zr	9981	6690	6367	1783	9846
ZrO_2	8760	13210	13640	19830	8942
Fe	40520	34140	42110	34050	51880
Mo	125	140	125	142	117
Sr	39.8	43.7	39.7	44.1	36.5
Ag	1410	1460	1410	1400	1400
Cd	36.0	38.0	36.0	36.0	36.0
In	431	433	431	430	430
Sb	0.11	0.31	0.11	0.60	0.05

TABLE 6.11. MELT CONTENT FOR SPECIES NOT SPECIFICALLY INCLUDED IN CORSOR CALCULATIONS FOR THE SURRY PLANT

Species	AB-δ Melt Content (kg)	TMLB-δ Melt Content (kg)	S_2D-ε Melt Content (kg)	S_2D-γ Melt Content (kg)	V Melt Content (kg)	Reference Species
Rb	0.0	0.1	0.0	0.0	0.0	Cs
Y	22.9	22.9	22.9	22.9	22.9	UO_2
Tc	36.4	36.7	36.4	36.7	36.0	Ru
Rh	20.5	20.7	20.5	20.7	20.3	Ru
Pd	51.5	52.0	51.5	52.0	51.0	Ru
La	62.3	62.3	62.3	62.3	62.2	UO_2
Ce	131	131	131	131	131	UO_2
Pr	50.7	50.7	50.7	50.7	50.6	UO_2
Nd	171	171	171	171	171	UO_2
Sm	34.0	34.0	34.0	34.0	34.0	UO_2
Pu	469	469	469	469	468	UO_2
Cr	6351	5411	6734	5411	8130	(a)
Mn	153	157	153	157	151	Fe
Ni	3528	3006	3741	3006	4517	(a)

(a) These values are taken from the MARCH code predictions.

TABLE 6.12. AEROSOL COMPOSITION AND TOTAL RELEASE RATE FOR SURRY AB EARLY, CORE-CONCRETE INTERACTION

Species, %	Time, sec											
	0	1200	2400	3600	4800	6000	7200	8400	9600	10800	12000	13200
FeO	--	12.1	9.93	7.56	9.67	14.0	18.9	1.01	0.90	0.90	0.82	0.72
Cr_2O_3	--	--	--	--	--	--	--	4×10^{-4}	1×10^{-3}	1×10^{-3}	2×10^{-3}	2×10^{-3}
Ni	2.43	0.44	1.89	4.76	2.46	0.26	0.10	0.25	0.20	0.21	0.18	0.16
Mo	3×10^{-6}	2×10^{-7}	2×10^{-6}	1×10^{-5}	4×10^{-6}	8×10^{-8}	2×10^{-8}	4×10^{-5}	3×10^{-5}	4×10^{-5}	4×10^{-5}	5×10^{-5}
Ru	3×10^{-5}	2×10^{-6}	2×10^{-5}	1×10^{-4}	3×10^{-5}	7×10^{-7}	1×10^{-7}	2×10^{-7}	1×10^{-7}	1×10^{-7}	1×10^{-7}	9×10^{-8}
Sn	0.19	0.06	0.14	0.24	0.16	0.04	0.02	0.18	0.17	0.18	0.17	0.17
Sb	3×10^{-5}	1×10^{-5}	2×10^{-5}	3×10^{-5}	2×10^{-5}	8×10^{-6}	6×10^{-6}	2×10^{-5}	2×10^{-5}	2×10^{-5}	2×10^{-5}	2×10^{-5}
Te	0.95	0.49	0.62	0.66	0.60	0.35	0.30	1.04	1.05	1.05	1.07	1.09
Ag	24.0	21.3	19.1	14.4	18.5	14.8	8.61	25.0	22.8	23.4	22.2	20.9
Mn	8.89	2.94	5.96	7.32	6.14	1.78	1.11	3.37	3.14	3.20	3.09	2.96
CaO	--	12.3	10.6	8.87	10.7	14.3	12.4	0.55	0.52	0.46	0.44	0.49
Al_2O_3	--	6×10^{-4}	4.50	6.79	5.46	1×10^{-3}	2×10^{-3}	8×10^{-3}	9×10^{-3}	0.01	0.01	0.01
Na_2O	--	7.22	6.05	4.63	5.90	8.33	11.0	5.34	5.46	5.48	5.49	5.41
K_2O	--	12.6	10.6	8.04	10.3	14.8	19.1	55.5	59.9	59.3	61.7	64.3
SiO_2	--	26.0	21.4	16.5	20.87	30.1	27.9	6.98	5.26	5.24	4.22	3.23
UO_2	3.24	0.35	1.43	3.95	1.67	0.13	0.06	0.63	0.53	0.54	0.51	0.48
ZrO_2	0.04	6×10^{-3}	0.02	0.08	0.03	6×10^{-3}	8×10^{-3}	0.03	0.03	0.03	0.03	0.03
Cs_2O	--	--	--	--	--	--	--	--	--	--	--	--
BaO	3.46	1.30	1.03	0.90	0.79	0.44	0.20	0.03	0.02	0.02	0.02	0.02
SrO	8.63	2.05	2.14	2.20	1.59	0.52	0.19	2×10^{-3}	2×10^{-3}	2×10^{-3}	2×10^{-3}	2×10^{-3}
La_2O_3	3.81	2×10^{-4}	2.04	6.62	2.52	1×10^{-4}	1×10^{-4}	4×10^{-4}	5×10^{-4}	4×10^{-4}	5×10^{-4}	5×10^{-4}
CeO_2	7.38	0.70	2.55	6.45	2.60	0.15	0.02	6×10^{-4}	9×10^{-4}	6×10^{-4}	7×10^{-4}	7×10^{-4}
Nb_2O_5	4×10^{-4}	2×10^{-5}	2×10^{-4}	1×10^{-3}	4×10^{-4}	1×10^{-5}	2×10^{-6}	7×10^{-6}	7×10^{-6}	7×10^{-6}	7×10^{-6}	7×10^{-6}
CsI	--	--	--	--	--	--	--	--	--	--	--	--
Cd	36.9	--	--	--	--	--	--	--	--	--	--	--
Source Rate g/sec	170	97.1	33.1	123	230	183	98.3	17.5	10.6	11.2	12.8	10.3

TABLE 6.12. (Continued)

Species, %	Time, sec							
	14400	15600	16800	18000	19200	20400	21600	22800
FeO	0.64	0.54	0.40	0.32	0.29	0.30	0.31	0.32
Cr_2O_3	3×10^{-3}	4×10^{-3}	5×10^{-3}	6×10^{-3}	7×10^{-3}	7×10^{-3}	7×10^{-3}	7×10^{-3}
Ni	0.14	0.12	0.09	0.07	0.07	0.07	0.07	0.07
Mo	7×10^{-5}	9×10^{-5}	1×10^{-4}	2×10^{-4}	6×10^{-4}	1×10^{-3}	1×10^{-3}	1×10^{-3}
Ru	--	--	--	--	--	--	--	--
Sn	0.18	0.18	0.17	0.18	0.21	0.24	0.25	0.26
Sb	2×10^{-5}	2×10^{-5}	2×10^{-5}	2×10^{-5}	2×10^{-5}	2×10^{-5}	3×10^{-5}	3×10^{-5}
Te	1.10	1.12	1.14	1.16	1.19	1.20	1.20	1.20
Ag	20.0	18.5	15.7	14.4	14.1	14.4	14.5	14.4
Mn	2.88	2.72	2.43	2.32	2.36	2.46	2.50	2.50
CaO	0.50	0.49	0.45	0.46	0.51	0.56	0.58	0.58
Al_2O_3	0.01	0.02	0.02	0.02	0.02	0.02	0.02	0.02
Na_2O	5.33	5.22	5.00	4.71	4.44	4.31	4.26	4.24
K_2O	66.0	68.7	73.0	75.1	75.6	75.2	75.0	75.1
SiO_2	2.58	1.88	1.12	0.75	0.59	0.55	0.54	0.53
UO_2	0.48	0.46	0.42	0.44	0.51	0.58	0.60	0.60
ZrO_2	0.03	0.04	0.04	0.04	0.05	0.05	0.04	0.04
Cs_2O	--	--	--	--	--	--	--	--
BaO	0.02	0.03	0.03	0.03	0.04	0.04	0.04	0.04
SrO	2×10^{-3}	2×10^{-3}	2×10^{-3}	2×10^{-3}	2×10^{-3}	2×10^{-3}	2×10^{-3}	2×10^{-3}
La_2O_3	5×10^{-4}	5×10^{-4}	6×10^{-4}	6×10^{-4}	7×10^{-4}	7×10^{-4}	7×10^{-4}	6×10^{-4}
CeO_2	7×10^{-4}	8×10^{-4}	9×10^{-4}	9×10^{-4}	1×10^{-3}	1×10^{-3}	1×10^{-3}	9×10^{-4}
Nb_2O_5	8×10^{-6}	8×10^{-6}	9×10^{-6}	9×10^{-6}	1×10^{-5}	1×10^{-5}	1×10^{-5}	1×10^{-5}
CsI	--	--	--	--	--	--	--	--
Cd	--	--	--	--	--	--	--	--
Source Rate g/sec	9.1	8.5	7.1	5.5	3.8	3.0	3.0	3.0

TABLE 6.13. AEROSOL COMPOSITION AND TOTAL RELEASE RATE FOR SURRY AB LATE, CORE-CONCRETE INTERACTION

Species %	Time, sec											
	0	1200	2400	3600	4800	6000	7200	8400	9600	10800	12000	13200
FeO	--	13.6	12.0	10.7	9.20	10.5	12.2	13.2	14.2	15.5	22.1	1.31
Cr_2O_3	--	--	--	--	--	--	--	--	--	--	--	0.12
Ni	2.43	0.22	0.47	1.20	2.60	1.55	0.52	0.38	0.26	0.20	0.21	0.39
Mo	3×10^{-6}	6×10^{-8}	2×10^{-7}	1×10^{-6}	5×10^{-6}	2×10^{-6}	3×10^{-7}	2×10^{-7}	8×10^{-8}	5×10^{-8}	4×10^{-8}	8×10^{-5}
Ru	3×10^{-5}	5×10^{-7}	2×10^{-6}	1×10^{-5}	4×10^{-5}	1×10^{-5}	2×10^{-6}	1×10^{-6}	7×10^{-7}	5×10^{-7}	4×10^{-7}	6×10^{-7}
Sn	0.19	0.04	0.06	0.11	0.17	0.12	0.06	0.05	0.04	0.03	0.04	0.23
Sb	3×10^{-5}	1×10^{-5}	1×10^{-5}	2×10^{-5}	3×10^{-5}	2×10^{-5}	1×10^{-5}	1×10^{-5}	8×10^{-6}	8×10^{-6}	9×10^{-6}	2×10^{-5}
Te	0.95	0.44	0.48	0.58	0.65	0.58	0.43	0.39	0.35	0.34	0.42	0.98
Ag	24.0	14.2	22.3	20.6	17.7	20.2	22.8	18.4	14.4	12.6	14.2	30.0
Mn	8.89	2.14	3.04	4.85	6.90	5.21	2.81	2.36	1.89	1.68	1.93	4.17
CaO	--	13.80	12.3	11.2	10.1	11.2	12.6	13.6	14.5	15.3	3.83	0.70
Al_2O_3	--	6×10^{-4}	7×10^{-4}	3.04	5.92	3.73	1×10^{-3}	1×10^{-3}	1×10^{-3}	1×10^{-3}	2×10^{-3}	6×10^{-3}
Na_2O	--	8.09	7.20	6.50	6.62	6.38	7.32	7.89	8.38	9.09	12.5	4.80
K_2O	--	14.2	12.8	11.4	9.79	11.20	13.0	13.9	14.7	15.6	20.2	44.1
SiO_2	--	29.4	25.8	23.1	19.9	22.6	26.2	28.4	30.5	29.0	24.3	12.2
UO_2	3.24	0.20	0.34	0.87	1.98	1.02	0.28	0.18	0.11	0.09	0.09	0.97
ZrO_2	0.04	0.007	0.006	0.015	0.035	0.018	0.006	0.006	0.006	0.006	0.009	0.02
Cs_2O	0	0	--	--	--	--	--	--	--	--	--	--
BaO	3.46	1.36	1.03	1.03	0.97	0.84	0.57	0.40	0.29	0.19	0.05	0.03
SrO	8.63	1.86	1.65	1.96	2.14	1.62	0.85	0.55	0.36	0.23	0.05	0.03
La_2O_3	3.81	2×10^{-4}	2×10^{-4}	1.15	3.01	1.44	$1 \times$	1×10^{-4}	1×10^{-4}	1×10^{-4}	1×10^{-4}	3×10^{-4}
CeO_2	7.38	0.36	0.63	1.59	3.39	1.71	0.	0.20	0.10	0.05	0.009	5×10^{-4}
Nb_2O_5	4×10^{-4}	3×10^{-6}	2×10^{-5}	1×10^{-4}	4×10^{-4}	2×10^{-4}	3×10^{-5}	2×10^{-5}	1×10^{-5}	2×10^{-6}	2×10^{-6}	5×10^{-6}
CsI	--	--	--	--	--	--	--	--	--	--	--	--
Cd	36.9	--	--	--	--	--	--	--	--	--	--	--
Source Rate (above pool) g/sec	158	80.5	205	214	73	136	119	84	73.1	62.2	45.3	17.6

TABLE 6.13. (Continued)

Species %	Time, sec 14400	15600	16800	18000	19200	20400	21600	22800	24000
FeO	1.22	1.07	0.91	0.80	0.69	0.59	0.43	0.36	0.33
Cr_2O_3	6×10^{-4}	1×10^{-3}	2×10^{-3}	2×10^{-3}	3×10^{-3}	4×10^{-3}	5×10^{-3}	5×10^{-3}	6×10^{-3}
Ni	0.33	0.27	0.22	0.18	0.16	0.13	0.09	0.08	0.07
Mo	7×10^{-5}	5×10^{-5}	6×10^{-5}	7×10^{-5}	8×10^{-5}	1×10^{-4}	1×10^{-4}	2×10^{-4}	3×10^{-4}
Ru	4×10^{-7}	2×10^{-7}	2×10^{-7}	1×10^{-7}	8×10^{-8}	--	--	--	--
Sn	0.22	0.20	0.20	0.19	0.19	0.19	0.17	0.18	0.20
Sb	2×10^{-5}	2×10^{-5}	2×10^{-5}	2×10^{-5}	2×10^{-5}	2×10^{-5}	2×10^{-5}	2×10^{-5}	2×10^{-5}
Te	1.01	1.06	1.09	1.11	1.13	1.15	1.17	1.19	1.21
Ag	28.3	26.0	23.8	22.2	20.7	19.3	15.9	14.9	14.7
Mn	4.01	3.78	3.55	3.38	3.22	3.06	2.66	2.58	2.60
CaO	0.60	0.52	0.52	0.54	0.53	0.52	0.46	0.47	0.50
Al_2O_3	7×10^{-3}	8×10^{-3}	0.01	0.01	0.01	0.01	0.018	0.02	0.02
Na_2O	5.06	5.30	5.38	5.36	5.33	5.24	5.05	4.82	4.64
K_2O	48.6	54.1	58.8	61.8	64.5	67.2	72.4	73.9	74.4
SiO_2	9.71	7.03	4.98	3.78	2.89	2.14	1.21	0.89	0.74
UO_2	0.82	0.67	0.58	0.54	0.50	0.48	0.42	0.44	0.48
ZrO_2	0.02	0.03	0.03	0.03	0.03	0.03	0.04	0.04	0.04
Cs_2O	--	--	--	--	--	--	--	--	--
BaO	2×10^{-3}	0.02	0.02	0.025	0.026	0.027	0.03	0.03	0.03
SrO	2×10^{-3}	2×10^{-3}	2×10^{-3}	2×10^{-3}	2×10^{-3}	2×10^{-3}	0.002	0.002	2×10^{-3}
La_2O_3	4×10^{-4}	4×10^{-4}	4×10^{-4}	5×10^{-4}	5×10^{-4}	5×10^{-4}	6×10^{-4}	6×10^{-4}	7×10^{-4}
CeO_2	5×10^{-4}	6×10^{-4}	6×10^{-4}	7×10^{-4}	7×10^{-4}	7×10^{-4}	9×10^{-4}	9×10^{-4}	9×10^{-4}
Nb_2O_5	5×10^{-6}	6×10^{-6}	7×10^{-6}	7×10^{-6}	7×10^{-6}	8×10^{-6}	9×10^{-4}	9×10^{-6}	1×10^{-5}
CsI	--	--	--	--	--	--	--	--	--
Cd	95.7	37.8	29.1	27.9	--	--	--	--	--
Source Rate g/sec	18.4	17.8	13.2	10.3	8.9	8.5	6.3	4.3	3.6

TABLE 6.14. AEROSOL COMPOSITION ANC TOTAL RELEASE RATE FOR SURRY TMLB, CORE-CONCRETE INTERACTION

Species, %	Time, sec											
	0	1200	2400	3600	4800	6000	7200	8400	9600	10800	12000	13200
FeO	--	12.5	10.3	10.8	13.8	15.2	16.2	16.9	18.2	21.0	1.04	1.15
Cr_2O_3	--	--	0.03	0.01	0.01	--	--	--	--	--	0.11	0.18
Ni	2×10^{-3}	6×10^{-2}	0.14	0.08	0.15	0.08	0.08	0.08	0.10	0.13	0.37	0.44
Mo	--	1×10^{-8}	4×10^{-8}	2×10^{-8}	4×10^{-8}	2×10^{-8}	1×10^{-8}	2×10^{-8}	2×10^{-8}	3×10^{-8}	9×10^{-5}	2×10^{-4}
Ru	--	9×10^{-8}	4×10^{-7}	2×10^{-7}	3×10^{-7}	1×10^{-7}	1×10^{-7}	1×10^{-7}	2×10^{-7}	2×10^{-7}	7×10^{-7}	1×10^{-6}
Sn	0.05	0.12	0.16	0.12	0.18	0.13	0.13	0.14	0.15	0.18	1.16	1.29
Sb	1×10^{-5}	3×10^{-5}	3×10^{-5}	3×10^{-5}	4×10^{-5}	3×10^{-5}	3×10^{-5}	3×10^{-5}	3×10^{-5}	4×10^{-5}	1×10^{-4}	1×10^{-4}
Te	0.25	0.39	0.43	0.37	0.51	0.44	0.43	0.44	0.48	0.54	1.38	1.26
Ag	1.20	7.94	12.2	8.96	14.0	9.71	9.43	10.3	11.6	13.99	38.2	40.0
Mn	0.29	1.41	2.02	1.53	2.34	1.69	1.64	1.77	1.98	2.36	6.34	6.46
CaO	--	1.14	4.28	6.99	13.6	12.9	13.0	12.6	11.0	5.26	0.39	0.51
Al_2O_3	--	5×10^{-5}	1×10^{-4}	3×10^{-4}	6×10^{-4}	8×10^{-4}	1×10^{-3}	1×10^{-3}	1×10^{-3}	2×10^{-3}	4×10^{-3}	4×10^{-3}
Na_2O	--	7.06	5.92	6.25	8.09	8.92	9.47	9.89	10.6	12.1	4.01	3.69
K_2O	--	11.2	9.76	10.7	14.0	15.8	16.7	17.3	18.1	20.0	35.9	31.6
SiO_2	--	15.4	21.0	23.1	29.7	32.8	31.3	29.3	26.8	24.0	9.90	11.9
UO_2	0.10	0.10	0.15	0.09	0.14	0.08	0.07	0.07	0.07	0.08	1.13	1.37
ZrO_2	0.02	9×10^{-3}	8×10^{-3}	7×10^{-3}	9×10^{-3}	9×10^{-3}	9×10^{-3}	9×10^{-3}	9×10^{-3}	0.01	0.02	0.02
Cs_2O	0.25	0.10	0.08	0.07	--	--	--	--	--	--	--	--
BaO	0.59	1.99	1.68	1.30	1.42	1.03	0.72	0.55	0.40	0.16	0.03	0.04
SrO	1.27	2.20	2.23	1.55	1.79	1.14	0.78	0.60	0.44	0.18	4×10^{-3}	5×10^{-3}
La_2O_3	4×10^{-4}	2×10^{-4}	2×10^{-4}	2×10^{-4}	2×10^{-4}	2×10^{-4}	2×10^{-4}	2×10^{-4}	2×10^{-4}	2×10^{-4}	4×10^{-4}	3×10^{-4}
CeO_2	6×10^{-4}	0.13	0.27	0.13	0.20	0.08	0.05	0.04	0.04	0.02	6×10^{-4}	5×10^{-4}
Nb_2O_5	6×10^{-6}	3×10^{-6}	3×10^{-6}	2×10^{-6}	3×10^{-6}	3×10^{-6}	2×10^{-6}	2×10^{-6}	2×10^{-6}	2×10^{-6}	5×10^{-6}	4×10^{-6}
CsI	0.16	0.40	0.24	0.28	0.01	1×10^{-3}	2×10^{-4}	7×10^{-5}	4×10^{-5}	2×10^{-5}	3×10^{-5}	2×10^{-5}
Cd	95.7	37.8	29.1	27.9	--	--	--	--	--	--	--	--
Source Rate (above pool) g/sec	1.9	3.1	50.0	58.2	76.8	85.4	55.8	47.8	43.6	40.3	12.6	7.9

TABLE 6.14. (Continued)

Species, %	Time, sec												
	14400	15600	16800	18000	19200	20400	21600	22800	24000	25200	26400	27600	28800
FeO	1.26	1.33	1.40	1.45	1.47	1.47	1.44	1.38	1.28	1.17	1.06	0.95	0.86
Cr_2O_3	0.23	0.27	0.30	0.32	0.33	0.31	0.28	0.24	0.20	0.16	2×10^{-3}	2×10^{-3}	2×10^{-3}
Ni	0.52	0.58	0.62	0.65	0.65	0.61	0.56	0.50	0.44	0.38	0.34	0.30	0.27
Mo	3×10^{-4}	3×10^{-4}	4×10^{-4}	5×10^{-4}	5×10^{-4}	5×10^{-4}	5×10^{-4}	5×10^{-4}	5×10^{-4}	5×10^{-4}	5×10^{-4}	6×10^{-4}	8×10^{-4}
Ru	2×10^{-6}	2×10^{-6}	3×10^{-6}	3×10^{-6}	3×10^{-6}	2×10^{-6}	2×10^{-6}	1×10^{-6}	1×10^{-6}	7×10^{-7}	5×10^{-7}	4×10^{-7}	3×10^{-7}
Sn	1.40	1.47	1.54	1.58	1.62	1.63	1.63	1.63	1.62	1.60	1.61	1.64	1.68
Sb	1×10^{-4}	9×10^{-5}	9×10^{-5}	9×10^{-5}	9×10^{-5}	9×10^{-5}	9×10^{-5}	9×10^{-5}	1×10^{-4}	1×10^{-4}	1×10^{-4}	1×10^{-4}	1×10^{-4}
Te	1.14	1.04	0.97	0.93	0.92	0.96	1.02	1.08	1.16	1.23	1.29	1.33	1.37
Ag	41.4	42.0	42.3	42.4	42.3	42.1	41.6	40.8	39.6	37.9	36.5	35.1	33.8
Mn	6.48	6.44	6.36	6.29	6.27	6.27	6.28	6.25	6.17	6.05	5.92	5.79	5.67
CaO	0.63	0.67	0.70	0.72	0.74	0.75	0.76	0.76	0.75	0.74	0.73	0.73	0.73
Al_2O_3	3×10^{-3}	3×10^{-3}	3×10^{-3}	2×10^{-3}	2×10^{-3}	3×10^{-3}	3×10^{-3}	4×10^{-3}	5×10^{-3}	6×10^{-3}	7×10^{-3}	8×10^{-3}	9×10^{-3}
Na_2O	3.35	3.10	2.93	2.83	2.87	3.03	3.26	3.50	3.77	3.98	4.13	4.21	4.25
K_2O	27.4	24.4	22.4	21.3	21.7	23.5	26.3	29.6	33.6	37.6	41.0	43.9	46.4
SiO_2	14.5	16.7	18.4	19.4	19.0	17.3	15.0	12.51	9.97	7.76	6.10	4.81	3.83
UO_2	1.65	1.87	2.04	2.14	2.13	2.01	1.84	1.67	1.48	1.33	1.24	1.17	1.14
ZrO_2	0.02	0.01	0.01	0.01	0.01	0.01	0.01	0.01	0.02	0.02	0.02	0.02	0.02
Cs_2O	--	--	--	--	--	--	--	--	--	--	--	--	--
BaO	0.04	0.04	0.04	0.04	0.04	0.04	0.04	0.04	0.04	0.04	0.05	0.05	0.05
SrO	6×10^{-3}	6×10^{-3}	5×10^{-3}	5×10^{-3}	5×10^{-3}	5×10^{-3}	5×10^{-3}	5×10^{-3}	3×10^{-3}	5×10^{-3}	5×10^{-3}	5×10^{-3}	5×10^{-3}
La_2O_3	2×10^{-4}	2×10^{-4}	2×10^{-4}	2×10^{-4}	2×10^{-4}	2×10^{-4}	2×10^{-4}	2×10^{-4}	3×10^{-4}	3×10^{-4}	3×10^{-4}	4×10^{-4}	4×10^{-4}
CeO_2	5×10^{-4}	4×10^{-4}	4×10^{-4}	4×10^{-4}	4×10^{-4}	4×10^{-4}	4×10^{-4}	4×10^{-4}	4×10^{-4}	5×10^{-4}	5×10^{-4}	5×10^{-4}	6×10^{-4}
Nb_2O_5	7×10^{-4}	9×10^{-4}	1×10^{-3}	1×10^{-3}	1×10^{-3}	1×10^{-3}	8×10^{-6}	3×10^{-6}	4×10^{-6}	4×10^{-6}	5×10^{-6}	5×10^{-6}	5×10^{-6}
CsI	2×10^{-5}	2×10^{-5}	1×10^{-5}	1×10^{-5}	--	--	--	--	--	--	--	--	--
Cd	--	--	--	--	--	--	--	--	--	--	--	--	--
Source Rate (above pool) g/sec	8.4	11.4	14.6	18.8	23.4	24.9	23.4	21.1	18.1	15.0	15.7	10.6	9.0

TABLE 6.15. AEROSOL COMPOSITION AND TOTAL RELEASE RATE FOR SURRY S_2D, CORE-CONCRETE INTERACTION

Species, %	Time, sec											
	0	1200	2400	3600	4800	6000	7200	8400	9600	10800	12000	13200
FeO	--	13.7	12.1	11.3	16.6	19.9	20.0	20.1	20.7	22.1	0.96	1.10
Cr_2O_3	--	--	0.02	0.01	--	--	--	--	--	--	2×10^{-4}	4×10^{-4}
Ni	8×10^{-4}	0.04	0.11	0.12	0.09	0.04	0.04	0.05	0.06	0.08	0.31	0.39
Mo	--	--	2×10^{-8}	2×10^{-8}	1×10^{-8}	--	--	--	--	--	4×10^{-5}	6×10^{-5}
Ru	--	3×10^{-8}	2×10^{-7}	2×10^{-7}	1×10^{-7}	3×10^{-8}	3×10^{-8}	4×10^{-8}	5×10^{-8}	7×10^{-8}	3×10^{-7}	5×10^{-7}
Sn	3×10^{-3}	0.01	0.02	0.02	0.02	0.01	0.01	0.02	0.02	0.02	0.22	0.26
Sb	6×10^{-7}	2×10^{-6}	4×10^{-6}	4×10^{-6}	4×10^{-6}	3×10^{-6}	3×10^{-6}	3×10^{-6}	3×10^{-6}	3×10^{-6}	2×10^{-5}	2×10^{-5}
Te	0.05	0.11	0.13	0.13	0.15	0.13	0.13	0.14	0.14	0.15	0.54	0.50
Ag	0.46	4.66	8.98	8.99	8.41	5.69	5.69	6.41	7.17	8.23	31.3	34.0
Mn	0.12	0.87	1.54	1.52	1.49	1.07	1.06	1.18	1.30	1.48	5.54	5.83
CaO	--	0.47	2.56	5.30	8.58	9.22	9.96	10.2	9.35	6.72	0.36	0.45
Al_2O_3	--	3×10^{-5}	1×10^{-4}	2×10^{-4}	5×10^{-4}	9×10^{-4}	1×10^{-3}	1×10^{-3}	1×10^{-3}	2×10^{-3}	6×10^{-3}	5×10^{-3}
Na_2O	--	7.70	6.91	6.50	9.64	11.6	11.6	11.7	12.0	12.8	4.86	4.56
K_2O	--	12.1	11.2	10.8	16.5	20.3	20.6	20.4	20.7	21.6	47.4	42.1
SiO_2	--	15.4	17.7	21.8	29.8	30.1	29.5	28.7	27.6	26.2	7.54	9.63
UO_2	0.03	0.08	0.14	0.12	0.11	0.08	0.06	0.06	0.06	0.06	0.91	1.12
ZrO_2	0.02	0.01	9×10^{-3}	8×10^{-3}	0.01	0.01	0.01	0.01	0.01	0.01	0.04	0.03
Cs_2O	--	--	--	--	--	--	--	--	--	--	--	--
BaO	0.22	1.16	1.36	1.10	1.22	0.73	0.52	0.42	0.33	0.21	0.03	0.03
SrO	0.69	1.60	1.95	1.61	1.56	1.03	0.72	0.57	0.43	0.26	4×10^{-3}	4×10^{-3}
La_2O_3	4×10^{-4}	2×10^{-4}	2×10^{-4}	2×10^{-4}	2×10^{-4}	2×10^{-4}	2×10^{-4}	2×10^{-4}	2×10^{-4}	2×10^{-4}	8×10^{-4}	8×10^{-4}
CeO_2	6×10^{-4}	0.07	0.19	0.18	0.11	0.04	0.03	0.03	0.02	0.02	8×10^{-4}	8×10^{-4}
Nb_2O_5	6×10^{-6}	4×10^{-6}	3×10^{-6}	3×10^{-6}	4×10^{-6}	3×10^{-6}	3×10^{-6}	3×10^{-6}	3×10^{-6}	3×10^{-6}	8×10^{-6}	8×10^{-4}
CsI	--	--	--	--	--	--	--	--	--	--	--	--
Cd	98.3	42.0	35.0	30.4	5.68	--	--	--	--	--	--	--
Source Rate (after pool) g/sec	0.8	8.1	20.0	32.2	51.4	59.6	45.0	40.1	38.2	38.4	8.8	5.3

TABLE 6.15. (Continued)

Species, %	Time, sec											
	14400	15600	16800	18000	19200	20400	21600	22800	24000	25200	26400	27600
FeO	1.24	1.37	1.47	1.55	1.62	1.67	1.71	1.72	1.71	1.65	1.56	1.44
Cr_2O_3	0.20	0.26	0.31	0.36	0.39	0.42	0.43	0.41	0.38	0.33	0.28	0.23
Ni	0.48	0.57	0.66	0.72	0.77	0.80	0.80	0.76	0.70	0.63	0.55	0.47
Mo	1×10^{-4}	2×10^{-4}	2×10^{-4}	3×10^{-4}	4×10^{-4}	4×10^{-4}	5×10^{-4}	4×10^{-4}	4×10^{-4}	3×10^{-4}	3×10^{-4}	3×10^{-4}
Ru	8×10^{-7}	1×10^{-6}	2×10^{-6}	2×10^{-6}	3×10^{-6}	3×10^{-6}	3×10^{-6}	3×10^{-6}	2×10^{-6}	2×10^{-6}	1×10^{-6}	8×10^{-7}
Sn	0.29	0.32	0.35	0.37	0.38	0.39	0.40	0.40	0.40	0.39	0.38	0.37
Sb	2×10^{-5}	2×10^{-5}	2×10^{-5}	2×10^{-5}	2×10^{-5}	2×10^{-5}	2×10^{-5}	2×10^{-5}	2×10^{-5}	2×10^{-5}	2×10^{-5}	2×10^{-5}
Te	0.46	0.41	0.38	0.34	0.32	0.31	0.30	0.32	0.34	0.36	0.39	0.42
Ag	36.1	37.8	38.6	39.0	39.0	38.9	38.8	38.7	38.4	37.7	36.6	35.2
Mn	6.00	6.07	6.06	5.98	5.80	5.70	5.66	5.80	5.82	5.82	5.77	5.65
CaO	0.59	0.67	0.71	0.74	0.77	0.79	0.81	0.82	0.82	0.82	0.81	0.79
Al_2O_3	4×10^{-3}	4×10^{-3}	3×10^{-3}	3×10^{-3}	2×10^{-3}	2×10^{-3}	2×10^{-3}	3×10^{-3}	3×10^{-3}	4×10^{-3}	5×10^{-3}	6×10^{-3}
Na_2O	4.17	3.80	3.48	3.23	3.06	2.96	2.96	3.13	3.40	3.72	4.03	4.31
K_2O	36.5	31.4	27.5	24.6	22.7	21.6	21.6	23.4	26.3	30.3	34.5	38.9
SiO_2	12.4	15.5	18.4	20.9	22.8	23.9	24.0	22.2	19.6	16.4	13.4	10.7
UO_2	1.40	1.70	1.96	2.18	2.33	2.42	2.42	2.27	2.06	1.81	1.58	1.38
ZrO_2	0.02	0.02	0.02	0.01	0.01	0.01	0.01	0.01	0.01	0.01	0.02	0.02
Cs_2O	--	--	--	--	--	--	--	--	--	--	--	--
BaO	0.04	0.04	0.04	0.04	0.04	0.03	0.03	0.03	0.03	0.03	0.04	0.04
SrO	5×10^{-3}	6×10^{-3}	6×10^{-3}	6×10^{-3}	6×10^{-3}	6×10^{-3}	5×10^{-3}	5×10^{-3}	5×10^{-3}	5×10^{-3}	5×10^{-3}	5×10^{-3}
La_2O_3	4×10^{-4}	3×10^{-4}	2×10^{-4}	2×10^{-4}	2×10^{-4}	2×10^{-4}	2×10^{-4}	2×10^{-4}	2×10^{-4}	2×10^{-4}	2×10^{-4}	3×10^{-4}
CeO_2	6×10^{-4}	5×10^{-4}	5×10^{-4}	5×10^{-4}	5×10^{-4}	5×10^{-4}	4×10^{-4}	4×10^{-4}	4×10^{-4}	4×10^{-4}	4×10^{-4}	5×10^{-4}
Nb_2O_5	5×10^{-6}	4×10^{-6}	9×10^{-4}	1×10^{-3}	1×10^{-3}	1×10^{-3}	1×10^{-3}	1×10^{-3}	1×10^{-3}	8×10^{-4}	4×10^{-6}	4×10^{-6}
CsI	--	--	--	--	--	--	--	--	--	--	--	--
Cd												
Source Rate (above pool) g/sec	4.9	6.2	8.4	11.2	14.2	17.0	21.9	24.6	23.8	21.0	18.0	15.2

TABLE 6.15. (Continued)

Species, %	Time, sec						
	28800	30000	31200	32400	33600	34800	36000
FeO	1.31	1.19	1.08	0.98	0.89	0.78	0.69
Cr_2O_3	2×10^{-3}	2×10^{-3}	3×10^{-3}	3×10^{-3}	3×10^{-3}	4×10^{-3}	4×10^{-3}
Ni	0.41	0.36	0.32	0.28	0.26	0.22	0.19
Mo	3×10^{-4}	3×10^{-4}	3×10^{-4}	3×10^{-4}	4×10^{-4}	4×10^{-4}	6×10^{-4}
Ru	6×10^{-7}	4×10^{-7}	3×10^{-7}	2×10^{-7}	2×10^{-7}	1×10^{-7}	1×10^{-7}
Sn	0.35	0.35	0.34	0.34	0.35	0.35	0.35
Sb	2×10^{-5}	2×10^{-5}	2×10^{-5}	2×10^{-5}	2×10^{-5}	2×10^{-5}	2×10^{-5}
Te	0.44	0.46	0.47	0.48	0.49	0.50	0.52
Ag	33.6	32.2	30.7	29.5	28.4	26.9	25.4
Mn	5.51	5.37	5.21	5.08	4.97	4.79	4.62
CaO	0.77	0.75	0.74	0.73	0.72	0.71	0.70
Al_2O_3	7×10^{-3}	8×10^{-3}	9×10^{-3}	0.01	0.01	0.01	0.01
Na_2O	4.55	4.69	4.78	4.82	4.83	4.82	4.77
K_2O	43.3	46.6	49.8	52.2	54.3	57.1	59.6
SiO_2	8.47	6.84	5.48	4.49	3.71	2.86	2.19
UO_2	1.21	1.11	1.02	0.97	0.94	0.89	0.86
ZrO_2	0.02	0.02	0.02	0.03	0.03	0.03	0.03
Cs_2O	--	--	--	--	--	--	--
BaO	0.04	0.04	0.04	0.04	0.04	0.04	0.04
SrO	5×10^{-3}	4×10^{-3}	4×10^{-3}	4×10^{-3}	4×10^{-3}	4×10^{-3}	4×10^{-3}
La_2O_3	3×10^{-4}	4×10^{-4}	4×10^{-4}	4×10^{-4}	4×10^{-4}	5×10^{-4}	5×10^{-4}
CeO_2	5×10^{-4}	5×10^{-4}	6×10^{-4}	6×10^{-4}	6×10^{-4}	7×10^{-4}	7×10^{-4}
Nb_2O_5	5×10^{-6}	5×10^{-6}	5×10^{-6}	6×10^{-6}	6×10^{-6}	6×10^{-6}	7×10^{-6}
CsI	--	--	--	--	--	--	--
Cd							
Source Rate (above pool) g/sec	12.6	10.6	9.1	7.9	7.5	7.0	6.2

TABLE 6.16. AEROSOL COMPOSITION AND TOTAL RELEASE RATE FOR SURRY V, CORE-CONCRETE INTERACTION

Species, %	Time, sec											
	0	1200	2400	3600	4800	6000	7200	8400	9600	10800	12000	13200
FeO	--	14.2	12.7	11.0	9.58	13.6	15.3	18.4	23.7	1.11	1.02	0.86
Cr_2O_3	--	--	--	--	--	--	--	--	--	4×10^{-4}	1×10^{-3}	2×10^{-3}
Ni	2.57	0.24	0.51	1.27	2.78	0.40	0.16	0.12	0.11	0.28	0.24	0.18
Mo	3×10^{-6}	5×10^{-8}	2×10^{-7}	9×10^{-7}	4×10^{-6}	1×10^{-7}	2×10^{-8}	1×10^{-8}	1×10^{-8}	3×10^{-5}	3×10^{-5}	2×10^{-5}
Ru	2×10^{-5}	4×10^{-7}	2×10^{-6}	8×10^{-6}	3×10^{-5}	1×10^{-6}	2×10^{-7}	1×10^{-7}	1×10^{-7}	2×10^{-7}	1×10^{-7}	9×10^{-8}
Sn	0.08	0.02	0.03	0.04	0.07	0.02	0.01	0.01	0.01	0.08	0.08	0.07
Sb	1×10^{-5}	3×10^{-6}	4×10^{-6}	6×10^{-6}	8×10^{-6}	3×10^{-6}	2×10^{-6}	2×10^{-6}	2×10^{-6}	8×10^{-6}	7×10^{-6}	7×10^{-6}
Te	0.70	0.32	0.36	0.43	0.48	0.32	0.25	0.25	0.28	0.88	0.89	0.91
Ag	25.5	12.1	19.3	21.2	18.4	16.2	8.96	7.89	8.04	22.6	21.0	18.8
Mn	7.55	1.84	2.66	4.14	5.95	2.19	1.28	1.16	1.21	3.49	3.31	3.03
CaO	--	14.4	13.0	11.6	10.6	13.9	15.5	13.4	4.53	0.59	0.48	0.42
Al_2O_3	--	6×10^{-4}	8×10^{-4}	2.53	4.97	1×10^{-3}	1×10^{-3}	2×10^{-3}	2×10^{-3}	8×10^{-3}	9×10^{-3}	0.01
Na_2O	--	8.40	7.60	6.65	5.81	8.10	9.01	10.8	13.5	5.55	5.70	5.77
K_2O	--	14.7	13.4	11.6	10.0	14.3	15.9	18.6	22.1	56.7	60.2	64.9
SiO_2	--	30.6	27.3	23.7	20.7	29.2	32.3	28.8	26.3	7.94	6.36	4.48
UO_2	3.43	0.20	0.35	0.89	2.06	0.22	0.08	0.06	0.06	0.68	0.58	0.47
ZrO_2	0.04	2×10^{-3}	7×10^{-3}	0.01	0.03	6×10^{-3}	7×10^{-3}	8×10^{-3}	9×10^{-3}	0.03	0.03	0.03
Cs_2O	--	--	--	--	--	--	--	--	--	--	--	--
BaO	2.64	1.00	0.99	0.74	0.71	0.49	0.28	0.18	0.06	0.02	0.02	0.02
SrO	7.48	1.59	1.42	1.64	1.81	0.81	0.37	0.23	0.07	3×10^{-3}	2×10^{-3}	2×10^{-3}
La_2O_3	3.82	2×10^{-4}	2×10^{-4}	1.12	2.37	1×10^{-4}	1×10^{-4}	1×10^{-4}	1×10^{-4}	5×10^{-4}	5×10^{-4}	5×10^{-4}
CeO_2	6.96	0.33	0.59	1.44	3.10	0.30	0.07	0.03	8×10^{-3}	6×10^{-4}	7×10^{-4}	7×10^{-4}
Nb_2O_5	4×10^{-4}	1×10^{-5}	3×10^{-5}	1×10^{-4}	5×10^{-4}	2×10^{-5}	2×10^{-6}	2×10^{-6}	2×10^{-6}	7×10^{-6}	7×10^{-6}	8×10^{-6}
CsI	--	--	--	--	--	--	--	--	--	--	--	--
Cd	39.2	--	--	--	--	--	--	--	--	--	--	--
Source Rate g/sec	156.0	81.4	20.7	24.6	147.0	157.0	100.0	66.0	49.9	14.4	16.0	13.3

TABLE 6.16. (Continued)

Species, %	Time, sec									
	14400	15600	16800	18000	19200	20400	21600	22800	24000	25200
FeO	0.79	0.72	0.66	0.66	0.56	0.43	0.38	0.36	0.32	0.32
Cr_2O_3	2×10^{-3}	3×10^{-3}	3×10^{-3}	4×10^{-3}	4×10^{-3}	5×10^{-3}	6×10^{-3}	6×10^{-3}	7×10^{-3}	7×10^{-3}
Ni	0.17	0.15	0.14	0.14	0.12	0.08	0.08	0.07	0.07	0.07
Mo	3×10^{-5}	3×10^{-5}	3×10^{-5}	5×10^{-5}	5×10^{-5}	5×10^{-5}	7×10^{-5}	1×10^{-4}	1×10^{-4}	2×10^{-4}
Ru	7×10^{-8}	--	--	--	--	--	--	--	--	--
Sm	0.07	0.07	0.07	0.07	0.07	0.06	0.06	0.07	0.07	0.08
Sb	7×10^{-6}	7×10^{-6}	7×10^{-6}	7×10^{-6}	7×10^{-6}	7×10^{-6}	7×10^{-6}	7×10^{-6}	7×10^{-6}	8×10^{-6}
Te	0.91	0.92	0.92	0.93	0.93	0.93	0.95	0.96	0.97	0.99
Ag	17.9	17.0	16.3	16.9	15.3	12.9	12.4	12.2	11.6	12.4
Mn	2.92	2.82	2.73	2.82	2.61	2.30	2.25	2.25	2.19	2.34
CaO	0.48	0.48	0.47	0.51	0.50	0.42	0.42	0.44	0.44	0.50
Al_2O_3	0.01	0.01	0.01	0.01	0.02	0.02	0.02	0.02	0.02	0.02
Na_2O	5.70	5.66	5.60	5.56	5.48	5.28	5.13	5.00	4.83	4.76
K_2O	66.9	68.5	70.0	69.3	72.1	75.9	76.9	77.3	78.3	77.2
SiO_2	3.69	3.11	2.60	2.60	1.95	1.24	1.01	0.88	0.72	0.72
UO_2	0.45	0.43	0.41	0.44	0.40	0.35	0.36	0.37	0.38	0.44
ZrO_2	0.03	0.03	0.04	0.03	0.04	0.04	0.04	0.04	0.04	0.04
Cs_2O	--	--	--	--	--	--	--	--	--	--
BaO	0.02	0.02	0.02	0.02	0.02	0.02	0.02	0.02	0.02	0.03
SrO	2×10^{-3}	2×10^{-3}	2×10^{-3}	2×10^{-3}	2×10^{-3}	2×10^{-3}	2×10^{-3}	2×10^{-3}	2×10^{-3}	2×10^{-3}
La_2O_3	5×10^{-4}	5×10^{-4}	5×10^{-4}	5×10^{-4}	5×10^{-4}	6×10^{-4}	6×10^{-4}	6×10^{-4}	7×10^{-4}	6×10^{-4}
CeO_2	7×10^{-4}	7×10^{-4}	8×10^{-4}	7×10^{-4}	8×10^{-4}	9×10^{-4}	9×10^{-4}	9×10^{-4}	9×10^{-4}	9×10^{-4}
Nb_2O_5	8×10^{-6}	8×10^{-6}	8×10^{-6}	7×10^{-6}	8×10^{-6}	9×10^{-6}	9×10^{-6}	9×10^{-6}	1×10^{-5}	9×10^{-6}
CsI	--	--	--	--	--	--	--	--	--	--
Cd	--	--	--	--	--	--	--	--	--	--
Source Rate g/sec	9.4	8.6	6.4	5.7	7.2	5.8	4.1	3.6	3.2	3.3

7. RESULTS AND DISCUSSION

7.1 Introduction

Results of calculations for the transport and deposition of radionuclides are presented and discussed in this section. The plants and sequences selected for consideration were discussed in Chapter 4, the analytical and calculational methods were described in Chapter 5, and the assumptions and bases for the calculations were described in Chapter 6. Results presented in this chapter include the deposition and release from the reactor coolant system of radionuclides leaving the core region. These results are based on TRAP-MELT code calculations. Also included as results are the masses of radionuclides airborne and deposited in the containment as well as the airborne materials leaked to the environment, based on NAUA-4 calculations.

Four basic system sequences were considered in the analyses: AB, TMLB', S_2D, and V. Combined with these sequences are several variations in the analyses, allowing for different assumptions of containment failure, compartmentalization of the containment, compartmentalization of the ECC injection piping for the V sequence, and heating of primary system structures by decay of deposited radionuclides.

7.2 Transport and Deposition in Primary System

7.2.1 RCS Transport and Deposition for Sequence AB

The AB sequences are characterized as low pressure, generally high flow rate scenarios with respect to RCS behavior. These sequences, considered here as hot leg breaks, offer the minimum volume of the RCS to the fission products being transported to the containment atmosphere. This, of course, usually minimizes the opportunity for retention in the primary system. A variety of containment failure modes have been examined for this sequence in the Surry plant and are reported in this volume.

The TRAP-MELT predictions of fission product retention for the AB sequence are found in Tables 7.1 and 7.2. The extent of retention is seen to be different for the various species, and the cause of the differences is

TABLE 7.1. CORSOR PREDICTIONS OF MASSES OF SPECIES RELEASED FROM THE CORE (TOTAL) AND TRAP-MELT PREDICTIONS OF MASSES RETAINED IN THE RCS (RET) DURING THE AB SEQUENCE FOR THE SURRY PLANT

(Times Measured from Start of Core Melting)

Time (s)	CsI		CsOH		Te		Aerosol	
	Ret (kg)	Total (kg)	Ret (kg)	Total (kg)	Ret (kg)	Total (kg)	Ret (kg)	Total (kg)
300	2.9	12.4	15.9	67.7	0.3	0.4	319	663
600	5.3	18.9	28.3	100	0.8	1.0	523	974
900	6.9	22.7	37.0	120	1.5	1.7	682	1235
1200	0.5	24.6	3.9	130	2.4	2.9	713	1810
1510	0.5	25.3	3.9	133	2.4	3.6	714	1875
2110	0.5	25.6	3.9	135	2.4	4.4	714	1900
2710	0.5	25.8	3.9	135	2.4	4.9	721	1920
3310	0.6	25.9	4.6	136	2.9	5.7	785	1990
3910	0.7	25.9	4.9	136	4.1	6.9	911	2120
4520	0.7	26.0	5.0	136	5.4	8.2	1030	2235
5120	0.7	26.0	5.1	136	6.5	9.3	1135	2340

TABLE 7.2. TRAP-MELT PREDICTIONS OF PRIMARY SYSTEM RETENTION FACTORS (RF) AND VOLUME SPECIFIC RETENTION FACTORS AS FUNCTIONS OF TIME FOR THE AB SEQUENCE FOR THE SURRY PLANT

Time (s)	CsI		CsOH		Te			Aerosol		
	RF	Core Plate	RF	Core Plate	RF	Core	Core Plate	RF	Core	Core Plate
300	.23	.22	.23	.23	.82	0	.78	.48	.32	.16
600	.28	.27	.28	.27	.86	0	.83	.54	.36	.17
900	.30	.29	.31	.30	.93	0	.91	.55	.37	.18
1200	.02	--	.03	.01	.85	--	.77	.39	.25	.13
1510	.02	--	.03	.01	.67	--	.61	.38	.25	.13
2110	.02	--	.03	.01	.55	--	.51	.38	.24	.12
2710	.02	--	.03	.01	.49	--	.45	.38	.24	.12
3310	.02	--	.03	.01	.51	.09	.39	.39	.27	.12
3910	.03	--	.04	.01	.60	.25	.32	.43	.31	.11
4520	.03	--	.04	.01	.66	.36	.27	.46	.35	.11
5120	.03	--	.04	.01	.70	.44	.24	.48	.38	.10

apparently in the RCS gas flow rates as a function of time. Examination of the gas flow rates leaving the core shows that for this sequence there is low flow for approximately the first 1000 s after the start of core melting. This low flow rate of gas through the upper plenum permits very efficient retention of Te vapor due to its rapid reaction with the structural surfaces. This behavior is illustrated in Figure 7.1. At about t = 1000 s, the RCS gas flow rates increase dramatically as portions of the core begin to slump into the water remaining in the lower plenum. Thus, while Te continues to be emitted by the melting fuel, it moves so rapidly through the upper plenum control volumes that practically no additional Te vapor is retained. After about 2500 s, the gas flow rate decreases to very low levels again because the water has been completely exhausted, and the additional release of Te is effectively scavenged.

The influence of the RCS thermal-hydraulics is also clear in Figures 7.2 and 7.3. For these species, the surface reaction is not nearly so rapid, and the mechanism of their retention is condensation on the particles followed by particle settling in the lower portion of the upper plenum. This is seen to occur until the gas flow rate increases greatly, at which time the temperature of the upper grid plate increases from 950 F to 1340 F, resulting in re-evaporation of the CsI and CsOH into the swiftly flowing gas stream. The temperatures of the gas and the upper plenum surfaces quickly decrease to values which would permit condensation, but because the inventory of Cs and I has been nearly expended by this time, there is almost no retention of these vapors in the RCS for this sequence.

The aerosol retention factor for the AB sequence is seen in Table 7.2 to be approximately 50 percent. Figure 7.4 illustrates that about one-half of the ultimately retained aerosol mass accumulates in the core and upper plenum during the first 1000 s, characterized by low flow and high aerosol generation. As one would expect, the high flow rate during the in-vessel phase of this accident sequence permits little added retention because of the low aerosol concentrations and residence times. After vessel dryout, nearly all the emitted aerosol is retained by means of gravitational settling.

The TRAP-MELT code was executed in a mode which permitted tracking of the WASH-1400 radionuclide groups (as described in Chapter 6) for this sequence, and the results are summarized in Table 7.2a. The correspondence

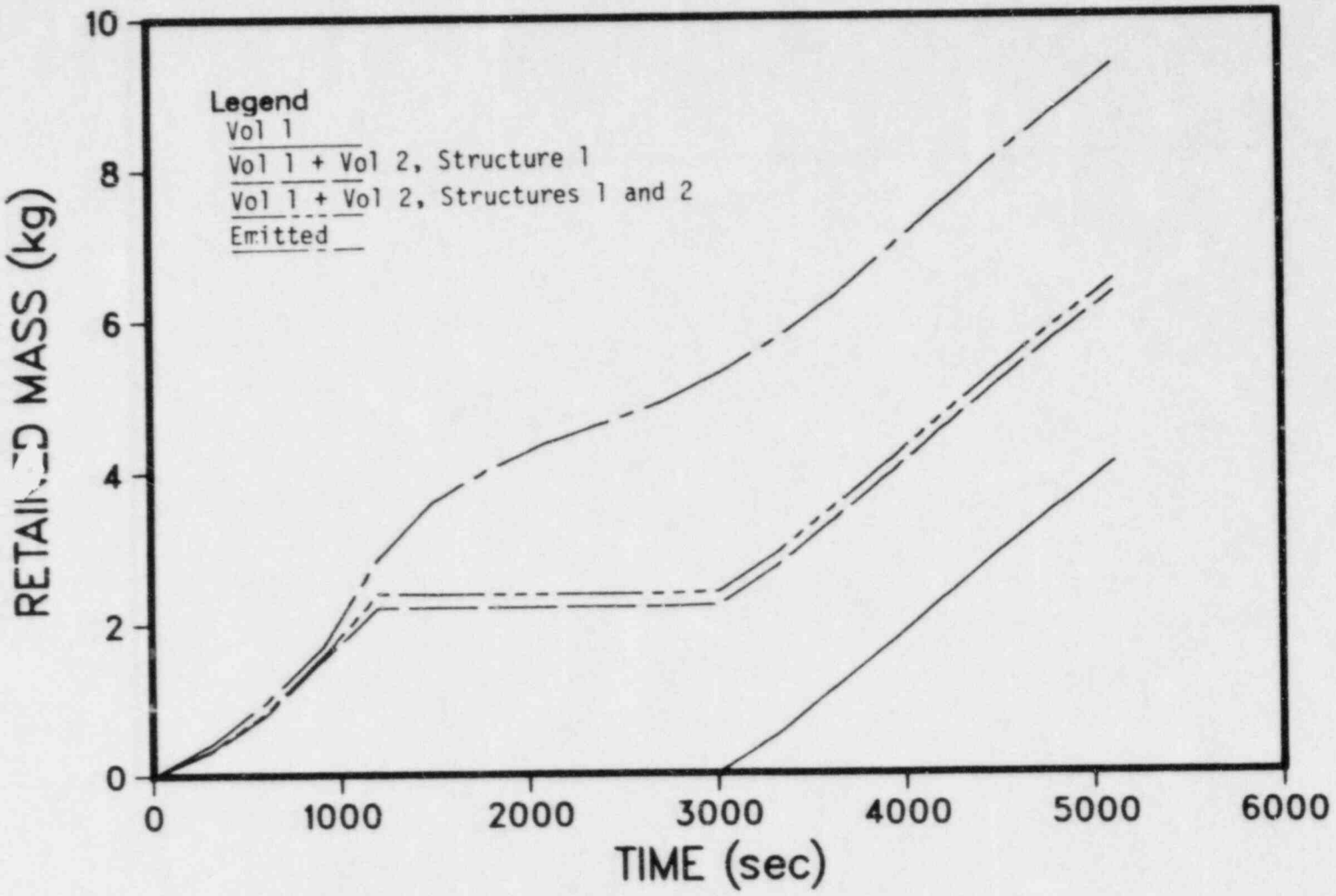

FIGURE 7.1. MASSES OF Te EMITTED FROM CORE AND RETAINED IN THE RCS CONTROL VOLUMES AS FUNCTIONS OF TIME FOR THE AB SEQUENCE (Vol 1 = Core; Vol 2, Structure 1 = Upper Grid Plate; Vol 3, Structure 2 = Guide Tubes). Times Measured from Start of Core Melting.

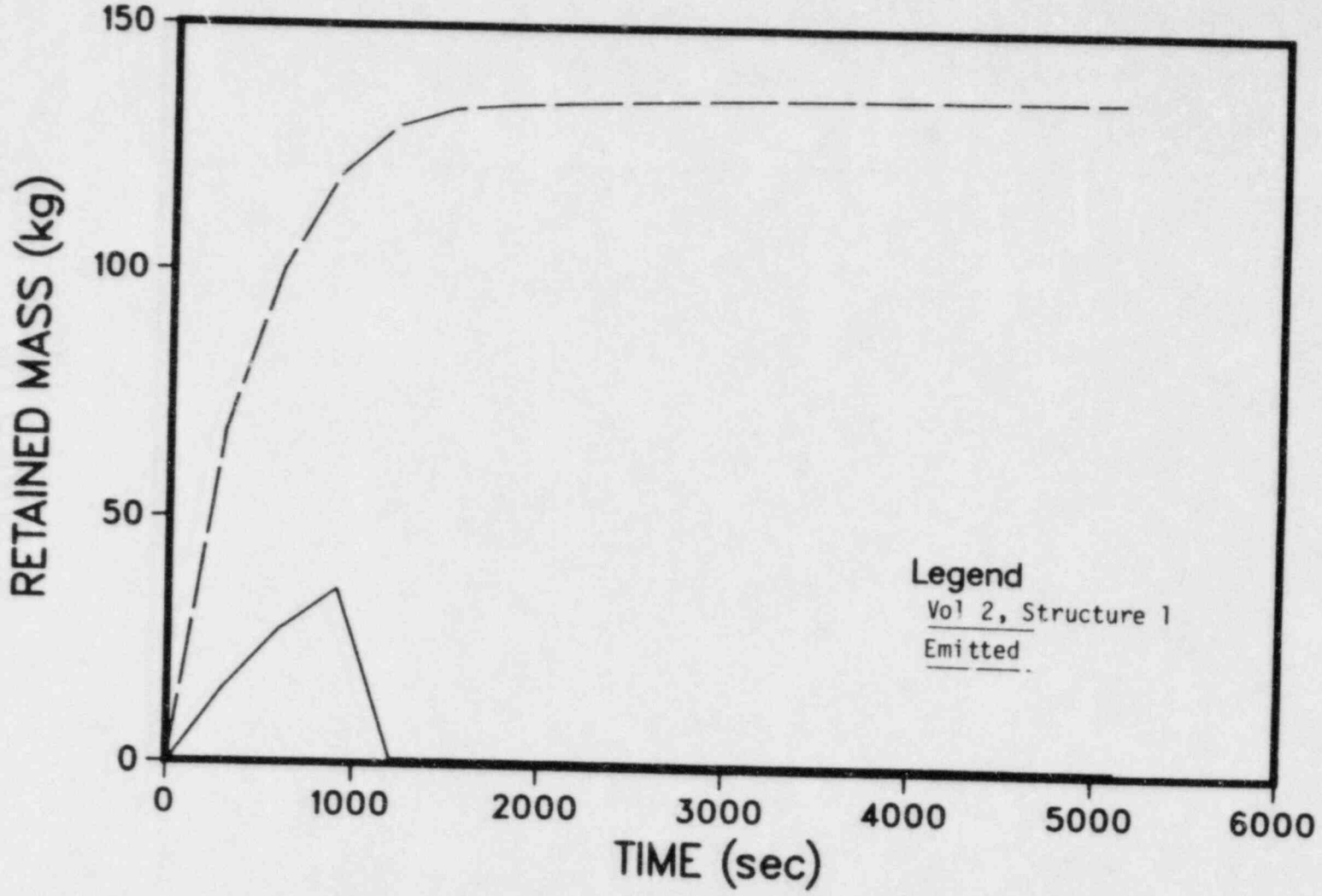

FIGURE 7.2. MASSES OF CsOH EMITTED FROM CORE AND RETAINED IN THE RCS CONTROL VOLUMES AS FUNCTIONS OF TIME FOR THE AB SEQUENCE (Vol 2, Structure 1 = Upper Grid Plate). Times Measured from Start of Core Melting.

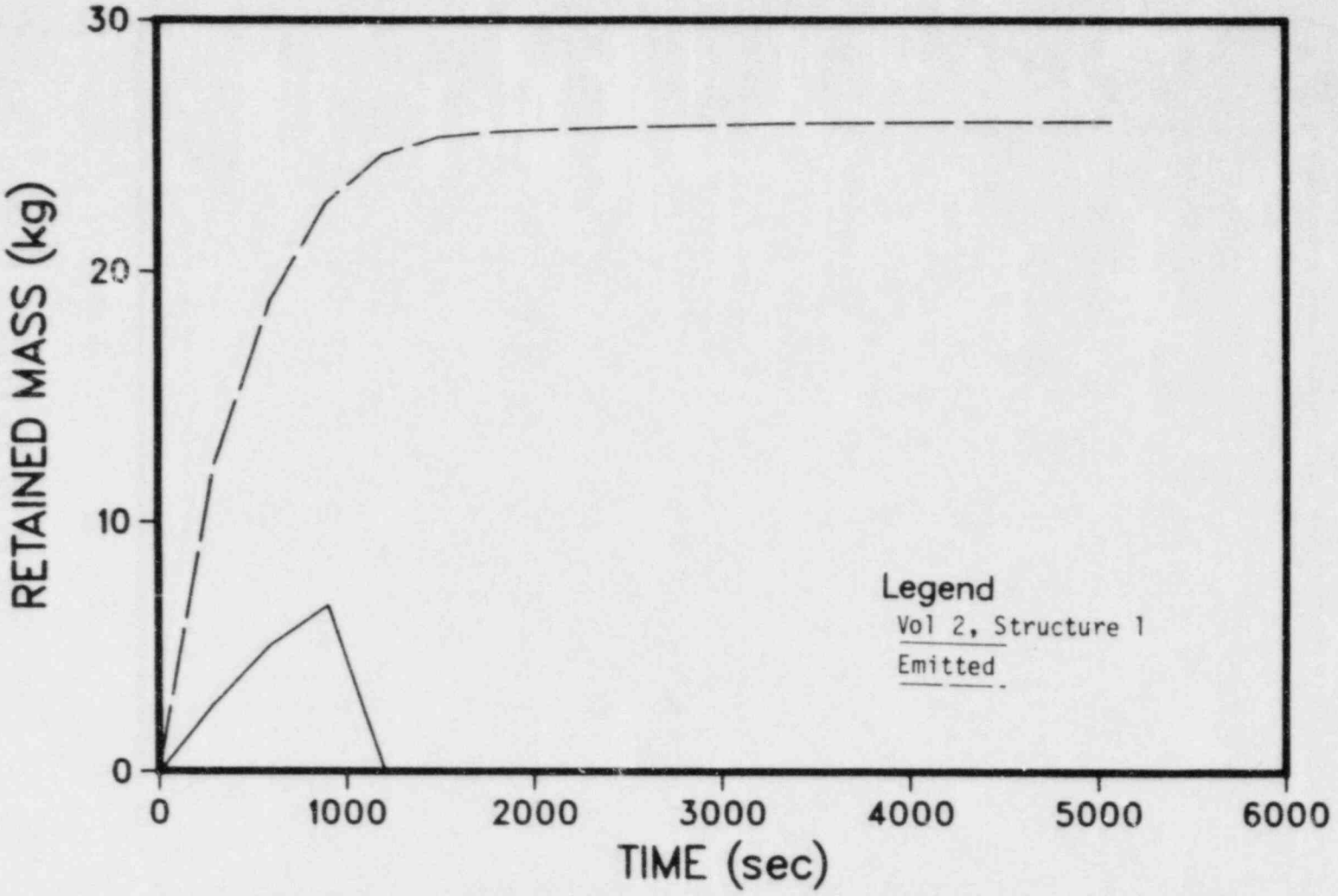

FIGURE 7.3. MASSES OF CsI EMITTED FROM CORE AND RETAINED IN THE RCS CONTROL VOLUMES AS FUNCTIONS OF TIME FOR THE AB SEQUENCE (Vol 2, Structure 1 = Upper Grid Plate). Times Measured from Start of Core Melting.

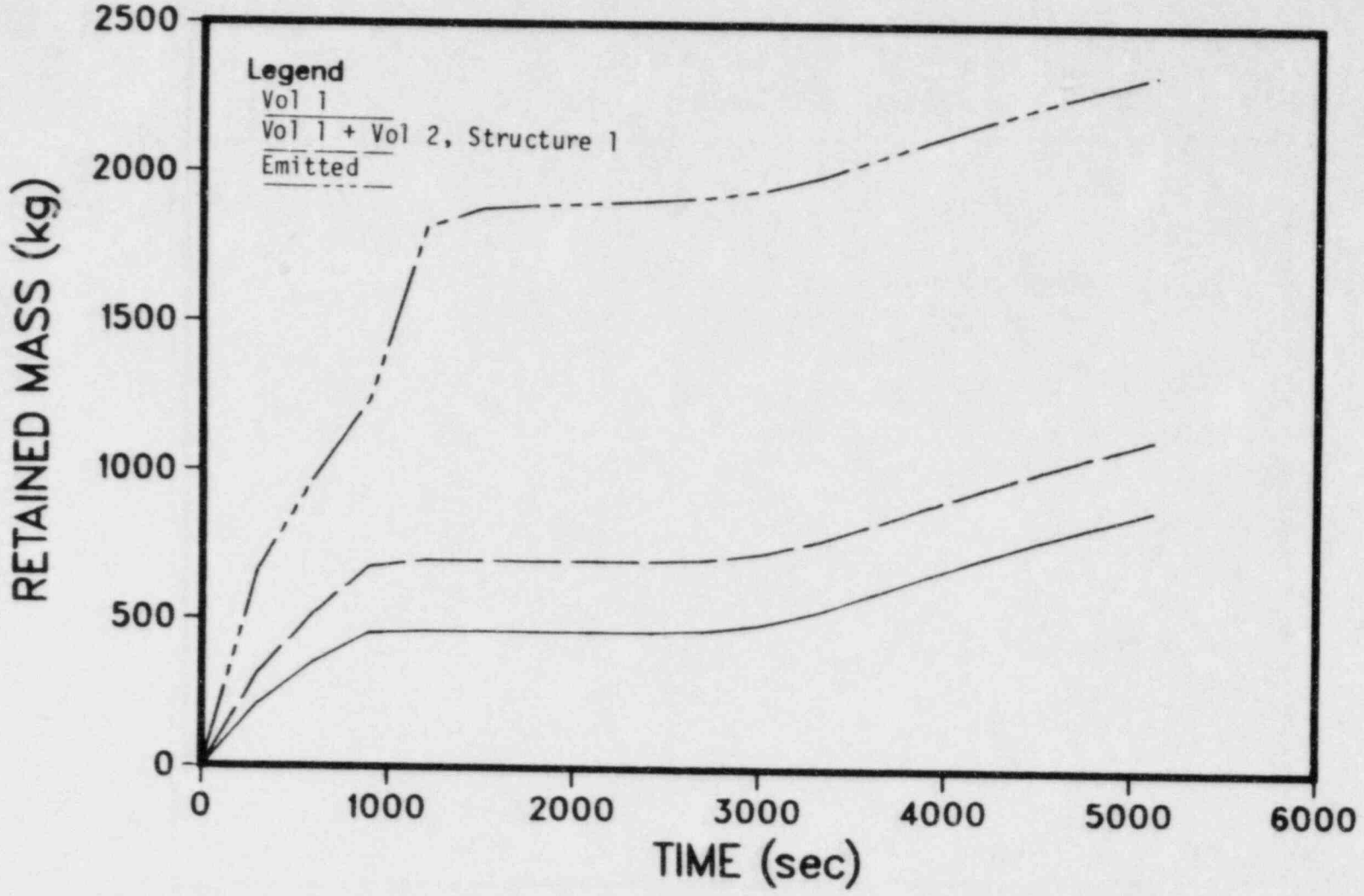

FIGURE 7.4. MASSES OF AEROSOL EMITTED FROM CORE AND RETAINED IN THE RCS CONTROL VOLUMES AS FUNCTIONS OF TIME FOR THE AB SEQUENCE (Vol 1 = Core; Vol 2, Structure 1 = Upper Grid Plate). Times Measured from Start of Core Melting.

TABLE 7.2a. CORSOR PREDICTIONS OF RELEASE FROM CORE AND TRAP-MELT PREDICTIONS OF PRIMARY SYSTEM RETENTION OF WASH-1400 GROUPS FOR AB-γ SEQUENCE

Group	Released (kg)	Retained (kg)
I	12.4	0.4
Cs	146	5.4
Te	9.3	6.5
Sr	71.1	51.1
Ru	34.7	24.4
La	0.8	0.7

*Groups are defined in Chapter 6.

between the results cited for CsI, CsOH, and Te and Groups 2, 3, and 4 is to be expected since this merely represents a regrouping of the species already considered. The results obtained for Groups 5, 6, and 7, however, are interesting since they display different overall RCS retention than does the total aerosol. While approximately 50 percent of the total aerosol mass released from the core is retained in the RCS, about 70 percent of Groups 5 and 6 and 90 percent of the Group 7 material is predicted to be retained. This is the case not because of any difference in physical or chemical properties of these groups, as they all behave identically in the code. Rather, the differing extents of retention are due to the relative timing of the releases of the various groups. Thus, the Group 7 species, which are emitted late in the in-vessel portion of the accident, are injected into the RCS during a period in which conditions, especially gas flow rates, are much more conducive to aerosol retention than is the case early in the sequence.

There are major differences in the input to the TRAP-MELT code for this analysis from that used in the initial analysis of Surry (presented in Volume 1 of this report). In this analysis, the upper plenum has been subdivided into four control volumes, and the geometries and masses of the structures in the upper plenum have been described more accurately. Another difference is the inclusion of control rod material in the aerosol inventory, leading to higher masses of aerosol being released from the core. The most significant difference in these results, however, is the lack of retention of fission products; this is a direct consequence both of the gas flow rates predicted by the MARCH code and of the timing of fission product release relative to the gas flow rates. The use of a different description of the core melting and slumping behavior appears to be a dominant influence on the predicted retention.

7.2.2 RCS Transport and Deposition for Sequence TMLB'

This sequence involves high primary system pressure with generally low flow rate, yielding long residence times of the emitted materials in the RCS. These long residence times lead to quite high retention factors for all the species considered, as seen in Tables 7.3 and 7.4. There is a significant difference in the flow rates through the RCS used in this analysis and those

TABLE 7.3. CORSOR PREDICTIONS OF MASSES OF SPECIES RELEASED FROM THE CORE (TOTAL) AND TRAP-MELT PREDICTIONS OF MASSES RETAINED IN THE RCS (RET) DURING THE TMLB SEQUENCE FOR THE SURRY PLANT

(Times Measured from Start of Core Melting)

Time (s)	CsI		CsOH		Te		Aerosol	
	Ret (kg)	Total (kg)	Ret (kg)	Total (kg)	Ret (kg)	Total (kg)	Ret (kg)	Total (kg)
106	0.2	2.9	1.8	22.1	--	0.1	218	265
306	0.9	8.2	6.1	52.2	--	0.2	436	470
611	1.7	14.0	11.9	85.5	--		699	719
1020	2.5	18.8	17.6	112.5	0.1	1.3	941	955
1426	3.7	21.7	23.8	129	0.1	2.3	1129	1139
1629	5.4	23.0	33.9	137	1.3	3.5	1241	1291
1934	21.1	24.7	125	147	6.5	6.9	1558	1688
2340	21.8	25.6	128	151	7.6	8.9	1612	1733

TABLE 7.4. TRAP-MELT PREDICTIONS OF PRIMARY SYSTEM RETENTION FACTORS (RF) AND VOLUME SPECIFIC RETENTION FACTORS AS FUNCTIONS OF TIME FOR THE TMLB SEQUENCE FOR THE SURRY PLANT

Time (s)	CsI				CsOH				Te			Aerosol		
	RF	Core Plate	Piping	Pres-surizer	RF	Core Plate	Piping	Pres-surizer	RF	Core	Core Plate	RF	Core	Core Plate
106	.07	.02	--	--	.02	.02	--	--	.04	0	.04	.82	.81	.01
306	.11	.04	--	--	.12	.05	--	--	.05	0	.05	.93	.91	.01
611	.12	.04	--	--	.14	.05	--	--	.05	0	.05	.98	.96	.01
1020	.13	.06	--	--	.16	.07	--	--	.04	0	.04	.99	.98	.01
1426	.17	.06	--	--	.18	.07	--	--	.04	0	.04	.99	.98	.01
1630	.24	.23	--	--	.23	.23	--	--	.37	0	.37	.96	.95	.01
1934	.85	.43	.18	.16	.86	.45	.18	.16	.93			.92	.77	.04
2340	.85	.43	.18	.16	.86	.45	.18	.16	.85	.17	.58	.93	.78	.04

used in the initial analysis of Surry (presented in Volume 1 of this report). In the previous analysis, the flow rate was so low as to prevent all but a few percent of the emitted materials from entering the containment until the time of bottom head failure, with nearly 75 percent of even the early emitted materials still residing in the core region, where gas and surface temperatures prohibit any condensation, at the time of vessel failure. This fact may well have led to large underestimates of the extent of the vapor species' retention.

In the present analysis, the low flow rates retain the emitted materials in the core region until just after t = 1500 s. Figure 7.5 shows that no significant retention of Te occurs until after this time. This is because the TRAP-MELT code, as used here, does not permit the surface reaction of Te to occur in the core region. As the gas flow rate from the core increases at 1500 s, the suspended vapors and particles are swept into the upper plenum control volumes, where the Te reaction leads to nearly complete scavenging by the structure surfaces. This period of high flow rates due to core slumping also leads to increased Zr cladding oxidation, which in turn increases the Te release rate from the melting fuel. As the gas flow rate continues to increase, eventually the material is transported through the RCS too quickly for the surface reaction to be completely effective, and the retention factor decreases, although it remains at a fairly high value.

The CsOH and CsI behavior indicated in Figures 7.6 and 7.7 is similar to that of Te. The cause of the small early retention of the Cs species is condensation of the vapors on particles which subsequently settle out in the upper plenum volumes. There is no retention of these species in the core volume because the high gas temperatures there prevent condensation of the vapors on the particles. As soon as the aerosol and vapors are transported into the relatively cool upper plenum, condensation and retention of these species occurs at a rapid rate. The process does not, however, go "to completion", being curtailed by the large velocities which are achieved and by the low emission rate of Cs and I after about 1400 s.

The aerosol retention factor reaches 90 percent for this transient sequence, which is similar to values obtained for such sequences in other plants. The explanation for this is found in the long RCS residence time the low flow rate affords the aerosol. This results in the particle mass median diameter being greater than 3 μm when the aerosol reaches the upper plenum, where there

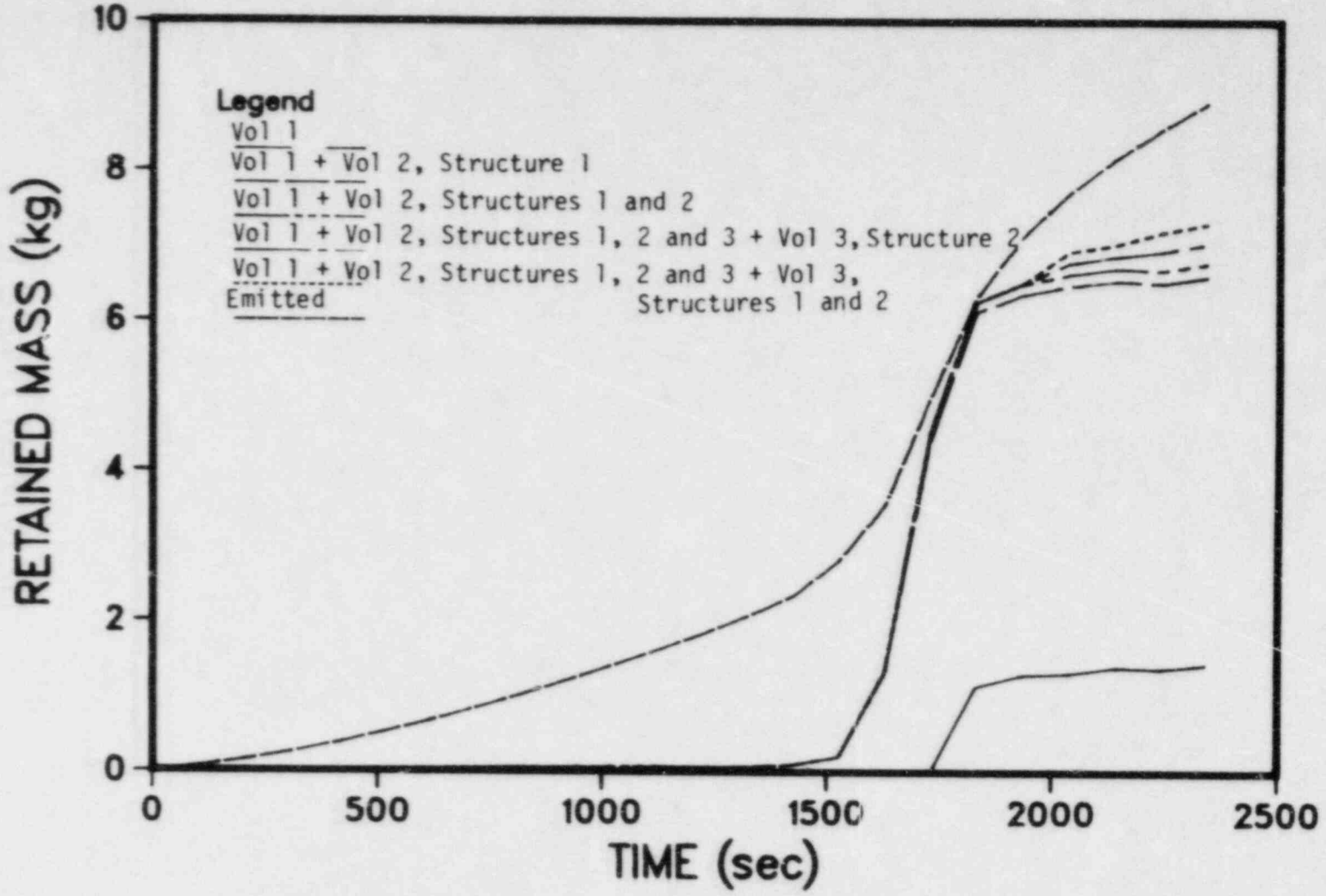

FIGURE 7.5. MASSES OF Te EMITTED FROM CORE AND RETAINED IN THE RCS CONTROL VOLUMES AS FUNCTIONS OF TIME FOR THE TMLB' SEQUENCE (Vol 1 = Core; Vol 2, Structure 1 = Upper Grid Plate; Vol 2, Structure 2 = Guide Tubes; Vol 2, Structure 3 = Core Barrel; Vol 3, Structure 1 = Pressurizer; Vol 3, Structure 2 = Hot Leg). Times Measured from Start of Core Melting.

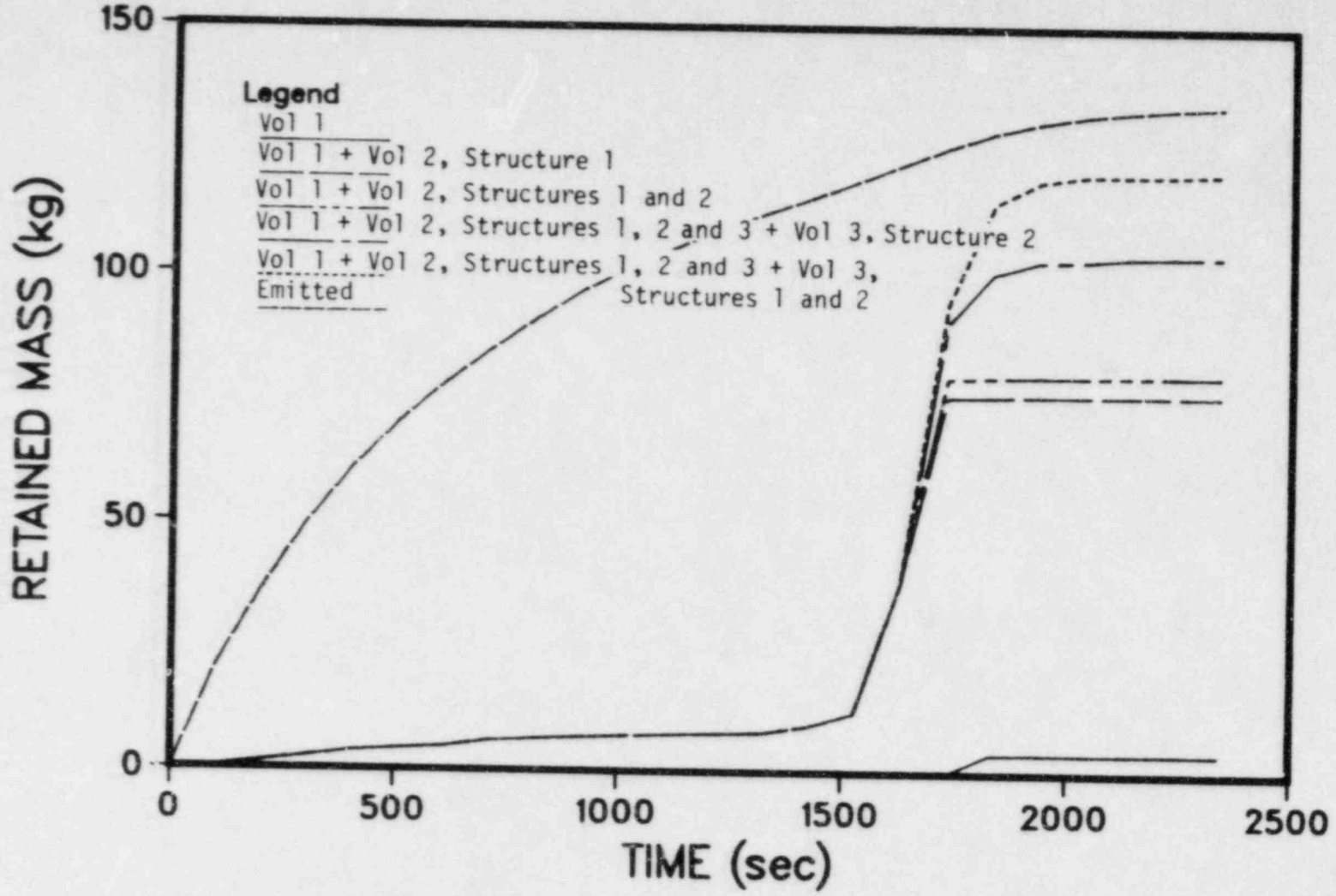

FIGURE 7.6. MASSES OF CsOH EMITTED FROM CORE AND RETAINED IN THE RCS CONTROL VOLUMES AS FUNCTIONS OF TIME FOR THE TMLB' SEQUENCE (Vol 1 = Core; Vol 2, Structure 1 = Upper Grid Plate; Vol 2, Structure 2 = Guide Tubes; Vol 2, Structure 3 = Core Barrel; Vol 3, Structure 1 = Pressurizer; Vol 3, Structure 2 = Hot Leg). Times Measured from Start of Core Melting.

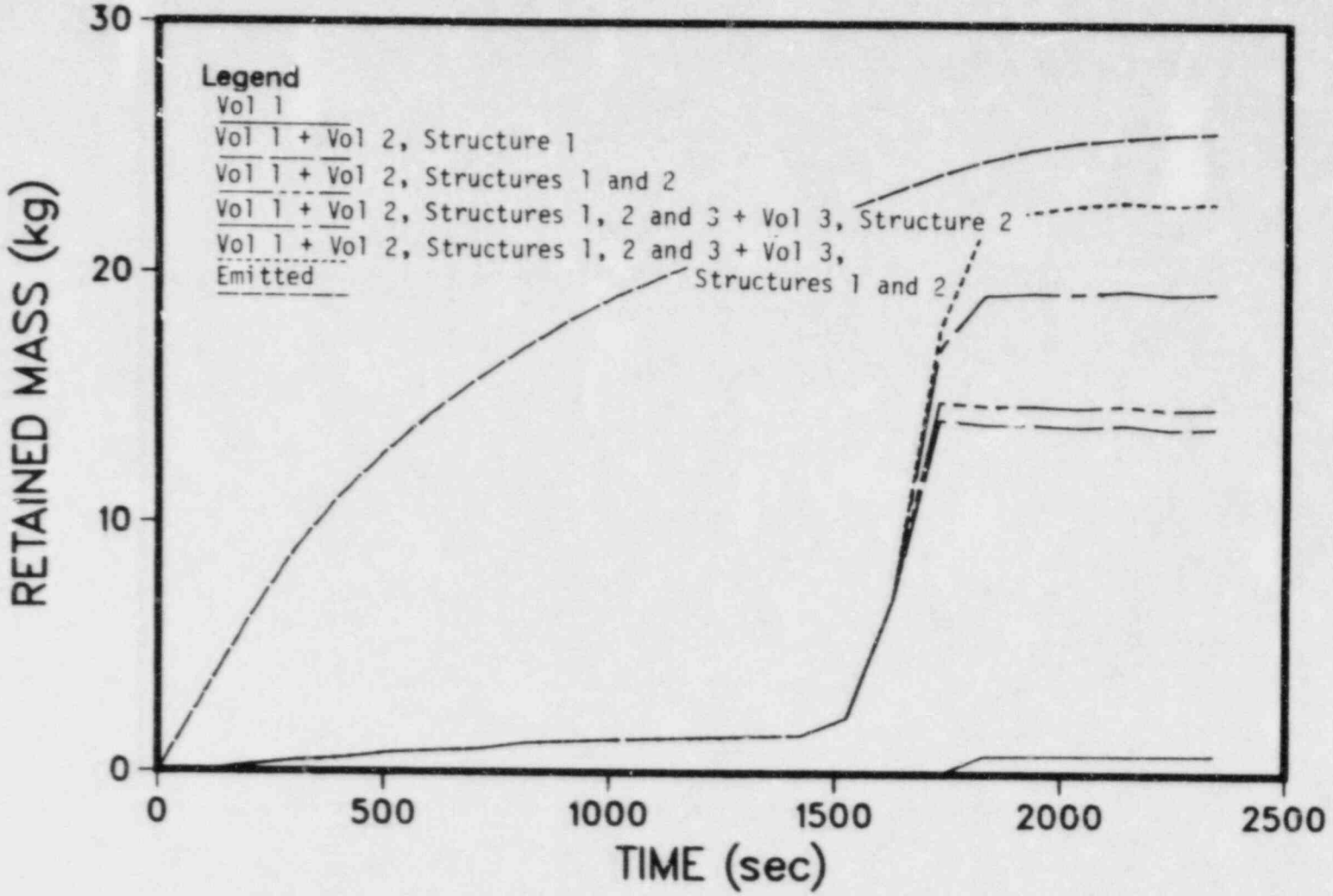

FIGURE 7.7. MASSES OF CsI EMITTED FROM CORE AND RETAINED IN THE RCS CONTROL VOLUMES AS FUNCTIONS OF TIME FOR THE TMLB' SEQUENCE (Vol 1 = Core; Vol 2, Structure 1 = Upper Grid Plate; Vol 2, Structure 2 = Guide Tubes; Vol 2, Structure 3 = Core Barrel; Vol 3, Structure 1 = Pressurizer; Vol 3, Structure 2 = Hot Leg). Times Measured from Start of Core Melting.

is a greater amount of horizontal surface area available for settling of the particles. This effect is clear in Figure 7.8. Significantly, the aerosol generation rate decreases greatly during the high flow rate period. This results in a lower amount of aerosol mass being injected into the containment than would occur for the case where aerosol generation proceeded at a high rate along with the high gas flows.

While the aerosol retention factors for this sequence as analyzed here and in Volume 1 are similar, the location of the retention is different because of the different flow rates used in the two TRAP-MELT analyses, and the total mass injected into the containment is nearly three times as great here (165 kg) because of the higher aerosol generation rates used in the current analyses.

TRAP-MELT predictions for the RCS retention of the WASH-1400 groups were obtained for this sequence and are summarized in Table 7.4a. As for the AB sequence above, the extent of retention of Groups 5, 6, and 7 vary somewhat due to the differences in the timing of their releases, but the variation seen here is less than in the AB case and is closely related to the total aerosol retention predicted by the code.

7.2.3 RCS Transport and Deposition for the Sequence V

The V sequence, from the perspective of the primary system, is much the same as an intermediate size break in the cold leg of a steam generator. The difference, which is very significant from a risk standpoint, is that the primary system communicates directly with the auxiliary building(s) through a long pipe. The gas flow through the primary circuit is fairly low during the first 1000 s after the start of core melting, and then reaches very high values until approximately 2400 s, at which time vessel dryout occurs. Bottom head failure is not predicted by MARCH to occur until about 4000 s after vessel dryout--resulting in a long period during which the melting core is emitting into a stagnant primary system. The total masses of the species of interest emitted from the core and retained throughout the primary system are given in Table 7.5, and the retention factors for the primary system and specific control volumes are given in Table 7.6.

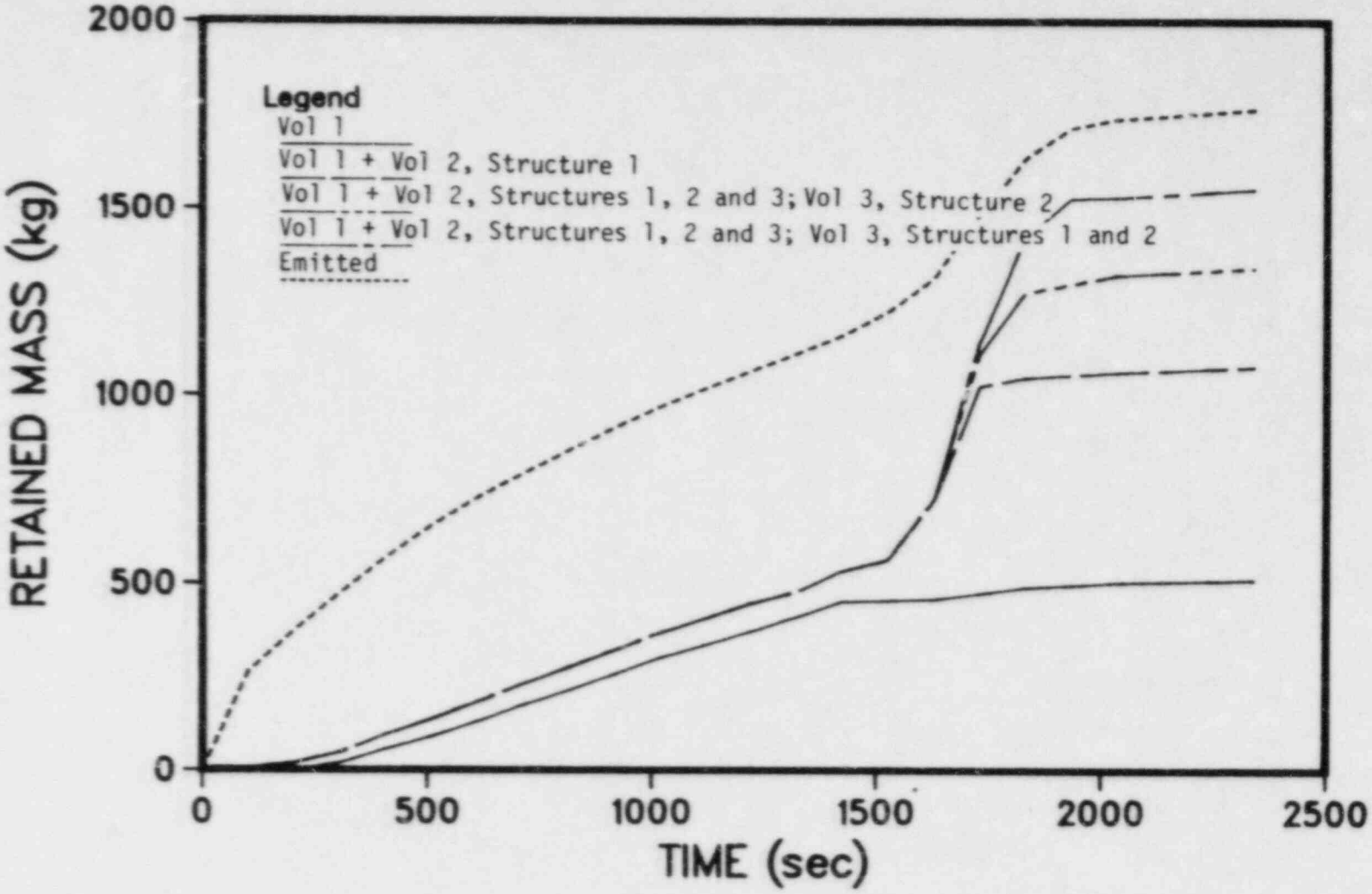

FIGURE 7.8. MASSES OF AEROSOL EMITTED FROM CORE AND RETAINED IN THE RCS CONTROL VOLUMES AS FUNCTIONS OF TIME FOR THE TMLB' SEQUENCE (Vol 1 = Core, Vol 2 = Upper Grid Plate, Vol 3 = Guide Tubes, Vol 4 = Upper Plenum Annulus, Vol 5 = Hot Leg, Vol 6 = Pressurizer). Times measured from start of core melting.

TABLE 7.4a. CORSOR PREDICTIONS OF RELEASE FROM CORE AND TRAP-MELT PREDICTIONS OF PRIMARY SYSTEM RETENTION OF WASH-1400 GROUPS FOR TMLB' SEQUENCE

Group	Released (kg)	Retained (kg)
I	12.3	10.6
Cs	145	125
Te	8.8	7.5
Sr	35.7	31.9
Ru	16.7	13.6
La	0.29	0.26

*Groups are defined in Chapter 6.

TABLE 7.5. CORSOR PREDICTIONS OF MASSES OF SPECIES RELEASED FROM THE CORE (TOTAL) AND TRAP-MELT PREDICTIONS OF MASSES RETAINED IN THE RCS (RET) DURING THE V SEQUENCE FOR THE SURRY PLANT

Time (s)	CsI		CsOH		Te		Aerosol	
	Ret (kg)	Total (kg)	Ret (kg)	Total (kg)	Ret (kg)	Total (kg)	Ret (kg)	Total (kg)
300	5.4	12.0	30.1	65.4	0.3	0.4	340	687
600	10.3	18.2	54.8	97.0	0.9	0.9	588	999
900	13.6	21.7	71.9	115	1.5	1.6	805	1240
1200	14.0	23.5	73.6	124	2.3	2.3	941	1520
1500	13.0	24.4	69.4	128	2.6	3.0	948	1680
2100	13.0	25.3	69.4	133	2.6	3.7	948	1690
2690	13.0	25.5	69.4	134	2.6	4.0	955	1710
3290	13.0	25.6	69.5	135	2.6	4.8	1005	1760
4190	13.0	25.8	69.6	136	2.7	6.5	1150	1910
5090	13.0	25.9	69.6	136	2.9	8.5	1330	2090
6585	13.1	25.9	69.7	136	3.2	11.4	1565	2320

TABLE 7.6. TRAP-MELT PREDICTIONS OF PRIMARY SYSTEM RETENTION FACTORS (RF) AND VOLUME SPECIFIC RETENTION FACTORS AS FUNCTIONS OF TIME FOR THE V SEQUENCE FOR THE SURRY PLANT

Time (s)	CsI			CsOH			Te		Aerosol			
	RF	Hot Leg	Piping	RF	Hot Leg	Piping	RF	Core Plate	RF	Core	Hot Leg	Piping
300	.45	.18	.20	.46	.18	.21	.90	.83	.50	.03	.18	.21
600	.56	.22	.23	.57	.21	.23	.91	.86	.59	.7	.20	.22
900	.63	.24	.24	.63	.23	.24	.93	.89	.65	.10	.20	.21
1200	.60	.24	.26	.60	.24	.25	.98	.90	.62	.09	.19	.21
1500	.53	.23	.25	.54	.23	.25	.86	.78	.56	.08	.17	.19
2100	.51	.22	.24	.52	.22	.24	.71	.64	.56	.08	.17	.19
2690	.51	.22	.24	.52	.22	.24	.64	.58	.56	.08	.17	.19
3290	.51	.22	.24	.52	.22	.23	.55	.49	.57	.11	.16	.18
4190	.50	.22	.23	.51	.22	.23	.42	.36	.60	.18	.15	.17
5090	.50	.22	.23	.51	.22	.23	.34	.29	.54	.25	.14	.16
6585	.50	.22	.23	.51	.22	.23	.28	.23	.67	.32	.12	.14

The behavior of the Te illustrated in Figure 7.9 can be explained entirely in terms of the gas flow through the RCS. During the initial period of low but non-zero flows, the Te is scavenged by the upper plenum surfaces very efficiently due to the long residence time in that region and Te's high rate of reaction. Since this reacted material is not liberated, except at very high temperatures, it is retained throughout the sequence. The lack of additional retention of the Te emitted beyond t = 1200 s is caused by two factors. Until 2400 s, the flow rate through the system is too high for the reaction with the surfaces to occur at a significant rate. Beyond this time (i.e., after vessel dryout), the lack of flow out of the core region results in the vapor remaining suspended in the core region until the bottom head fails, at which time it is injected into the containment atmosphere.

The primary system retention of CsOH and CsI is depicted in Figures 7.10 and 7.11. In this sequence, the materials which are retained in the first 1000 s (principally via condensation on particles which are subsequently deposited), are partially liberated by the surface heatup that occurs at about 1200 s, when the gas flow increases dramatically. After this time, the surfaces cool sufficiently to permit condensation, but the inventory of Cs and I has been nearly exhausted so that no further retention is possible.

Approximately two-thirds of the aerosol mass emitted from the core in this sequence is retained within the RCS. It is clear in Figure 7.12 that from t = 1200 s to t = 2400 s, the high flow rates (or very short RCS residence times) lead to no aerosol retention on the surfaces. After vessel dryout, however, almost all further emission of aerosol is retained. As a result, there is but little aerosol injected into the containment at the time of vessel failure. Figure 7.12 also illustrates that the ECC piping--Volume 5 in the figure--is an important, though not dominant, contributor to aerosol retention in this sequence. The total mass retained in this piping is predicted by TRAP-MELT to be 323 kg at the time of bottom head failure. This is equivalent to a deposition of just over 50 g of aerosol per cm of pipe, leading to questions concerning whether this is physically possible. As the aerosol deposit in the pipe increases, one would expect the constriction in the flow path to lead to higher gas flow velocities. These higher velocities could, in turn, result in resuspension of deposited aerosol, reducing retention. A plug of deposited

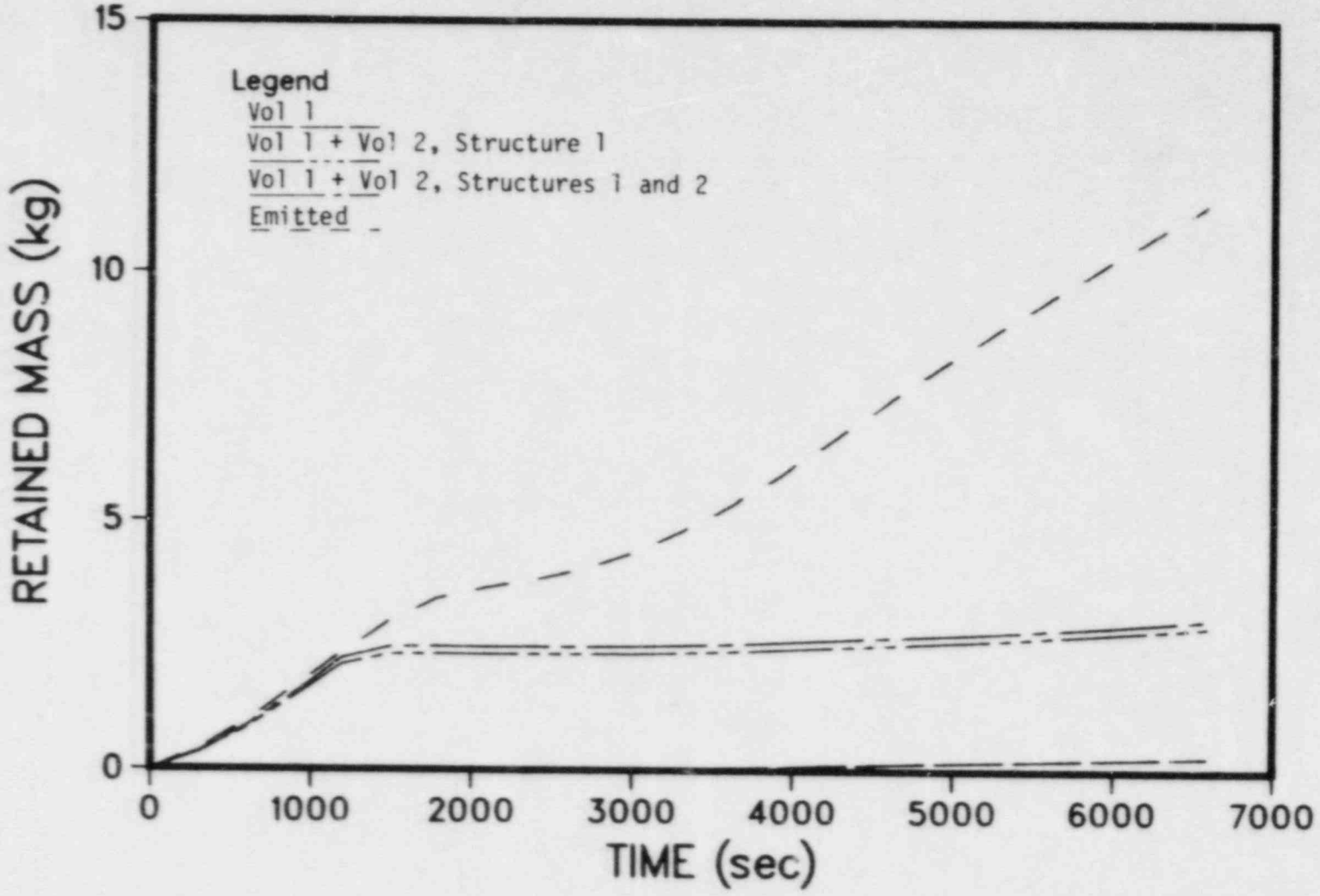

FIGURE 7.9. MASSES OF Te EMITTED FROM CORE AND RETAINED IN THE RCS CONTROL VOLUMES AS FUNCTIONS OF TIME FOR THE V SEQUENCE (Vol 1 = Core; Vol 2, Structure 1 = Upper Grid Plate; Vol 2, Structure 2 = Guide Tubes). Times Measured from Start of Core Melting.

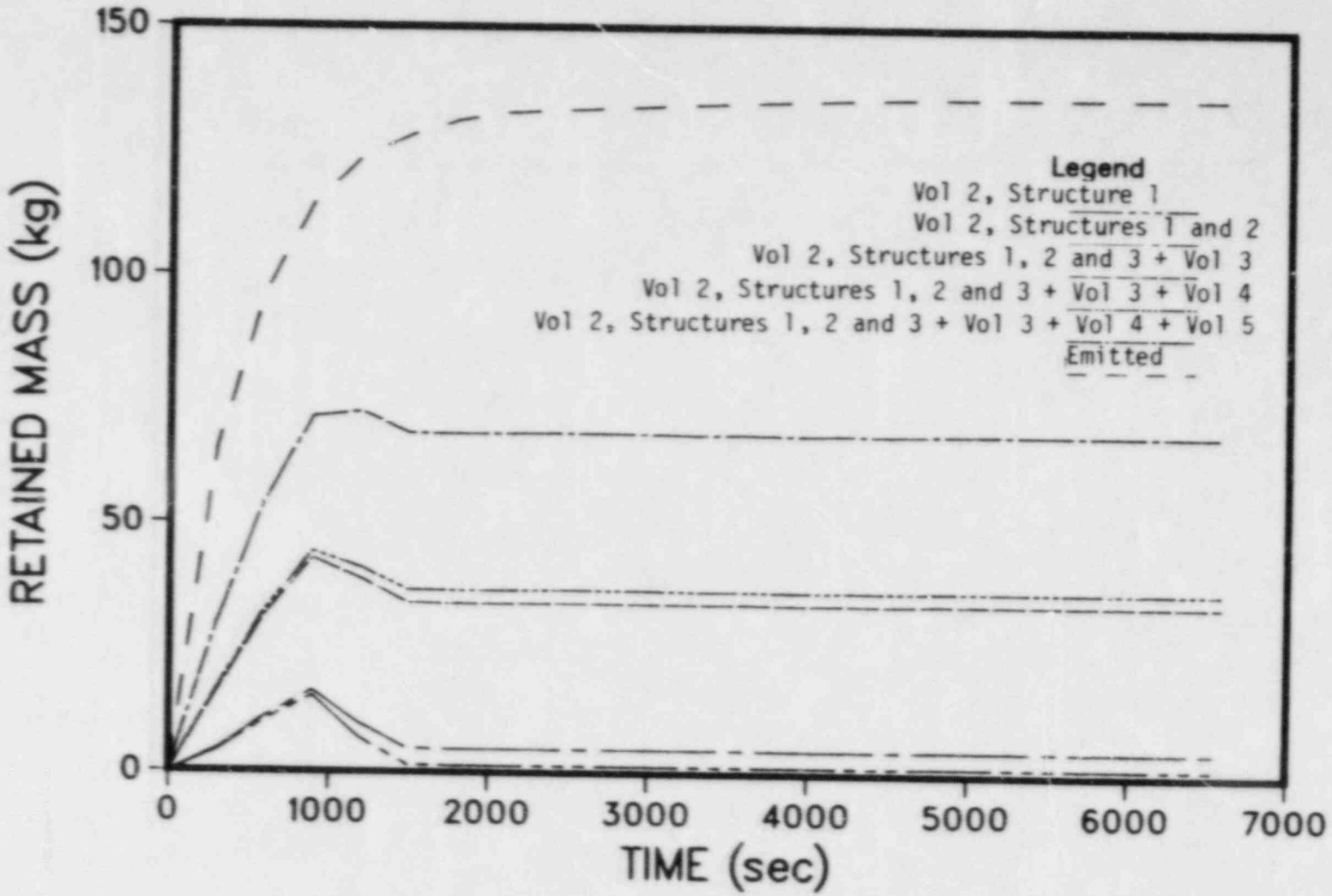

FIGURE 7.10. MASSES OF CsOH EMITTED FROM CORE AND RETAINED IN THE RCS CONTROL VOLUMES AS FUNCTIONS OF TIME FOR THE V SEQUENCE (Vol 2, Structure 1 = Upper Grid Plate; Vol 2, Structure 2 = Guide Tubes; Vol 2, Structure 3 = Core Barrel; Vol 3 = Hot Leg; Vol 4 = Steam Generator; Vol 5 = Piping). Times Measured from Start of Core Melting.

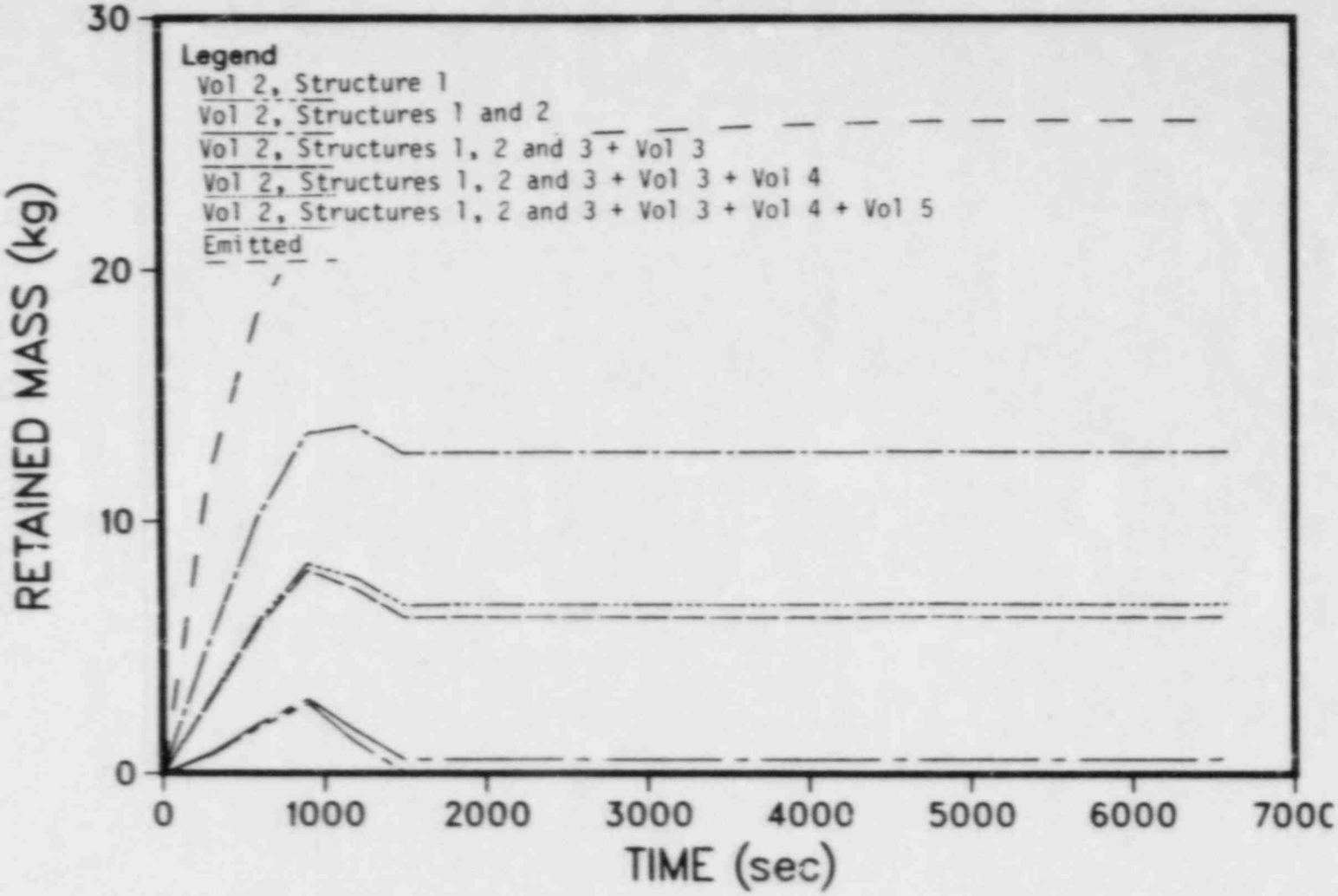

FIGURE 7.11. MASSES OF CsI EMITTED FROM CORE AND RETAINED IN THE RCS CONTROL VOLUMES AS FUNCTIONS OF TIME FOR THE V SEQUENCE (Vol 2, Structure 1 = Upper Grid Plate; Vol 2, Structure 2 = Guide Tubes; Vol 2, Structure 3 = Core Barrel; Vol 3 = Hot Leg; Vol 4 = Steam Generator; Vol 5 = Piping). Times Measured from Start of Core Melting.

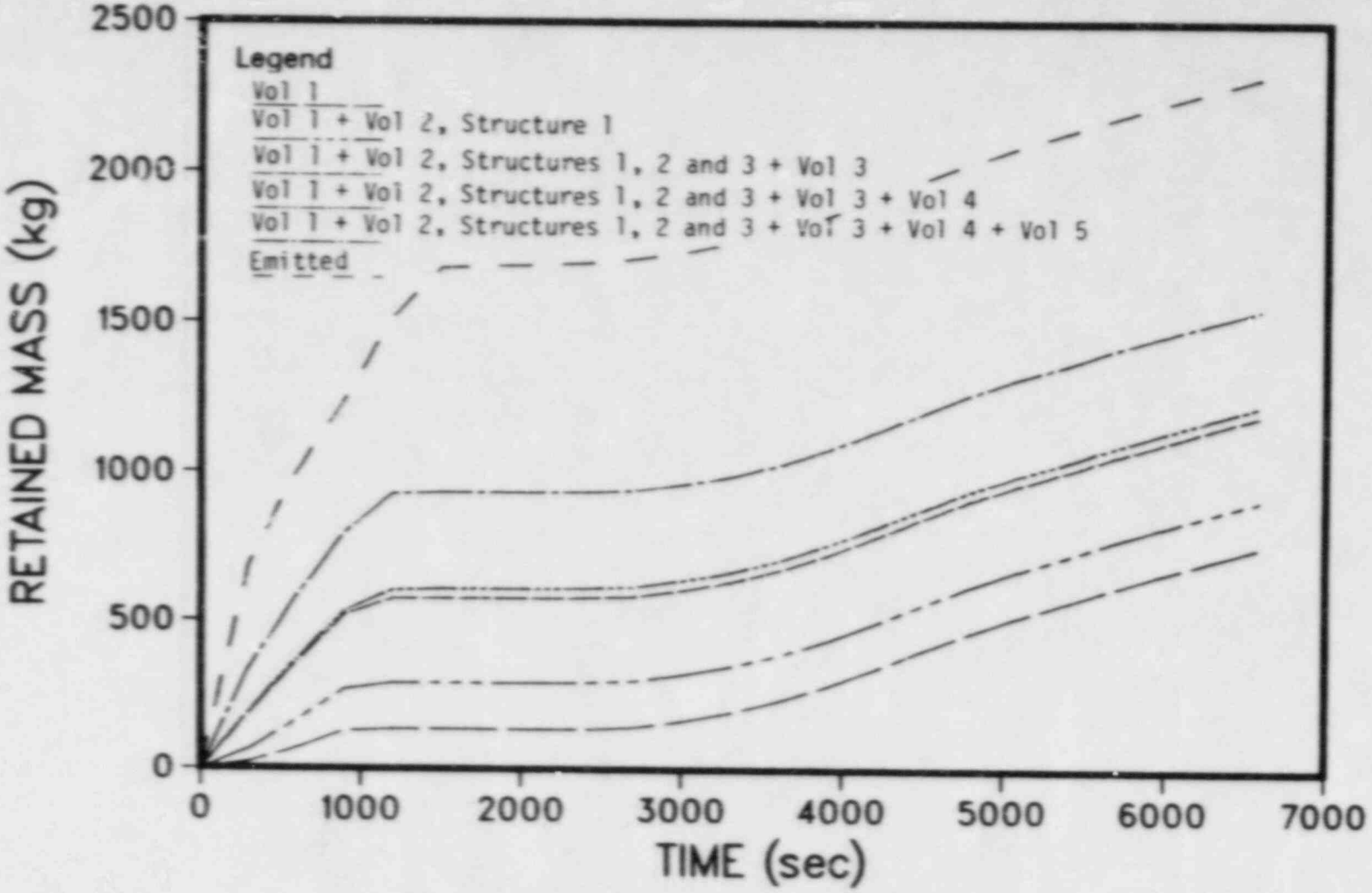

FIGURE 7.12. MASSES OF AEROSOL EMITTED FROM CORE AND RETAINED IN THE RCS CONTROL VOLUMES AS FUNCTIONS OF TIME FOR THE V SEQUENCE (Vol 1 = Core; Vol 2, Structure 1 = Upper Grid Plate; Vol 2, Structure 2 = Guide Tubes; Vol 2, Structure 3 = Core Barrel; Vol 3 = Hot Leg; Vol 4 = Steam Generator; Vol 5 = Piping). Times Measured from Start of Core Melting.

material could form in the pipe, but the existence of system pressures in excess of 100 psi make this open to question also.

7.2.4 RCS Transport and Deposition for the S_2D-c (Cold Leg) Sequence

This sequence exhibits low flow and intermediate pressure in the RCS. The principal contributors to fission product retention in the primary system are the core region, the upper plenum annulus, and the steam generators.

Tables 7.7 and 7.8 illustrate the release of the species of interest from the core and the retention and distribution of retained masses throughout the RCS during the in-vessel phase of the sequence. The high overall retention factors for each species are characteristic of a low flow, high residence time sequence such as this one.

The retention of Te in this sequence is nearly complete; the largest portion is retained on the first post-core surface, which is the upper grid plate. This retention is due exclusively to the chemical reaction of tellurium with system surfaces. The high retention decreases slightly starting at 4100 seconds because of vessel dryout and the coupled loss of flow of emitted vapors from the core. Figure 7.13 illustrates the behavior of tellurium in the RCS.

CsI and CsOH are retained throughout the system in a common pattern, as shown in Figures 7.14 and 7.15. At 840 seconds, each displays a drop in retention in the core plate and guide tubes. The core has slumped at this time, and the resultant increase in surface temperature to 1900 F in these volumes causes re-evaporation of the two Cs species and their transport to downstream volumes. Emission of CsI and CsOH from the core is essentially complete at 1200 s, and the retention of the two species undergoes little change after that time. The steam generators are seen to be the site of the bulk of the retention of the Cs species.

Aerosol retention, as illustrated in the tables and Figure 7.16, shows a less pronounced response to the core slump. Retention continues to increase, but at a slightly reduced rate. The increased flow rates accompanying steam generated when the core slumps serve to reduce agglomeration by reducing aerosol concentrations and residence times. This is evident in the aerosol mass median diameters calculated by the TRAP-MELT code. In the core region, the particle diameter falls from 3.6 μm at 560 s to 1.0 μm at 840 s.

TABLE 7.7. TRAP-MELT PREDICTIONS OF PRIMARY SYSTEM RETENTION FACTORS (RF) AND VOLUME SPECIFIC RETENTION FACTORS AS FUNCTIONS OF TIME FOR THE S_2D-ϵ (COLD LEG) SEQUENCE FOR THE SURRY PLANT

	CsI			CsOH			Te		Aerosol				
Time (s)	RF	Upper Plenum Annulus	Steam Gen	RF	Upper Plenum Annulus	Steam Gen	RF	Upper Grid Plate	RF	Core	Upper Grid Plate	Upper Plenum Annulus	Steam Gen
280	.48	.17	.06	.54	.17	.07	.74	.72	.71	.24	.18	.16	.07
560	.73	.22	.11	.75	.21	.11	.80	.78	.82	.30	.19	.18	.08
840	.81	.21	.35	.83	.20	.30	.99	.93	.85	.24	.16	.19	.19
1400	.77	.19	.34	.79	.19	.29	.97	.91	.78	.22	.14	.16	.20
1960	.76	.19	.33	.78	.18	.29	.97	.90	.77	.22	.14	.16	.20
2800	.75	.19	.33	.77	.18	.28	.96	.90	.76	.21	.13	.16	.19
3630	.74	.18	.33	.77	.18	.28	.96	.89	.73	.20	.13	.15	.19
5591	.74	.18	.32	.76	.18	.28	.90	.84	.73	.29	.11	.13	.16

TABLE 7.8. CORSOR PREDICTIONS OF MASSES OF SPECIES RELEASED FROM THE CORE (TOTAL) AND TRAP-MELT PREDICTIONS OF MASSES RETAINED IN THE RCS (RET) DURING THE S_2D-ϵ (COLD LEG) SEQUENCE FOR THE SURRY PLANT

Time (s)	CsI		CsOH		Te		Aerosol	
	Ret (kg)	Total (kg)	Ret (kg)	Total (kg)	Ret (kg)	Total (kg)	Ret (kg)	Total (kg)
280	3.9	8.0	24.3	45.3	1.0	1.4	351	492
560	12.5	17.2	68.6	91.8	5.0	6.2	771	935
840	18.2	22.3	97.9	117	12.9	13.1	1150	1360
1400	18.6	24.1	100	126	14.4	14.8	1240	1590
1960	18.6	24.5	100	128	14.8	15.3	1240	1600
2800	18.7	24.9	101	131	15.8	16.5	1250	1650
3630	18.8	25.3	101	132	16.9	17.7	1280	1760
5591	18.9	25.6	102	134	17.4	19.3	1570	2140

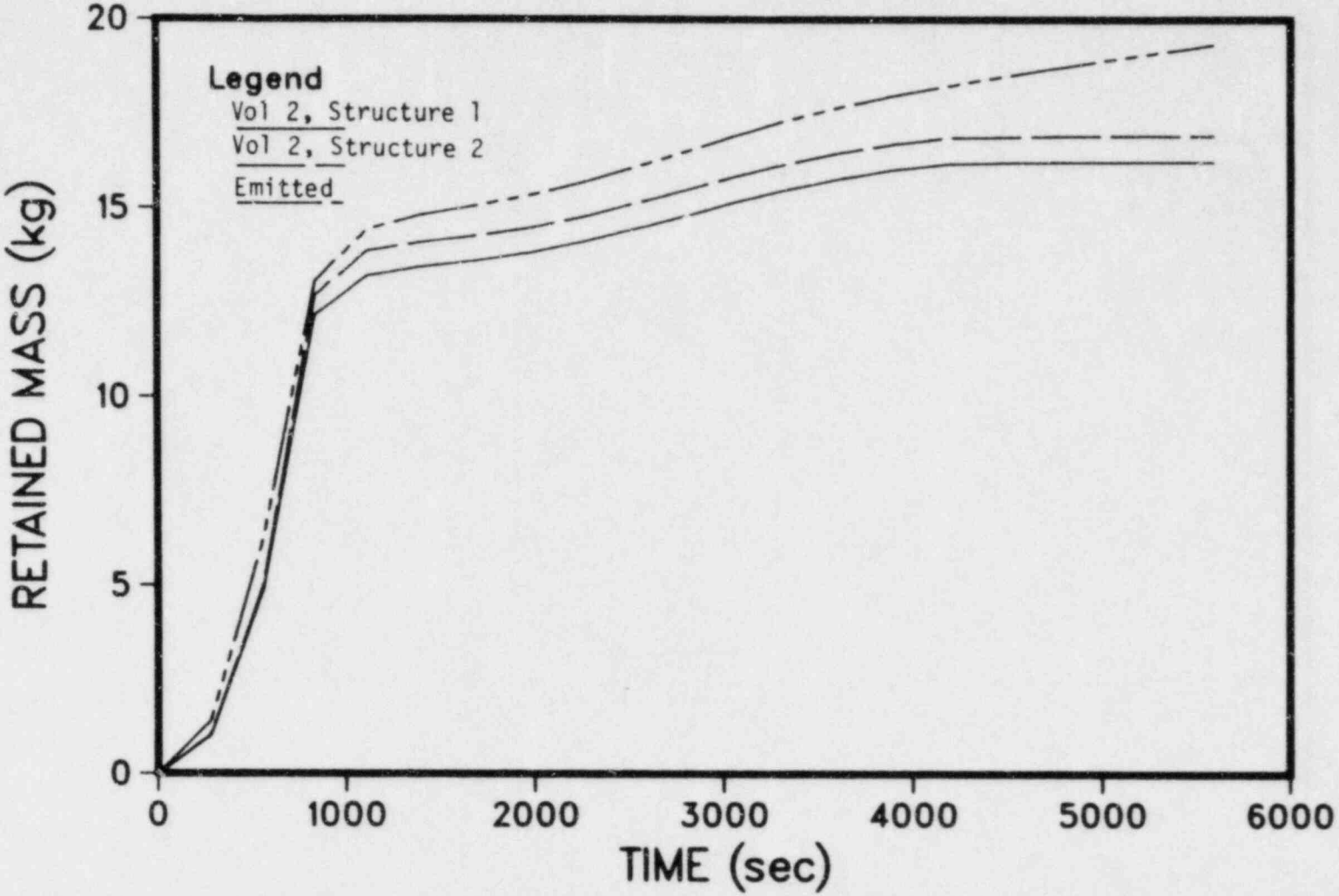

FIGURE 7.13. MASSES OF Te EMITTED FROM CORE AND RETAINED IN THE RCS CONTROL VOLUMES AS FUNCTIONS OF TIME FOR THE S_2D-ϵ (COLD LEG) SEQUENCE (Vol 2, Structure 1 = Upper Grid Plate; Vol 2, Structure 2 = Guide Tubes). Times Measured from Start of Core Melting.

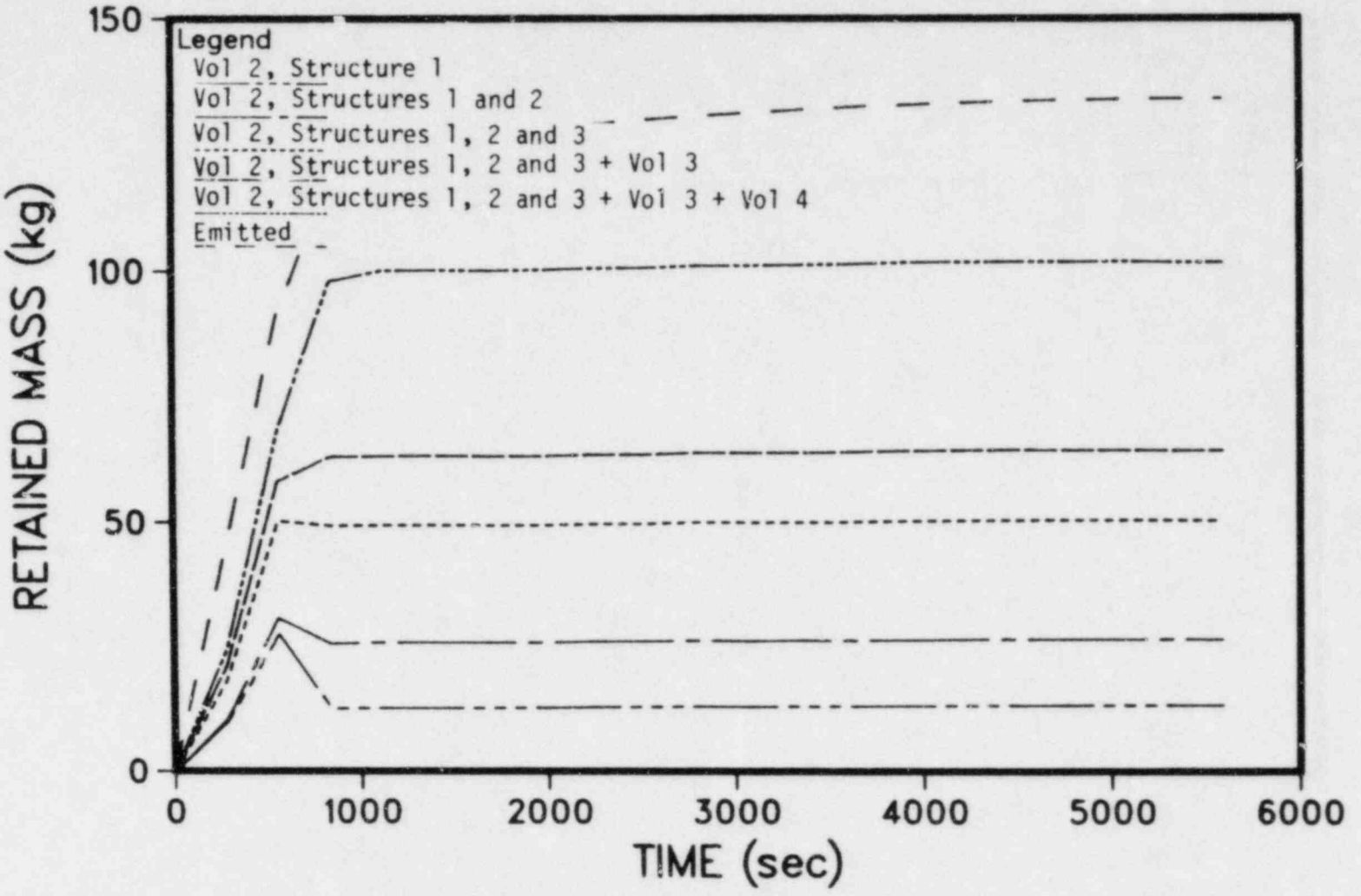

FIGURE 7.14. MASSES OF CsOH EMITTED FROM CORE AND RETAINED IN THE RCS CONTROL VOLUMES AS FUNCTIONS OF TIME FOR THE S_2D-ϵ (COLD LEG) SEQUENCE (Vol 1 = Core; Vol 2, Structure 1 = Upper Grid Plate; Vol 2, Structure 2 = Guide Tubes; Vol 2, Structure 3 = Core Barrel; Vol 3 = Hot Leg; Vol 4 = Steam Generator). Times Measured from Start of Core Melting.

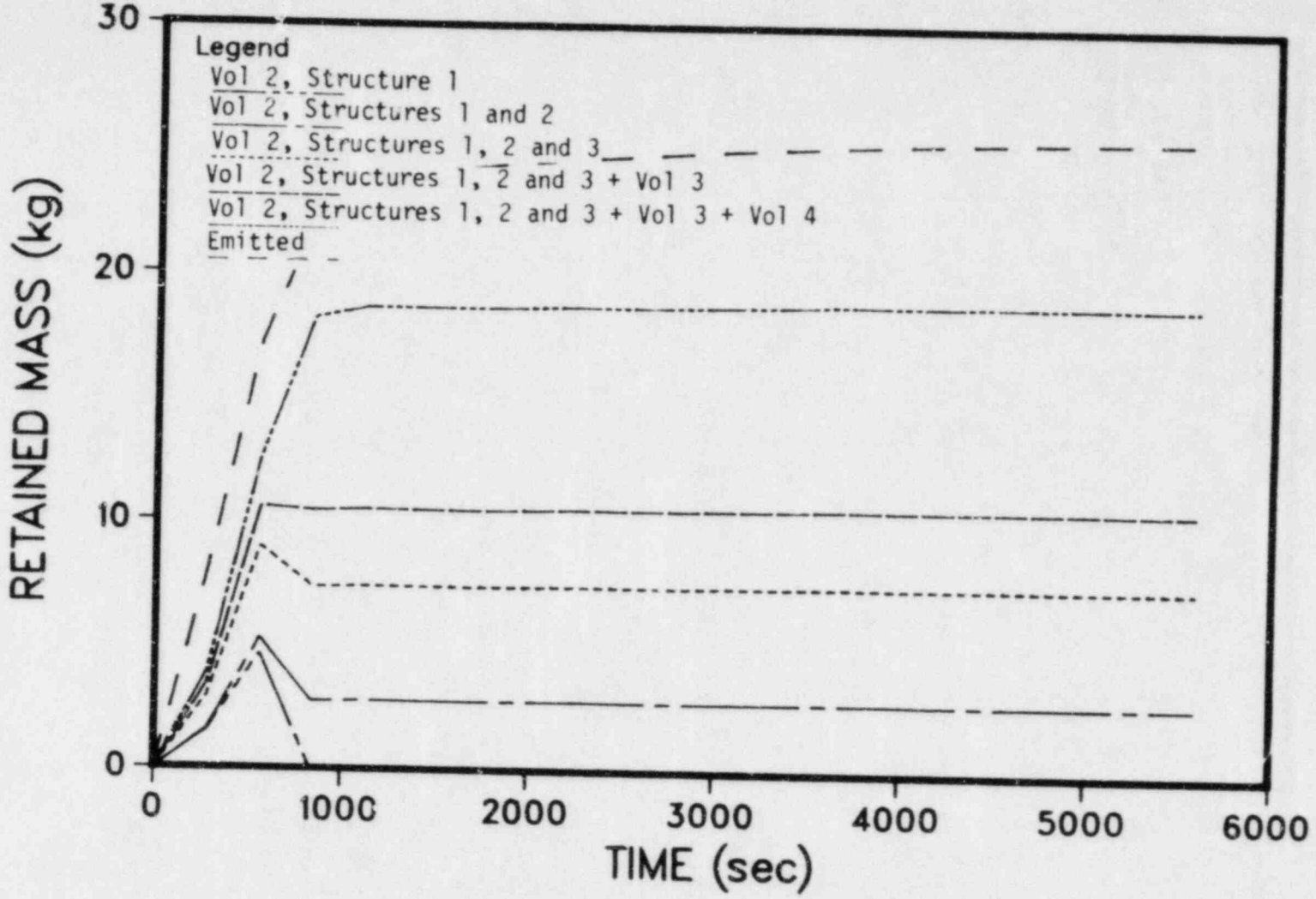

FIGURE 7.15. MASSES OF CsI EMITTED FROM CORE AND RETAINED IN THE RCS CONTROL VOLUMES AS FUNCTIONS OF TIME FOR THE S_2D-ϵ (COLD LEG) SEQUENCE (Vol 1 = Core; Vol 2, Structure 1 = Upper Grid Plate; Vol 2, Structure 2 = Guide Tubes; Vol 2, Structure 3 = Core Barrel; Vol 3 = Hot Leg; Vol 4 = Steam Generator). Times Measured from Start of Core Melting.

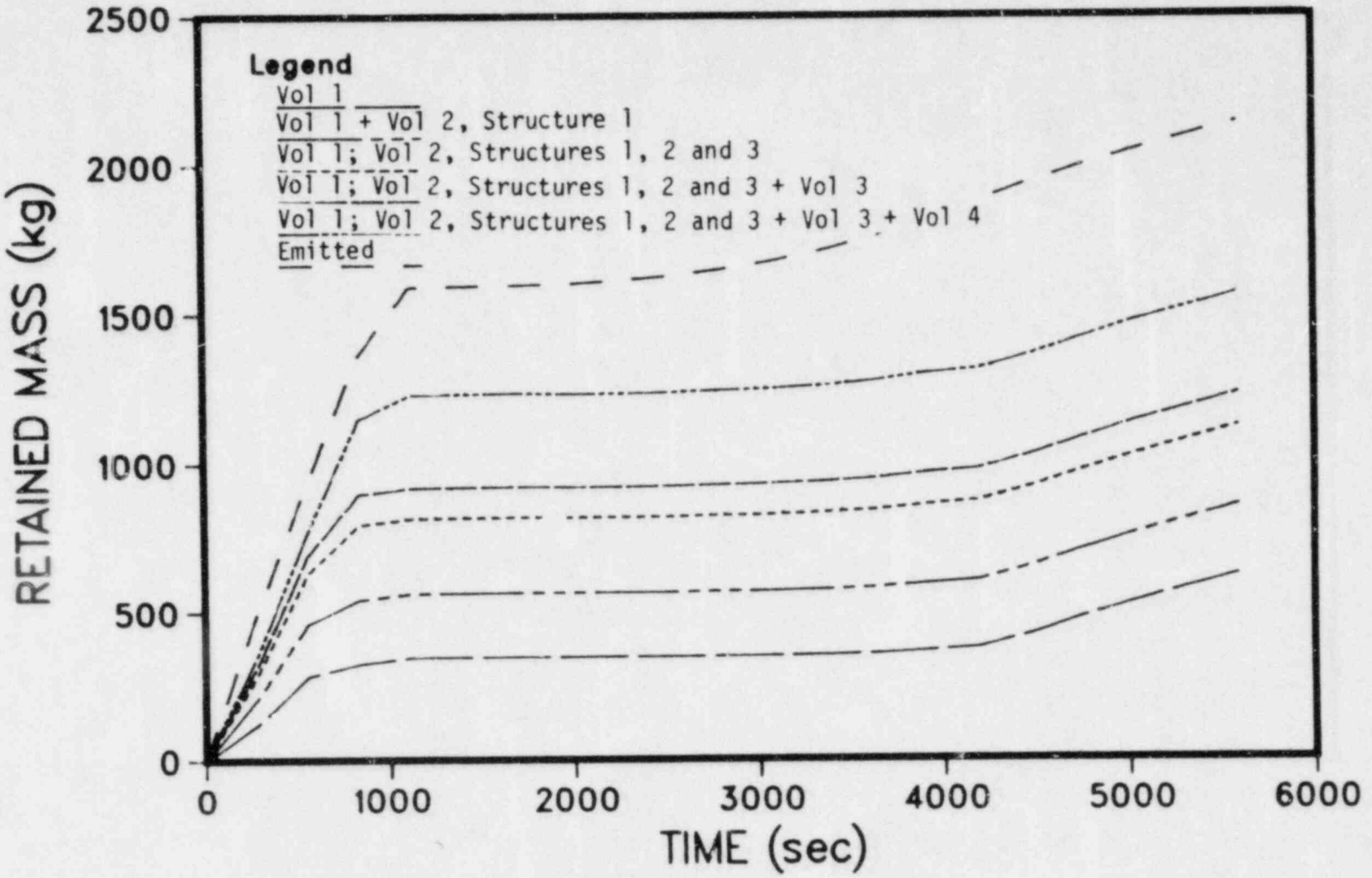

FIGURE 7.16. MASSES OF AEROSOL EMITTED FROM CORE AND RETAINED IN THE RCS CONTROL VOLUMES AS FUNCTIONS OF TIME FOR THE S_2D-ϵ (COLD LEG) SEQUENCE (Vol 1 = Core; Vol 2, Structure 1 = Upper Grid Plate; Vol 2, Structure 2 = Guide Tubes; Vol 2, Structure 3 = Core Barrel; Vol 3 = Hot Leg; Vol 4 = Steam Generator). Times Measured from Start of Core Melting.

Gravitational settling in the core region continues at a reduced rate, and transport to cooler volumes allows continued retention. After this time, retention shows little change as aerosol emission from the core slows considerably, until 4100 s. At this time flow has stopped, the freshly emitted aerosol staying in the core region, where gravitational settling effects an increase in overall retention.

7.2.5 RCS Transport and Deposition for the S_2D (Hot Leg) Sequence

This sequence is characterized by low flow and intermediate pressure in the RCS. Retention occurs primarily in the core region and the upper plenum annulus. Use of the hot leg as the site of the small pipe break removes the steam generators from analysis. The resulting decrease in overall retention, except for tellurium, is the most noticeable feature when this sequence is compared to the previous one. Tables 7.9 and 7.10, along with Figures 7.17 through 7.20, illustrate the release, retention, and distribution of species of interest.

Tellurium shows increased retention, when compared to the cold leg case, because the flow in this sequence does not subside after core slump. This results from the shorter duration of the in-vessel portion of the accident, 1750 s versus 5600 s.

The Cs species again show the decrease in retention attributable to core slump at 720 s, with its resultant temperature increase from 1530 F to 1980 F. CsI has a negligible surface reaction rate compared to that of CsOH, and it shows the more abrupt decrease in retention at this time. Retention for both species has recovered by 1100 s, at which time Cs emission from the core has slowed considerably. Retention is essentially unchanged from this time to the end of the sequence.

The aerosol retention pattern is similar to that of the previous sequence with one exception, as illustrated in Figure 7.20 at 1100 s. While emission from the core continues, retention has stopped. This is due to the increased flow beginning at 1070 s, which results from the core slump and subsequent steam generation and pressure increase. The mass median diameter drops from 3.27 μm to 1.79 μm in the core region, and from 5.1 μm to 2.5 μm in the

TABLE 7.9. CORSOR PREDICTIONS OF MASSES OF SPECIES RELEASED FROM THE CORE (TOTAL) AND TRAP-MELT PREDICTIONS OF MASSES RETAINED IN THE RCS (RET) DURING THE S_2D (HOT LEG) SEQUENCE FOR THE SURRY PLANT

Time (s)	CsI		CsOH		Te		Aerosol	
	Ret (kg)	Total (kg)	Ret (kg)	Total (kg)	Ret (kg)	Total (kg)	Ret (kg)	Total (kg)
103	1.0	3.8	7.5	24.4	0.1	0.3	224	336
206	3.1	7.6	19.9	43.5	0.8	1.2	348	494
309	5.8	11.5	34.1	63.2	1.7	2.3	481	652
412	8.5	14.9	47.8	80.4	3.0	4.2	629	815
514	11.2	17.9	61.9	95.3	5.3	7.0	776	974
617	13.6	20.3	75.9	108	8.4	9.9	907	1130
720	11.7	22.0	76.9	116	11.3	12.1	1040	1290
1029	12.6	24.5	78.1	129	17.0	18.1	1190	1610
1337	12.3	25.5	76.7	134	22.6	23.0	1240	1790
1749	12.3	25.7	76.5	135	23.8	24.3	1240	1870

TABLE 7.10. TRAP-MELT PREDICTIONS OF PRIMARY SYSTEM RETENTION FACTORS (RF) AND VOLUME SPECIFIC RETENTION FACTORS AS FUNCTIONS OF TIME FOR THE S_2D (HOT LEG) SEQUENCE FOR THE SURRY PLANT

	CsI					CsOH					Te		Aerosol			
Time (s)	RF	Upper Grid Plate	Guide Tubes	Upper Plenum Annulus	Hot Leg	RF	Upper Grid Plate	Guide Tubes	Upper Plenum Annulus	Hot Leg	RF	Upper Grid Plate	RF	Core	Upper Grid Plate	Upper Plenum Annulus
103	.25	.18	--	.06	.02	.31	.21	--	.07	.02	.46	.45	.64	.40	.16	.06
206	.41	.22	--	.15	.05	.46	.25	.01	.15	.05	.66	.64	.70	.37	.18	.11
309	.51	.25	--	.20	.06	.54	.27	.01	.20	.06	.74	.72	.74	.37	.19	.14
412	.57	.27	.01	.22	.07	.59	.30	.01	.22	.07	.71	.70	.77	.39	.19	.14
514	.63	.30	.02	.23	.08	.65	.33	.02	.22	.08	.76	.74	.80	.40	.20	.15
617	.67	.32	.05	.22	.09	.71	.36	.04	.22	.09	.85	.83	.80	.40	.20	.16
720	.52	.12	.09	.21	.11	.66	.28	.08	.21	.10	.93	.91	.81	.38	.20	.17
1029	.51	0	.15	.21	.15	.61	.14	.13	.21	.13	.94	.91	.74	.32	.17	.18
1337	.48	--	.13	.20	.15	.57	.14	.12	.19	.12	.98	.93	.69	.30	.16	.17
1749	.48	--	.13	.20	.15	.57	.14	.12	.19	.12	.98	.92	.67	.28	.15	.16

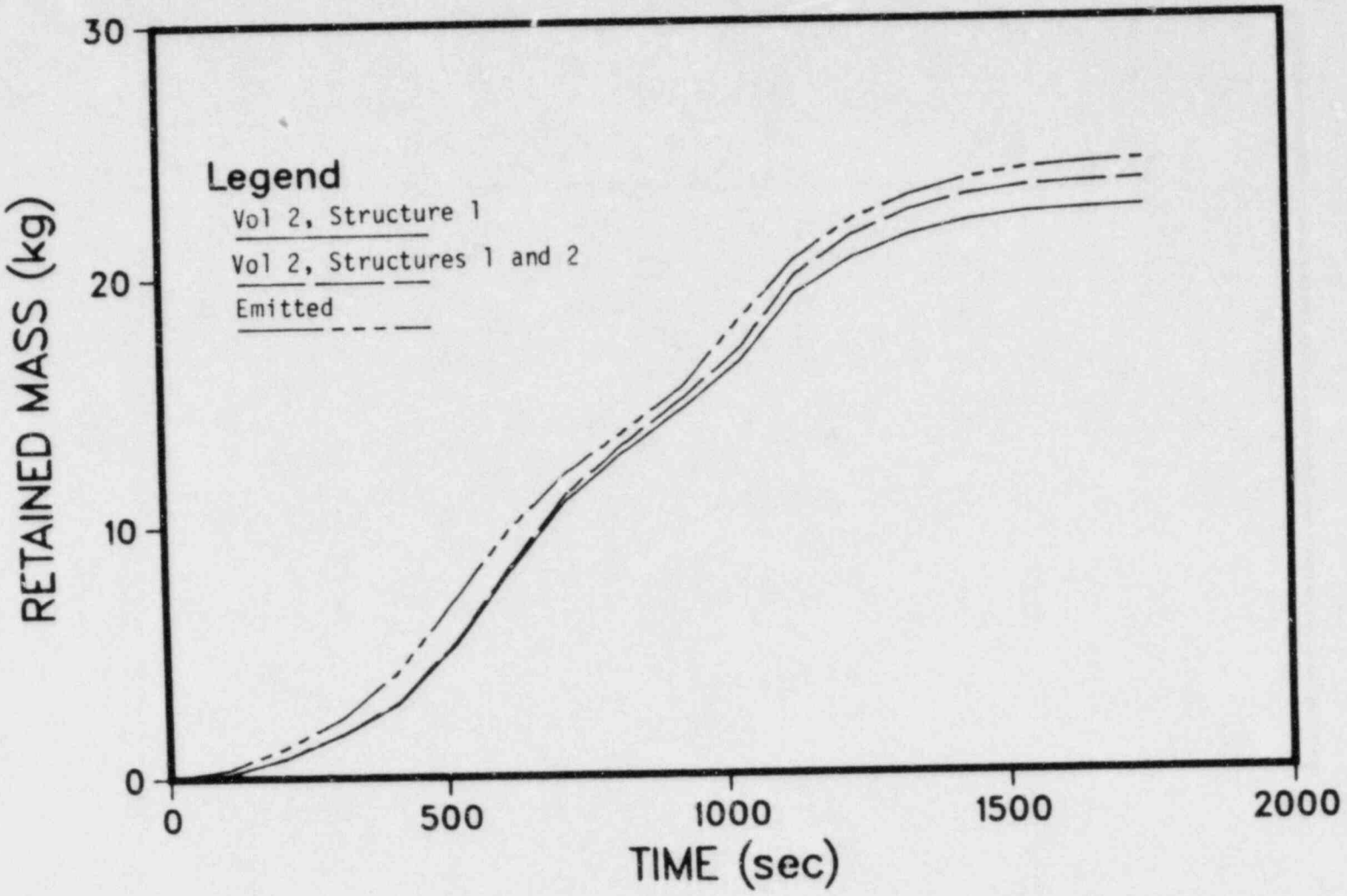

FIGURE 7.17. MASSES OF Te EMITTED FROM CORE AND RETAINED IN THE RCS CONTROL VOLUMES AS FUNCTIONS OF TIME FOR THE S_2D-γ (HOT LEG) SEQUENCE (Vol 2, Structure 1 = Upper Grid Plate; Vol 2, Structure 2 = Guide Tubes). Times Measured from Start of Core Melting.

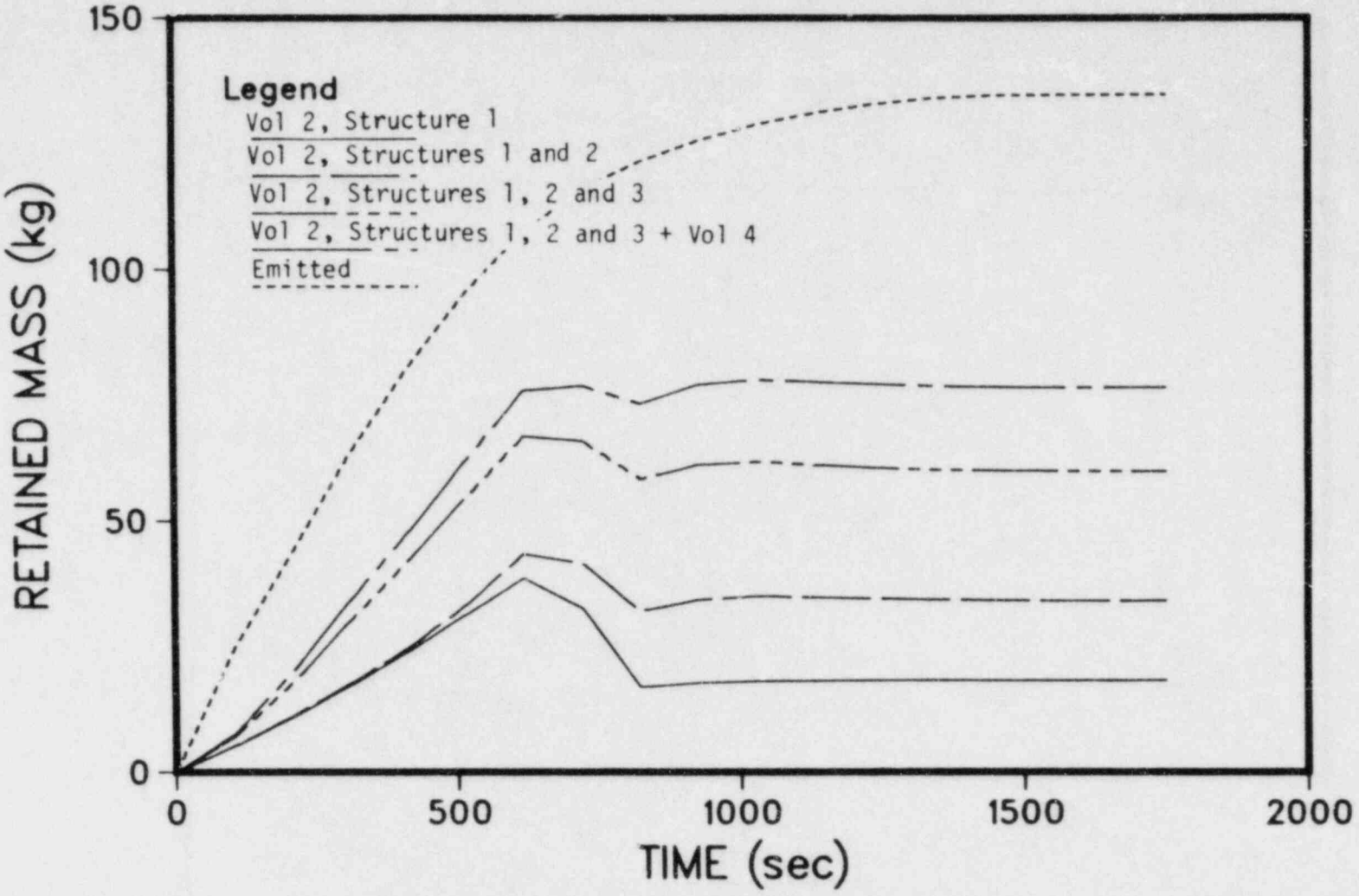

FIGURE 7.18. MASSES OF CsOH EMITTED FROM CORE AND RETAINED IN THE RCS CONTROL VOLUMES AS FUNCTIONS OF TIME FOR THE S_2D-γ (HOT LEG) SEQUENCE (Vol 2, Structure 1 = Upper Grid Plate; Vol 2, Structure 2 = Grid Plate; Vol 2, Structure 3 = Guide Tubes; Vol 3 = Hot Leg). Times Measured from Start of Core Melting.

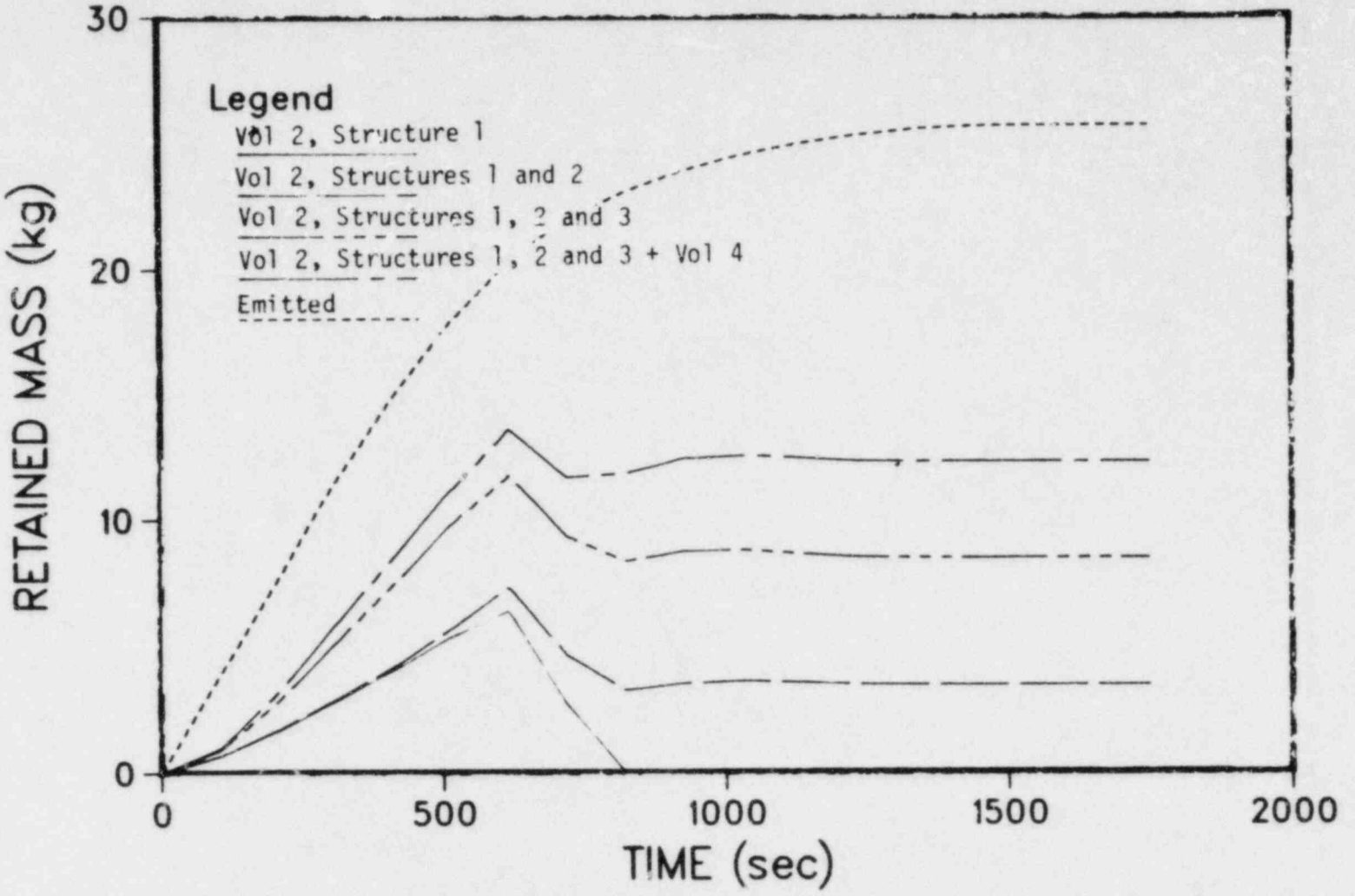

FIGURE 7.19. MASSES OF CsI EMITTED FROM CORE AND RETAINED IN THE RCS CONTROL VOLUMES AS FUNCTIONS OF TIME FOR THE S_2D-γ (HOT LEG) SEQUENCE (Vol 2, Structure 1 = Upper Grid Plate; Vol 2, Structure 2 = Grid Plate; Vol 2, Structure 3 = Guide Tubes; Vol 3 = Hot Leg). Times Measured from Start of Core Melting.

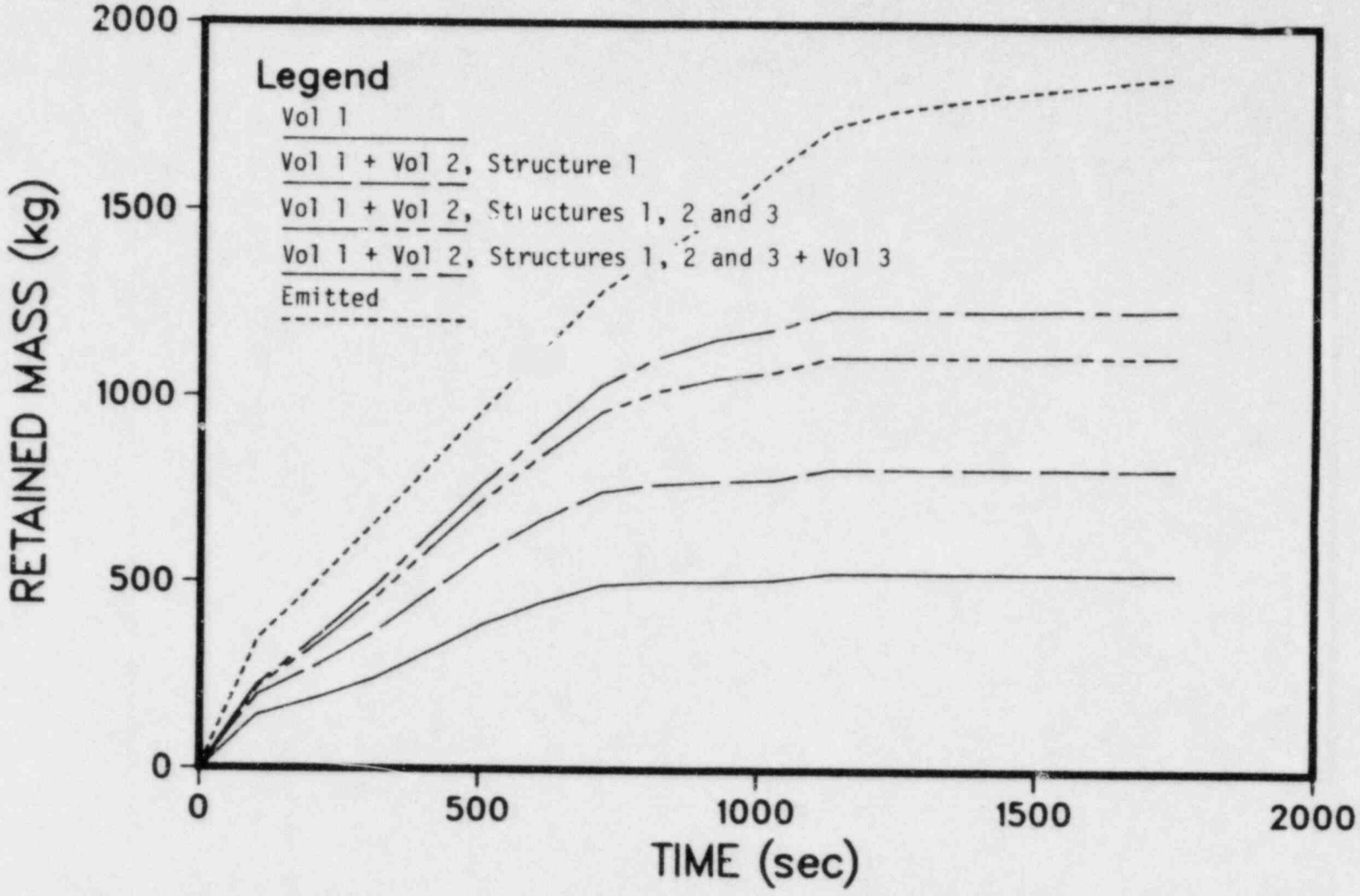

FIGURE 7.20. MASSES OF AEROSOL EMITTED FROM CORE AND RETAINED IN THE RCS CONTROL VOLUMES AS FUNCTIONS OF TIME FOR THE S_2D-γ (HOT LEG) SEQUENCE (Vol 1 = Core; Vol 2, Structure 1 = Upper Grid Plate; Vol 2, Structure 2 = Grid Plate; Vol 2, Structure 3 = Guide Tubes; Vol 3 = Hot Leg). Times Measured from Start of Core Melting.

hot leg, from 1030 s to 1130 s. The shorter residence times and reduced agglomeration halt the gravitational settling in all volumes.

7.3 Transport, Deposition and Leakage in Containment

Calculated results are presented in this section for analyses performed to examine the transport and retention of various fission products in the containment. The NAUA code that was described previously was utilized in the analyses.

In general, the NAUA code used here needs information on the thermal-hydraulic conditions of an accident of interest. The conditions provided by the MARCH computer calculation were used. The typical required thermal hydraulic conditions are time-dependent containment temperature, pressure, and wall temperature, and the rates at which steam enters the containment, condenses on the containment structure, and leaks from the containment.

Perhaps the most important and critical input that the NAUA code also needs is the fission product source term for particulates. The source rates calculated as release from the primary system (TRAP-MELT code) and the VANESA calculations for release during the core-concrete interaction were taken for the melt and vaporization releases, respectively. For the NAUA calculations, CsI, CsOH, and Te were considered separately. All these species were assumed to be in the particulate form in the containment atmosphere because the temperature and pressure under the containment conditions indicate that these species will remain as particulates for all practical circumstances. Although it is assumed in the calculation that individual species are distributed evenly over all sizes of particulates, the different amounts of these species at a given time due to different source timings were taken into consideration in the calculations.

The aerosol behavior mechanisms considered in the present calculations include agglomeration due to Brownian diffusion and due to sequential gravitational settling, particle size change due to steam condensation/evaporation, sedimentation, Brownian diffusion, and diffusiophoresis. Additionally, homogeneous nucleation of water vapor was included to model the water droplet formation in the containment. It should be noted that diffusiophoresis and

homogeneous nucleation of water vapor were not considered in the initial calculations for Surry (presented in Volume 1 of this report).

Four different accident sequences--AB, TMLB', S_2D, and V--were considered in the present calculations. The timing of the fission product source for the containment calculations was permitted to coincide with the prescribed accident sequence that was listed in Chapter 6. Thus, the melt release of aerosol mass occurs as the core starts melting, and the vaporization release takes place as the core-concrete interaction begins. The time-dependent source rates in mass per unit time were provided as input to the NAUA calculations. In certain cases, the effects of multiple compartment modeling (notably for the AB-β and V sequences), were further examined. The timing of accident events for each accident sequence considered in the present calculations is summarized in Chapter 6.

The formation of or reevolution as volatile iodine species in the containment is noted where this effect may be important. In general, if the fraction of the iodine inventory released to the environment for a sequence is in excess of about 0.001, then the volatile iodine is probably an insignificant contributor to total iodine release based on the procedures for estimating this source discussed in Chapter 6. For the final released fractions lower than 0.001, the effect of volatile iodine species is noted on the release summary tables.

7.3.1 AB Sequence

This accident represents the sequence in which a minimum retention of fission products is expected to occur in the primary system due to the presence of relatively rapid steam flow conditions combined with a short transport pathway. For analysis of the AB sequence, three different containment failure modes were applied and these are identified using WASH 1400 nomenclature as AB-β, AB-γ, and AB-ε. The containment failure times corresponding to these sequences are shown in Chapter 6. The safeguard building was included in the analysis of the AB-β sequence. As mentioned previously, calculations based on a multi-compartment model were additionally made to compare with those based on a reduced volume assumption for the AB-β sequence.

7.3.1.1 AB-β. This containment isolation failure mode was analyzed using two compartment models. The NAUA code was run sequentially to calculate the aerosol behavior in the containment and in the safeguard building. Figures 7.21 and 7.22 show the airborne mass in the containment and safeguard building, and Figure 7.23 shows the accumulated mass released to the environment from the safeguard building. Figures 7.24 and 7.25 present the particle size distribution in the containment and safeguard building. The location of each species after the accident is completed is shown in Table 7.12. Table 7.12 shows that a core inventory fraction less than 5 percent for the CsI and CsOH species is retained in the primary system due to relatively high flow velocity. As a result, nearly 80 percent of the CsI and CsOH inventories are retained in the containment and the safeguard building. The distribution of Te is seen to be substantially different from that of CsI and CsOH in the table. As already discussed in Section 7.2, the timing of the Te release during the melt release is considerably delayed, and a substantial portion of the Te core inventory is released directly into the containment during the core-concrete interaction, causing the distribution of Te to differ from that of CsI and CsOH.

To examine the effects of multi-compartment modeling on the calculated release fraction, the containment was divided into four separate volumes and similar calculations were performed. The calculated results showing the locational distribution of the CsI, CsOH, and Te species are shown in Table 7.13. It is interesting to note that the fraction of core inventory for each species that is released to the environment is smaller than the corresponding fraction shown in Table 7.12. While it is rather difficult to assess precisely the effect of the multi-compartment calculation on radionuclide behavior, the observed increase in retention appears to result primarily from altered flow patterns and thermo-hydraulic conditions, such as recirculated and periodic reverse flows, as modeled by the MARCH calculation.

7.3.1.2 AB-γ. This containment failure mode represents an early overpressure failure due to hydrogen burning. The containment failure takes place at 269 minutes, which is about 159 minutes after the vessel failure. The VANESA calculation results shown in Table 6.13 were used as the source during the core-concrete interaction for this sequence and for the AB-β sequence.

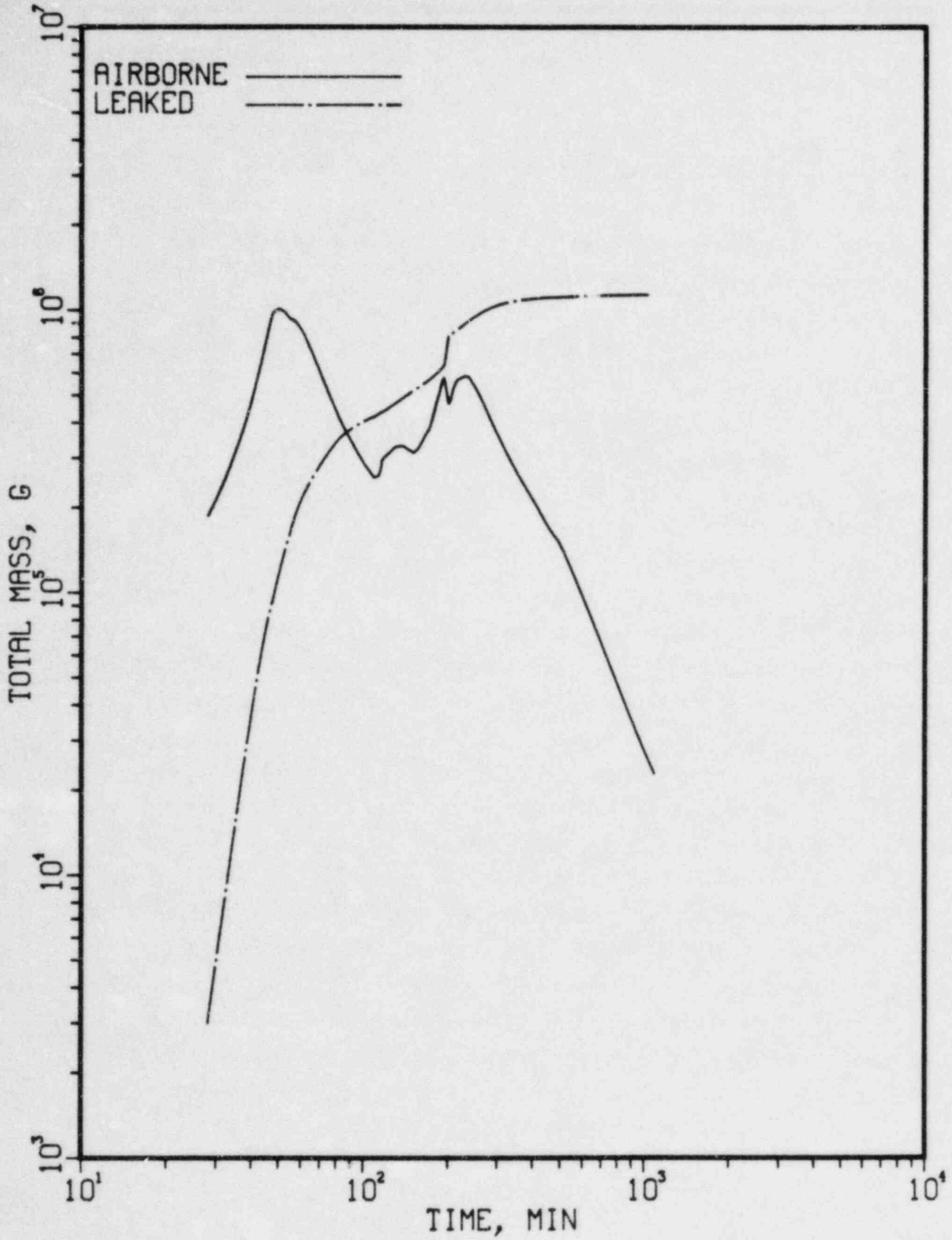

FIGURE 7.21. AIRBORNE AND LEAKED MASSES, AB-B (Safeguard Building).

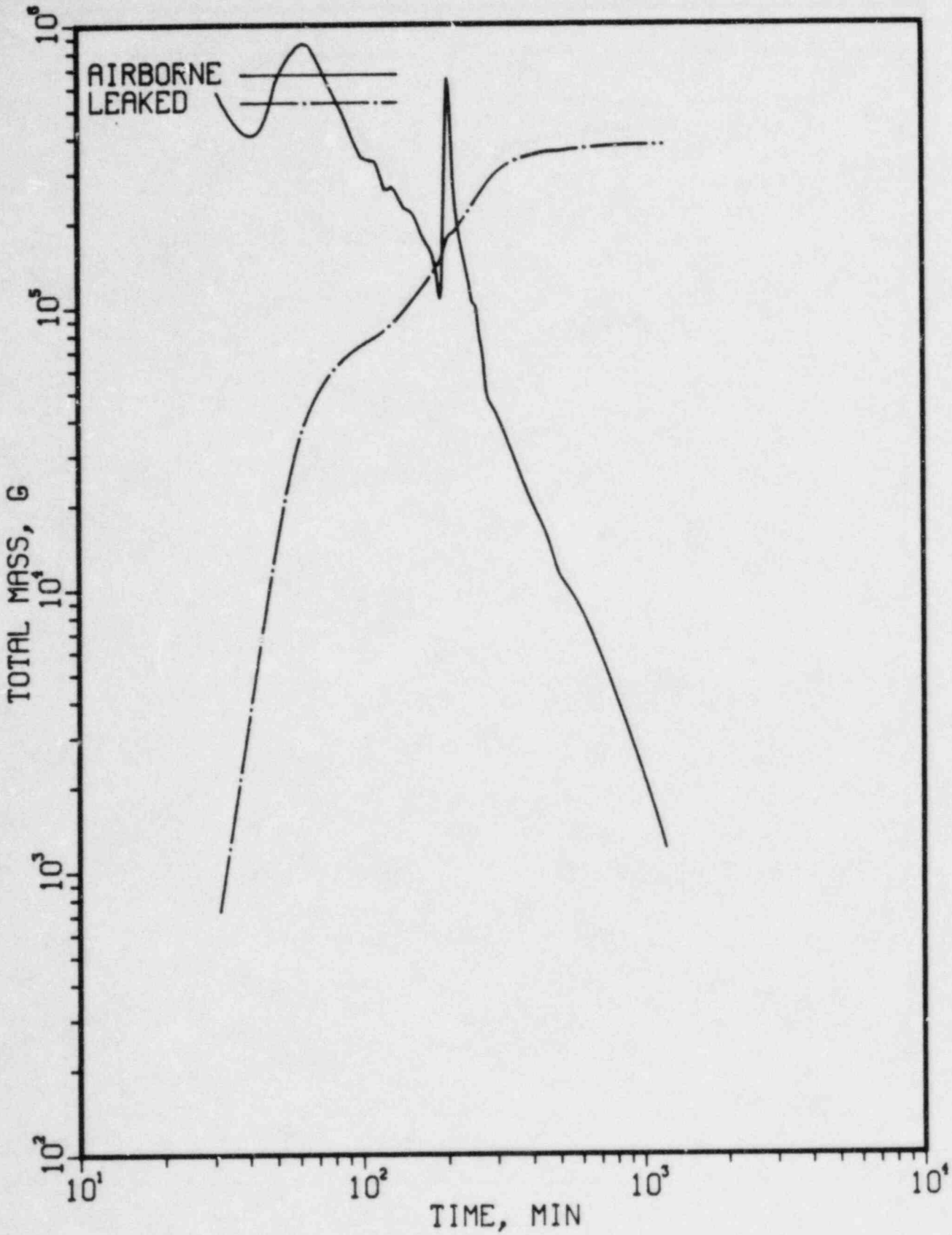

FIGURE 7.22. AIRBORNE AND LEAKED MASSES, AB-B (Safeguard Building)

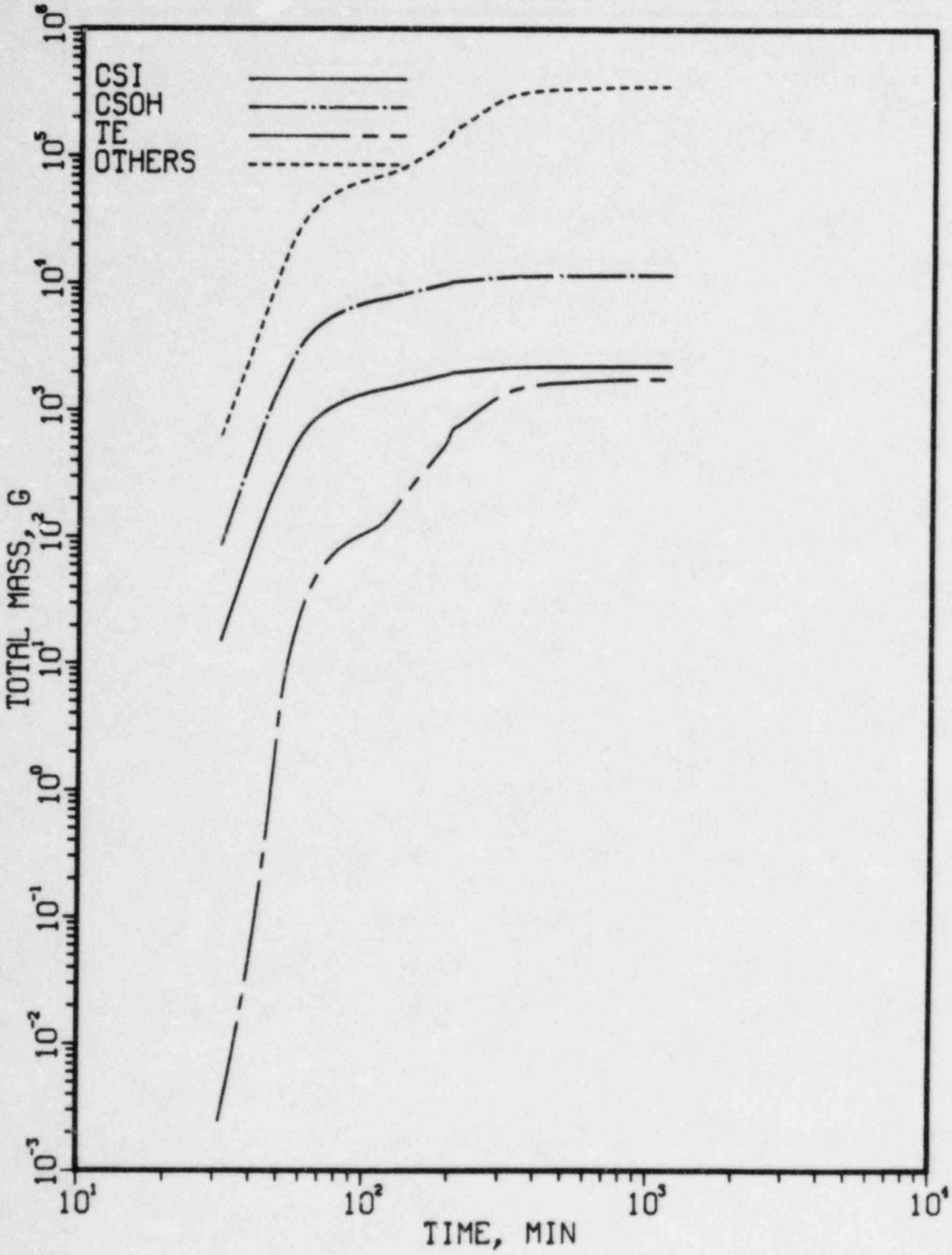

FIGURE 7.23. ACCUMULATED LEAKED NUCLIDES, AB-B

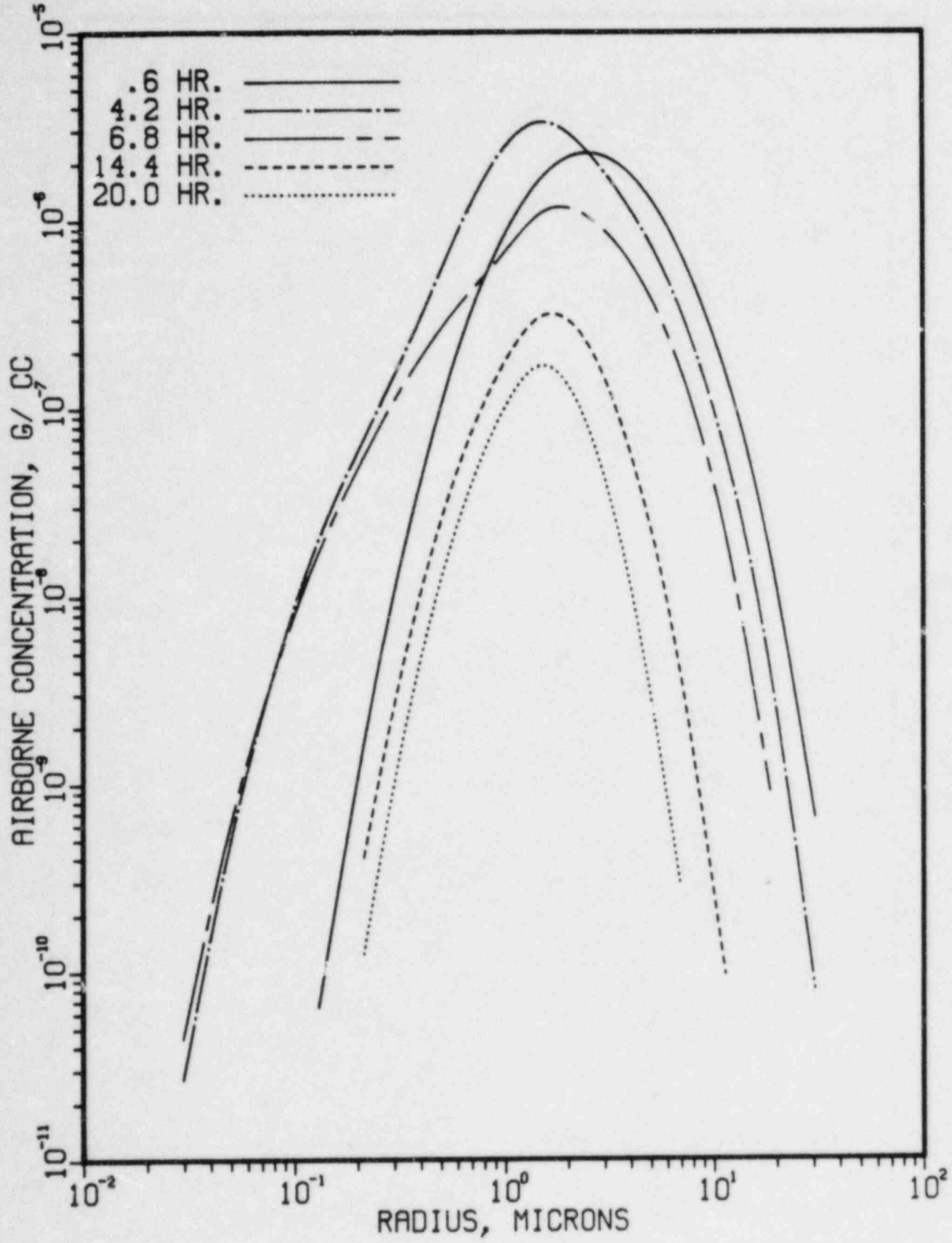

FIGURE 7.24 PARTICLE SIZE DISTRIBUTION, AB-R (Containment)

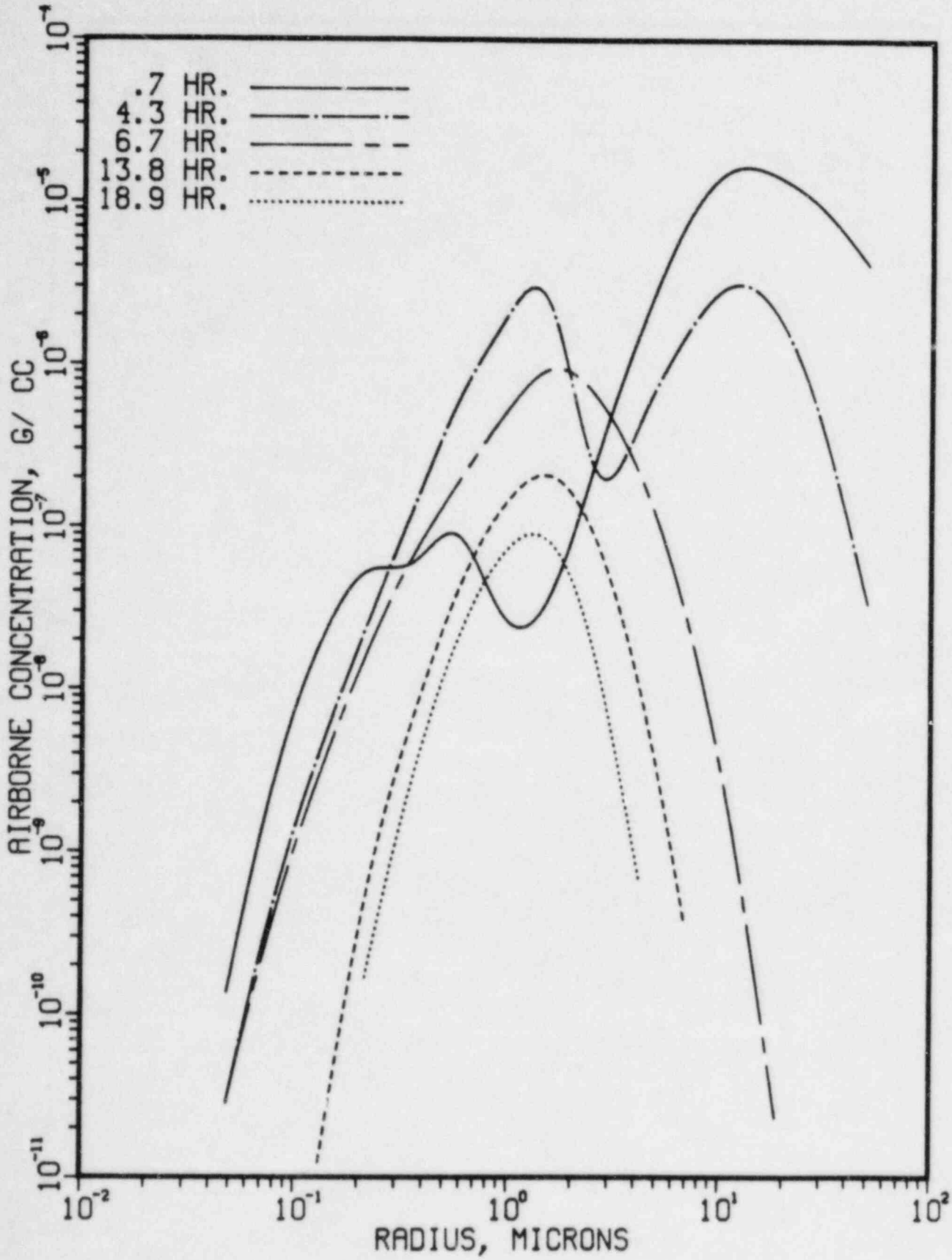

FIGURE 7.25 PARTICLE SIZE DISTRIBUTION, AB-β (Safeguard Building)

TABLE 7.12. LOCATIONAL DISTRIBUTION OF SPECIES AFTER ACCIDENT IS COMPLETED, AB-B

Species	Fraction of Core Inventory			
	RCS	Containment	Safeguard Building	Environment
CsI	2.7×10^{-2}	0.59	0.29	8.7×10^{-2}
CsOH	3.8×10^{-2}	0.59	0.29	8.5×10^{-2}
Te	0.26	0.19	0.12	7.0×10^{-2}

TABLE 7.13. LOCATIONAL DISTRIBUTION OF SPECIES AFTER ACCIDENT IS COMPLETED, AB-β (4 Volume)

Species	Fraction of Core Inventory					
	RCS	Vol.1	Vol. 2	Vol. 3	Vol. 4	Environment
CsI	2.7×10^{-2}	0.33	0.36	0.23	1.8×10^{-3}	5.0×10^{-2}
CsOH	3.8×10^{-2}	0.33	0.36	0.23	2.2×10^{-3}	4.9×10^{-2}
Te	0.26	4.3×10^{-2}	5.3×10^{-2}	0.19	4.9×10^{-2}	4.2×10^{-2}

Figures 7.26 through 7.28 show the airborne mass, the accumulated mass leaked, and the particle size distribution for this case. Table 7.14 is the locational distribution of each species after a long period of time elapsed. Table 7.14 shows that compared with the calculated CsI and CsOH fractions released into the environment (as shown in Table 7.12) for the AB-β sequence, slightly lower fractions are found to escape the containment in the AB-γ sequence. However, the Te release fraction is substantially higher because more Te is available in this sequence than in the AB-β sequence.

7.3.1.3 AB-ε. Figures 7.29 through 7.31 show the airborne mass, the accumulated mass leaked to the environment, and the airborne particulate size distribution at various times for the AB-ε sequence. As shown in Chapter 6, the containment does not fail until a time of 1450 minutes in this sequence. The first peak in the airborne mass shown in Figure 7.29 represents the source from the RCS prior to the bottom head failure; the second peak represents the source during the core-concrete interaction. The particle size distribution shown in Figure 7.31 attains a bimodal distribution, apparently due to the condensation of steam vapor onto particulates. However, when the thermal-hydraulic conditions in the containment become such that there is no further condensation, the size distribution becomes a unimodal distribution which seems to fit approximately the lognormal function. Table 7.15 shows the results of the fraction of core inventory for each species located in various compartments. Note that for the failure mode the calculated release of fission products is into the ground rather than to the outside atmosphere. A substantial additional decontamination factor would be expected for the source term to the atmosphere.

7.3.2 TMLB' Sequence

Two containment failure modes were examined for this accident sequence. The first, designated TMLB'-δ, is an early overpressure failure resulting from steam and noncondensible gases. In this failure mode, the containment fails 152 minutes after the core uncovers; this coincides with the time at which the bottom head fails. At this point, the containment pressure reaches 89 psi. The second containment failure mode considered here, designated

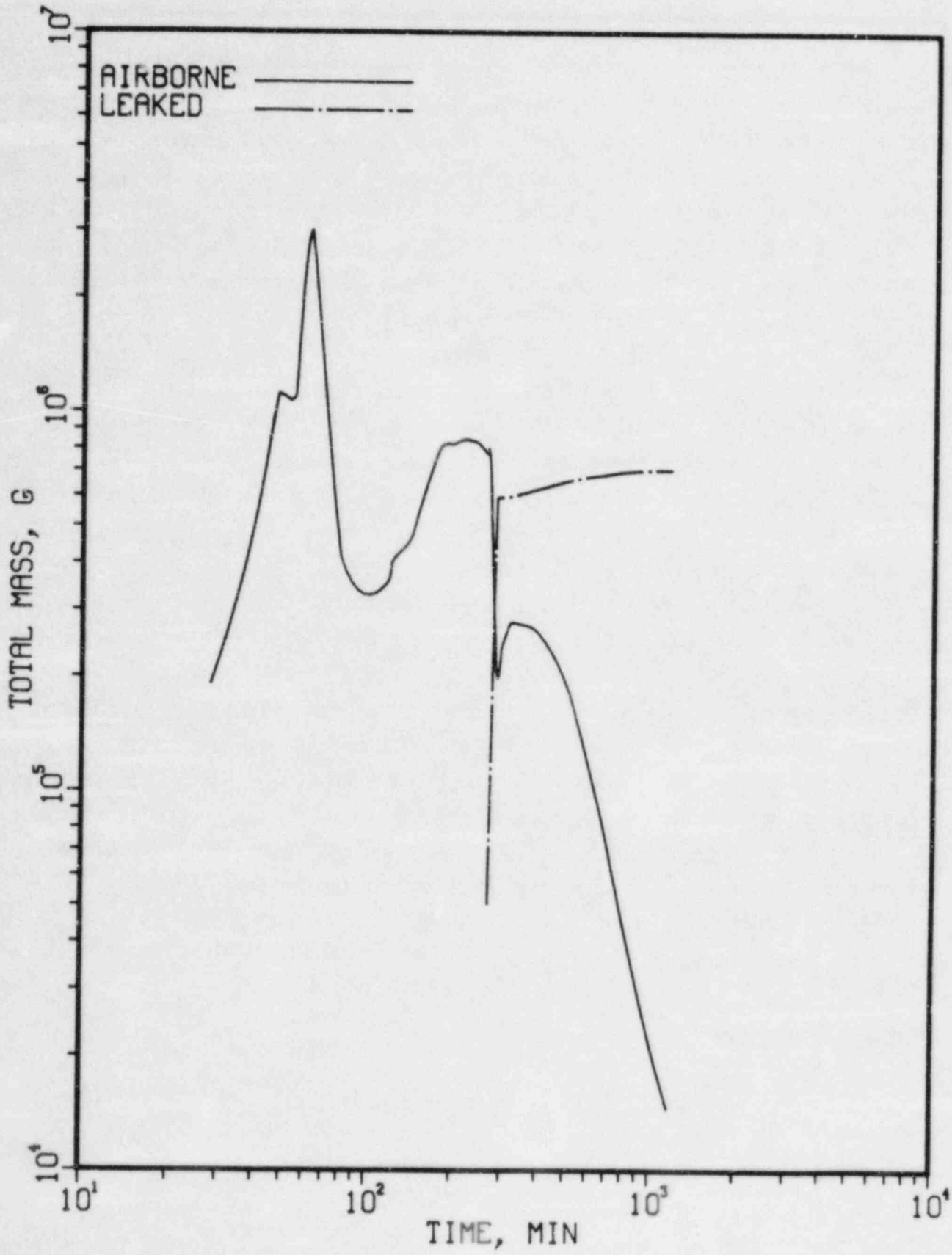

FIGURE 7.26. AIRBORNE AND LEAKED MASSES, AB-$_Y$

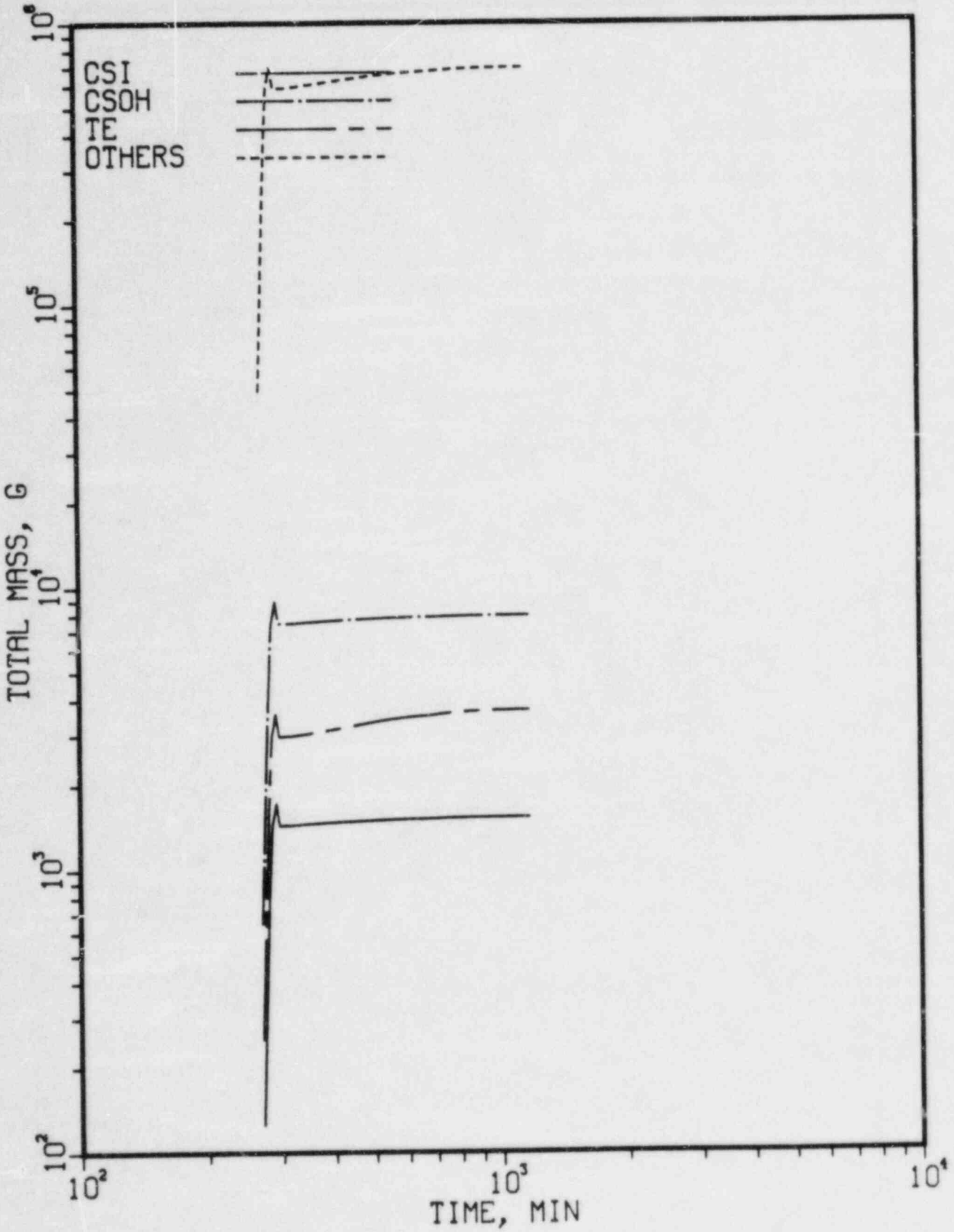

FIGURE 7.27. ACCUMULATED LEAKED NUCLIDES, AB-γ

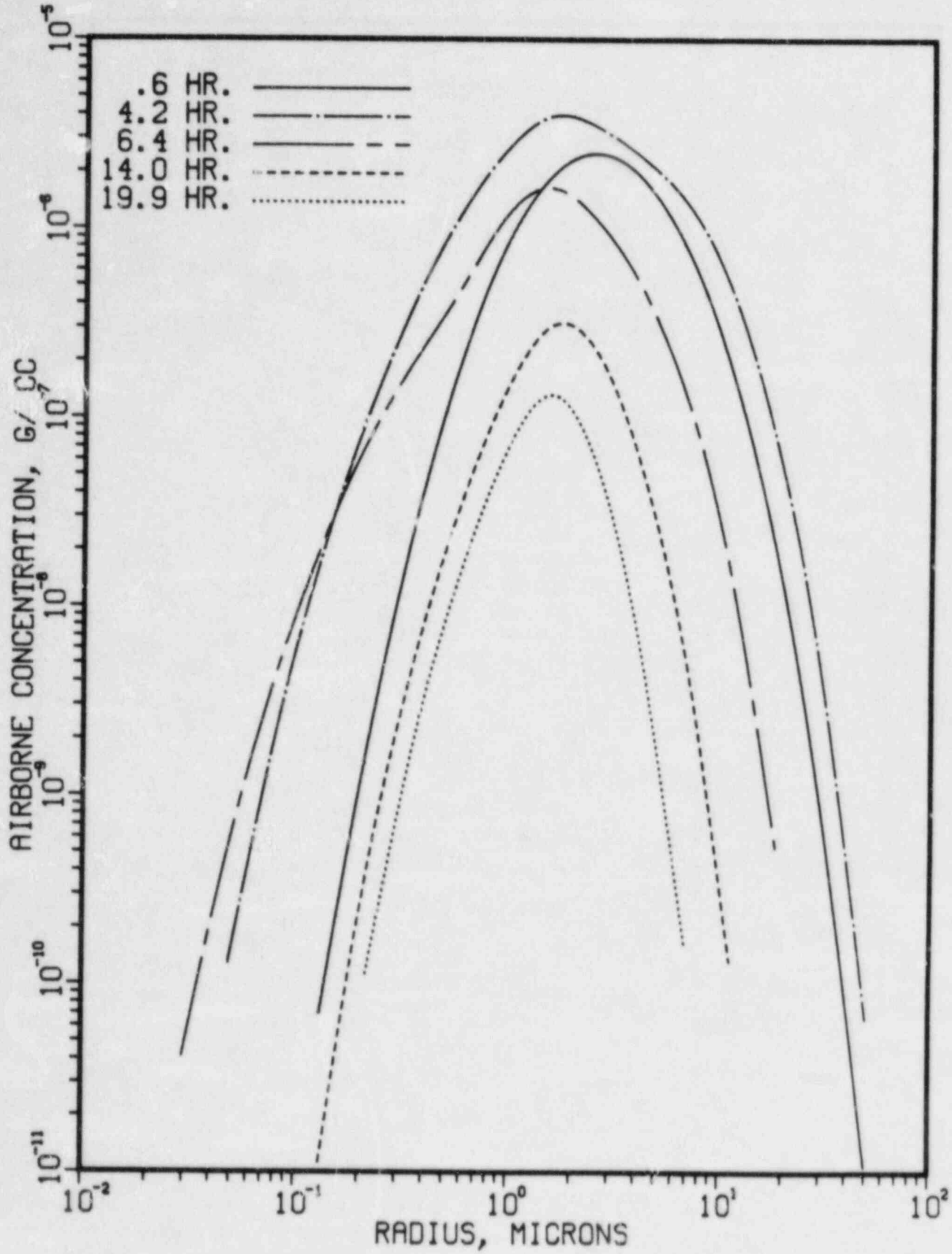

FIGURE 7.28. PARTICLE SIZE DISTRIBUTION AB-γ

TABLE 7.14 LOCATIONAL DISTRIBUTION OF SPECIES AFTER ACCIDENT IS COMPLETED, AB-γ

Species	Fraction of Core Inventory		
	RCS	Containment	Environment
CsI	2.7×10^{-2}	0.92	5.7×10^{-2}
CsOH	3.8×10^{-2}	0.90	5.9×10^{-2}
Te	0.26	0.31	0.14

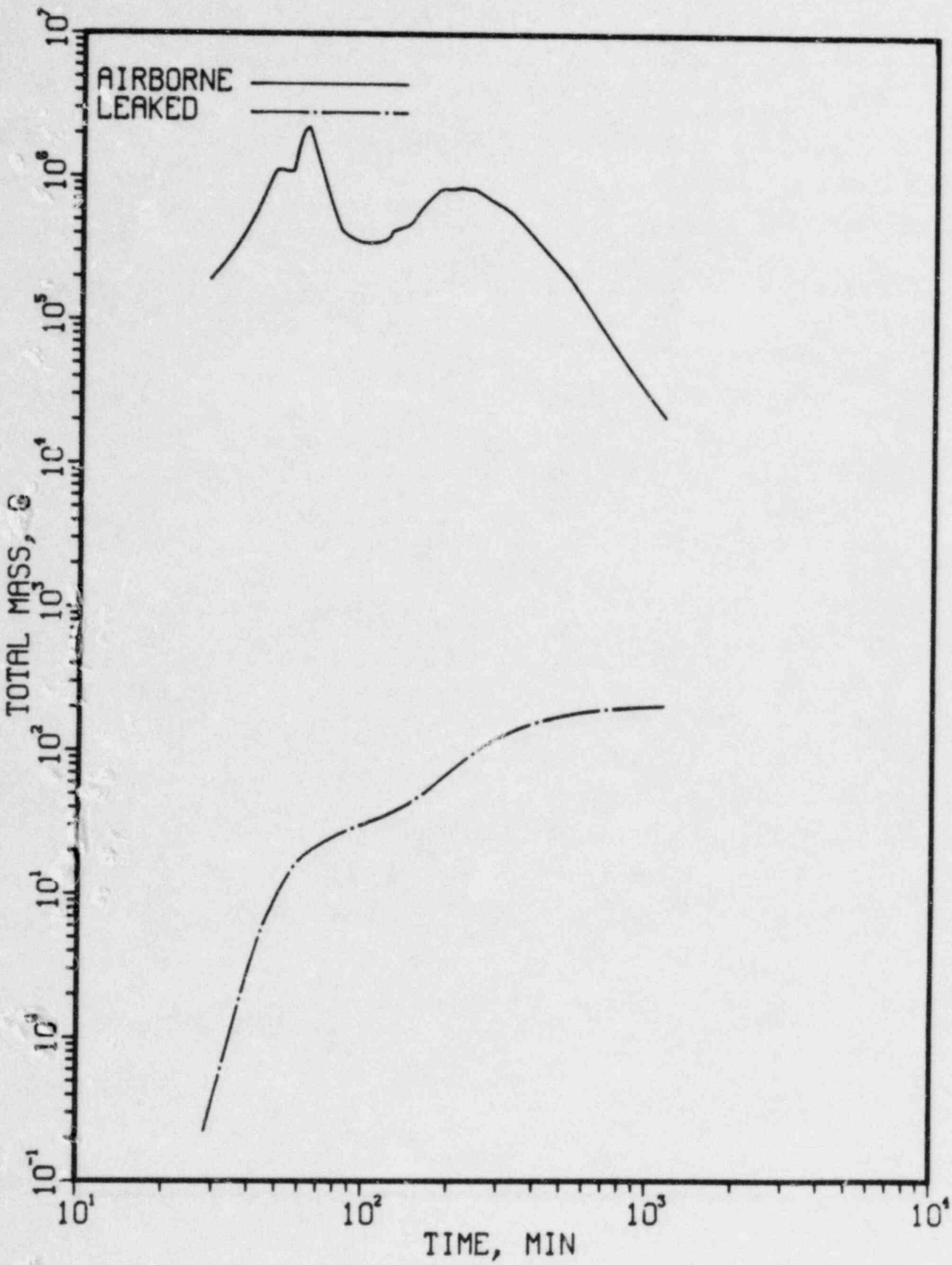

FIGURE 7.29. AIRBORNE AND LEAKED MASSES, AB-ε

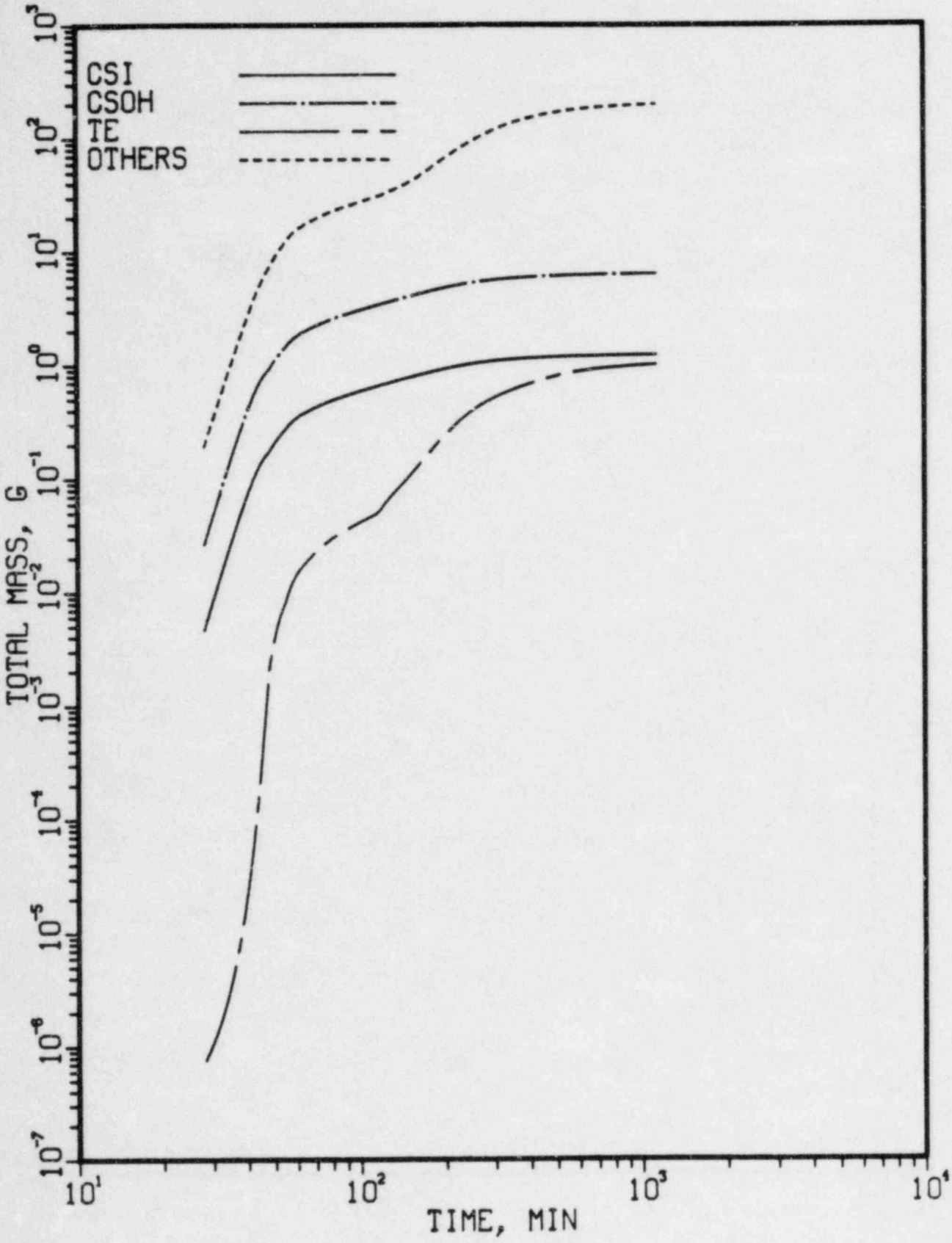

FIGURE 7.30. ACCUMULATED LEAKED NUCLIDES, AB-ε

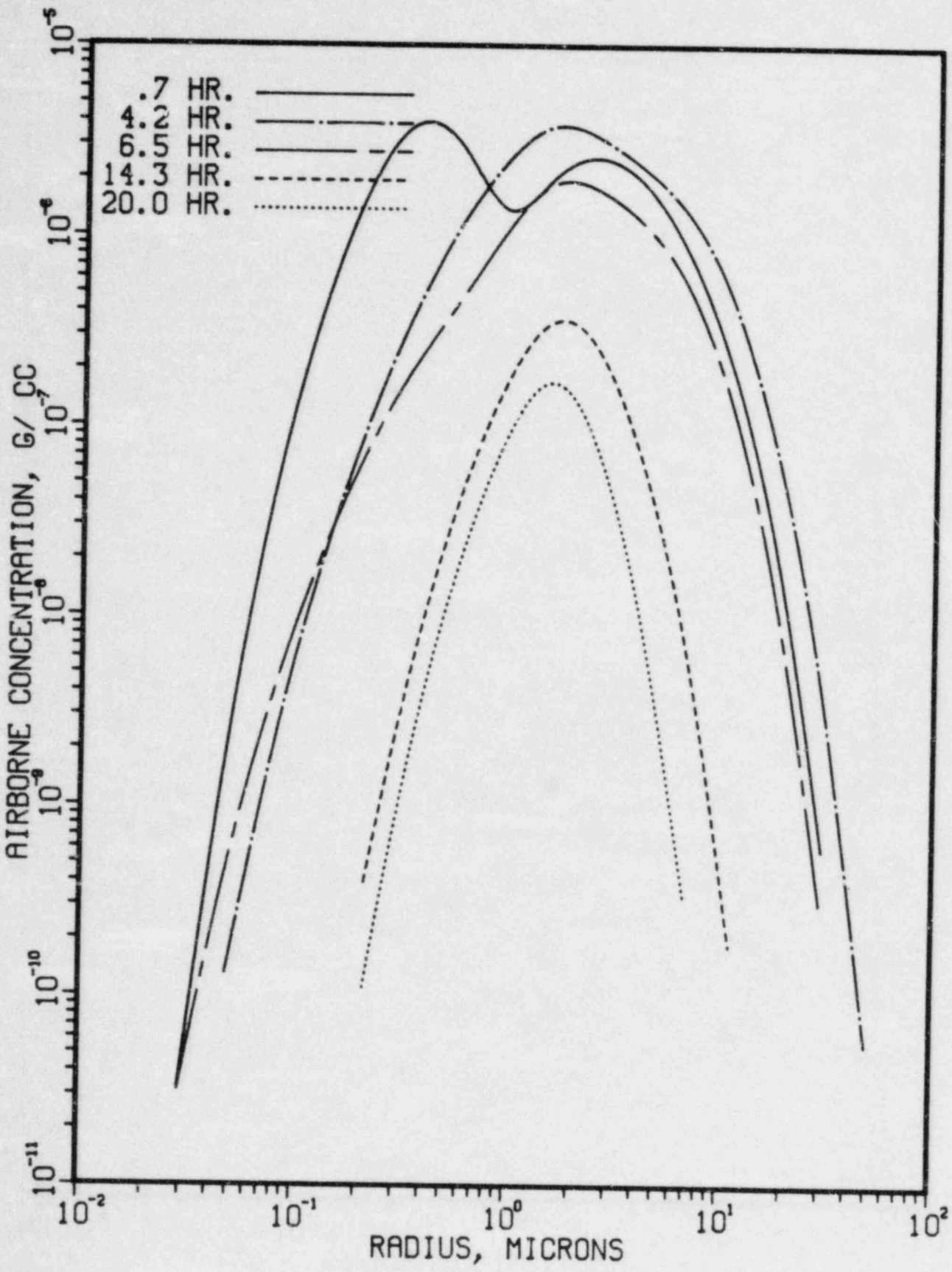

FIGURE 7.31. PARTICLE SIZE DISTRIBUTION, AB-ε

TABLE 7.15. LOCATIONAL DISTRIBUTION OF SPECIES AFTER ACCIDENT IS COMPLETED, AB-ε

Species	Fraction of Core Inventory		
	RCS	Containment	Environment*
CsI	2.7×10^{-2}	0.97	4.8×10^{-5}
CsOH	3.8×10^{-2}	0.96	4.7×10^{-5}
Te	0.26	0.45	4.0×10^{-5}

*Released to the ground below the containment building. Values for CsI is as an aerosol and does not reflect possible iodine release as a volatile iodide.

TMLB-δ, considers basemat melt-through. In this failure mode, the containment fails at a time of 738 minutes with a containment pressure of 55 psi. Unlike the AB accident sequences, in which fission products have a minimum retention in the primary system due to a relatively short pathway, 90 percent of the CsI and CsOH core inventories are retained in the TMLB' sequence (as discussed previously in Section 7.2).

7.3.2.1 TMLB'-δ. In TMLB'-δ, the containment fails shortly after the reactor vessel is ruptured. Compared with the TMLB'-ε sequence, the source particulates released from the primary system and from the core-concrete interaction tend to escape the containment before encountering significant natural retention. No engineered safety features are assumed available in this sequence.

The calculated results for the airborne mass and accumulated leaked mass for the containment for the TMLB'-δ sequence are shown in Figures 7.32 and 7.33. The locational distribution of species after a long period of time elapsed is shown in Table 7.16. The calculated core inventory fractions shown in the table are comparable to those obtained for the AB-γ sequence shown in Table 7.14 but are somewhat lower than those for the AB-β sequence shown in Table 7.12.

7.3.2.2 TMLB'-ε. The calculated results for the airborne mass and the accumulated leaked mass in the containment for the TMLB'-ε sequence are shown in Figures 7.34 and 7.35. In this accident sequence, the containment melt-through occurs at a time of 738 minutes. The containment pressure reaches about 55 psi at this time. As traditionally assumed, no engineered safety features such as sprays are operating due to the loss of all AC power. Details on the accident event timetable and the time-dependent pressure and temperature conditions can be referred to in Section 6.1.

Figure 7.34 shows the mass of the total airborne particulates as a function of time. Again, the first peak of the curve represents the melt release prior to the bottom head failure and the subsequent increase is due to the release, calculated from VANESA, during the core-concrete interaction. It should be noted that in this accident sequence, a water mass of 1.117×10^5 kg at 326 K is assumed present at the time of head failure (t = 157 min), and it is further assumed that the mass evaporates over a time period of approximately

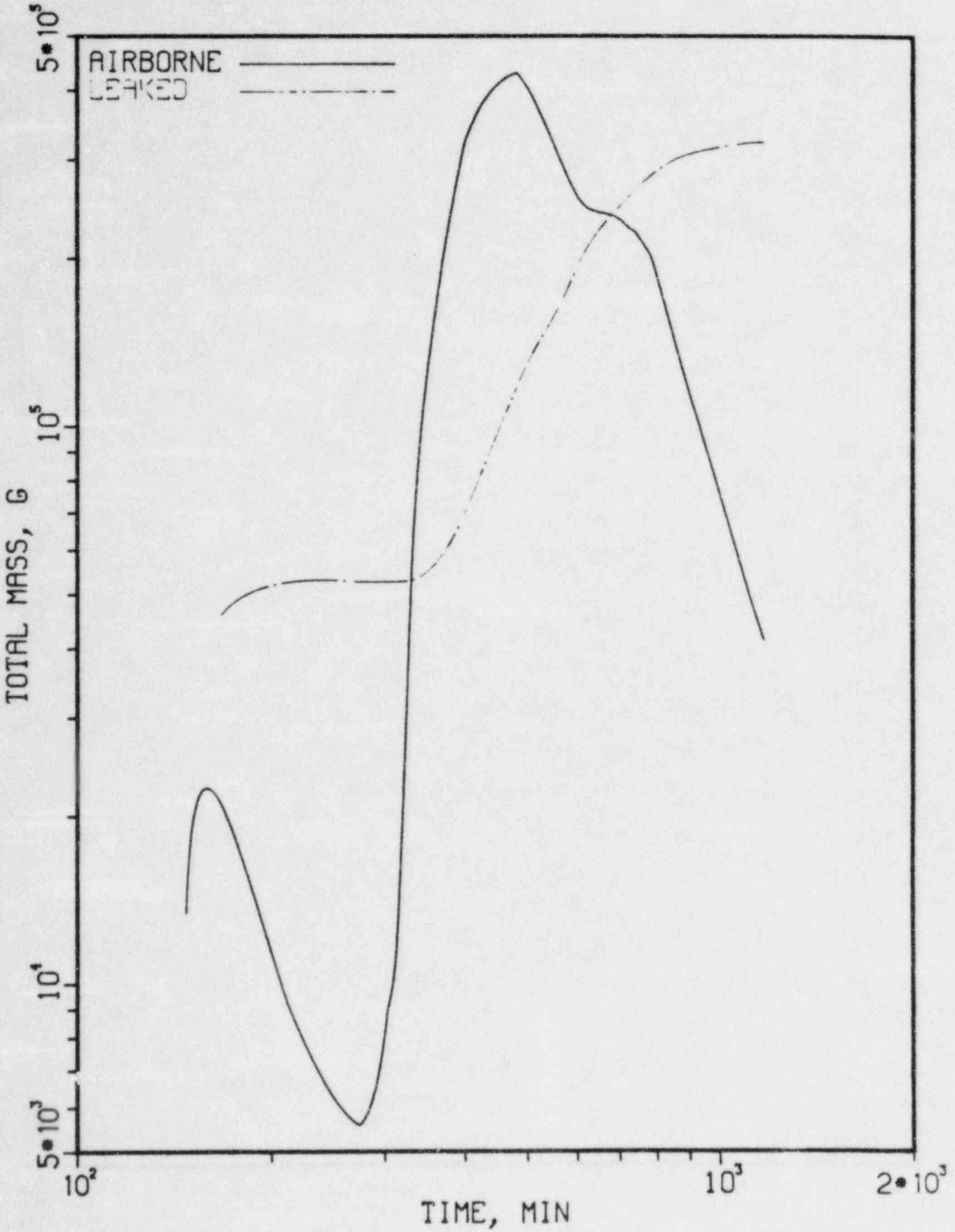

FIGURE 7.32. AIRBORNE AND LEAKED MASSES, TMLB'-8

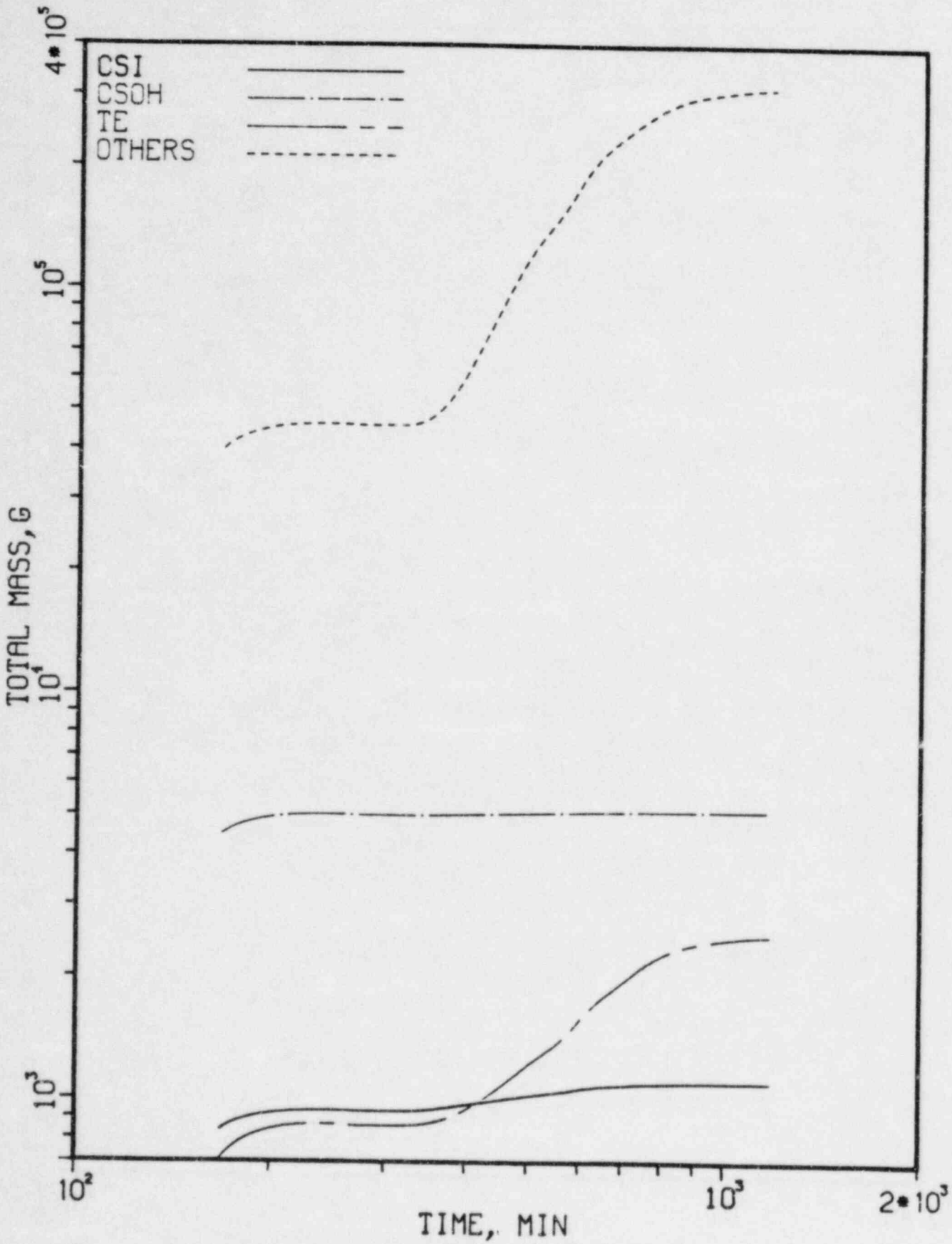

FIGURE 7.33. ACCUMULATED LEAKED NUCLIDES, TMLB'-6

TABLE 7.16 LOCATIONAL DISTRIBUTION OF SPECIES AFTER ACCIDENT IS COMPLETED, TMLB'-6

Species	Fraction of Core Inventory		
	RCS	Containment	Environment
CsI	0.85	0.11	4.6×10^{-2}
CsOH	0.86	0.10	3.9×10^{-2}
Te	0.30	0.16	0.11

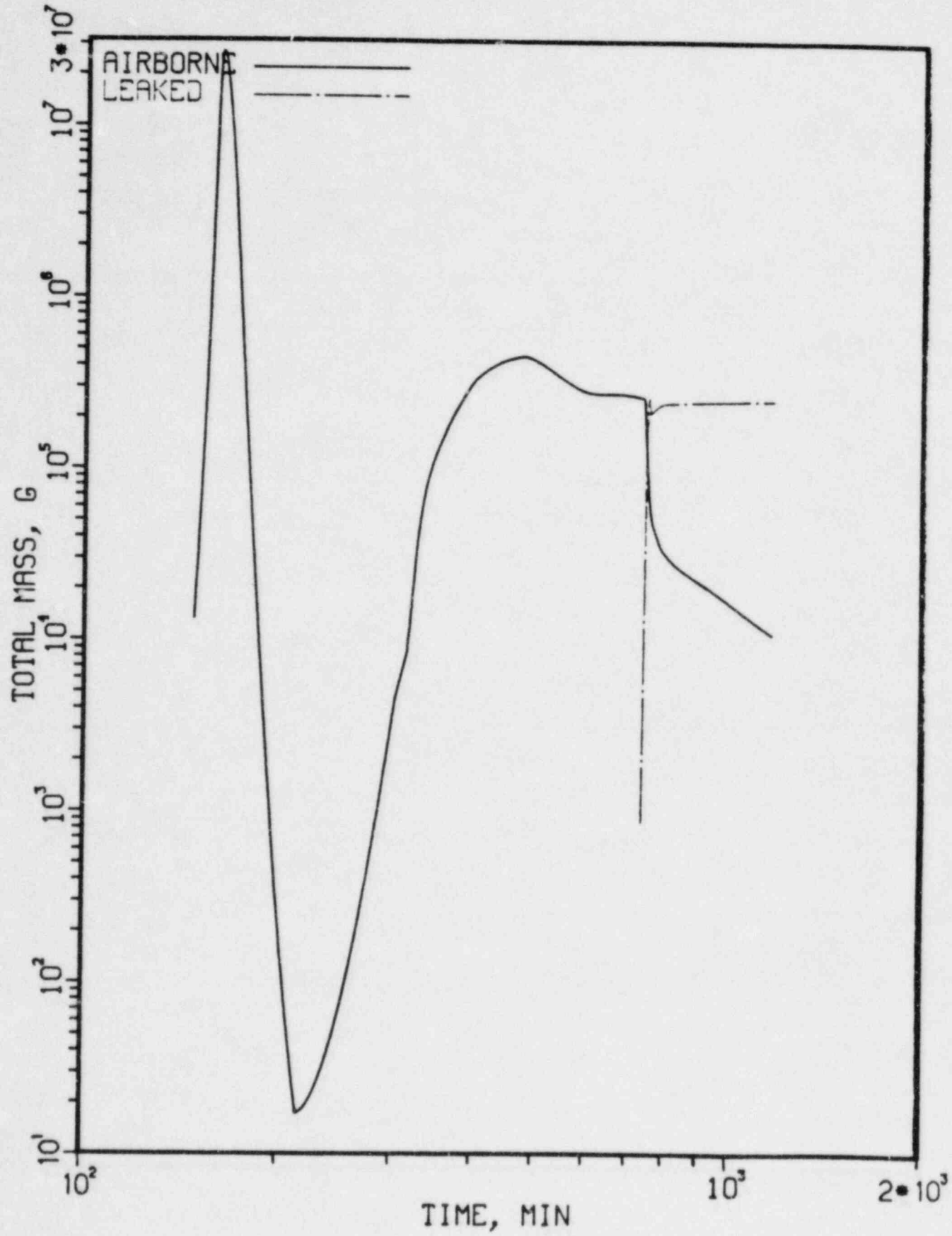

FIGURE 7.34. AIRBORNE AND LEAKED MASSES, TMLB'-ε

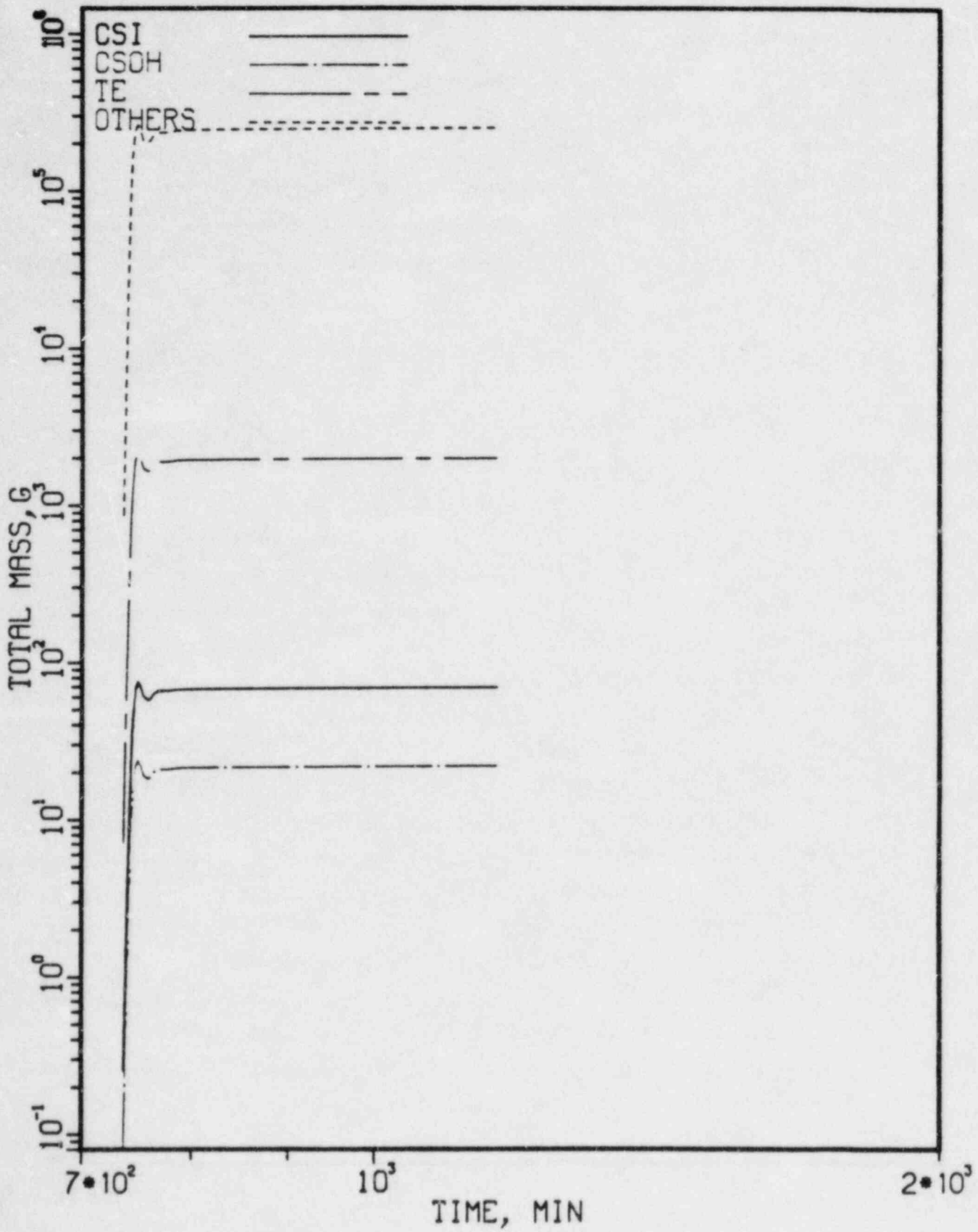

FIGURE 7.35. ACCUMULATED LEAKED NUCLIDES, TMLB'-ε

1 hour. The presence of water, of course, delays the vaporization release substantially. Figure 7.35 shows the accumulated leaked mass for CsI, CsOH, and Te as a function of time. Table 7.17 summarizes the calculated distribution of the core inventory fractions. For the ε failure mode release is to the ground rather than directly to the outside atmosphere. A substantial additional attenuation factor would be expected for the atmospheric source term.

7.3.3 V Sequence

This sequence represents one of the accidents that potentially permits a large amount of fission products to escape to the atmosphere. In this event, the check valves that provide a barrier between the RCS piping and the low pressure ECC system fail, and fission products can bypass the containment safety features and be released to the auxiliary building. If the auxiliary building is treated as a containment for modeling purposes, calculational methods identical to those used for the other accident sequences can be applied. Results calculated with the TRAP-MELT code were used for the melt release source for NAUA containment calculations. In treating the vaporization release, it was assumed that no attenuation of particulates occurs in their passage from the reactor cavity through the primary system. This simplification is expected to overestimate the amount of fission products released to the environment. To simulate this sequence more rigorously, it may be necessary to use a multivolume approach to assess the effects of retention of particulate material in the primary system for the vaporization release term. Two separate TRAP-MELT calculations would be necessary in that approach.

The fractions of core inventory of various species released to the atmosphere as predicted by the NAUA code are listed in Table 7.18a. As expected, the calculated results show that this accident sequence is still one of the most important in terms of total release, with the release fractions being about 40 percent of the Cs and I inventories. The airborne mass, accumulated leaked mass of each species, and the size distribution in the safeguard building are shown in Figures 7.36 through 7.38.

If scrubbing in a water pool on entry into the safeguards building is considered, the results are as shown in Table 7.18b. It is seen that the

TABLE 7.17. LOCATIONAL DISTRIBUTION OF SPECIES AFTER ACCIDENT IS COMPLETED, TMLB'-ε

Species	Fraction of Core Inventory		
	RCS	Containment	Environment*
CsI	0.85	0.15	2.8×10^{-3}
CsOH	0.86	0.14	1.7×10^{-4}
Te	0.30	0.19	8.1×10^{-2}

*Released to the ground below the containment building.

TABLE 7.18a. LOCATIONAL DISTRIBUTION OF SPECIES AFTER ACCIDENT IS COMPLETED, V

Species	Fraction of Core Inventory			
	RCS	Containment	Safeguards Building	Environment
CsI	0.50	1.8×10^{-2}	6.9×10^{-2}	0.41
CsOH	0.51	1.7×10^{-2}	7.1×10^{-2}	0.40
Te	0.13	0.71	4.4×10^{-2}	0.12

TABLE 7.18b. LOCATIONAL DISTRIBUTION OF SPECIES AFTER ACCIDENT IS COMPLETED, V WITH WATER

Species	Fraction of Core Inventory			
	RCS	Containment	Safeguards Building*	Environment
CsI	0.50	1.8×10^{-2}	0.40	7.9×10^{-2}
CsOH	0.51	1.7×10^{-2}	0.40	7.3×10^{-2}
Te	0.13	0.71	0.14	2.5×10^{-2}

*A water depth of 3 feet is assumed.

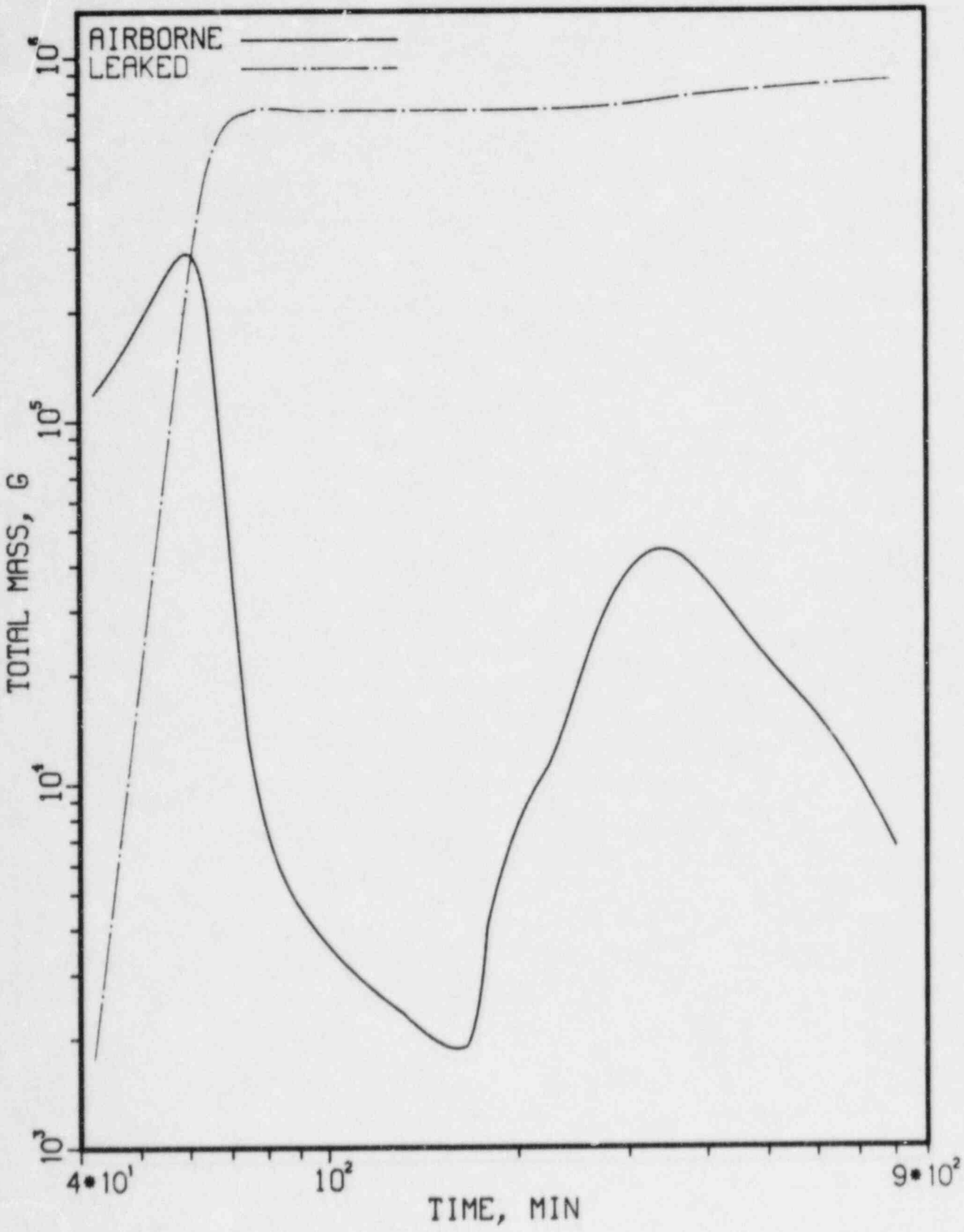

FIGURE 7.36. AIRBORNE AND LEAKED MASSES, V (Safeguard Building)

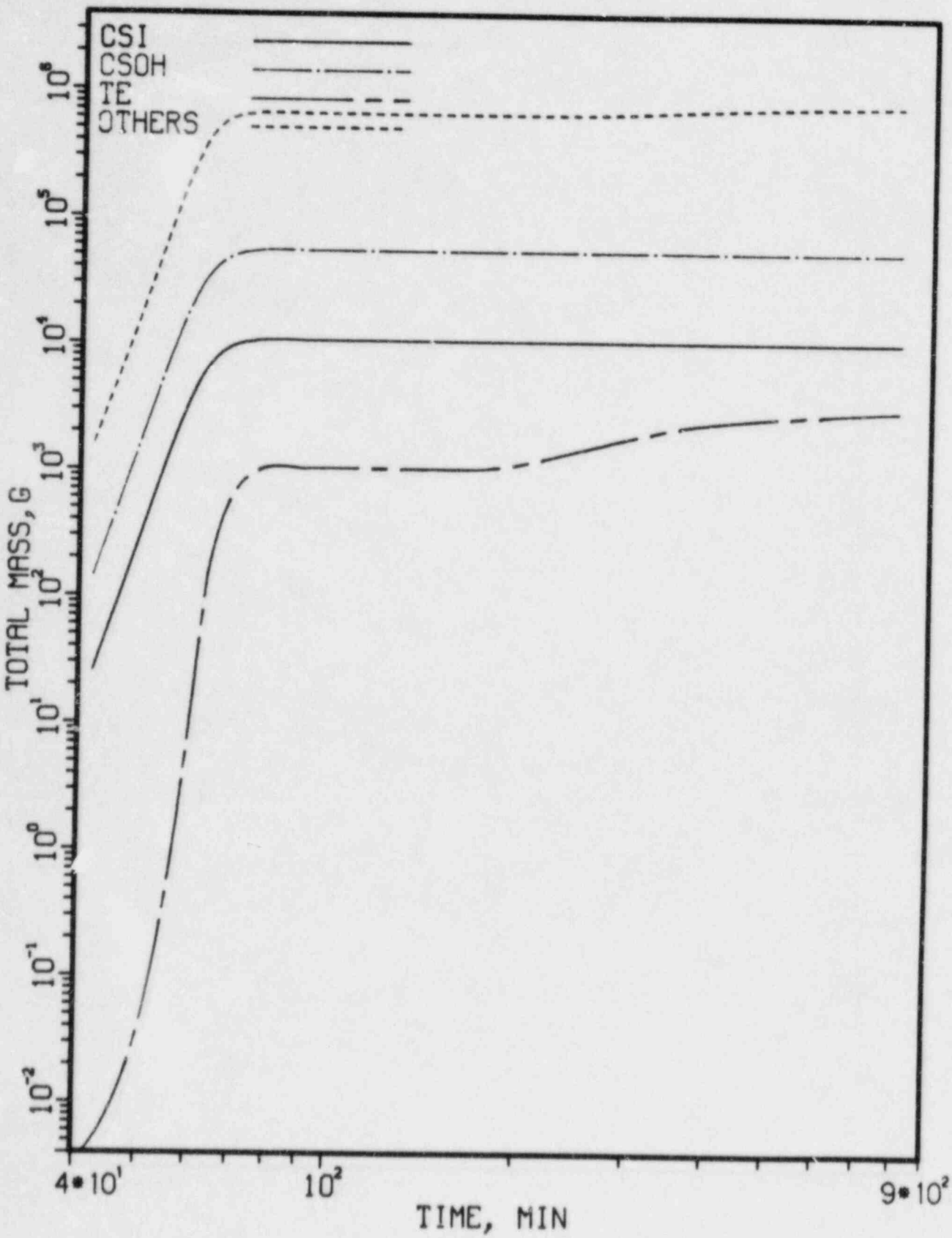

FIGURE 7.37. ACCUMULATED LEAKED NUCLIDES, V (Safeguard Building)

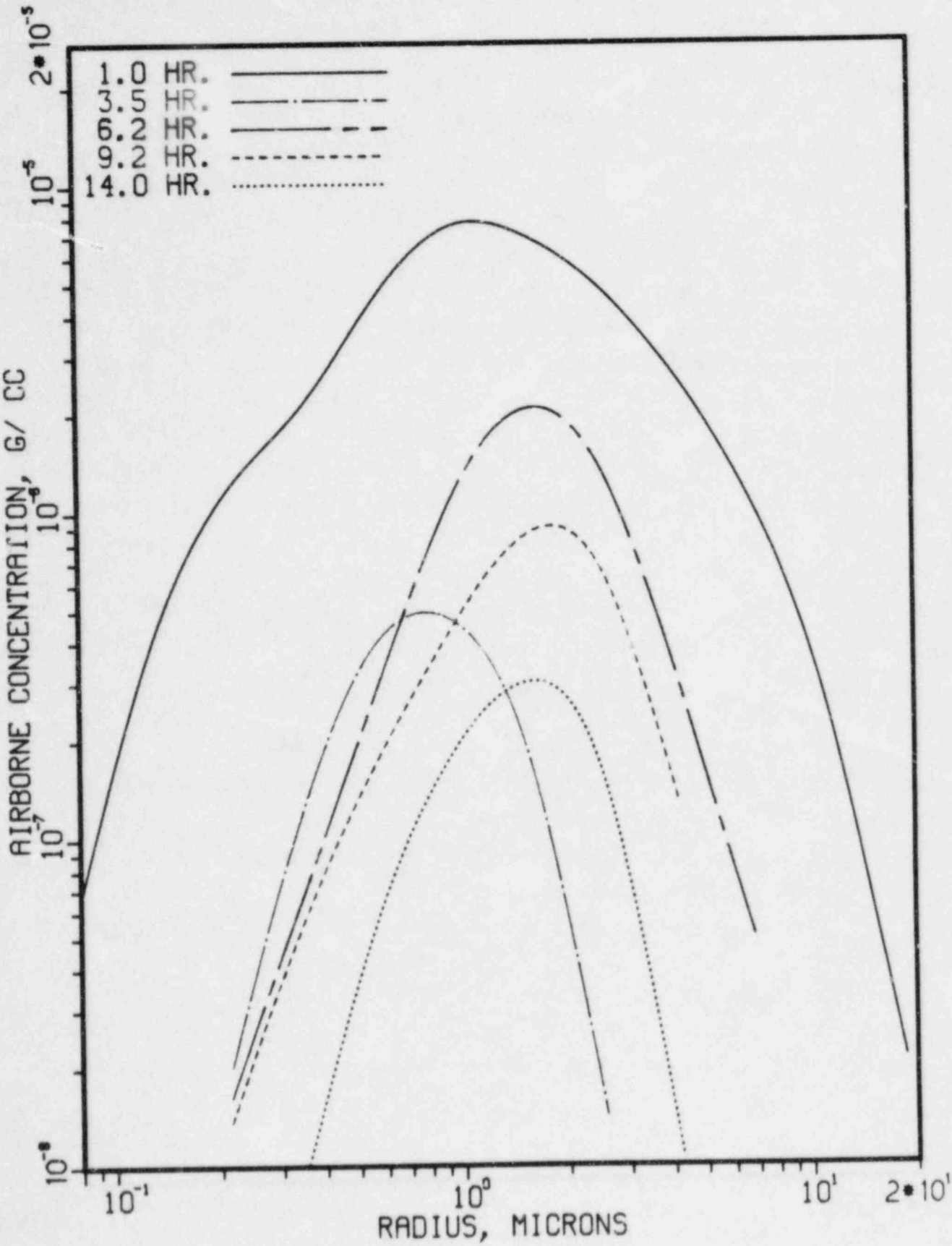

FIGURE 7.38. PARTICLE SIZE DISTRIBUTION, V (Safeguard Building)

presence of gas flow through a hot pool only 3 feet deep has a significant effect with the fractional release to the environment being about 0. for CsI and CsOH as compared with values of about 0.4 if the water pool is ignored.

7.3.4 S_2D Sequence

The S_2D sequence is a small pipe break accident. The containment failure modes examined were overpressure due to hydrogen burning (S_2D-γ) and basemat melt-through (S_2D-ε). Unlike the AB and TMLB' accident sequences, containment spray systems operate during this sequence; this allows steam to condense and containment pressure to be reduced. Since the original NAUA code had no provision for accounting for the role of engineered safeguard, calculations were made by adding the removal mechanism of aerosol particles due to spraying. Details of the modification of the NAUA code were discussed in Chapter 5.

In general, spraying systems are highly effective in removing aerosol particles, and it is expected that the spraying mechanism will dominate all natural retention mechanisms in the case of the S_2D sequence.

7.3.4.1 S_2D-γ. In this sequence, containment failure results from overpressure due to hydrogen burning. The spray systems were assumed to cease operating when the containment failure occurs.

Figure 7.39 shows the time-dependent airborne mass for this failure mode. In Figure 7.39, it is seen that, as expected, the airborne mass remains very low during the melt release period due to the high removal effectiveness of spraying coupled with the relatively high retention of particulates in the primary system. It should be noted that in the S_2D calculation shown in Figure 7.39, a drop size of 400 m was used. Figure 7.40 shows the leaked mass, and Table 7.19 shows the fraction of core inventory leaked to the environment.

7.3.4.2 S_2D-ε. This accident sequence is similar to the S_2D-γ sequence except that containment failure does not occur until the basemat melts through and that containment sprays continue to operate throughout all the accident events. Due to the quantity of water in the reactor cavity during

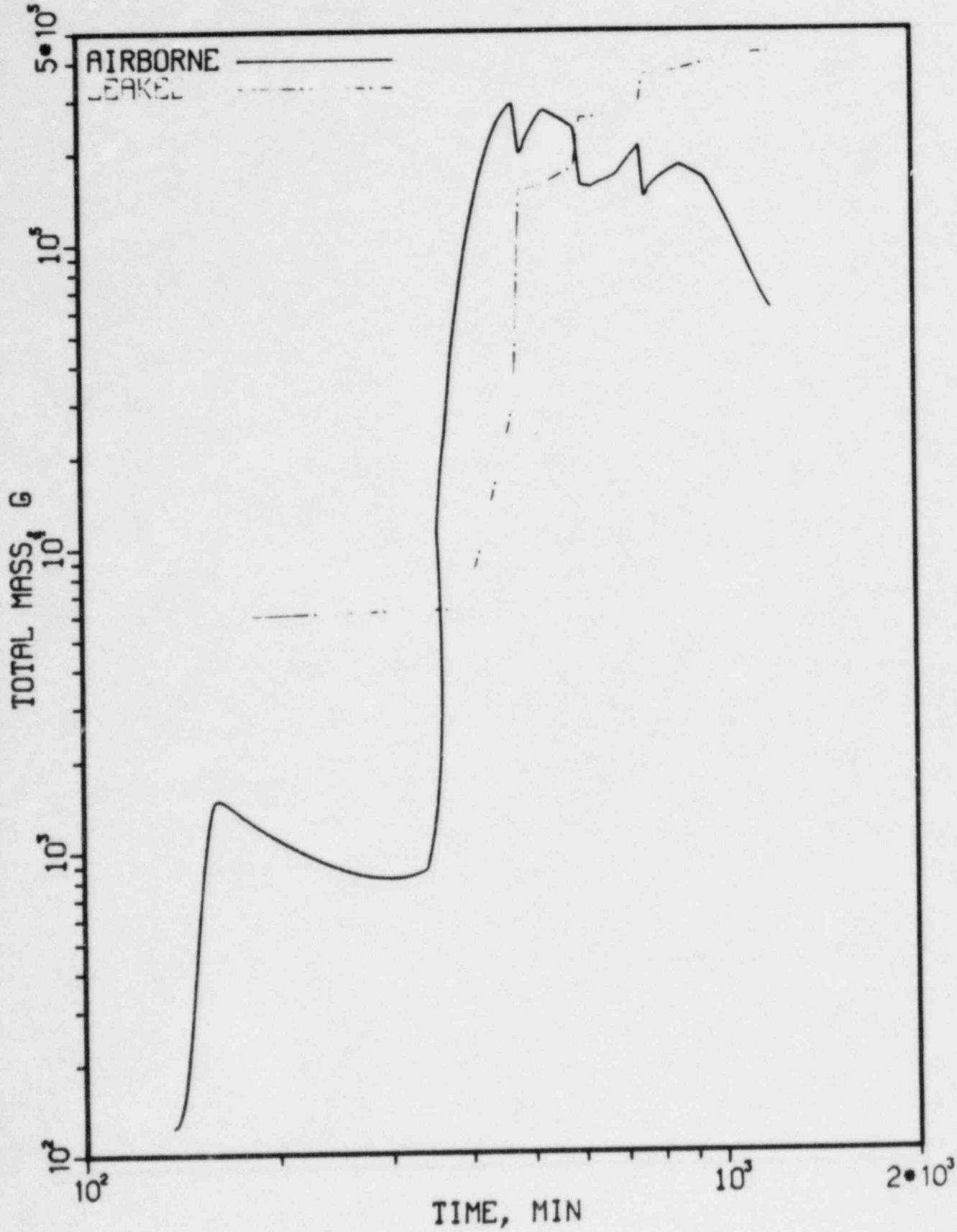

FIGURE 7.39. AIRBORNE AND LEAKED MASSES, S$_2$D-$_Y$

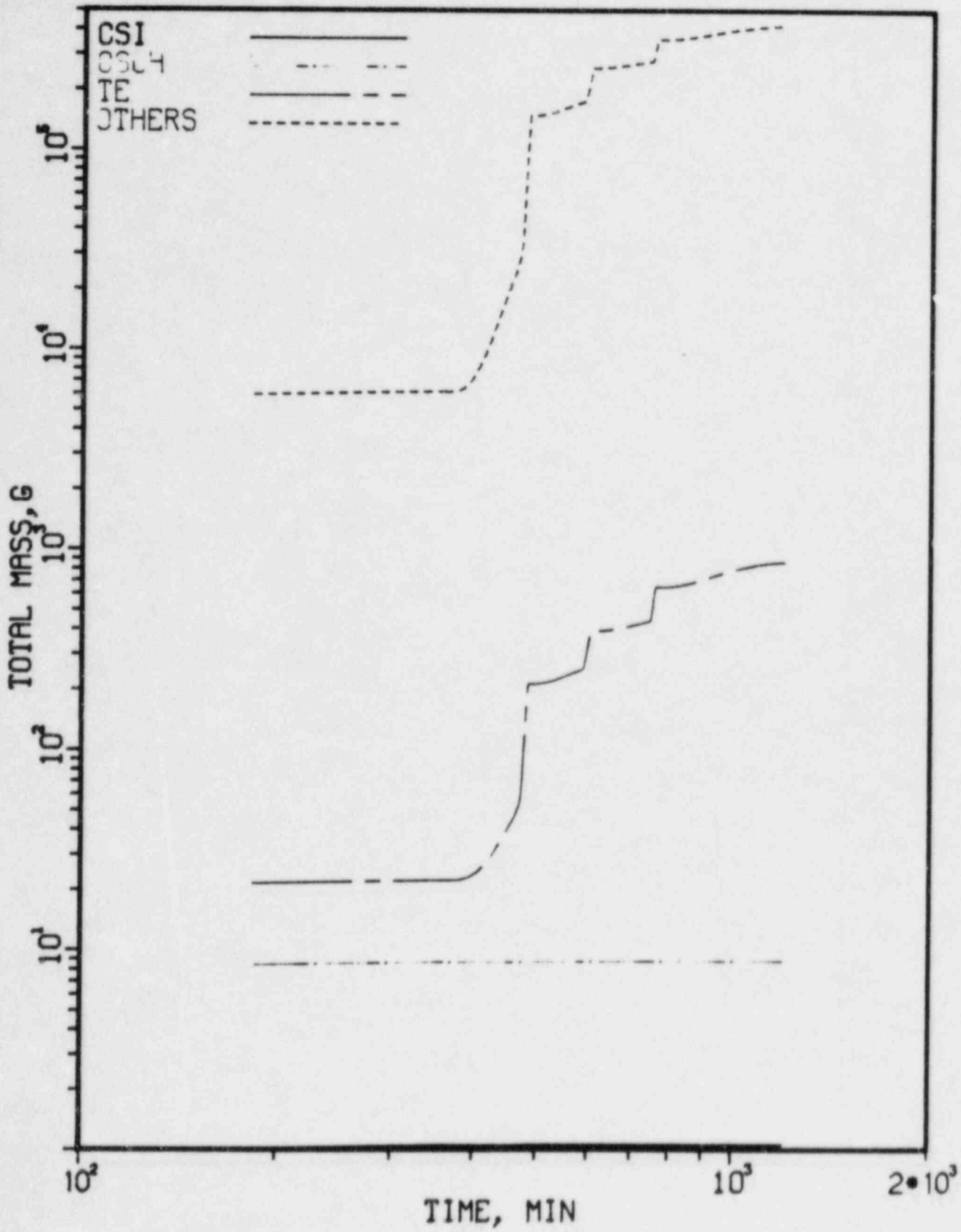

FIGURE 7.40. ACCUMULATED LEAKED NUCLIDES, S_2D-Y

TABLE 7.19 LOCATIONAL DISTRIBUTION AFTER THE CALCULATION IS COMPLETED, S_2D-γ

Species	Fraction of Core Inventory		
	RCS	Containment	Environment
CsI	0.48	0.52	4.2×10^{-5}*
CsOH	0.57	0.43	6.4×10^{-5}
Te	0.91	5.8×10^{-2}	3.3×10^{-2}

*This value is for CsI as an aerosol and does not indicate iodine release if volatile iodides are formed in the containment. Estimated release for volatile iodides is about 10^{-3}.

the core-concrete interaction, the VANESA calculation accounts for the presence of water; these calculations were utilized as the source term during the vaporization phase. Figures 7.41 and 7.42 show the airborne mass and accumulated leaked mass of species for the S_2D-ε sequence, and Table 7.20 presents the locational distribution of the CsI, CsOH, and Te species. For the ε failure mode the release is into the ground rather than to the outside atmosphere.

7.3.5 Results for Groups of Reactor Safety Study

As discussed, the results of calculations presented so far distinguished CsI, CsOH, and Te. In general, one can keep track of an increased number of species in the calculation. In order to demonstrate this capability, additional NAUA calculations were performed for the AB and TMLB sequences. The groups and the corresponding species accounted for in these additional calculations were already discussed in Section 6.2.1. Since the VANESA calculations for the release during the core-concrete interaction did not include all the species to be tracked, it was assumed that the species in a group not included in the original VANESA calculation are released at a rate identical to that for the species in the same group. For example, the release rate for Tc, Rh, and Pd in Group 6 was assumed to be the same as that for Ru and Mo combined after accounting for their core inventories. It should also be noted that Group 1 was not included in the NAUA calculation since Kr and Xe are in the vapor form. Table 7.4 lists the calculated fraction of core inventory released to the environment as a function of both time and group for AB-β, AB-γ, AB-ε, TMLB'-δ, and TMLB'-ε. The calculated fraction for AB-β is based on a two-volume model.

It is seen from the table that the containment failure time shows pronounced effects on the amount of release to the environment as expected. Compared with the results of the calculations for CsI, CsOH, and Te given earlier in Tables 7.12, 7.14, 7.15, 7.16, and 7.17, the results listed in Table 7.21 for Groups 2, 3, and 4 are slightly different because of the regrouping of the species. In general, the release fraction for Group 6 is seen to be the lowest because of its relatively low release from the fuel.

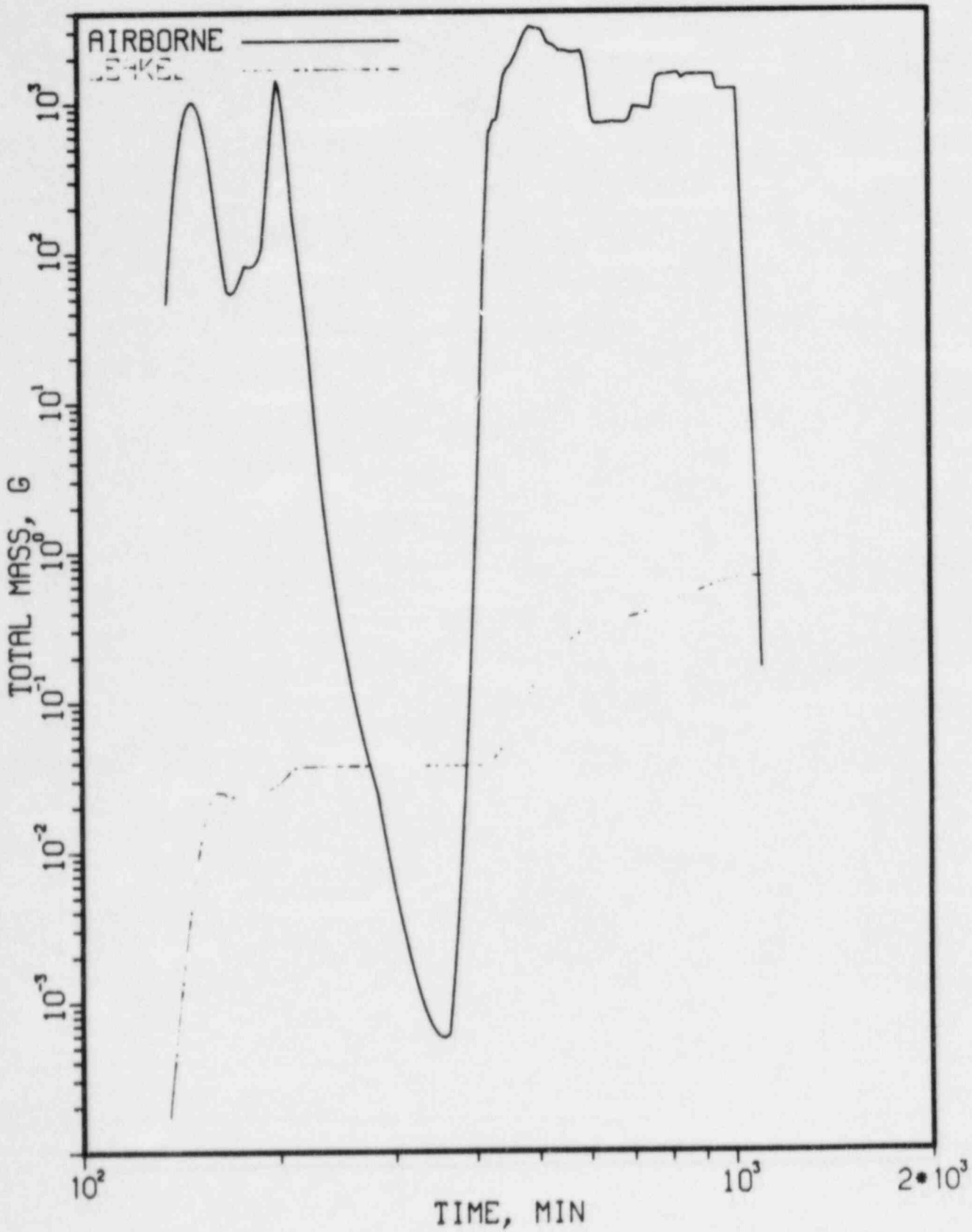

FIGURE 7.41. AIRBORNE AND LEAKED MASSES, S_2D-c

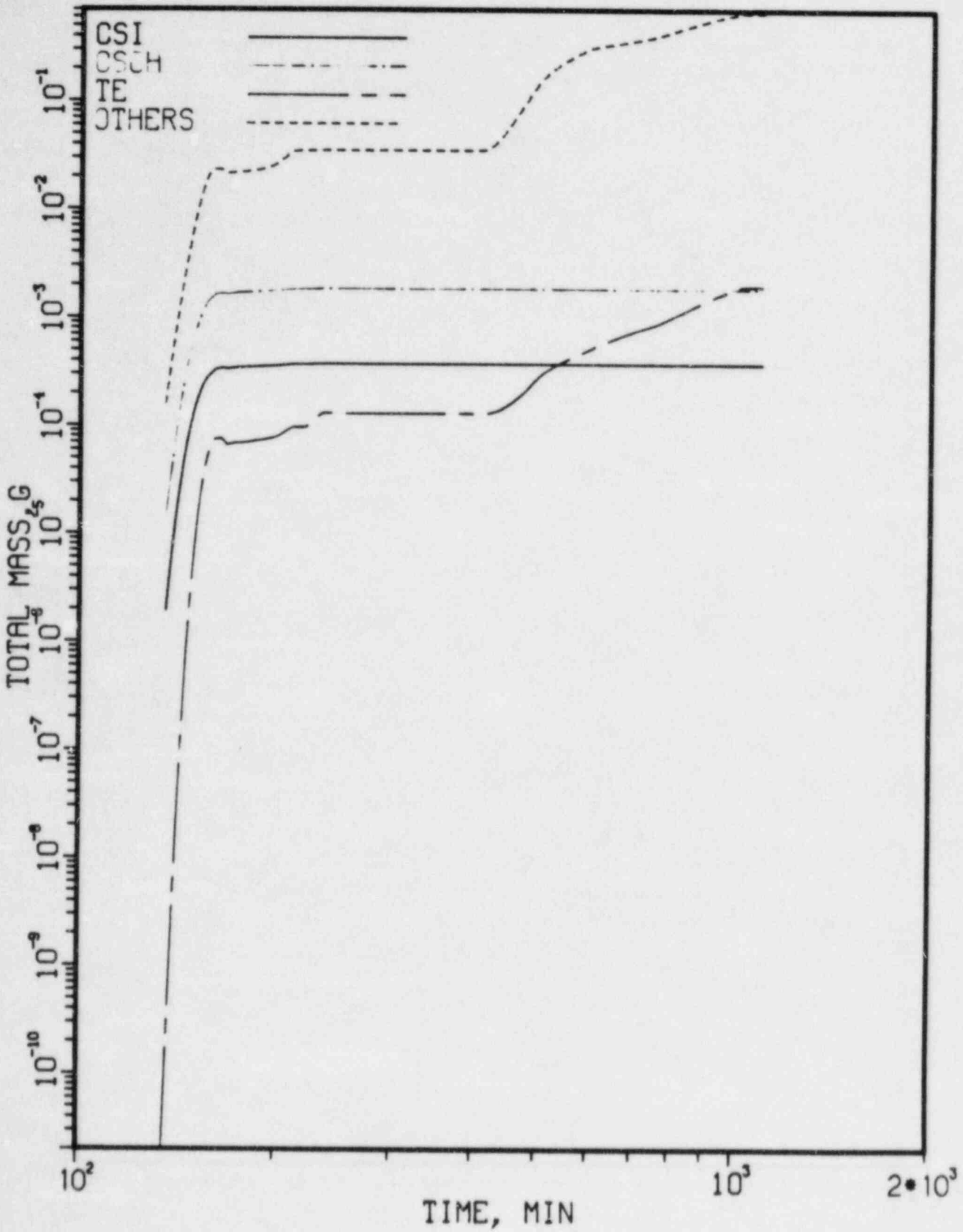

FIGURE 7.42. ACCUMULATED LEAKED NUCLIDES, S_2D-ϵ

TABLE 7.20 LOCATIONAL DISTRIBUTION AFTER THE CALCULATION IS COMPLETED, S_2D-c

Species	Fraction of Core Inventory		
	RCS	Containment	Environment*
CsI	0.74	0.26	1.5×10^{-8}
CsOH	0.76	0.24	1.4×10^{-8}
Te	0.69	0.15	7.7×10^{-8}

*Released to the ground below the containment building. Value for CsI is as an aerosol and does not reflect possible iodine release as a volatile iodide.

TABLE 7.21. FRACTION OF CORE INVENTORY RELEASED TO THE ATMOSPHERE

Time (hr)	I Group 2	Cs Group 3	Te Group 4	Sr Group 5	Ru Group 6	La Group 7
			AB-β			
0.5	4.2×10^{-4}	4.5×10^{-4}	6.4×10^{-8}	1.7×10^{-5}	2.4×10^{-6}	1.0×10^{-8}
1	2.4×10^{-2}	2.4×10^{-2}	8.5×10^{-4}	3.1×10^{-3}	4.1×10^{-4}	2.6×10^{-6}
2	5.8×10^{-2}	5.7×10^{-2}	4.9×10^{-3}	1.1×10^{-2}	1.5×10^{-3}	4.8×10^{-4}
4	8.1×10^{-2}	8.0×10^{-2}	3.4×10^{-2}	5.1×10^{-2}	2.5×10^{-3}	2.6×10^{-2}
7	8.7×10^{-2}	8.6×10^{-2}	6.0×10^{-2}	7.2×10^{-2}	2.9×10^{-3}	4.3×10^{-2}
10	8.7×10^{-2}	8.7×10^{-2}	6.3×10^{-2}	7.4×10^{-2}	2.9×10^{-3}	4.4×10^{-2}
15	8.7×10^{-2}	8.7×10^{-2}	6.6×10^{-2}	7.5×10^{-2}	2.9×10^{-3}	4.5×10^{-2}
20	8.7×10^{-2}	8.7×10^{-2}	6.6×10^{-2}	7.6×10^{-2}	2.9×10^{-3}	4.5×10^{-2}
			AB-γ			
0.5	1.9×10^{-7}	2.0×10^{-7}	3.0×10^{-11}	1.6×10^{-9}	1.6×10^{-10}	7.3×10^{-11}
1	1.3×10^{-5}	1.3×10^{-5}	5.5×10^{-7}	4.2×10^{-7}	4.0×10^{-8}	2.5×10^{-8}
2	2.6×10^{-5}	2.6×10^{-5}	2.2×10^{-6}	1.5×10^{-6}	1.0×10^{-7}	5.0×10^{-7}
4	4.0×10^{-5}	4.0×10^{-5}	1.4×10^{-5}	2.4×10^{-5}	1.9×10^{-7}	1.7×10^{-5}
7	5.6×10^{-2}	5.8×10^{-2}	1.2×10^{-1}	9.4×10^{-2}	2.3×10^{-3}	4.5×10^{-2}
10	5.7×10^{-2}	5.9×10^{-2}	1.3×10^{-1}	9.6×10^{-2}	2.3×10^{-3}	4.6×10^{-2}
15	5.7×10^{-2}	6.0×10^{-2}	1.4×10^{-1}	9.7×10^{-2}	2.4×10^{-3}	4.7×10^{-2}
20	5.7×10^{-2}	6.0×10^{-2}	1.4×10^{-1}	9.7×10^{-2}	2.4×10^{-3}	4.7×10^{-2}
			AB-ε*			
0.5	1.9×10^{-7}	2.0×10^{-7}	3.0×10^{-11}	1.6×10^{-9}	1.6×10^{-10}	7.3×10^{-11}
1	1.3×10^{-5}	1.3×10^{-5}	5.5×10^{-7}	4.2×10^{-7}	4.0×10^{-8}	2.5×10^{-8}
2	2.6×10^{-5}	2.6×10^{-5}	2.2×10^{-6}	1.5×10^{-6}	1.0×10^{-7}	5.0×10^{-7}
4	4.0×10^{-5}	4.0×10^{-5}	1.4×10^{-5}	2.4×10^{-5}	1.9×10^{-7}	1.7×10^{-5}
7	4.5×10^{-5}	4.5×10^{-5}	2.8×10^{-5}	4.2×10^{-5}	2.3×10^{-7}	3.0×10^{-5}
10	4.7×10^{-5}	4.6×10^{-5}	3.4×10^{-5}	4.6×10^{-5}	2.4×10^{-7}	3.4×10^{-5}
15	4.8×10^{-5}	4.7×10^{-5}	3.8×10^{-5}	4.9×10^{-5}	2.4×10^{-7}	3.5×10^{-5}
20	4.8×10^{-5}	4.7×10^{-5}	4.0×10^{-5}	4.9×10^{-5}	2.4×10^{-7}	3.6×10^{-5}

UNITED STATES
NUCLEAR REGULATORY COMMISSION
WASHINGTON, D. C. 20555

July 27, 1984

ERRATA SHEET

for

BMI-2104, Volume V
DRAFT

Radionuclide Release Under
Specific LWR Accident Conditions

Prepared by

Batelle Columbus Laboratories

for the

U.S. Nuclear Regulatory Commission

Please replace page 7-81 with the
attached revised page.

DIVISION OF TECHNICAL INFORMATION
AND
DOCUMENT CONTROL

TABLE 7.21. (Continued)

Time (hr)	I Group 2	Cs Group 3	Te Group 4	Sr Group 5	Ru Group 6	La Group 7
			TMLB-δ			
2	0	0	0	0	0	0
4	3.9×10^{-2}	3.7×10^{-2}	3.0×10^{-2}	1.8×10^{-2}	4.8×10^{-3}	1.4×10^{-5}
7	4.1×10^{-2}	3.8×10^{-2}	3.5×10^{-2}	2.5×10^{-2}	4.8×10^{-3}	2.1×10^{-4}
10	4.4×10^{-2}	3.9×10^{-2}	5.7×10^{-2}	4.3×10^{-2}	4.9×10^{-3}	7.0×10^{-4}
15	4.6×10^{-2}	3.9×10^{-2}	9.1×10^{-2}	5.3×10^{-3}	5.0×10^{-3}	9.4×10^{-4}
20	4.6×10^{-2}	3.9×10^{-2}	9.7×10^{-2}	5.4×10^{-2}	5.0×10^{-3}	9.6×10^{-4}
50	4.6×10^{-2}	3.9×10^{-2}	1.0×10^{-1}	5.5×10^{-2}	5.0×10^{-3}	9.9×10^{-4}
			TMLB-ε*			
10	0	0	0	0	0	0
15	2.7×10^{-3}	3.7×10^{-4}	8.1×10^{-2}	1.8×10^{-2}	3.1×10^{-6}	4.6×10^{-4}
20	2.8×10^{-3}	3.8×10^{-4}	8.3×10^{-2}	1.8×10^{-2}	3.2×10^{-6}	4.7×10^{-4}
70	2.8×10^{-3}	3.9×10^{-4}	8.5×10^{-2}	1.8×10^{-2}	3.3×10^{-6}	4.7×10^{-4}

*Released with gas flow to ground beneath reactor building. Values for iodine (Group 2) releases could be increased by approximately an additional 10^{-3} if accounting were made for volatile iodide formation.

UNITED STATES
NUCLEAR REGULATORY COMMISSION
WASHINGTON, D.C. 20555

TABLE 7.21. (Continued)

Time (hr)	I Group 2	Cs Group 3	Te Group 4	Sr Group 5	Ru Group 6	La Group 7
			TMLB-δ			
2	0	0	0	0	0	0
4	6.1×10^{-2}	5.9×10^{-2}	3.0×10^{-2}	1.9×10^{-2}	5.0×10^{-3}	1.5×10^{-5}
7	6.4×10^{-2}	6.0×10^{-2}	3.5×10^{-2}	2.6×10^{-2}	5.1×10^{-3}	2.2×10^{-4}
10	6.8×10^{-2}	6.1×10^{-2}	5.9×10^{-2}	4.6×10^{-2}	5.2×10^{-3}	7.3×10^{-4}
15	7.0×10^{-2}	6.2×10^{-2}	9.3×10^{-2}	5.6×10^{-2}	5.3×10^{-3}	9.7×10^{-4}
20	7.0×10^{-2}	6.2×10^{-2}	9.8×10^{-2}	5.7×10^{-2}	5.3×10^{-3}	1.0×10^{-3}
50	7.0×10^{-2}	6.2×10^{-2}	1.0×10^{-1}	5.8×10^{-2}	5.3×10^{-3}	1.0×10^{-3}
			TMLB-ε*			
7	0	0	0	0	0	0
10	0	0	0	0	0	0
15	2.7×10^{-3}	5.8×10^{-4}	8.1×10^{-2}	1.7×10^{-2}	2.3×10^{-5}	4.3×10^{-4}
20	2.7×10^{-3}	5.9×10^{-4}	8.3×10^{-2}	1.7×10^{-2}	2.3×10^{-5}	4.4×10^{-4}
70	2.8×10^{-3}	6.0×10^{-4}	8.5×10^{-2}	1.7×10^{-2}	2.4×10^{-5}	4.4×10^{-4}

*Released with gas flow to ground beneath reactor building. Values for iodine (Group 2) releases could be increased by approximately an additional 10^{-3} if accounting were made for volatile iodide formation.

7.3.6 General Observations

Based on the results of nine NAUA calculations, the following observations can be made on transport and retention of fission products in the containment. The amount of particulates escaping the containment is largely dependent upon the timing of the two releases from the fuel (melt and vaporization) and upon containment failure time. As demonstrated in calculations for the sequences involving an early containment failure (AB-β, AB-γ, TMLB-δ, and V), these accidents lead to the highest release fractions.

It is worthwhile to note that the retention of fission products in the flow path of the primary system for sequences involving early containment failure reduces the source term to the containment and will directly reduce the amount of fission products that escapes the containment. However, the retention effects of the primary system on the release to the environment would not be so apparent for accidents involving a late containment failure mode. In such accident sequences, the fission products that are not retained in the primary system will be retained in the containment due to prolonged residence times.

7.4 Discussion

In July, 1983, Volume 1 of BMI-2104 was issued in draft form. Volume 1 provided analyses for essentially the same sequences as this report. A number of improvements have been made in the methods of analysis in the intervening period between the reports, such as use of the MARCH 2 rather than the MARCH 1.1 code, a more realistic fuel slumping model, more accurate representation of upper plenum structures, and inclusion of diffusiophoretic removal terms in the containment transport analysis. It is important to compare the results obtained in Volume 1 with those of Volume 5 to determine the effects of these modeling changes. Such a comparison may also provide answers to other critical questions. Rapid advancement has been made in the last few years in understanding the processes that influence severe accident source terms. How mature is our calculational methodology? Will future improvements in the methodology dramatically affect the results we are obtaining with the current

methods? Comparisons between Volume 1 and Volume 5 cannot provide definitive answers to these difficult questions but they may provide insights. In this section of the report results obtained with the current methodology will be compared to those obtained in WASH-1400 for the same sequences and the same plant design.

In Table 7.22 results obtained in this study for the release of fission products from the fuel are compared with the WASH-1400 release terms. The comparison between the results is quite close. In both cases essentially all of the volatile fission products are predicted to be completely released from the fuel, either while the core is heating and melting or during the period of concrete attack. The current release estimates during the core meltdown phase are higher for the strontium and ruthenium groups than the WASH-1400 fractions but are substantially less for the least volatile Group 7 which includes lanthanum, uranium, and plutonium. The results obtained in Volume 1 were also quite similar to the current results. Higher release fractions were obtained for Group 7 in the Volume 1 analyses because higher fuel temperatures were obtained in the MARCH 1.1 analyses. It should be recognized in the interpretation of these results that the treatment of fuel melting in the MARCH codes is overly simplified. Indeed the manner in which the single melting temperature in the MARCH model has been used in the BMI-2104 analyses may tend to underpredict the release of low volatility elements from the fuel.

In WASH-1400 no credit was assumed for the retention of fission products during transport through the reactor coolant system. In Volume 1 analyses of these accident sequences predicted retention of the important volatile species, iodine and cesium, varied over a range depending on the accident sequence, from approximately 60 percent in the V and S_2D sequences down to approximately 20 percent in TMLB' and essentially zero in AB. In the more recent analyses the principal difference is in the TMLB' sequence where the predicted retention is substantially higher (~85 percent). This difference is primarily due to the prediction of very low flow rates during core melting in the MARCH 1.1 analyses which did not enable the fission products to be transported out of the core region prior to vessel failure.

The reader should be particularly cautious in the interpretation of results presented in this report for retention in the reactor coolant system. These analyses did not include the effect of the feedback of decay heat from

TABLE 7.22. FISSION PRODUCT RELEASE FROM FUEL

Group	1	2	3	4	5	6	7
Principal Element	Xe	I	Cs	Te	Sr	Ru	La
			Current Study*				
Gap/melt	1.0	1.0	1.0	0.35	0.33	0.045	2.9×10^{-4}
Vaporization	--	--	--	0.22	0.10	--	2.8×10^{-3}
Total	1.0	1.0	1.0	0.59	0.43	0.045	3.1×10^{-3}
			WASH-1400				
Gap/melt	0.90	0.90	0.81	0.15	0.10	0.03	0.03
Vaporization	0.10	0.10	0.19	0.85	0.01	0.003	0.01
Total	1.0	1.0	1.0	1.0	0.11	0.033	0.013

*TMLB' results are used in the example.

deposited fission products leading to the heating of surfaces and the reevolution of deposited fission products. This effect has been demonstrated to be potentially important in this study. Reevolution is being investigated in follow-on analyses that will be provided at a later time as an Appendix.

In Table 7.23 the overall results for the current study are compared with results from WASH-1400. In some cases where analyses were not performed for the same specific case in WASH-1400, the results of similar sequences are substituted. In many important sequences, the releases predicted with the current methodology are substantially lower than the WASH-1400 results. In TMLB'-δ for example, the predicted release is more than an order of magnitude lower. Most of the difference can be attributed to the predicted retention in the reactor coolant system in this study. Greater retention is also predicted within the containment volume with the NAUA code than was predicted for elemental iodine retention using the WASH-1400 CORRAL code. The high release value obtained in Volume 1 resulted from a combination of low retention on surfaces in the reactor coolant system and release to the containment at the time of containment failure. Under those conditions there was little opportunity for removal in the containment prior to release.

For the AB-β sequence the increased retention in the current analyses comes from additional retention in the secondary building into which containment leakage occurs. Most but not all isolation failures would be expected to release into a building of this type. The reduced release in the AB-γ sequence is the result of longer time to containment failure. In the MARCH 2 analysis a 2-1/2-hour delay was predicted from the time of lower head failure to the time of the global hydrogen burn which was predicted to fail the containment. Aerosol deposition in this time period was effective in reducing the eventual release of fission products at the time of containment failure.

The important sequence for which the predicted release was not reduced dramatically is V. It has been agreed that the V sequence in Surry should actually involve scrubbing of fission products through water which has been discharged to the safeguards building. No credit has been assumed in this analysis for decontamination in a water pool because of major uncertainties regarding the location of the failure and the structural condition of the safeguards building. As the result of procedural changes introduced subsequent to WASH-1400, the likelihood of event V is believed to have been reduced

TABLE 7.23. RELEASE FRACTIONS FOR IODINE*

Sequence	Current Estimate	Draft Volume 1	WASH-1400
AB-β	9×10^{-2}	0.4	0.4
AB-γ	6×10^{-2}	0.3	0.7
AB-ε	5×10^{-5}	3×10^{-4}	3×10^{-3}
TMLB'-δ	5×10^{-2}	0.7	0.7
TMLB'-ε	3×10^{-3}	1×10^{-3}	3×10^{-3}
V	0.4**	0.2	0.7
S_2D-ε	2×10^{-8}	6×10^{-7}	2×10^{-5}

* Does not include consideration for volatile iodide formation.

** Release fraction reduced to 0.09 if scrubbing by water in safeguards building is considered.

substantially so that it is no longer considered a principal contributor to the risk. Thus, if the release fractions in Table 7.23 were used to reestimate the risk to the public, a substantially smaller risk would be predicted. In terms of the risk of latent fatalities, the reduction would be essentially proportional to the reduction in the source term of the volatile fission products (e.g., an order of magnitude reduction). Because of the threshold nature of early fatalities, the reduction in the predicted risk would be more dramatic.

Again the reader is cautioned to recognize the magnitude of the uncertainties in the methods of analysis. Work is continuing to improve and validate the methods which could lead to changes in source term estimates in the future. In particular, the analysis of fission product reevolution from reactor coolant system surfaces should be recognized as a potential source of nonconservatism in the analysis.

*U.S. GOVERNMENT PRINTING OFFICE : 1984 0-421-297/4035